Microrheology of Fibrin Clots

Peter Allan

Submitted in accordance with the requirements for the degree of
Doctor of Philosophy

The University of Leeds
School of Physics and Astronomy

April 2012

The candidate confirms that the work submitted is his own, except where work which has formed part of jointly-authored publications has been included. The contribution of the candidate and the other authors to this work has been explicitly indicated below. The candidate confirms that appropriate credit has been given within the thesis where reference has been made to the work of others.

Publications

1. **Allan, P.**, S. Uitte de Willige, R. H. Abou-Saleh, S. D. Connell, and R. A. S. Ariëns. 2012. Evidence that fibrinogen directly interferes with protofibril growth: implications for fibrin structure and clot stiffness. *J Thromb Haemost* **10**:1072-1080.

The author helped in the design of the study, performed all experiments, analyzed and interpreted all the data, and wrote the manuscript; S. Uitte de Willige helped in the design of the study, performed the anion exchange chromatography, helped interpret the data and critically reviewed the manuscript; R. Abou-Saleh assisted in AFM analysis; S. D. Connell helped in the design of the study, helped interpret the data and critically reviewed the manuscript; R. A. S. Ariens designed the study, helped interpret the data and critically reviewed the manuscript.

2. Konings, J., J. W. P. Govers-Riemslag, H. Philippou, N. J. Mutch, J. I. Borissoff, **P. Allan**, S. Mohan, G. Tans, H. ten Cate, and R. A. S. Ariëns. 2011. Factor XIIa regulates the structure of the fibrin clot independently of thrombin generation through direct interaction with fibrin. *Blood* **118**:3942-3951.

The author performed magnetic microrheometer experiments, analyzed the data and assisted in their interpretation. It is this work which is included within this thesis, it has been explicitly stated where reference has been made to the work of others taken from this publication.

I dedicate this thesis to my mother and father David and Vivien Allan.

Acknowledgements

Firstly, I would like to thank my supervisors Dr Robert Ariëns and Dr Simon Connell for their guidance and support during my PhD. I would also like to thank Dr Lars Jeuken and Dr Mike Evans for their extremely useful feedback during my first year transfer viva.

I wish to thank Radwa Abou-Saleh and Daniel Billingsley for their assistance in AFM sample preparation and the 'dark art' of AFM imaging. Similarly, I wish to thank Daniel Whalley for his help in SEM sample preparation and imaging. I would also like to thank Gareth Howell of the Leeds Bio-imaging facility for his training and assistance in confocal microscopy. In addition, thanks go to Dr Shirely Uitte de Willige for preparing the γ' samples and her assistance in the biological aspects of the work.

I wish to thank everyone, past and present, in the Molecular and Nanoscale physics group for all your support and numerous cups of tea over the years. I would like to thank the following people from the LIGHT institute; Emma Smith, Amy Cilia La Corte, Helen Philippou, Cedric Duval and all those who attended the ISTH in Japan. I would also like to thank everyone involved or associated with the White Rose DTC, in particular Dan (again), Tom Forth, Louise Way and Simon England for some great times in Sheffield and Leeds.

I would like to thank Jan Clarke and Mark Johnson for letting me take over their flat while I wrote up my thesis, and in particular for the extremely reasonable rent they charged (£0).

Finally, I wish to thank my wife for all her help and support during some of the hardest years. And more importantly, for always putting up with me, a task that probably rivals doing a PhD.

Abstract

An active particle tracking microrheology technique has been developed to study the viscoelastic properties of human fibrin and plasma clots. In order to perform microrheology measurements, a magnetic microrheometer device has been adapted and a technique developed, following the procedure of Evans *et al*., to measure the frequency dependent viscoelastic moduli ($G'(\omega)$ and $G''(\omega)$). This technique has been supported by complementary investigation methodologies, such as protein analysis, turbidity, and multiple microscopy techniques.

As a result of this study new insights into the viscoelastic dynamics of fibrin have been revealed. Three stress relaxation mechanisms, as predicted by Morse *et al*. for networks of semi-flexible fibres, were observed and occur on distinctly different timescales. The scaling of the tension dominated contribution was measured to scale as $G' \sim c^{2.7 \pm 0.2}$ in agreement with the prediction of Mackintosh. The presence of FXIII resulted in stiffer less deformable clots but was found to have no effect on the viscoelastic dynamics of clots. Frequency measurements of the loss tangent revealed that on timescales intermediate between stress relaxation modes clots were much more susceptible to permanent deformation. The effect of fibrinogen, thrombin and calcium on the viscoelastic behaviour of clots was also investigated. Increased fibrinogen levels produced clots which displayed predominantly elastic behaviour on shorter time-scales .

The molecular mechanism underpinning the role of fibrinogen γ' in fibrin clot polymerisation, structure and viscoelasticity was also investigated. We report new data which show that fibrinogen γ' is associated with the formation of mechanically weaker, non-uniform clots composed of thinner fibres. This is caused by direct disruption of protofibril formation by γ' and not through thrombin inhibition or binding to FXIII. In addition, the effects of the plasma proteins FVIIa, FIXa, FXIIa and FXIII on clot properties are also reported.

Table of Contents

List of figures

List of Tables

Chapter 1

1 Introduction

1.1 Haemostasis

Haemostasis is the physiological process which protects the integrity of the vascular system (1). An extremely important function of the haemostatic process is the ability to minimise blood loss in the event of vessel trauma. The body's ability to stem the flow of blood is commonly referred to as coagulation; this process is of central importance to life as it prevents an organism from bleeding to death. In the event of damage to a blood vessel several steps occur to arrest the flow of blood:

- Vasoconstriction: blood vessels constrict minimising their diameter and reducing the flow of blood.

- Primary haemostasis: exposed collagen in the damaged cells of the blood vessel lining activate platelets leading to their attachment to the damaged cells and to themselves (2). These platelets aggregate into a 'haemostatic plug', forming within seconds after vessel trauma.
- Secondary haemostasis (coagulation): Tissue factor exposed by damage of the vascular wall binds factor VII and initiates coagulation. In addition, platelet activation leads to the exposure of negatively charged phospholipids on the platelet membrane and to the release of procoagulant factors from the platelet granules, further activating the common and contact pathways of coagulation. The final result is the formation of a blood clot.
- Finally, Plasmin begins to dissolve the clot; a process termed fibrinolysis, in order to restore normal blood flow after tissue repair.

Two pathways exist to initiate coagulation; termed contact activation pathway (intrinsic) and tissue factor pathway (extrinsic) (Figure 1-1). Both coagulation pathways rely on inactive enzyme precursors (zymogens) becoming activated through limited proteolysis by an upstream coagulation factor and initiating the next stage of coagulation. The enzymes involved in coagulation are serine proteases (the active site of the enzyme possesses a serine residue), all of which cleave peptide bonds of proteins. Only factor XIII (FXIII) is a different zymogen, being a protransglutaminase, which on activation by thrombin cross-links proteins such as fibrin and collagen by forming covalent bonds between the γ-chains and between γ- and Aα-chains (3).

The intrinsic pathway, activated when zymogen FXII comes into contact with a negative surface, is believed to play a relatively minor role in the haemostatic response. The role of FXII has been contested as people with FXII deficiency, unlike other coagulation factor deficiencies, do not suffer from major bleeding (4). Recent *in vivo* data show that FXII inhibition or deficiency in rodent models reduces blood clot formation whilst maintaining

normal bleeding times (5-8), suggesting a role for FXII in pathological thrombus formation but not normal haemostasis.

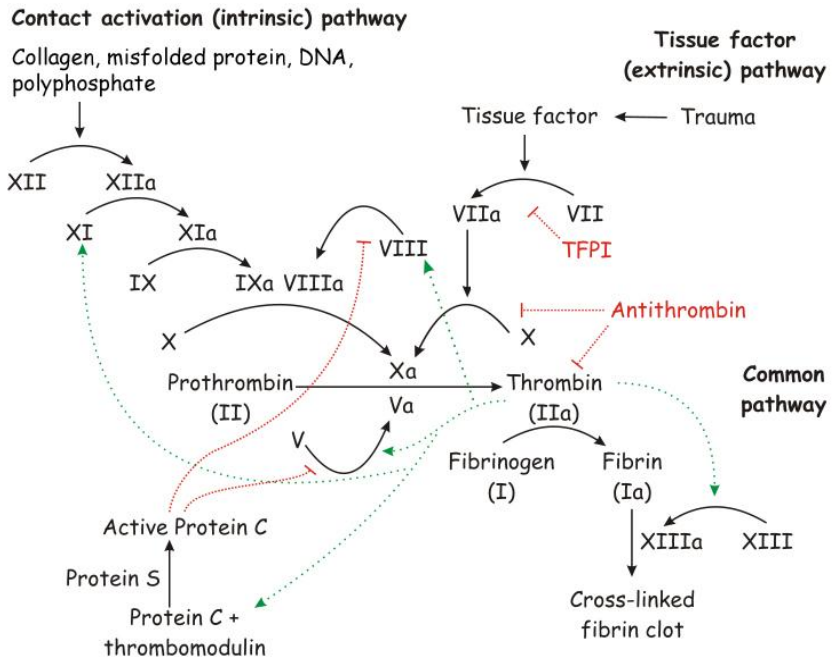

Figure 1-1: The intrinsic and extrinsic coagulation cascade (adapted from (5)). The intrinsic pathway is activated via FXII through several mechanisms while the extrinsic pathway is activated by blood vessel trauma. Both responses culminate in the formation of a fibrin clot.

The extrinsic pathway plays a much more vital role and is activated upon damage to blood vessels which exposes tissue factor (TF), a transmembrane protein expressed on perivascular cells. FVII is activated by TF, and has been shown to demonstrate auto-catalytic activity, and by thrombin (once initial minute amounts have been generated). FVIIa then reacts with TF to from TF-VIIa, which in turn activates factors IX and X. FXa and its cofactor Va and several other molecules form a complex called prothrombinase. This complex (on the surface of activated platelets) converts prothrombin (FII) into thrombin (FIIa). Thrombin then initiates a number of reactions (including activation of factors V and VIII) that result in further activation of FX; this produces a self-enhancing cycle which rapidly increases the amount of thrombin and consolidates the haemostatic response.

The main role of thrombin is to convert the precursor fibrinogen (FI) into its active form fibrin (FIa) which then self-assembles to form a fibrin clot, termed the common pathway. Thrombin also activates FXIII which forms covalent bonds between fibrin molecules; this is termed cross-linking (or ligation) and results in a more stable clot. The terms cross-linking and ligation are used interchangeable throughout the literature. The term cross-link is commonly used in haemostasis and thrombosis to indicate the product of FXIII activity, therefore throughout this work the term cross-link will be used to identify these types of covalent bonds produced by FXIIIa.

1.2 Fibrin Clot Formation

Fibrinogen, the primary structural protein of a blood clot, has a molecular weight of 340 KDa, is ~45 nm in length, ~4 nm in diameter, and consists of two identical halves each containing an outer D-region connected by a coiled-coil segment to a central E-region (Figure 1-2 A) (6, 7). These connecting coiled-coil segments consist of three polypeptide chains termed Aα, Bβ and γ and all have their amino termini joined together in the central E-region via five symmetrical disulfide bridges (8-12). Anti-parallel disulfide bridges form a 'disulfide ring' within this region (8, 9). Disulphide bonds also hold the chains in place at various other locations across the structure.

The Aα-chain consists of 610, the Bβ-chain 461, and the major γ-chain form, γA, 411 amino acid residues respectively (10). A minor γ-chain variant termed γ' accounts for between 8 to 15% of the total fibrinogen γ-chain population and is composed of 427 residues (7). The Bβ and γ chains carboxyl-termini reside in the D-region, while that of the Aα chain loops back towards the central region of the fibrinogen molecule (Figure 1-2 A) (7).

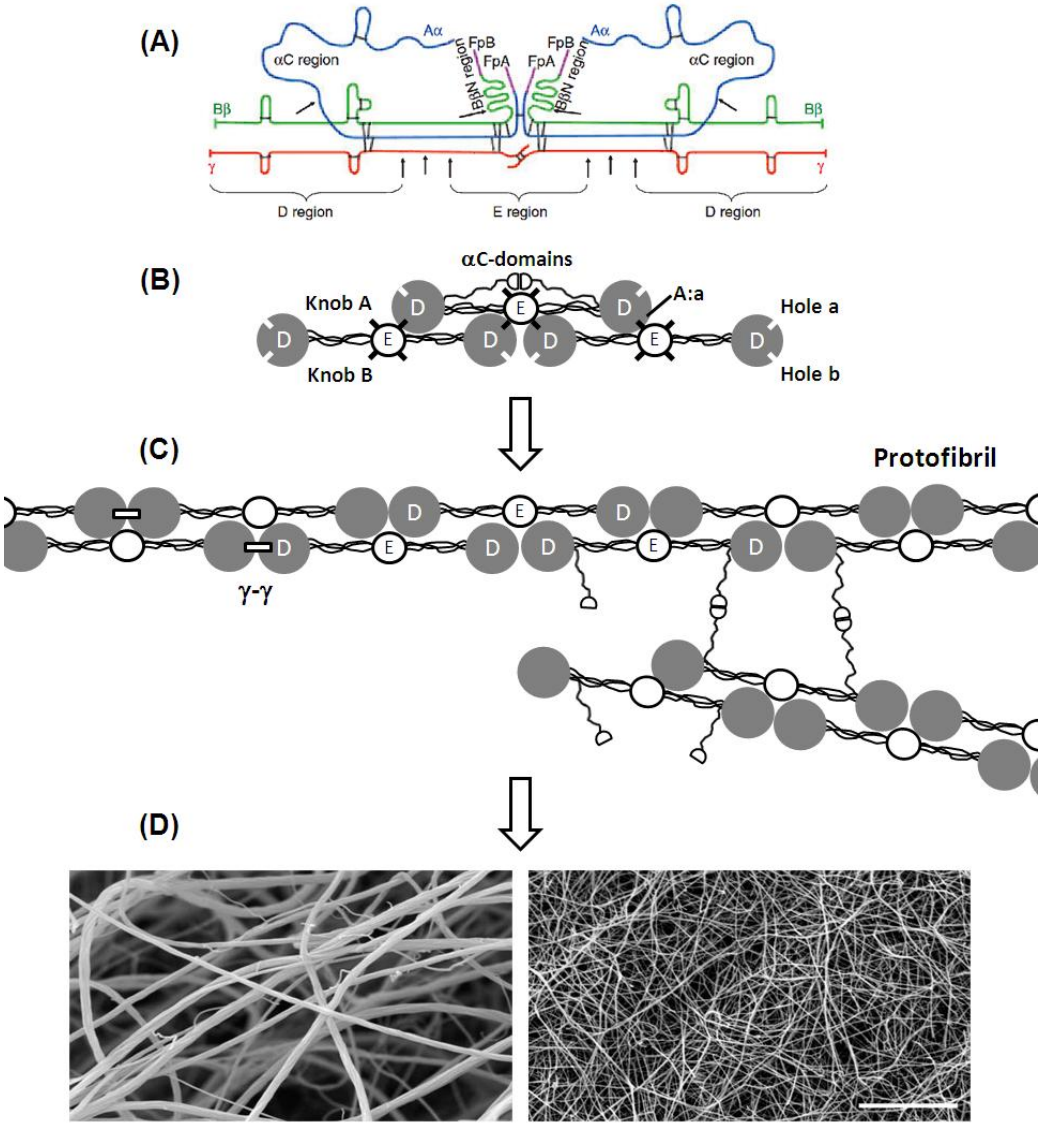

Figure 1-2: Fibrinogen structure and fibrin polymerisation (adapted from (11)). (A) Polypeptide chain structure of fibrinogen (12). The Aα, Bβ and γ polypeptide chains are blue, green and red respectively. The numerous disulfide bonds are represented by black bars. Fibrinopeptides A and B (FpA and FpB) are magenta. **(B)** Schematic representing the "knob-to-hole" interaction of fibrin showing A:a bonding. The αC-domains, which interact intramolecularly, are shown only in the upper molecule for clarity. **(C)** Schematic representing protofibrils and intermolecular interaction between the αC-domains upon lateral aggregation of protofibrils. The γ-γ cross-links between D regions are represented by small open rectangles. They are shown only between the D-D ends for simplicity, however they may also occur in a transverse manner (Figure 1-5) (11). **(D)** Scanning electron micrographs of fibrin clots (images taken from (13)). **Left:** clot with thick, long fibres and few branch points formed with a low thrombin concentration (Coarse). **Right**: clot with thin, short fibres and many branch points formed with a high thrombin concentration (Fine). Scale bar = 5μm.

Two fibrinopeptides termed A (FpA) and B (FpB) reside at the N-termini of the Aα and Bβ chains respectively (Figure 1-2 A). FpA and FpB are negatively charged and prevent fibrinogen molecules from aggregating in the absence of blood vessel damage (14). During clotting thrombin converts fibrinogen into fibrin by cleaving FpA and FpB from the central E-region of the molecule. This exposes knobs (A and B) which can then interact with complementary holes (a and b) that are always exposed in the D-regions of the fibrinogen molecule (Figure 1-2 B) (15).

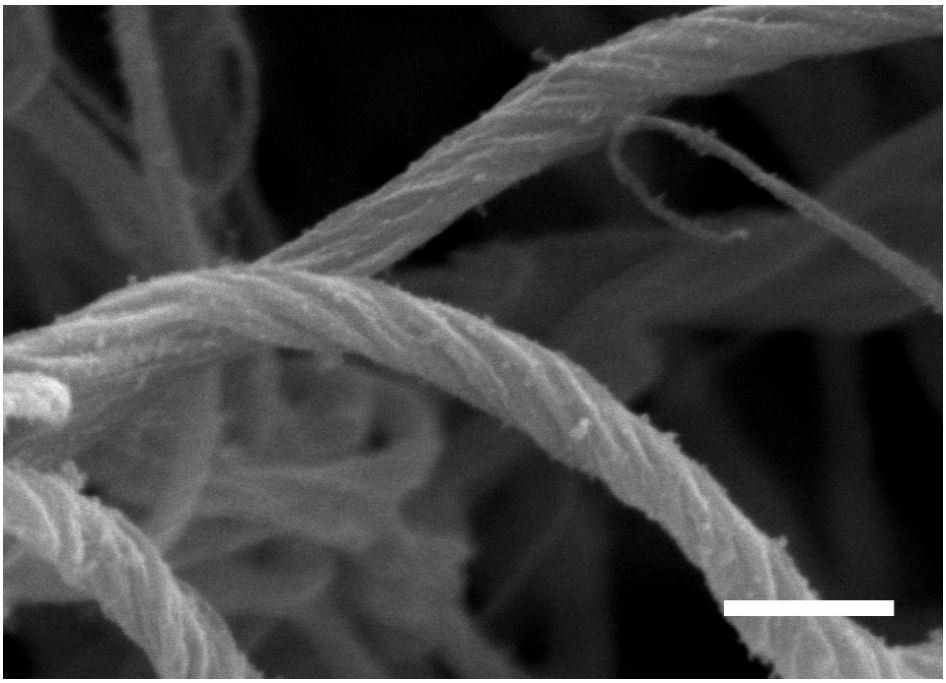

Figure 1-3: Scanning electron micrograph of fibres in a fibrin clot. The surface appearance of the fibres indicates that fibrin fibres can produce rope-like twisted structures. Image kindly provided by Sumitra Mohan. Scale bar = 500 nm.

Cleavage of FpA exposes a Gly-Pro-Arg (GPR) sequence while cleavage of FpB exposes a Gly-His-Arg-Pro (GHRP) sequence. Specific A:a interactions (16) are responsible for the longitudinal growth of fibrin monomers into a half staggered structure called the proto-fibril (Figure 1-2 B and C), which has a periodicity of 22.5 nm. This periodicity of the protofibril is responsible for the

banding pattern of fibrin fibres observed by scanningelectron microscopy (Figure 1-3).

Thrombin cleaves FpA more rapidly than FpB and this is sufficient to initiate fibrin polymerisation (16). The snake venom batroxobin cleaves FpA without cleaving FpB to produce the desA-fibrin monomer. Polymerisation of desA-fibrin results in a network similar to normal fibrin except for some differences in ultra structure (17). The stiffness of clots formed from thrombin is 2- to 4-times greater than clots formed only by cleavage of FpA (18), indicating a role for B-b bonding in enhancing the molecular interactions involved in protofibril assembly. The majority of FpBs are cleaved after the process of fibrin assembly has been initiated and fibrin polymers have formed (19, 20). The role of B:b interactions has been studied in one of two ways; either using fibrinogen with impaired FpA release, or enzymes which specifically remove FpB to produce desB-fibrin. These variants were all able to form a β-fibrin clot (14, 21, 22). It has been suggested however that polymerisation in the latter case arises through B:a instead of B:b interactions (23).

FpB release has been reported to result in the formation of thicker fibres by enhancing lateral aggregation of growing protofibrils (14, 24). The release of the αC-domains after FpB has been removed is thought to aid lateral aggregation by molecular interactions of the αC-domains in the intra-protofibril space (Figure 1-2 C) (25). The work of Litvinov *et al*. used optical tweezers to measure the forces of individual knob-hole interactions underlying fibrin polymerisation (16). They found polymerisation was mainly driven by strong, stable and highly specific A:a bonding, where the strength of binding is of the order of 250 pN.

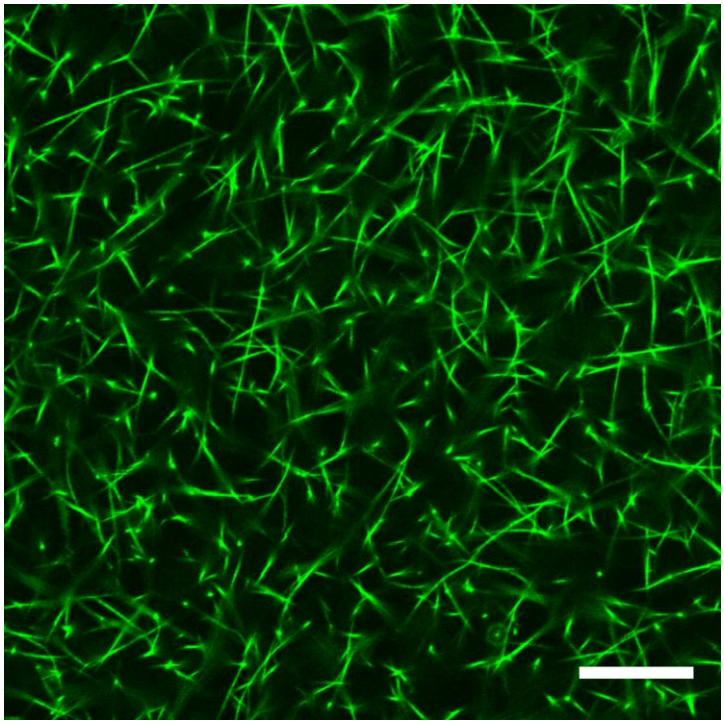

Figure 1-4: Confocal microscopy image of a fibrin clot. The image is of a single optical plane within a fibrin clot which contains fluorescently labelled fibrinogen. Note the vast majority of fibres are extremely straight in this type of imaging. Image obtained by the author of this work, further details provided in chapter 2. Scale bar = 20 μm.

Once proto-fibrils have grown sufficiently, up to around 15 monomers in length (26), they begin to aggregate laterally and form fibres (Figure 1-2 C). Fibres display a twisted, rope-like structures on their exterior (Figure 1-3). When protofibrils aggregate to form fibres this seems to suggest that they twist around one another (27). This twisting limits the radial growth of fibres if we assume that the protofibril periodicity of 22.5 nm needs to be maintained. Increasing the diameter of a fibre requires stretching a protofibril in order to increase its path length; this sets an upper limit on the radial size of fibrin fibres to 50 nm (28). This increases up to 100 nm when accounting for the flexibility of fibrinogen molecules. Fibres may also aggregate to form even thicker fibres. Fibre growth halts when the energy required to stretch an added protofibril exceeds the energy of bonding. Thus, protofibrils on the exterior are under tension and this accounts for the observation that fibres making up a clot are extremely straight when observed under fully hydrated

conditions such as with the laser scanning confocal microscope (Figure 1-4). The fact that fibres are under tension will have important implications for the viscoelastic properties of a clot.

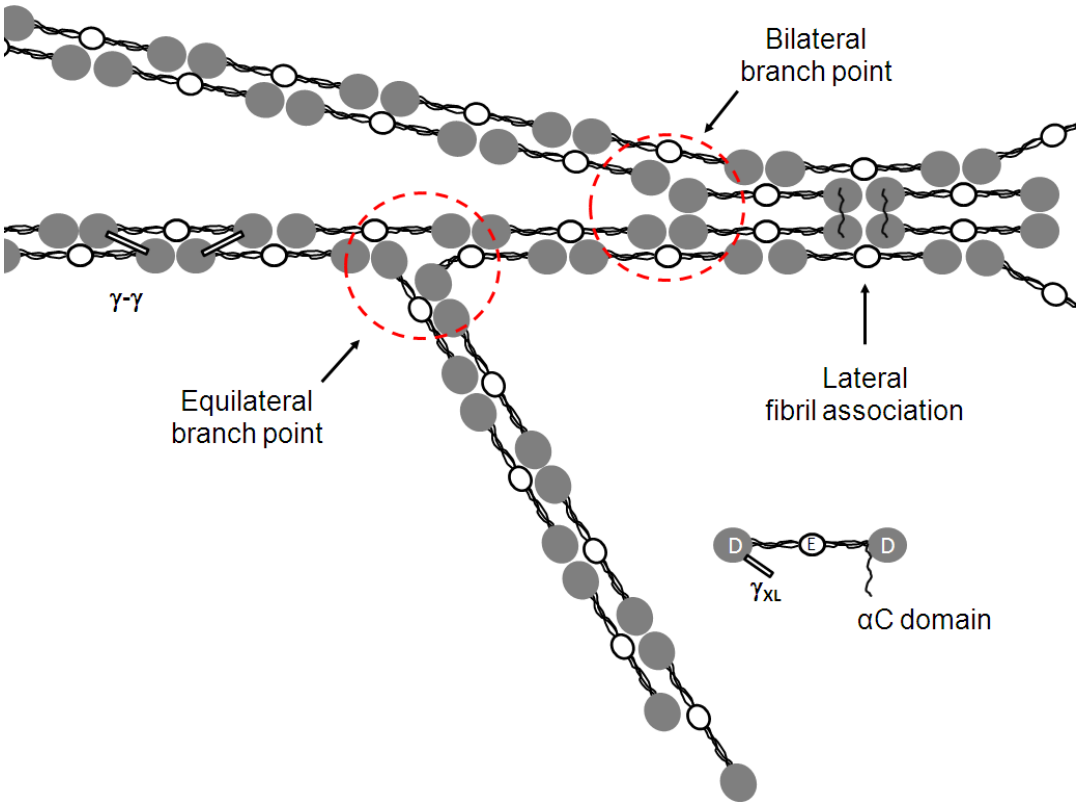

Figure 1-5: Schematic diagram of fibrin assembly, branching, lateral fibril association, and γ-chain cross-linking (adapted from (7)). Cross-linked γ-chains are positioned 'transversely' between fibril strands are represented by small open rectangles.

Fibrin fibres form branches with one another resulting in a 3-dimensional fibrous network (Figure 1-2 D). This forms the structural basis, or scaffold, of a blood clot. It was initially proposed by Ferry *et al*. that a fine clot consisted of a random assembly of long stiff fibres which did not branch (29). However, it has since been shown that fibrin fibres do branch, forming an intricate interlinked network. Free fibre ends are rarely observed in an undamaged normal clot (30). They may occur when the fibrin clot is lysed by plasmin, which cuts perpendicularly through a fibrin fibre. Two types of branching exist in fibrin networks (Figure 1-5), termed bilateral and equilateral branch points (31, 32). Bilateral branching occurs when a double-stranded protofibril

converges laterally with another fibril to form a four-stranded fibril junction. Equilateral branching forms by convergent interactions between three fibrin molecules giving rise to three fibres at a junction. It has been suggested that equilateral junctions are the dominant branch point type and form with far greater frequency than bilateral branches (22, 33). However, recent evidence suggests that branch points may be more complex in structure and form triangular structures, with struts crossing from one leg to the other, particularly when placed under mechanical stress (34).

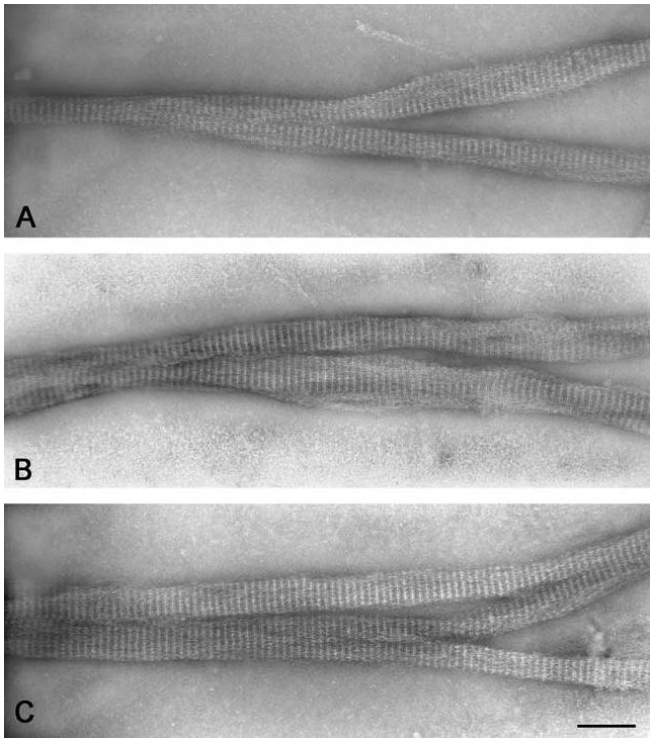

Figure 1-6: Transmission electron micrographs of negatively contrasted fibrin fibres that show the substructure of branch point (figure from (35)). The majority of branch points consist of three fibre segments of approximately equal diameters which join together at small acute angles with their band patterns aligned. The 22.5 nm band pattern characteristic of fibrin can be easily observed. Scale bar = 0.2 μm.

The structure of branch points in coarse clots has been studied using the electron microscope (35) and stained human fibrin (Figure 1-6). Stain distribution is directly related to protein density; stain is excluded from regions of high protein density, appearing bright, while stain penetrates

regions of lower protein density, appearing darker. These results suggest that branch points arise due to the divergence of fibrils that were associated with one another as a fibre and these formed early in polymerisation with additional protofibrils added to all parts of the network (13). Fibres form by the lateral aggregation of protofibrils while branch points form by the divergence of protofibrils from one another. So, a high degree of lateral aggregation during polymerisation will result in a network of thick fibres with low branching (Figure 1-2 D Left), while more protofibril divergence will result in a clot consisting of thin fibres and many branches (Figure 1-2 D Right).

Once a fibrin clot has formed it must remain at the site of a wound to stem the flow of blood while any vessel damage is repaired, after this, the clot must be broken down and removed so as not to cause any serious pathological complications e.g. heart attack or stroke. The viscoelastic properties of a clot are crucial to its function; a clot must display both the elastic properties of a solid and the viscous properties of a fluid. Blood clots must be strong enough to stop bleeding and withstand the pressure of blood flow while at the same time be easily digestible by enzymes in order to be removed. Clot structure plays a simultaneous role in modulating both the viscoelastic properties and the mechanism of fibrinolysis. The structure must be finely tuned in order to strike the right balance between halting bleeding and minimising the effects of cardiovascular disease.

The physiological importance of blood clot viscoelasticity is demonstrated by the effect different haemostatic disorders have upon a clot's physical properties. Patients with myocardial infarction, whereby interruption of the blood flow to the heart leads to subsequent heart muscle damage, form clots with a much tighter and more rigid fibrin network compared with healthy controls (36, 37). Similarly, patients who suffered from heart attacks at an early age posses clots with an increased stiffness of around 50%, compared with control clots (38). On the other hand factor VIII-and factor IX- deficient patients (haemophiliacs) form clots with a reduced stiffness that is 3- to 5-times lower than clots formed by healthy subjects (39). Other studies of

patients with an auto-antibody inhibiting cross-linking involving the α-chain showed clots with a stiffness 4-times lower than that of fully cross-linked clots (40). Achieving an optimal viscoelastic balance in a clot's mechanical properties is therefore critical to prevent disorders of either bleeding or thrombosis with their associated high degrees of morbidity and mortality.

1.3 The Mechanical Properties of Fibrin Clots

From a clinical perspective, the study of the mechanical properties of blood clots is an extremely important area. Very little is known of the mechanical properties of *in vivo* clots. Better understanding of a clot's mechanical properties could help to underpin mechanisms involved in vascular disease and should ultimately lead to the development of better treatments and preventions. Establishing the origin of blood clot viscoelasticity is also an active area in the field of biophysics and has been studied extensively for over five decades (33, 41-54).

The study of the mechanical properties in blood clots from clinical samples is typically carried out using the technique of thromboelastography (TEG), which is also used to assess the overall efficiency of blood coagulation (55, 56). It was first developed by the German Dr. Hellmut Hartert at University of Heidelberg School of Medicine in 1948 (57). Thromboelastography works by placing a small sample of blood (typically 0.36 ml) into a cup (heated to 37°C) which is slowly oscillated. Coagulation is induced by the addition of activator, typically tissue factor or kaolin. A pin suspended freely from a torsion wire is placed into the blood. As the clot forms the fibrin strands couple the motion of the cup to the pin; the response of the clot to this torsional stress is transmitted through the pin and recorded. By measuring the response of a clot in this way many parameters governing blood coagulation may be extracted e.g. clot formation time, rate of clotting, and R_{max}, an indicator of maximal clot firmness. However, the latter mechanical property has not been related to the viscoelastic properties commonly used

to characterise materials and therefore has no physical meaning other than in comparison with other such thromboelastography measurements.

Fibrin networks are viscoelastic polymers which exhibit both viscous and elastic characteristics. Elastic materials obey Hooke's law which states that stress (the force applied per unit area) is directly proportional to strain, but independent of the rate of strain. For a purely elastic material the stress, σ is given by:

$$\sigma = G\gamma \qquad 1\text{-}1$$

where G is the elastic modulus and γ is the strain. Viscous materials obey Newton's law, which states that stress is directly proportional to the rate of strain but independent of the strain itself (58). For a purely viscous material the stress is given by:

$$\sigma = \eta\dot{\gamma} \qquad 1\text{-}2$$

where η is the viscosity and $\dot{\gamma}$ is the rate of strain ($d\gamma/dt$). Most materials can be classified as either solid (elastic) or liquid (viscous) and this is based upon the time frame in which we observe and interact with them. However, there is also a class of materials which behave viscoelastically. One example is silly putty (polydimethylsiloxane (PDMS)), which when thrown against a wall (short timescale) will behave elastically and bounce off the wall. When left for a long period (long timescale) it will behave viscously and flows like a liquid.

An oscillatory force applied to an elastic material will produce a strain which is transmitted almost instantaneously, thus the stress and strain are in phase with one another. The same force applied to a viscous material will result in the fluid flowing and deforming. As the rate of stress is increased, the time available for this flow to occur is reduced and the strain increases. The stress and strain are out of phase by $\pi/4$. Thus, a viscoelastic material will exhibit a phase shift which varies between 0 and $\pi/4$, depending on the frequency of

oscillation. The maximum stress, σ_0 and strain, γ_0 are constant for any given frequency. The ratio of these two quantities:

$$\left|G^*\right| = \frac{\sigma_0}{\gamma_0} \qquad 1\text{-}3$$

is known as the complex modulus, where G* is a complex number where G′ represents the real and G′′ represents the imaginary parts:

$$G^* = G' + iG'' \qquad 1\text{-}4$$

The storage modulus, G′ represents the elastic properties and is widely used to characterise clot stiffness, while the loss modulus, G′′ represents the inelastic, or viscous properties and is used to characterise the amount of energy dissipated by a clot (59). Also used to characterise clot viscoelasticity is the loss tangent:

$$\tan\delta = \frac{G''}{G'} \qquad 1\text{-}5$$

which gives the ratio of energy lost to energy stored in a cyclic deformation (33). For a viscous liquid tanδ >> 0 i.e. G′′ >> G′, and the viscous behaviour dominates. For an elastic solid tanδ << 0 i.e. G′ >> G′′, and the elastic behaviour dominates. For a viscoelastic material with tanδ = 1 then it dissipates and stores equal amounts of energy.

The viscoelastic properties of a clot determine how it responds when subjected to a force. Physiological forces arise from either venous or arterial blood flow which will apply substantial and varying shear forces upon a clot; venous wall shear rates are <300 s^{-1} (60), arterial ~650 s^{-1} and in stenosed arteries shear rates increase to 2600 s^{-1} (61). The venous system is characterised by low flow and low pressure conditions as opposed to the high flow and high pressure in the arterial system. A stiff clot, one possessing

a large elastic component and a small viscous component will deform very little to a given stress and return to its original shape. A weaker clot; one possessing a large viscous component and a small elastic component under the influence of the same stress will incur a large and more permanent deformation. As indicated above, a clot with very similar elastic and viscous components will incur a permanent deformation of similar magnitude to the reversible deformation.

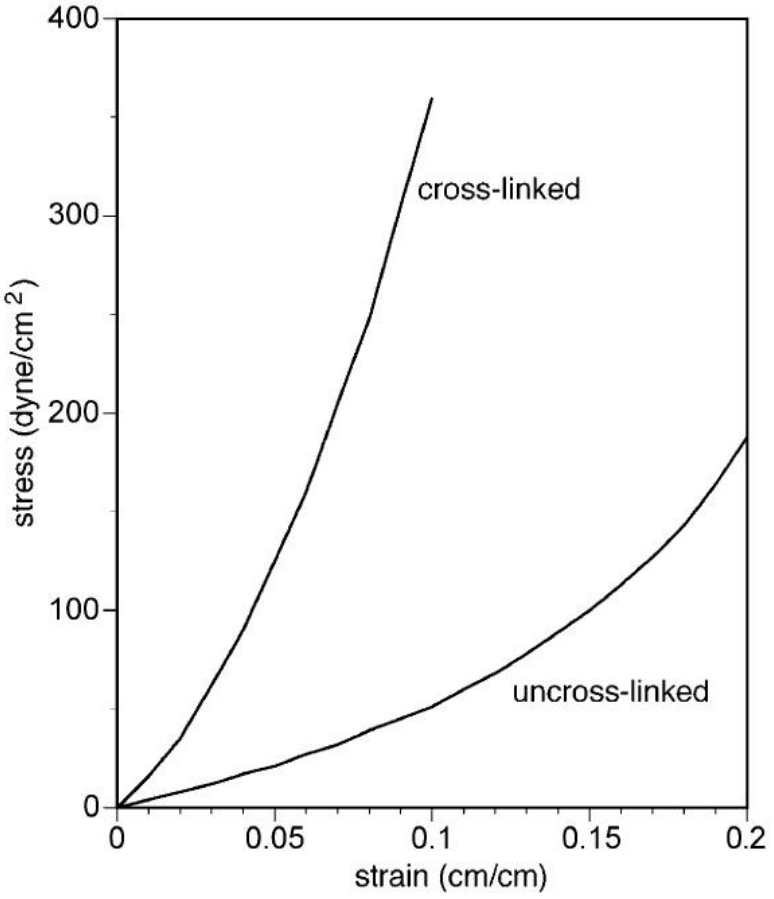

Figure 1-7: Stress vs. strain curves for cross-linked and uncross-linked fibrin clots (data from (62), figure from (63)). The elastic modulus is determined from the slope of each curve. Strain hardening is apparent in both clots by the non-linear stress-strain response.

In order to measure the viscoelastic properties of any material a stress must be applied and the resulting strain measured. A stress-strain curve can be used to determine the elastic modulus, G′ of a material, a quantity which is

independent of both the size and shape of the material (58, 62). An example of this can be seen between a clot with and without cross-linking (Figure 1-7), which is known to increase a material's stiffness. For the same stress you get a much larger strain in uncross-linked clots; indicative of a much weaker network. Cross-linking increases a clot's stiffness by the formation of bonds between individual fibrin monomers (Figure 1-12). The nature of these cross-links and their effect on clot stiffness is still currently in debate.

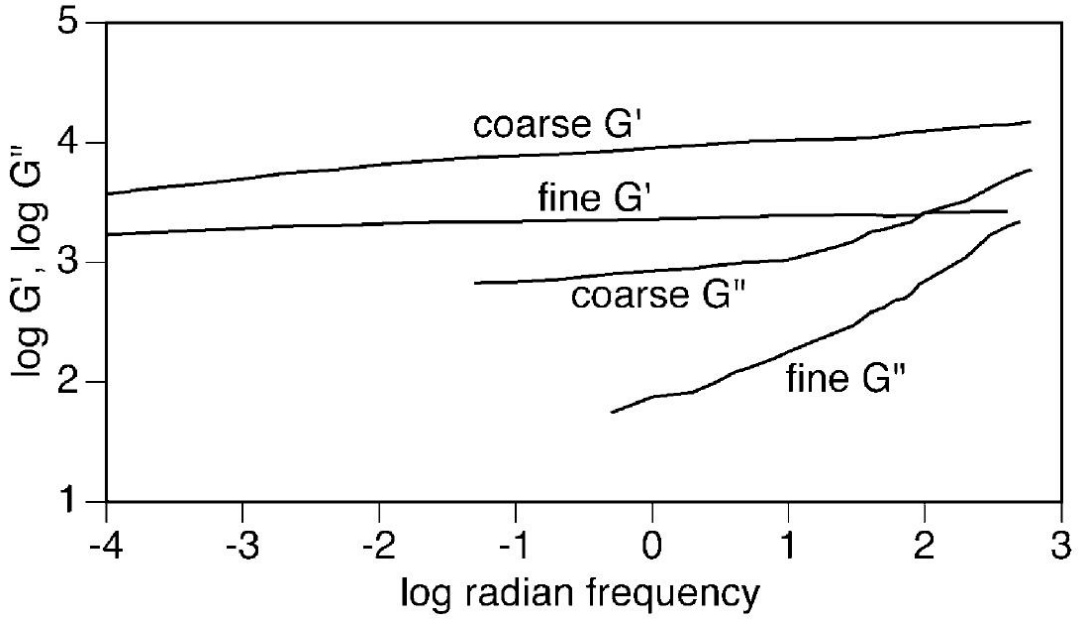

Figure 1-8: Log-log plot of the storage (G′) and loss (G″) moduli as a function of frequency for fine and coarse clots (data from (44), figure from (63)).

Viscoelastic measurements are typically carried out by placing a material between two circular plates or a cone and plate (58): the bottom plate is kept stationary while the top is rotated in order to produce a shear stress. This type of stress is applied parallel to the face of a material and in this way one part of the material moves with respect to another. Measurements can be applied either dynamically where the top plate is oscillated, or statically where the top plate is rotated and held to apply a constant stress and the resulting strain is measured (creep experiments).

The first major study into the viscoelasticity of clots came from Ferry *et al*. (44) who looked at the dynamic viscoelastic properties of human fibrin clots. Two different types of clot structure as determined by the pH and ionic strength were investigated: termed “fine” and “coarse” (Figure 1-2 D). Clots formed with a low thrombin concentration have a high opacity and consist of thick fibres (coarse) while clots formed with a high thrombin concentration have a very low opacity and consist of thin fibres (fine). Opacity can be used as a measure of the typical diameter of fibres within a clot. It has been shown from turbidity measurements that it is possible to estimate the size and density of fibrin fibres within a clot (64).

Ferry *et al*. measured the storage and loss moduli of clots over a frequency range of 0.01 to 160 Hz with a Birnboim transducer apparatus; a stainless steel cell and rod. This allowed the viscoelastic behaviour of clots to be studied over a range of timescales, i.e. slow and fast deformations. For fine and coarse clots G′ and G′′ (in dynes cm^{-2}) are plotted as a function of frequency (Figure 1-8). For fine clots, G′ is independent of frequency, suggesting fibrin clots are nearly a perfect elastic system. This consistency in a clot’s elasticity means that the stiffness of a clot is the same irrespective of the rate of application of stress. Such behaviour suggests a clot’s stiffness must be important physiologically as the rate of application of stress is likely to vary greatly depending upon where a clot is located within the body.

For coarse clots, G′ was found to be higher suggesting that clot structure has a significant effect upon clot stiffness. The storage modulus of coarse clots showed a slight dependence upon frequency suggesting a small inelastic component. For both fine and coarse clots their inelastic components show a dependency upon frequency. At low frequencies, i.e. slow changes in deformation, G′′ is small and clots behave elastically. While at much higher frequencies i.e. fast changes, clots begin to deform irreversibly and are beginning to display viscous behaviour.

The work of Ferry *et al*. continued onto studying the linear viscoelastic behaviour of fine and coarse clots, on much longer time scales, from 20 up to 10^4 s, through the measurement of shear creep and creep recovery in small deformations (45). A torsional rheometer was used for this work where clots are formed between two circular plates. A large change in the compliance of coarse clots between those with and without cross-linking was observed and attributed to increased stiffening. The discovery that cross-linking increases clot stiffness, contrary to their earlier work (44), was also confirmed by other studies at the time (46-48).

The dependency of the initial modulus, corresponding to 20 – 30 s after stress has been applied, upon fibrin concentration was also investigated for non-cross-linked and cross-linked coarse clots. The dependency for non-cross-linked clots was $G' \sim c^{1.5}$ while for cross-linked clots it was $G' \sim c^{2.3}$. The modulus of fine non-cross-linked clots was also found to vary as $G' \sim c^{1.5}$. Different concentration dependences of G' have been reported by many other studies: $G' \sim c^{1.67}$ (fibrin clots formed with 0 - 6mg/ml fibrinogen (33)), $G' \sim c^2$ (fibrin clots formed with 0.05 - 0.8mg/ml fibrinogen (48)), $G' \sim c^{2.1}$ (fibrin clots formed with 5 - 20 mg/ml fibrinogen (65)), $G' \sim c^{1.7}$ (plasma clots (65)), $G' \sim c$ (platelet free plasma clots (66)) and most recently $G' \sim c^{2.22}$ (fibrin clots formed with 0 - 40mg/ml fibrinogen (67)).

Mackintosh *et al*. developed a model for networks of semi-flexible biopolymers in which the elastic properties arise from chains that are very straight between entanglements and branches (68). A semi-flexible polymer is defined as having a persistence length, ℓ_p (distance along the polymer chain over which vectors drawn tangent to the chain become uncorrelated) equal to the contour length, ℓ_c (distance between branch points or filament length). The persistence length increases with increasing filament rigidity and decreases with increasing temperature. For a flexible polymer $\ell_c >> \ell_p$ and for a rigid polymer $\ell_p >> \ell_c$. Their model predicts the concentration dependence of the storage modulus for both entangled and branched networks. An entangled network is one which consists of filaments which can cross and

loop around one another forming transient branches. For an entangled solution the storage modulus scales with monomer concentration, c as:

$$G' \sim c^{2.2} \qquad 1\text{-}6$$

For densely cross-linked gels, i.e. a branched network, the storage modulus displays a stronger dependence upon the concentration:

$$G' \sim c^{2.5} \qquad 1\text{-}7$$

The majority of studies find concentration dependencies which fall below that predicted by this model. Discrepancies may arise due to the different systems and concentration ranges used. In addition, features and fundamental assumptions of the model may also account for any differences observed.

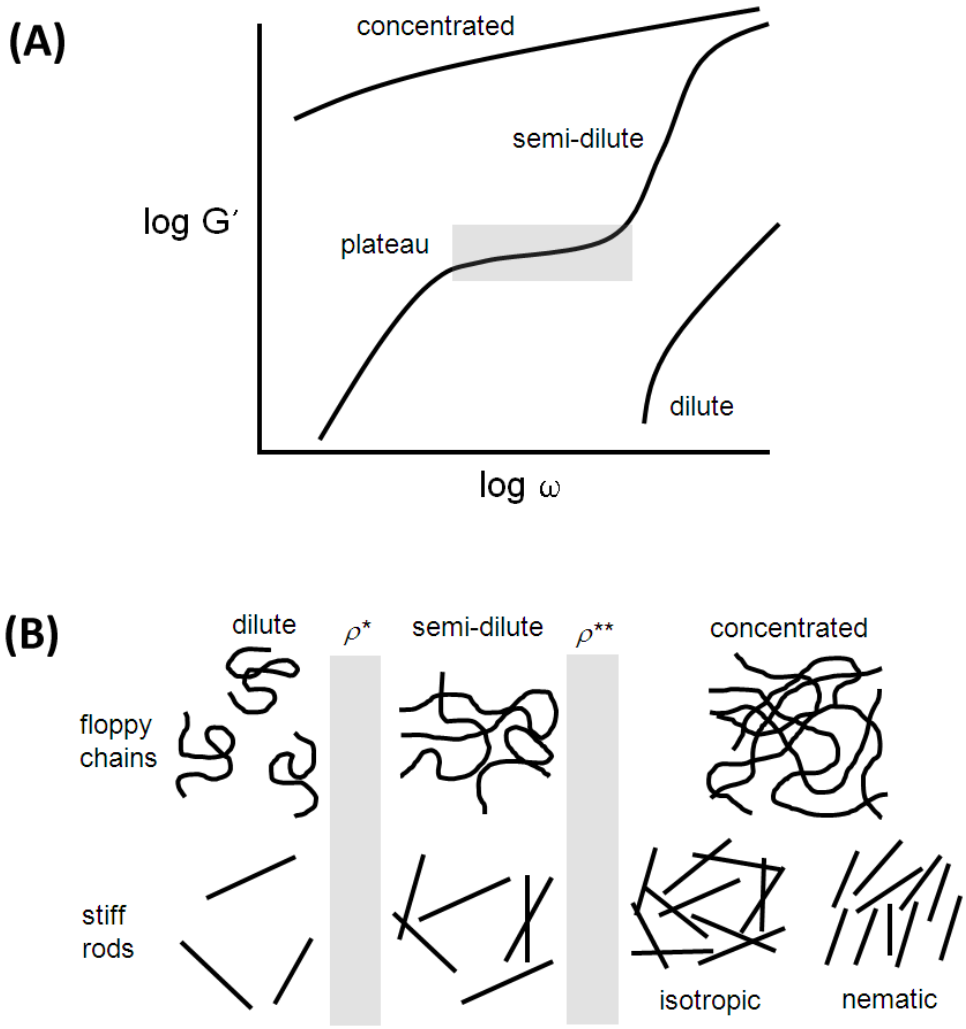

Figure 1-9: (A) Schematic representation of G′ versus ω for the three sample concentrations depicted in (B) (adapted from (69)). The three concentrations are dilute, semi-dilute and concentrated. Their generic behaviour as a function of chain density is shown in (B) where density increases from left to right. Note physical systems range between the examples shown here.

Figure 1-9 depicts the frequency behaviour of G′ for three different polymeric samples. For dilute solutions displaying fluid-like behaviour then G′ should fall with decreasing frequency. These materials display some of the smallest storage moduli, while concentrated polymer solutions have some of the highest storage moduli. Semi-dilute solutions range between these two examples. For long times (small frequencies) they display little resistance and behave like fluids. At short times (high frequencies) they begin to display

high resistance. In between these timescales, G′ displays varying behaviour associated with polymer entanglements (plateau region in Figure 1-9).

Boal *et al*. provides a qualitative explanation for the different shear relaxation modes which can occur on each distinct timescale (69). At short times only molecular rearrangements and transitions can occur. While at long times large scale motion of the polymer chains can occur. On intermediate timescales the polymer chains move on length scales characterised by distances between entanglement points. These are loops and knots which form between polymer chains as they move around one another. Here the polymer chains are behaving like a network of branched chains resulting in a frequency-independent shear resistance. This model describes the viscoelastic behaviour of flexible polymer solutions where chains cross and loop around one another but do not form a permanent branched network like fibrin.

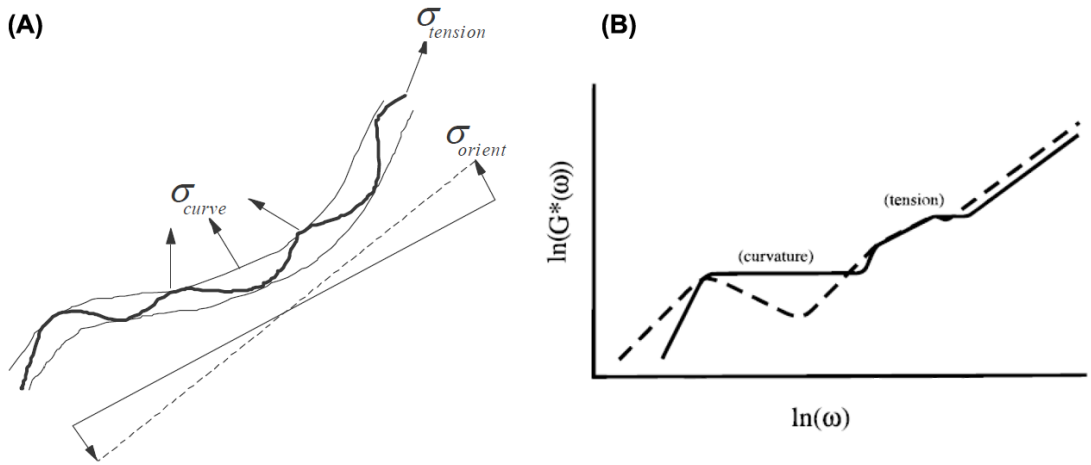

Figure 1-10: (A) Schematic representation of the different stress contributions (figure from (70)). (B) Schematic of G′(ω) (solid line) and G′′(ω) (dashed line) for a solution of coil-like chains (figure from (71)). Each plateau in G′ indicates frequency regimes where G*(ω) is dominated by either curvature or tension contributions. A low frequency orientation plateau is assumed to make a negligible contribution on all times for coil-like polymer solutions and is thus ignored.

A more complete mathematical treatment is provided by Morse's model (71-73) which describes the viscoelastic properties of semi-flexible polymer solutions between the rod-like ($\ell_p >> \ell_c$) and coil-like ($\ell_c >> \ell_p$) limits. Morse derives a general expression for the stress tensor for a solution of worm-like chains and identifies three stress contributions:

- σ_{tens}: a tension contribution arising from tangential forces that resist stretching or compression of the chain
- σ_{curve}: a curvature contribution arising from forces that oppose transverse deformation or rotation of chain segments
- σ_{orient}: an orientational contribution arising from forces that resist movement of the entire chain

These different stress contributions are depicted in Figure 1-10 A. The general expression of the stress tensor may be applied to any concentration regime and from this a prediction of the behaviour of $G^*(\omega)$ can be calculated (Figure 1-10B) for a whole host of parameters e.g. ℓ_p, ℓ_c and ℓ_e, the entanglement length (defined as the distance between polymer entanglements) (71). One such example, for a solution of coil-like chains in the tightly-entangled regime ($\ell_p >> \ell_e$), is given in Figure 1-10 B. This predicts the existence of a low-frequency, curvature dominated plateau and a higher-frequency, tension-dominated plateau. This behaviour corresponds with the qualitative description of Boal *et al*. (69) presented above and in addition, the high-frequency tension dominated plateau predicted by Morse's model is the same one as that predicted by Mackintosh *et al*. (68) (Equation 1-6).

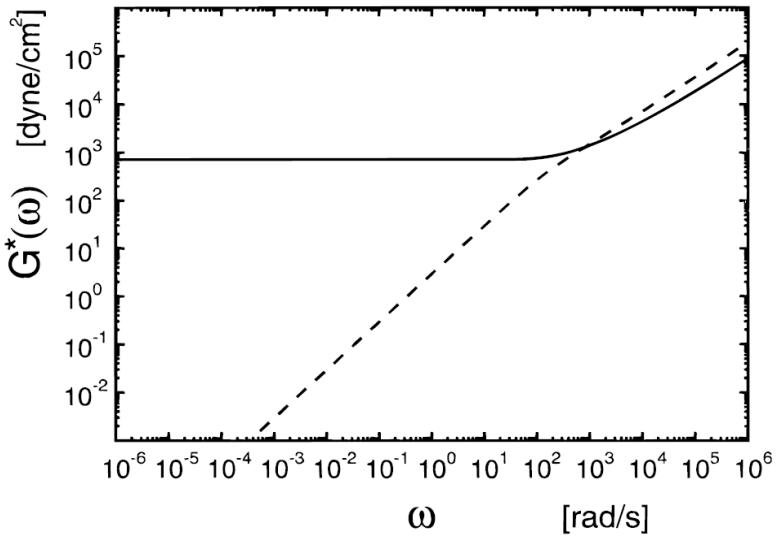

Figure 1-11: Values of G′(ω) (solid line) and G′′(ω) (dashed line) which is an approximation to the behaviour of a lightly branched gel (figure from (71)). The model parameters were chosen to be representative of a 1 mg/ml solution of F-actin. Note the plateau in G′ which extends to lower frequencies while G′′ diverges to lower and lower values.

Morse also looked at the effect of branching on the viscoelastic behaviour of a solution of worm-like chains. This model assumed relatively few free filament ends and that each filament was relatively straight between branches; a scenario not to dissimilar to the physical architecture of fibrin networks. The calculated behaviour of $G^*(\omega)$ is presented in Figure 1-11. The storage modulus is predicted to plateau while the loss modulus diverges becoming smaller and smaller. Thus, it appears that the effect of branching is to dramatically alter the stress relaxation behaviour at lower frequencies.

Ferry *et al*. went onto measure the effects of strain and clot age on creep and creep recovery (45). For old (6 hours+) coarse cross-linked clots it was found that compliance during creep is independent of strain magnitude indicating linear viscoelastic behaviour; after 10^3 seconds, recovery is more than 98% complete. Such recovery is attributed to the fact that the clot is fully formed before creep experiments begin; none of the network is formed under strain. For young (<4 hours) coarse cross-linked clots the compliance is smaller

indicating a stiffer clot and recovery is very different; differences are explained by the fact that the clot is formed under strain. This suggests clots subjected to stresses before they are fully formed can result in a much stiffer clot with altered elastic properties. This will have interesting implications for the interpretation of *in vitro* data where experiments are typically carried out under static flow conditions.

Next, Ferry *et al*. studied the behaviour of fine cross-linked and coarse non-cross-linked clots (41). It was found that fine clots subjected to small strains obey Hooke's law and display no inelastic behaviour. The dependence of the storage modulus on fibrin concentration for fine cross-linked and coarse non-cross-linked clots was $G' \sim c^{1.5}$. The dependence of G' for fine cross-linked clots is very close to that reported previously for fine non-cross-linked clots (45). This is attributed to the fact that cross-linking may not have been completely absent from their earlier work. It was found in both fine and coarse clots that creep is largely suppressed by cross-linking and this involves only the γ-chains as indicated by gel electrophoresis.

The work of Mockros *et al*. looked at the viscoelastic properties of cross-link inhibited clots using a cone-plate rheometer (46). It was found that cross-linking increased clot stiffness in both plasma and purified clots. The introduction of inhibitors produced a substantial reduction in clot stiffness; at high enough inhibitor concentration clot stiffness approached that of non-cross-linked clots. A dependence of the storage modulus and loss tangent upon total ionic strength, μ was found, with a peak stiffness and minimum dissipation at $\mu = 0.17$..

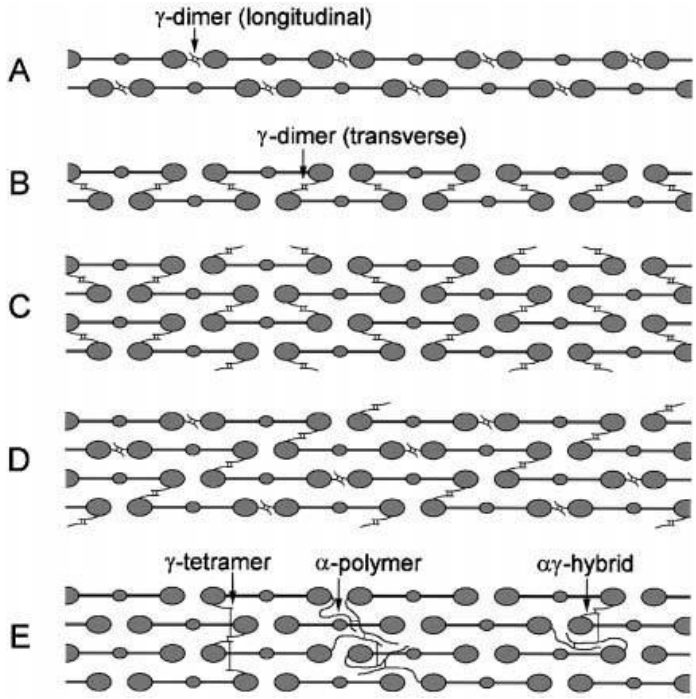

Figure 1-12: Schematic model of the possible orientations of cross-links in fibrin protofibrils (figure from (54)). A: longitudinal orientation of γ-chain cross-links. **B:** Transverse cross-links of γ-dimers. In this diagram, transverse crosslinks occur only between molecules within the same double-stranded protofibril. **C:** transverse dimeric cross-links of γ-chains between adjacent protofibrils. **D:** longitudinal and transverse cross-links of γ-chains between adjacent protofibrils. The patterns of cross-links shown in **C** and **D** are only two of many that may potentially be formed between protofibrils arranged within a three-dimensional fibre. **E:** possible orientation of γ-tetramers, α-polymers and αγ-hybrid polymers between two adjacent protofibrils.

Other related work at the time of that being carried out by Ferry *et al*. were studies into the effects of calcium ion and cross-linking upon fibrin structure and elasticity by Shen *et al*. (47). It was found that the presence of calcium results in the development of a clot with a much higher elastic modulus. By measuring the development of cross-linking activated by FXIIIa, it was found that cross-linking of the α-chains results in an increase in the elastic modulus while cross-linking of the γ-chains does not, contrary to previous work by Ferry *et al*. (41).

More recently Ryan *et al*. studied the effects of natural and synthetic inhibitors of FXIIIa in order to determine which cross-linking species are responsible for augmenting clot stiffness (54). Cross-linking was controlled using two inhibitors, cross-linked chains were identified by SDS-PAGE analysis and clot stiffness was measured using a cone-plate rheometer. The formation of γ-dimers, γ-multimers, α-polymers and αγ-hybrids (Figure 1-12) were all detected. It was found that FXIIIa-induced dimeric cross-linking of the γ-chains alone is not sufficient to stiffen the fibrin network but that clot stiffness was more strongly correlated with the formation of γ-multimers, α-polymers, and αγ-hybrids.

Collet *et al*. used a fibrinogen with a truncated α-chain in order to study cross-linking (74). They also report a lower effect of γ-chain cross-linking on clot stiffness. A study by Standeven *et al*. (75) investigated FXIIIa cross-linking using recombinant fibrinogens with modified FXIII cross-linking sites on the γ-chain. In this study, γ-chain cross-linking contributed significantly to clot stiffness through the formation of γ-dimers while αγ-hybrids had the smallest effect on clot stiffness. In addition, no differences in clot morphology, polymerisation and fibrinolysis rate were reported for the recombinant cross-linking variant. The apparent discrepancy between these observations and that of previous authors may be attributed to the interference of antibodies and inhibitors along with the removal of substantial parts of the fibrinogen molecule as in the studies of Ryan *et al*. (54) whilst in the study of Standeven *et al*. (75) cross-linking was controlled by specific, small mutations in the cross-linking sites.

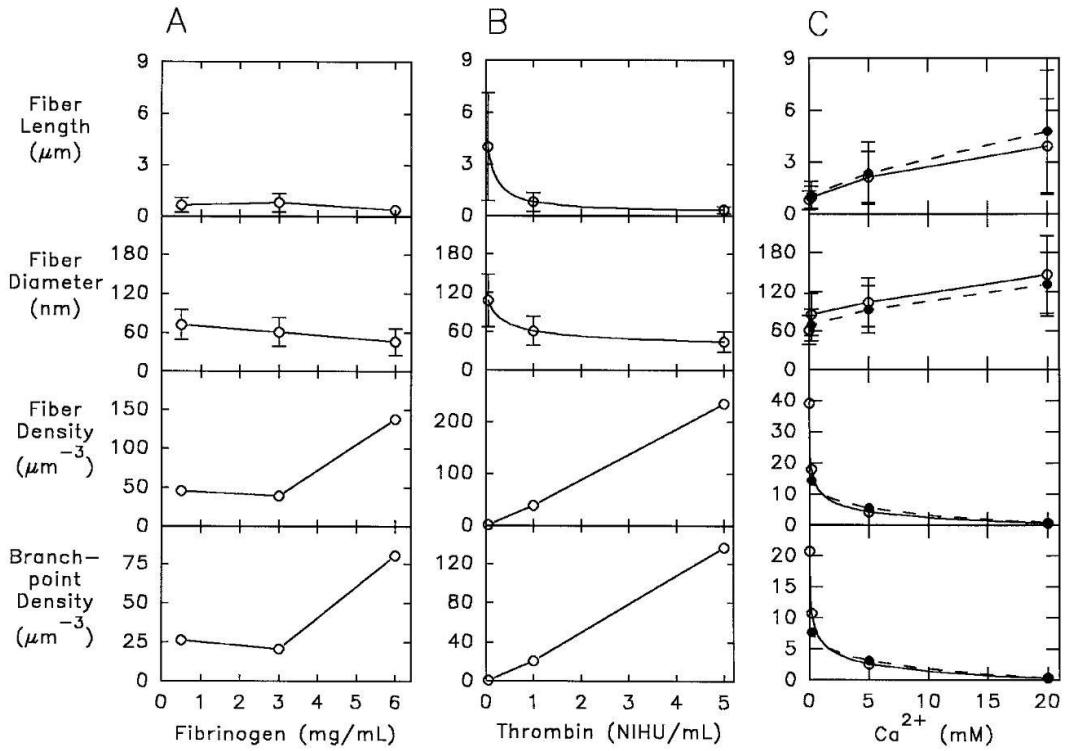

Figure 1-13: Quantitative data of fibrin network architecture as a function of fibrinogen, thrombin and $CaCl_2$ concentration (figure from (33)). A: effects of fibrinogen concentration on non-cross-linked fibrin networks. **B:** effects of thrombin concentration on non-cross-linked fibrin networks. **C:** Effects of calcium concentration on fibrin networks. Clots were formed with either 0 mM (solid symbols) or 1 mM (open symbols) FXIIIa inhibitor.

In order to understand the role of clot structure in modulating clot viscoelasticity Ryan *et al*. carried out detailed structural analysis upon a variety of clot architectures and correlated this with viscoelastic measurements (33). Network architecture was manipulated by varying fibrinogen, thrombin and $CaCl_2$ concentrations. Quantitative measurements of clot architecture (Figure 1-13) were made by analysing computerised three-dimensional models which were constructed from stereo pairs of scanning electron micrographs (76).

Large fibre diameters and lengths were established only when branching was minimal. Increases in fibre length were generally associated with increases in fibre diameter. Viscoelastic properties of clots were measured

with a cone-plate rheometer and correlated with structural features of the networks. Clot stiffness increased with increasing fibrinogen concentration. This was attributed to increased fibre and branch point density as fibre length and diameters were relatively insensitive to fibrinogen concentration. At constant fibrinogen but varying thrombin and calcium concentrations, maximal rigidities were established in samples (both cross-linked and non-cross-linked) which displayed a balance between large fibre sizes and a high degree of branching. Clot stiffness decreases with increasing thrombin (after 0.5U/ml concentration) and calcium concentration (after 1.5 mM). The effect of FXIIIa upon network structure was minimal, with a slight increase in fibre length and decrease in fibre diameter being observed. This suggests increased clot rigidity most likely arises from the stiffening of the individual fibres as opposed to structural alterations at the network level.

Another aspect of fibrin clot viscoelasticity is the phenomenon of strain-hardening. At low strains stress is directly proportional to strain (Hooke's law) and the elastic modulus is constant (41). At larger strains the elastic modulus begins to increase and a clot becomes stiffer, increasing by up to a factor of 20 (51). Strain-hardening is also apparent in clots with and without cross-linking. Roberts *et al.* (62) observed a non-linear stress-strain response in cross-linked and non-cross-linked fibrin clots at strains above 10% (Figure 1-7). The work of Shah *et al.* (77) showed that the addition of platelets to both human plasma and fibrin clots increases clot stiffness and eliminates strain-hardening.

The molecular origin of strain-hardening in fibrin clots is currently unknown. The theory of Doi *et al.* proposes that the elasticity of gels consisting of stiff rod-like polymer chains arises from the elastic deformation of the chains which are forced to bend under strain (78). Janmey *et al.* used this theory to interpret strain-hardening as arising from the increased number of contacts between fibres at large deformations (79). Within this framework an increase in elastic modulus is due to an increase in the number of elastically active network junctions. This interpretation accounts for the increase in stiffness at

moderate strains, however fails at larger strains. The effect of platelets which eliminates strain-hardening as observed by Shah *et al*. is explained by the platelets applying tension to the fibres and pulling out the slack which increases fibre stiffness as opposed to increasing the number of elastically active junctions (77).

Storm *et al*. report a theory that accounts for strain-hardening in a range of semi-flexible polymer networks at low to intermediate strain (80). The model links the theoretical force-extension behaviour of single fibres, based upon a worm-like chain (WLC) model, to the bulk modulus of the network. They predict that strain-hardening is intrinsic to all similar filamentous networks and they stiffen at low strains without requiring multiple elements of different intrinsic stiffness. That is, strain-hardening arises due to the entropic response of the individual fibres which then contributes to the overall macroscopic response.

A review by Weisel proposed that if the bending of fibres gives rise to clot elasticity then the stretching of fibres could play an important role at larger strains and account for strain-hardening behaviour (13). Very recently work into the multiscale mechanics of fibrin clots has begun to shed light on the mechanisms responsible for strain hardening. Brown *et al.* (81) report that fibrin fibres orient themselves and stretch along the direction of the applied strain. At low strains fibres can stretch as the constituent protofibrils straighten and untwist within the fibre. Next, they propose molecular unfolding occurs and this could be responsible for the linear strain response up to higher strains. However, once the coiled coils, or some other compact structures in fibrin such as the D-region, have completely unfolded this leads to strain-hardening. To test this mechanism they modelled the stress-strain behaviour using the model of Storm *et al*. (80) and find that protein unfolding is required to fit the model to the experimental data.

Hudson *et al*. report an interesting consequence of strain-hardening on the mechanical behaviour of fibrin clots (82). Using a combined

fluorescence/AFM nanomanipulation system they stretched 2D fibrin networks suspended over channels. They find that fibre strain-hardening distributes strain more evenly throughout the network i.e. once a fibre begins strain-hardening it pulls on any adjoining fibres transferring strain to them. This reduces the strain maxima and increases network strength. They find the behaviour observed in their experiments doesn't fit easily with the model of Storm *et al*. (80) but suggest that accounting for protein unfolding could resolve inconsistencies.

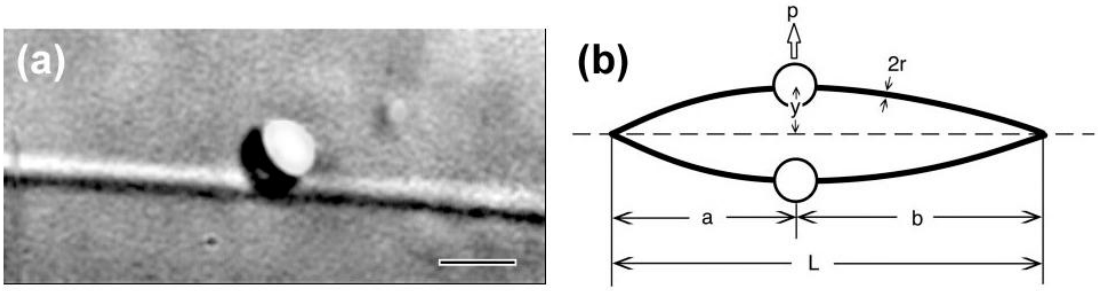

Figure 1-14: (a): an individual fibrin fibre with a polystyrene bead attached (figure from (83)). A force is exerted on a bead using optical tweezers in order to either stretch or bend a fibre (scale bar = 1μm). **(b):** schematic diagram of a fibre bending showing the measured parameters used for the calculation of the elastic modulus.

Work by Collet *et al*. measured the properties of individual fibres in clots with and without cross-linking (83). They used optical tweezers to either bend or stretch individual fibres (Figure 1-14). The elastic moduli measured for individual fibres in plasma clots was 1.7 and 14.5 MPa for non-cross-linked and cross-linked fibres respectively. This agrees with the earlier work of Ryan *et al*. (84) who suggested that FXIIIa cross-linking increases clot stiffness via the stiffening of individual fibres. It is also reported that fibres were much stiffer for stretching than for bending, as expected from their diameter to length ratio. The elastic moduli of non-cross-linked fibres was 1.7 MPa for bending and 1.9 MPa for stretching and for cross-linked clots was 14.5 MPa for bending and 11.5 MPa for stretching. This suggests cross-linking makes a fibre more flexible for stretching. In addition, this work

supports Weisel's theory that fibre stretching plays a role in the strain-hardening response of fibrin clots.

Measurements on single fibres have also been carried out by Guthold *et al*. using the Atomic Force Microscope (AFM) (26, 85, 86). They have developed a technique to image and mechanically manipulate individual fibrin fibres. The first of these studies (26) used the AFM to image then stretch individual fibrin fibres upon mica surfaces. Fibres were stretched until they snapped and the rupture force was determined as a function of fibre diameter.

Rupture force increased with increasing diameter as $F_R \sim d^{1.30\pm0.06}$. It was also observed that the light intensity (number of molecules per cross-section) of single fibres as a function of their diameter increased as $I \sim d^{1.25\pm0.11}$. This suggests that fibrin fibres are fractals where the number of molecules per cross-section increases as $d^{1.3}$, which implies that the molecular density varies as $\rho(d) \sim d^{-0.7}$. That is, thinner fibres are denser than thicker fibres; this points towards the idea that fibrin fibres are extremely porous. Considering the average concentration of fibrinogen in the blood is around 2.5 mg/ml, a clot made from fibrinogen at this concentration is only 0.25 g out of 100 ml of volume, meaning fibrin constitutes ~0.25% of the total clot volume (63). The remaining 99.75% of the clot consists of liquid which occupies the space between protofibrils in the fibres and the much larger spaces between the fibres (pores).

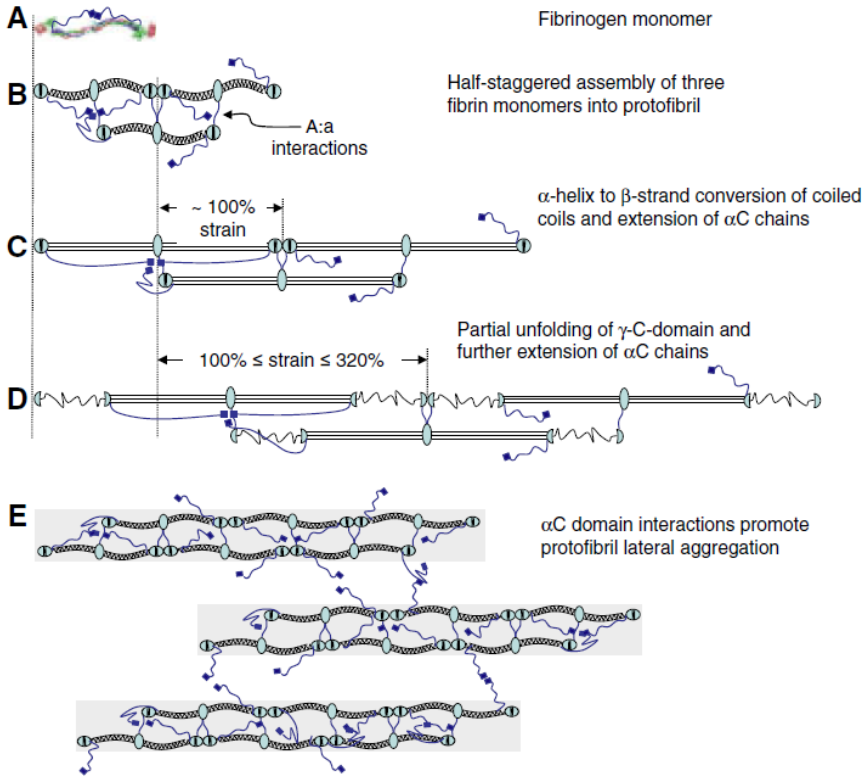

Figure 1-15: Model for fibre extension (figure from (86)). A: crystal structure of fibrinogen. A cartoon depiction of the αC domain is added to the crystal structure as a blue line with a blue square; αC domains can interact with one another within a protofibril and between protofibrils. **B:** schematic model of half-staggered assembly of three fibrin monomers into a protofibril. **C:** α-helix to β-strand conversion of the coiled coil and a straightening and alignment of the molecules could account for ~100% strain. **D:** strains up to 320% could be accommodated by a partial unfolding of the globular γ-nodule; 230% strain is depicted. Further extension of the αC domains could occur **E:** αC domains promote lateral aggregation of protofibrils; they can be elastically extended.

Later studies (85, 86) built on the previous work by using the AFM to manipulate single fibres suspended over 12 µm wide channels. They report that cross-linking renders fibres less extensible, stiffer and less elastic than non-cross-linked fibres. In order to explain their findings they propose a molecular model for the stretching of fibrin fibres (Figure 1-15). They also propose a longitudinal, as opposed to transverse, orientation for γ-γ cross-links (Figure 1-12).

In addition, Guthold *et al*. used the AFM to investigate the mechanical properties of branch points (34). In this instance they suspended branched fibres over channels and stretched them until they ruptured. They find that non-cross-linked and cross-linked branches show different rupture behaviour. Non-cross-linked branches ruptured 68.5% of the time at the branch and 31.5% of the time along the fibre. In contrast, cross-linked branches ruptured 39.5% of the time at the branch and 60.5% along the fibre. This suggests cross-linked branches are stronger than cross-linked fibres, while the opposite is true for non-cross-linked fibres. This could be explained by the lower extensibility of cross-linked fibres.

There has been much debate over the longitudinal versus transverse orientation of γ-γ cross-links within the literature (87, 88). Mosesson (7) proposes that γ-chain cross-links are orientated transversally between molecules of different fibrin strands (Figure 1-16). Cross-linking is represented in this way in order to explain the important viscoelastic response of fibrin, that after a maximum stretch of 1.8-times, cross-linked fibrin is able to recover its original form (89), while non-cross-linked fibrin cannot (90). The precise location of cross-linked -chains has been debated for many years but as yet has not been agreed upon.

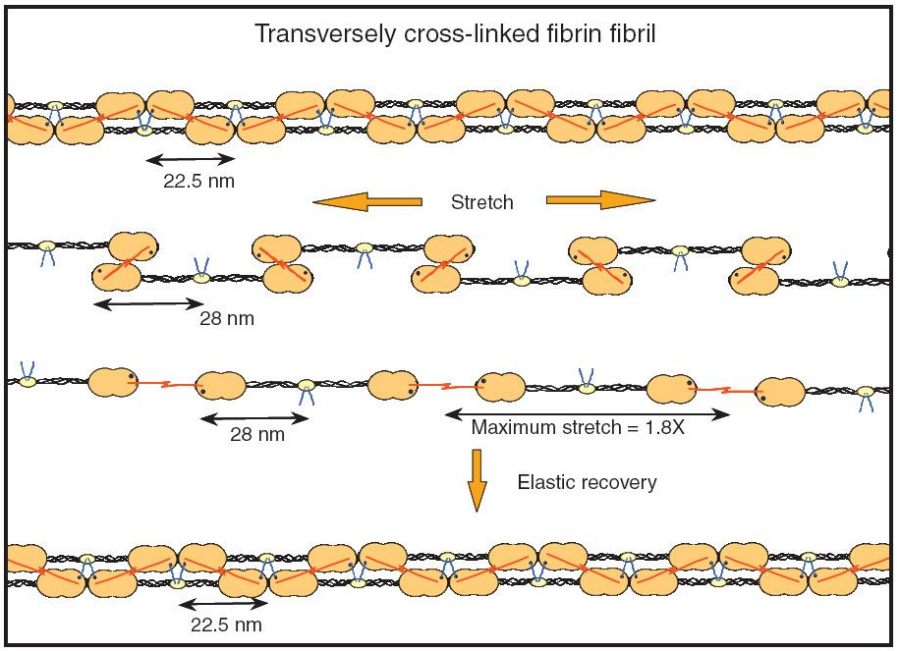

Figure 1-16: Schematic diagram of a transversely cross-linked fibrin fibril being stretched and relaxed (figure from (7)). When a double-stranded fibril is maximally stretched 1.8 times it becomes single-stranded, and the individual fibrin molecules remain connected to one another through covalently cross-linked γ-chains. Upon relaxation, the fibril recovers its original form. It is suggested by Mosesson that only cross-linked γ-chains positioned transversely between fibril strands can account for this behaviour.

The work of Collet *et al*. (83) suggested the origin of clot elasticity arises from the bending of fibres; however no indication as to the underlying molecular basis of clot elasticity was presented. Recently, two independent studies (91, 92) have attempted to elucidate the molecular origin of clot elasticity by suggesting that the coiled-coils of fibrinogen are responsible. Both studies used the AFM to mechanically unfold fibrinogen molecules (Figure 1-17). In the first of these studies by Brown *et al*. (91), forced unfolding was performed upon engineered linear oligomers of fibrinogen; multiple fibrinogen molecules joined end-to-end. It was found that the force extension curves of these oligomers produced saw tooth patterns with a peak-to-peak length consistent with the independent unfolding of the coiled-coils. This work suggests that the coiled-coil of fibrinogen is more than just a passive structural element and that their unfolding could account for the large extensibilities recently

observed in fibrin fibres (86). This also demonstrates the biological function of protein unfolding (94).

The second of these studies by Lim *et al*. (92) used the AFM to probe the mechanical properties of single fibrinogen molecules and fibrin protofibrils. They found that the mechanical unfolding of fibrinogen's coiled-coil domains is characterised by a distinctive intermediate force plateau in the systems' force-extension curve. This force plateau is related not only to the unfolding of fibrinogen's coiled coils but also of its central E domain. This highlights the complex nature of the unfolding events within fibrinogen.

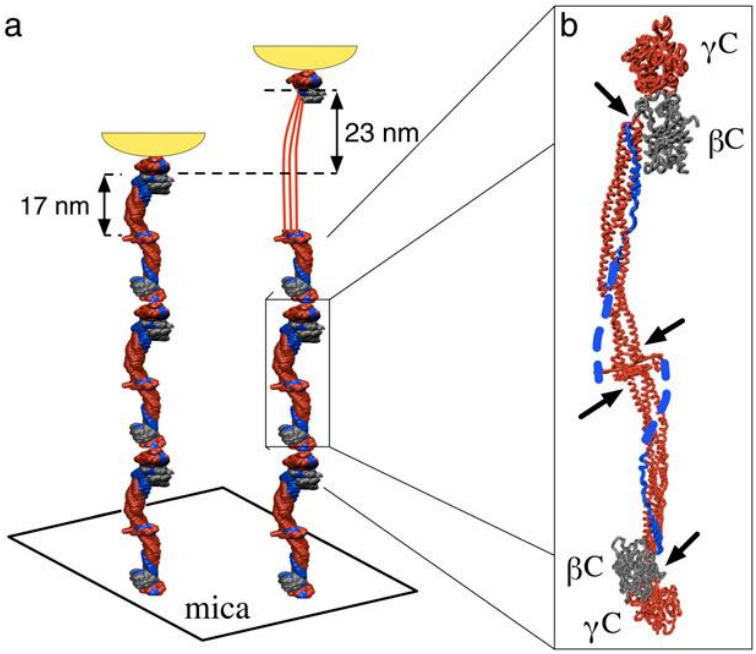

Figure 1-17: Schematic of the experimental pulling geometry of fibrinogen molecules using the AFM (figure from (91)). Fibrinogen oligomers adsorbed on mica were extended by the AFM tip shown in yellow. When a single coiled-coil is unfolded the oligomer contour length increases by 23 nm.

The C-terminal region of the Aα-chain forms the fourth strand of the quadruple-helical portion of the coiled-coil (Figure 1-2 A) and is known to interact with the central region through the αC-domain (93). It has been suggested by Brown *et al*. (91) that this structural feature may reduce

refolding and contribute to the mechanical stability of fibrinogen. Lim *et al*. (92) observed sequential unfolding of coiled coils in a protofibril as opposed to simultaneous unfolding of all coiled coils and attributed this behaviour to the fourth helical strand located at the C terminus of each set of coiled-coils. Again, it is suggested that interactions occurring here may restrict the unfolding of fibrinogen and help to buffer forces between connected fibrinogen molecules. However, it is difficult to speculate exactly what is occurring due to the unique architecture of this region. Improved simulations on more appropriate timescales to identify which domains of fibrinogen are stable along with the use of recombinant fibrinogens lacking the αC-domain will help to underpin these questions.

1.4 Thesis Aims

The main aim of this project was to develop an experimental method to study the viscoelastic behaviour of fibrin clots. This thesis will seek to describe the viscoelastic properties of fibrin clots studied using this technique. Throughout this work the effects of fibrinogen, along with many other blood proteins involved in coagulation, will be studied in order to better understand their role within fibrin clot viscoelasticity. In addition, studying clot polymerisation and structure through various complimentary techniques will provide a better understanding of the role of viscoelasticity in clot structure and function. The specific aims of this work are listed in detail here:

- Develop an experimental technique to measure the frequency dependent viscoelastic moduli of fibrin clots using a magnetic microrheometer.
- Using this technique, study the viscoelastic properties of fibrin clots and compare these measurements with current theories on the behaviour of viscoelastic networks. In particular, determine the effects of FXIII on clot viscoelasticity which has been widely reported upon in

the literature. Such measurements will serve as a good validation to the experimental technique developed in this work.

- Study the effects of fibrinogen, thrombin and $CaCl_2$ concentration on fibrin clot viscoelasticity, all of which are known to modulate fibrin clot structure. In this way it will be possible to correlate variations in clot structure with changes in clot viscoelasticity. The role of these reactants in modulating clot viscoelasticity is still not fully understood.
- In addition, study the effects of the fibrinogen γ chain splice variant γ' on fibrin clot physical properties and determine the molecular mechanism underpinning the variations observed. Currently, there is much debate on the effects of fibrinogen γ' in clot structure and function along with its role in cardiovascular disease.
- Finally, study the effects of the plasma proteins FVII, FIX, FXII and FXIII on polymerisation, structure and viscoelasticity of plasma clots. This will lead to a better understanding of how the coagulation cascade modulates the viscoelastic properties of clots.

Chapter 2

2 Materials and Methods

This chapter outlines all the biological materials and reagents used throughout this work. An introduction to standard experimental techniques and sample preparation are also provided. The techniques and preparations described here will be utilised throughout the remainder of this work, when procedures and preparations differ, changes will be explicitly stated.

2.1 Materials

The main constituents used to assemble fibrin clots are thrombin and fibrinogen. Thrombin (human alpha-thrombin, American Diagnostica, CT, US) was diluted in distilled water (dH_2O) to a final concentration of 250 NIHU/ml (NIHU is a National Institiue of Health standard Unit). The concentration of thrombin is measured in active units where 1 NIHU/ml = 9.16 nM (94). Thrombin loses activity rapidly at room temperature so after dilution it was immediately

aliquoted (on ice) and stored at -80ºC. Before use, thrombin was defrosted, diluted in TBS buffer (50 mM Tris, 150 mM NaCl, pH 7.4) to the required concentration and then used immediately. Clotting was also performed using Reptilase (Diagnostica Stago, Asnières sur Seine, France), a snake venom which cleaves FpA only. This was diluted in dH_2O to 20 BU/ml and stored at -80ºC.

For the majority of experiments standard commercially available human fibrinogen (Plasminogen, von Willebrand Factor and Fibronectin depleted, Enzyme Research Laboratories (ERL), Swansea, UK) was used. This fibrinogen is purified from frozen plasma and received in lyophilised form. It was prepared by reconstituting in TBS buffer heated to 37ºC; upon reconstitution the solution was diluted in TBS buffer to a stock concentration of 2 mg/ml and then aliquoted and stored at -80ºC. Fibrinogen concentration is determined by absorbance at 280 nm using an extinction coefficient of 1.51 (95) with a Nanodrop Spectrophotometer (Labtech International, UK).

γA/γA and γA/γ′ fibrinogens were purified from human plasminogen-depleted fibrinogen (ERL) as described previously (96) using anion exchange chromatography. This work was carried out by Dr Shirley Uitte de Willige (Division of Cardiovascular and Diabetes research, Section on Mechanisms of Thrombosis, Faculty of Medicine and Health, University of Leeds, Leeds, UK).

Fluorescently labelled fibrinogen (fibrinogen from human plasma, Alexa Fluor® 488, Paisley, UK) was used for confocal microscopy imaging. It was prepared by dissolution in dH_2O to a concentration of 2.0 mg/ml and then aliquoted and stored at -80ºC until use.

All deficient human plasmas (FVII-DP, FIX-DP, FXII-DP and FXIII-DP) were obtained from ERL. The plasma was thawed by heating to 37ºC in a waterbath for 5 minutes, aliquoted and then flash-frozen in liquid nitrogen and stored at -80ºC until use. Human plasma proteins (FVIIa, FIXa, FXIIa and FXIII) were also obtained from ERL. The lyophilised proteins were dissolved in dH_2O to a

concentration of 50 µg/ml (FVIIa), 1.29 mg/ml (FIXa), 400 µg/ml (FXIIa) and 110 µg/ml (FXIII); they were then aliquoted and stored at -80ºC until use.

Cross-linking of fibrin by FXIIIa was controlled with the synthetic inhibitor 1, 3, 4, 5-tetramethyl-2[(2-oxopropy-1)thio]imidazolium chloride (L682777, ZEDIRA GmbH, Darmstadt, Germany), which was dissolved in DMSO and further diluted in dH_2O to a concentration of 40 mM and stored at -20ºC until use. This inhibitor is highly specific for the active site of the FXIII A-subunit (97).

2.2 Methods

2.2.1 SDS-Polyacrylamide Gel Electrophoresis

SDS-PAGE (sodium dodecyl sulfate polyacrylamide gel electrophoresis) is a technique which separates proteins according to their molecular weight. Proteins are mixed with an SDS detergent which denatures secondary and tertiary structure and applies a negative charge to the protein in proportion to its mass, i.e. the larger the protein the greater the charge. Next, the protein is heated to near boiling point in reducing sample buffer which further denatures the protein's structure; breaking up tertiary protein folding and quaternary structure. These denatured proteins are then applied to one end of a polyacrylamide gel which is submerged in buffer and an electric field is applied across the gel for a set amount of time. The negatively charged proteins migrate through the gel, each protein migrates at a different rate depending upon its size (charge), resulting in a separation of protein by molecular weight. After this, a gel is stained in order to image the separated proteins. A molecular marker of known molecular weight is run in a separate lane on the gel to identify different proteins chains.

SDS-PAGE was used to separate fibrinogen polypeptide chains and FXIII cross-linked chains according to their molecular weight. Fibrinogen samples were prepared in 5 µl of blue NuPAGE loading dye (Invitrogen, Paisley, UK) and 2.5 µl of reducing sample buffer and then heated to 95ºC for 10mins with a hot

plate. For cross-linking reactions, fibrinogen (final concentration 0.5 mg/ml), $CaCl_2$ (2.5 mM) and either inhibitor (1 mM) for no cross-linking or FXIII (3.7 µg/ml) for cross-linking were diluted in TBS buffer, and pre-mixed in 0.5-ml Eppendorf tubes. Thrombin (1.0 U/ml) was then added to initiate clotting, which was allowed to proceed for 0, 1, 2, 5, 15, 30, 60, 120 and 360 minutes at room temperature. The clotting reaction was stopped by the addition of loading dye and reducing sample buffer and then heating. For the 0 minute time point reactions loading dye and reducing sample buffer were added prior to thrombin injection and heating proceeded immediately after.

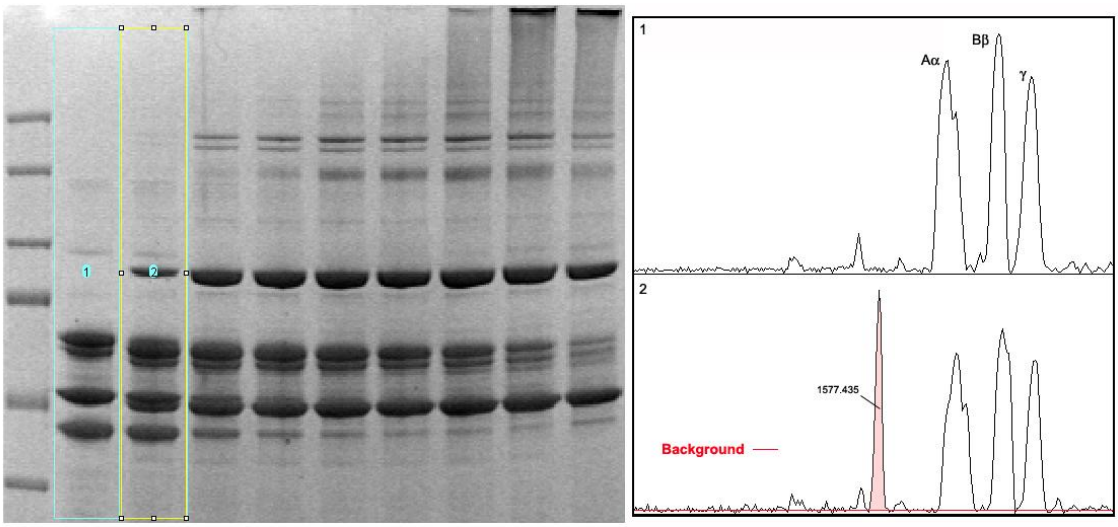

Figure 2-1: SDS-PAGE gel analysis. Left: ImageJ screenshot of a cross-linking gel showing the software selection of 2 lanes. **Right**: software plots of the two lanes; each peak corresponds to a polypeptide chain band on the gel. The background level of a lane is set by the red line. Here the contrast intensity of a band relating to the γ dimer cross-linking product has been measured.

Samples were then either frozen at -80ºC or immediately loaded onto a gel. 20 µl of sample were loaded into each well of a 4 - 12% Bis-Tris gradient gel (Invitrogen, Paisley, UK) and electrophoresis was carried out using a NuPAGE unit (Invitrogen, Paisley, UK). 200V was applied across the gel for 90 mins in MOPS running buffer (Invitrogen, Paisley, UK). After this time, the gel was removed and washed in dH_2O (3 times for 5 minutes each on a shaker at room temperature) and then stained with Gelcode blue protein stain (Pierce,

Rockford, IL, USA) for 1 hour. Gels were then de-stained with dH_2O on a shaker at room temperature overnight. Finally, the gel was photographed digitally using an Alpha Innotech (San Leandro, CA, USA) gel-documentation system.

All digital images of gels were analysed using the software ImageJ (National Institute of Health, Bethesda, MD, USA). This program has a feature which enables the bands of a gel to be quantified. In brief, each lane was selected with a rectangular region which encapsulates the polypeptide chain bands; from this a plot is produced (see Figure 2-1). This plot is a 2D representation of the 3D rectangular region where the x axis represents the molecular weight and the y axis is the contrast intensity of the gel. The background intensity was then set by drawing a line along the plot which defines the background level. Finally, the area under a peak can be measured giving the intensity of that polypeptide band. Each band is normalised to the Bβ chain band (which is not subject to cross-linking by FXIIIa) of that same lane. This allows quantitative information to be extracted from a gel, e.g. the relative amount of cross-linking and kinetics.

2.2.2 Turbidity

Turbidity is a technique which measures the level of cloudiness of a fluid i.e. measures the amount of suspended matter. Light is passed through a solution and scattered by any intervening matter, a detector measures the amount of transmitted light and therefore the relative amount of matter present.

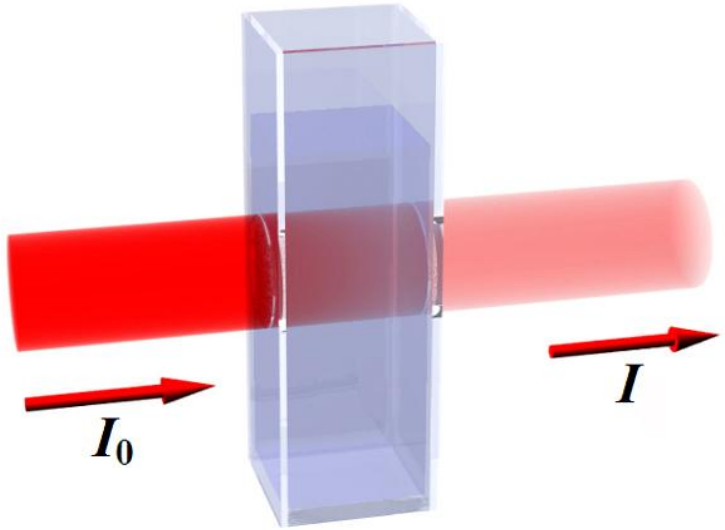

Figure 2-2: Schematic diagram representing an experimental turbidity setup (adapted from (98)). The intensities of the incident light (I_0) and transmitted light (I) are used to determine the absorbance (A_λ) of the intervening solution via Equation 2-1.

Turbidity can be expressed as the absorbance A_λ (also termed the optical density) by measuring the intensity of the incident light (I_0) and the intensity of the transmitted light (I) through a solution (see Figure 2-2) and using the following equation:

$$A_\lambda = \log\left(\frac{I_0}{I}\right) \qquad 2\text{-}1$$

Turbidity is a common technique used to measure the time development of fibrin polymerisation. The absorbance typically displays an initial lag phase followed by a rapid increase which then reachs a plateau (see Figure 2-3). The lag phase corresponds to the formation of protofibrils from fibrin monomer after fibrinopeptide cleavage. The rapid rise in optical density results from lateral aggregation of protofibrils that have reached a minimum length. The final value of turbidity, at the plateau, is directly related to the average size of the fibres or fibre bundles (30). It has been shown that turbidity is directly proportional to the average cross-sectional area of fibres (64), with a high level of absorbance indicating larger fibre diameters.

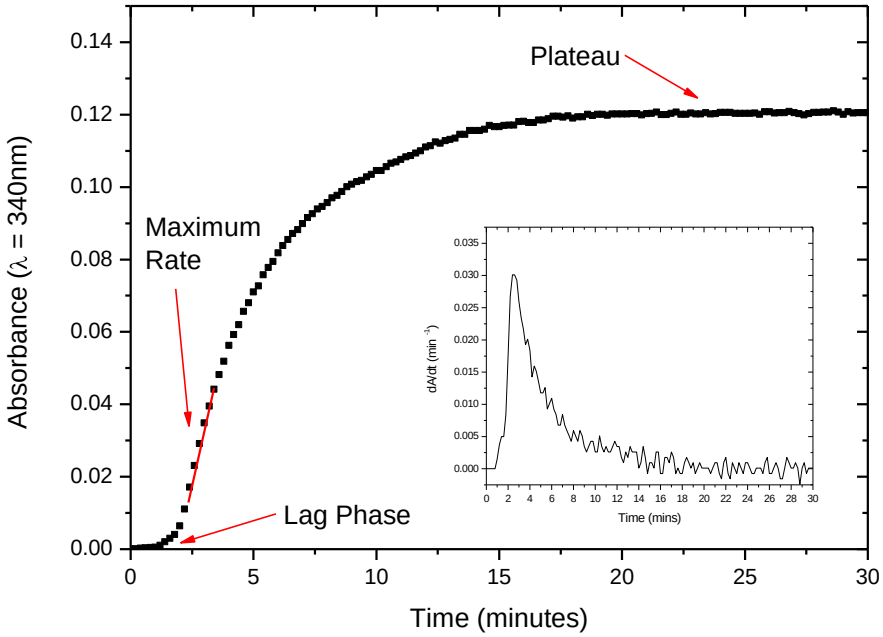

Figure 2-3: Turbidity curve of a fibrin clot during the first 30mins of polymerisation. Insert: the first derivative of the absorbance (dA/dt) as a function of time.

In addition to fibrin polymerisation, turbidity can also be used to monitor fibrin clot lysis (fibrinolysis). Again, the absorbance displays a rapid increase as the network forms and fibres grow. However, instead of a plateau in the absorbance there is a peak after which the absorbance begins to decrease as the network is broken down by plasmin generated from plasminogen by tissue plasminogen activator (tPA), added to the activation mixture at the start of the experiment.

All turbidity experiments were performed in 96-well plates using a BioTek ELX808 micro plate reader supplied by Labtech International (Ringmer, UK). Typically, in a single well 90 µl of fibrinogen (final concentration 0.5 mg/ml), $CaCl_2$ (2.5 – 7.5 mM), TBS buffer and any other reagents (e.g. FXIII (3.7 µg/ml)) were premixed, after which 10 µl of thrombin (0.5 – 1.0 U/ml) was added to initiate coagulation. For lysis experiments the fibrinogen was incubated with plasminogen (0.3 µM) and the thrombin (1.0 U/ml) with tPA (1 nM). Upon the addition of the thrombin-tPA mixture clotting and lysis proceed simultaneously. Immediately after the addition of thrombin the plate was transferred to the reader and measurements were taken at regular intervals e.g. every 12s for 1

hour (unless otherwise stated), at a wavelength of 340 nm at room temperature (unless otherwise stated). Generally, each clot was prepared in triplicate.

Data analysis was performed using the software OriginPro 8 (OriginLab, MA, USA). In order to compare the kinetics and structure of different fibrin clots 4 parameters were extracted: the lag time, maximum rate, final absorbance and plateau time. The lag time is measured as the time elapsed until an increase in absorbance is observed (99). The maximum rate is defined as the maximum rate of change in the absorbance. The final absorbance is taken once the curve has reached a plateau and no further increases in absorbance are observed. And the plateau time is the time taken to reach the final absorbance. For lysis experiments, the lysis time is also determined and defined as the time taken for the maximum absorbance to reduce by half.

The first time derivative of the absorbance (dA/dt) was calculated and plotted to assist in determining these quantities (see Figure 2-3 insert). This plot shows the rate of change of absorbance with time. Over the first minute of clotting dA/dt = 0 indicating no change in the absorbance; this defines the lag time. The curve rapidly increases, then peaks and begins to decrease; the peak in dA/dt is the maximum rate. The lag time and maximum rate give kinetic information on the rate of protofibril and fibre formation respectively. The final absorbance gives information on the average fibre diameter while the plateau time gives a measure of time taken for the entire network to form.

2.2.3 Measurement of Clotting Time

The clotting time, or gel point as it is referred to in polymer chemistry, is the point at which a substance turns from liquid to solid. Within a clot this is the time at which a minimum number of fibrils interconnect and span a length scale of the clot such that the clot becomes a gel (100). The gel point can be detected manually or automatically. Manual inspection typically involves forming a clot in a tube which is then tilted periodically until clot formation is detected by eye (33).

For manual inspection in this thesis, clots were formed in Eppendorf tubes in 20 µl final volumes and the timer was started. At set times (30, 35, 40, 45, 50, 55 s) a pipette was used to draw up some of the clot mixture. Prior to the gel point the clot can easily be drawn up into the pipette. After the gel point, once it has clotted, the mixture cannot be drawn up and a piece of clot is attached to the end of the pipette.

Automatic determination of the gel point was carried out using an Amelung coagulometer. Samples were pre-mixed in plastic cuvettes; a small ball bearing (~2 mm in diameter) was placed inside the mixture. The setup and the geometry of the cuvette are such that the ball bearing stays stationary while the cuvette rotates. The cuvette was placed within the coagulometer where it was heated to 37ºC and slowly rotated. Next thrombin was added to initiate coagulation and timing commenced automatically. Once the clot gels, the ball bearing is captured within the network and begins to rotate, this motion is detected electromagnetically and the time at which this occurs is recorded. Each sample was repeated 5 times.

2.2.4 Confocal Microscopy

Confocal Microscopy is an optical imaging technique which allows visualisation deep into samples, the creation of 3D images and the observation of biological processes. Confocal microscopy, unlike conventional microscopy, uses point illumination and a confocal pinhole positioned in front of a detector to remove out-of-focus light, only allowing light from the focal plane to reach the detector (see Figure 2-4). This dramatically improves image quality and allows the collection of optical slices to construct a 3D representation of a sample.

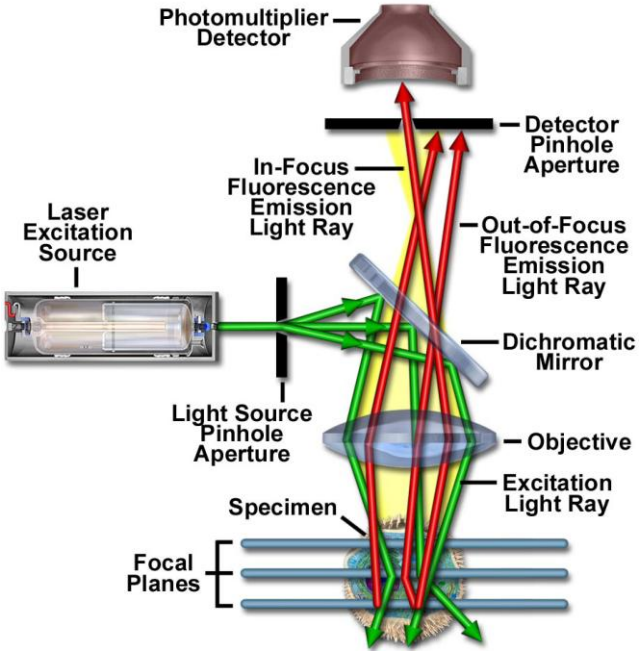

Figure 2-4: Schematic diagram of laser scanning confocal microscopy (LSCM) setup (figure from (101)). A laser spot produced by a pinhole aperture is scanned over a specimen exciting the fluorescent dye present in a focal plane. The light from only this focal plane is collected by a detector.

For this work, laser scanning confocal microscopy (LSCM) was utilised (Figure 2-4 shows a typical LSCM setup) to image fibrin network structures in fully hydrated form and in 3D. Coherent laser light (excitation source) is passed through a pinhole aperture to produce a point illumination source which is focused onto a dichromatic mirror. The reflected light from the mirror is scanned across a sample in a defined focal plane exciting the fluorescent emitting dye. This produces secondary fluorescence emission which passes back through the dichromatic mirror and is focused into a point at the detector pinhole aperture. A significant amount of fluorescence emission occurs above and below the focal plane. This is termed out-of-focus light and is removed by another pinhole aperture positioned at the detector. Light from above or below the focal plane focuses either in front or behind the pinhole aperture and is therefore physically blocked or misses the detector. Light originating from within the focal plane is focused at the pinhole aperture and passes through to the detector. As only a small fraction of out-of-focus light passes through the pinhole aperture the majority remains undetected and does not contribute to the resulting image. The

fluorescent light which passes through the pinhole aperture is collected by a photomultiplier tube (PMT) which converts the light into an electrical signal which is then sent to a PC where the resulting image is processed and constructed.

Scanning a single focal plane pixel by pixel creates an optical slice of a sample. Combining multiple scans of different focal planes allows the construction of a 3D image. By repeating this process over time a series of images can be collected and reconstructed in order to observe biological processes.

For a typical experiment fibrinogen (final concentration 0.5 mg/ml), $CaCl_2$ (2.5 mM), 5% fluorescently labelled fibrinogen (0.5 mg/ml) and any other reagents were diluted in TBS buffer and pre-mixed in 0.5 ml Eppendorf tubes. After the addition of thrombin (1.0 U/ml) to initiate clotting, the reaction components were quickly, but gently, vortexed to ensure they were thoroughly mixed and then immediately transferred into square glass capillaries of internal diameter 0.5 mm. The capillary was placed inside the mixture which was drawn up through capillary action. All confocal imaging for this work was carried out using an upright Zeiss LSM 510 META Axioplan 2 microscope (Carl Zeiss Ltd., UK) with 40 x (low magnification) and 63 x (high magnification) oil immersion objectives. For each clot type studied, multiple single optical sections (100 x 100 μm and 200 x 200 μm) were taken at different areas throughout the clot. Also, multiple optical sections were taken and combined to form three-dimensional reconstructed images of each clot. A measure of fibre density was determined by drawing a line through a micrograph and counting the number of fibres which cross it. This was repeated 5 times in 5 different 100 x 100 μm micrographs.

2.2.5 Scanning Electron Microscopy

The scanning electron microscope (SEM) was first developed by M. Knoll in 1935 (102) whereby a focused beam of electrons was scanned across a sample surface by magnetic deflection. A typical SEM setup consists of an electron gun (cathode and anode), two condenser lenses, two pairs of beam deflection coils,

an objective lens and some apertures (see Figure 2-5). Within the sample chamber are the sample stage and the detectors for the different signals generated by the electron-sample interaction. The SEM is maintained under vacuum to ensure the beam electrons have minimal interaction with any intervening gas molecules on their way to the sample.

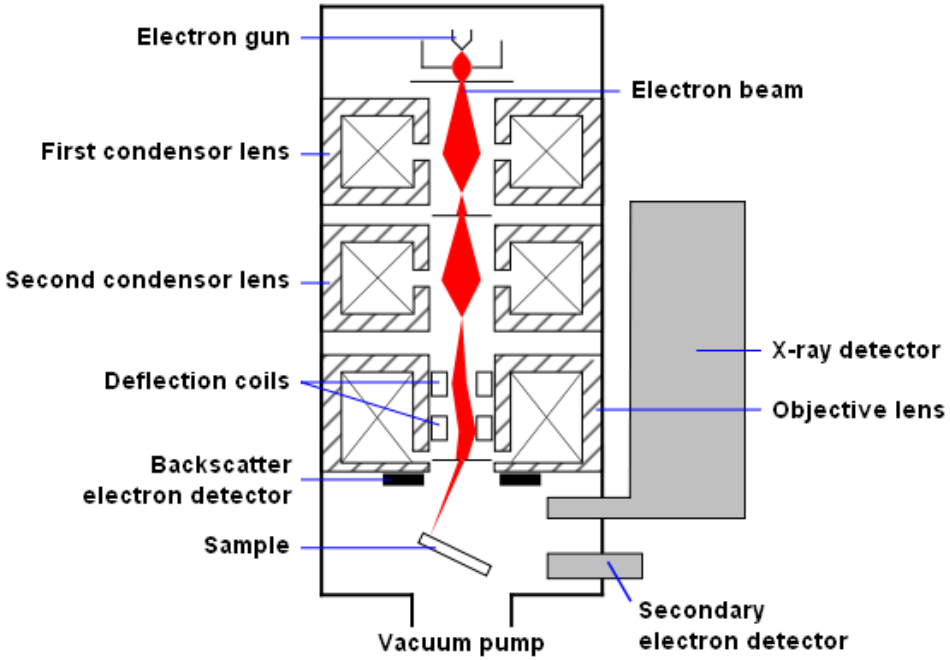

Figure 2-5: Schematic diagram of an scanning electron microscope (SEM) setup (figure from (103)). Electrons are focused by a series of lenses and then scanned over a sample. The various signals produced from the electron-sample interaction are collected by detectors which surround the sample.

Beam electrons are emitted from the cathode and accelerated by a voltage to the anode. The electrons then pass through condenser lenses which focus the beam down into a small spot, around 5 – 10 nm in diameter (104). The objective lens ensures a large working distance (distance from the objective to the sample) which allows the various signals produced from the sample to be collected efficiently. The deflection coils deflect the beam in the x and y axes allowing the sample to be raster scanned.

As the beam scans a sample the incident electrons interact with the surface and produce various signals: cathodoluminescence, X-rays, along with back-

scattered, transmission and secondary electrons. Imaging throughout this work used secondary electron detection. These are the electrons which are excited and emitted from the sample surface. These are collected by a detector, the signal is then amplified and sent to a PC where the resulting image is processed and constructed.

In contrast to confocal microscopy, SEM is a surface imaging technique and therefore does not allow visualisation deep inside a sample. It does however provide much greater spatial resolution, of the order of nm compared with hundreds of nm for confocal microscopy.

Scanning electron microscopy was used to investigate the structure of fibrin clots. Typically, fibrinogen (final concentration 0.5 mg/ml), $CaCl_2$ (2.5 – 7.5 mM) and any other reagents were diluted in TBS buffer and pre-mixed in 0.5 ml Eppendorf tubes in 110 μl volumes; thrombin (0.5 – 1.0 U/ml) was then added to initiate clotting. The mixtures were immediately transferred in volumes of 50 μl to Eppendorf lids which were pierced multiple times with a sharp syringe in order to assist solvent permeation. The lids were wrapped in parafilm in order to prevent clot leakage during formation. Clots were allowed to form in a humidity chamber at room temperature for the required time. After this period clots were washed in sodium cacodylate buffer (67 mM $C_2H_6AsNaO_2$, pH 7.4) to remove excess salt.

In order to image biological samples with the SEM, chemical fixation is required to preserve and stabilise the structure. Clots were fixed in 2% glutaraldehyde overnight. Clots were again washed in sodium cacodylate buffer and then dehydrated in a series of increasing acetone concentrations (30 - 100%) overnight. Clots must be dehydrated as imaging is performed under vacuum. Clots were further dried using a critical point drier. Here, the acetone present within the sample is replaced with liquid CO_2. The clots are then heated to ~31°C where the CO_2 evaporates leaving the samples dry. After this, samples are mounted onto SEM stubs and then sputter-coated with platinum using a Cressington sputter coater 208 HR (Cressington Scientific Instruments Ltd., Watford, UK).

Each clot type studied was photographed in at least 5 different areas at 5,000, 20,000 and 100,000 x magnifications using an FEI Quanta 200 FEG SEM (FEI, Hillsboro, OR). Average fibre diameters were measured from at least 50 random fibres in each sample using ImageJ software. A region of a micrograph is selected at random and the diameter of every fibre in that area is measured. This will ensure no bias towards, for example, thicker or well focused fibres thus minimises any sampling effects. A measure of fibre density was obtained in the same way as for confocal microscopy.

2.2.6 Atomic Force Microscopy

The atomic force microscope (AFM) was first developed in 1986 by Binnig *et al*. (105) and is part of the scanning probe microscope (SPM) class of instruments. SPMs operate by scanning a probe over the surface of a sample whereby images are built up a line at a time by recording the physical interaction between probe and sample. The AFM probe consists of a very sharp tip (radius of curvature of the order of nanometres) mounted onto a flexible cantilever (see Figure 2-6 Insert) which is oscillated at or near its natural resonant frequency (~kHz). This mode of operation is termed tapping mode (TM) since the probe is in intermittent contact with the surface, i.e. it taps over the surface. TM-AFM is particularly useful for studying biomolecules as it eliminates the lateral shear forces generated when using contact mode. In this mode of operation the tip is in continuous contact with the surface as it scans and as such can damage and displace weakly bound molecules. As a result TM-AFM has been used extensively to study biological systems (106), (107).

The AFM forms an image by detecting very small deflections in the cantilever caused by interaction forces which arise between the tip and sample. The optical lever method (108), the most common detection technique, uses a laser which is reflected off the back of the cantilever onto a split photodiode detector to measure this interaction (see Figure 2-6). The laser beam will strike the centre of the detector, with equal amounts of light in each quadrant when there

is zero deflection. However, when the cantilever is deflected this will change the angle of the cantilever and hence the beam spot will move position on the detector. By measuring the amount of laser light in each quadrant the deflection of the cantilever can be inferred.

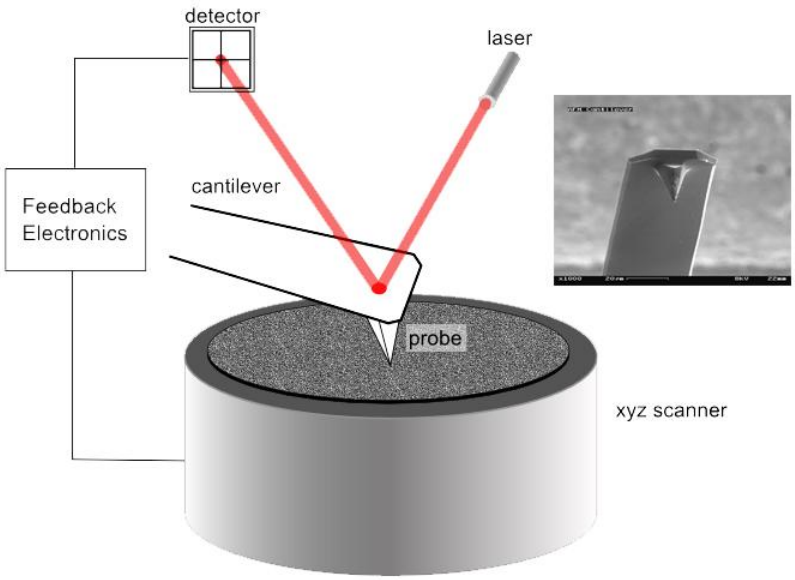

Figure 2-6: Schematic diagram of an atomic force microscope setup. Insert: SEM image of the tip-cantilever assembly (adapted from (109) and (110)).

As the tip is in intermittent contact with the surface at the extreme of its oscillation, this leads to dissipation of energy from the cantilever and a decrease in the amplitude of oscillation. This allows the amplitude to be used as a set-point parameter, which is defined by the user. Thus, when the tip encounters a surface feature and is deflected, the feedback loop maintains the pre-defined amplitude by varying the tip-sample separation. In this way, the tip tracks the topography of the surface and by repeating this process line-by-line a topographical map of the surface is constructed. Precise scanning in the x and y axes is achieved with piezoelectric scanners which are capable of nanometre positioning resolution.

The AFM was used to image the very early stages (< 1 minute) of polymerisation to investigate any differences between γA/γA and γA/γ′ fibrinogen protofibril assembly (see chapter 7). Samples were prepared following the

procedure of Abou-Saleh *et al*. (107). Fibrinogen (final concentration 0.5 mg/ml), $CaCl_2$ (2.5 mM) and TBS buffer were pre-mixed in 1.5 ml Eppendorf tubes to a final volume of 20 μl. After the addition of thrombin (1.0 U/ml) to initiate clotting, the reaction components were quickly vortexed and then allowed to clot for 10, 20, 30, 40 and 50 s. After the required time, the reaction was stopped by dilution by adding 1480 μl of TBS buffer to the clot. 50 μl of this mixture was then deposited onto a freshly cleaved mica disc (pre-treated with 2 mM $NiCl_2$ for 5 mins) and allowed to incubate for 2 minutes. After this time the disc was rinsed with dH_2O and dried with nitrogen gas. Samples were then imaged in air with a Nanoscope IIIa MultiMode AFM (Veeco Instruments, Santa Barbara, CA) operated in tapping mode. Image processing and analysis were performed with Nanoscope (Veeco Instruments) and ImageJ software.

2.2.7 Magnetic Microrheology

Microrheology is the study of how materials store and dissipate energy on the micrometre or sub-micrometre length scale (111). This presents a major technical obstacle as optical methods of mechanical spectroscopy are generally set at the micrometre length scale. Thanks to multiple technological and theoretical advances over the past few decades the study of physical phenomenon on the very smallest of length scales has been made possible. The review of T. A. Waigh (112) gives a good introduction to these techniques.

A major advantage of microrheology is that only small quantities of material (~10 - 20 μl) are required. This has allowed microrheological techniques to be readily applied to biological systems such as single molecules and living cells. There has been particular success in the field of fibrin research where samples purified from a patient's blood or those from recombinant fibrinogens are particularly time consuming to create and result in limited quantities. Microrheological measurements can also be performed in much more physiological environments than those achieved via bulk rheology, e.g. inside a living cell. Furthermore, many important biological processes occur on the

micrometre scale, as it is here where much of the mechanics of cells and biopolymers operate.

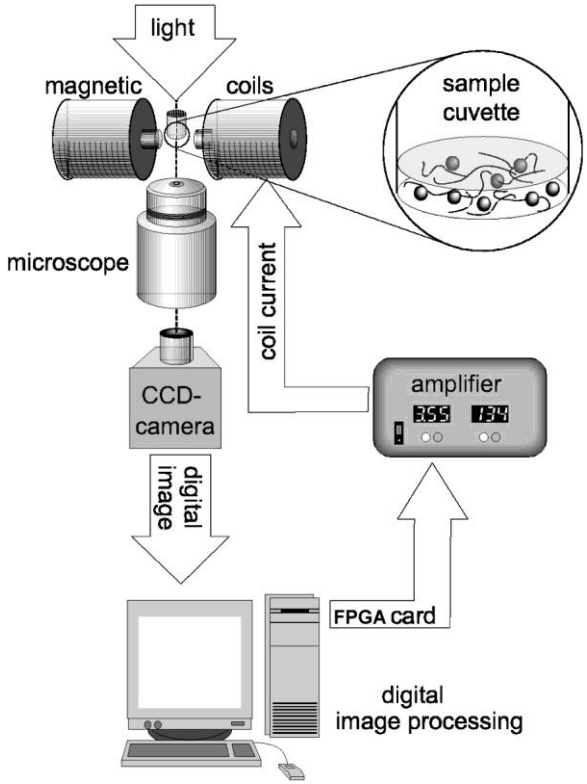

Figure 2-7: Schematic diagram of a magnetic microrheometer system for particle manipulation (figure from (113)). A close up of the sample region is shown, which is surrounded by 2 electromagnets and a microscope. Images from the microscope are captured by a CCD camera and fed to a PC for processing and analysis. Amplifies supplying current to the electromagnets are interfaced to the PC by a Field Programmable Gate Array (FPGA) card.

Active microrheology is a technique which measures the rheological properties of a material by applying forces to probe particles. In this instance, the probe particle interacts with the material it's embedded within and from the displacement response, the viscoelastic moduli may be extracted (114). In the field of magnetic microrheology, instruments utilise strong electromagnets coupled with imaging microscopy to manipulate particles and measure their movement.

The idea of magnetic microrheometers was first conceived in 1949 by Crick and Hughes in an experiment in which magnetic particles inside living cells were

manipulated using a permanent magnet (115). The idea of manipulating magnetic particles using magnetic fields is the basic principle behind magnetic microrheology and is still in use today. However, apparatus are much more advanced employing sophisticated optics and multiple electromagnets in conjunction with computer systems allowing 3D manipulation, oscillation and rotation of particles (see Figure 2-7 for a typical schematic of a magnetic microrheometer). In the literature 1D, 2D and 3D devices have been reported (113, 116-118) with wide ranging applications.

Magnetic microrheometers work by exerting a force upon a magnetic particle using an external magnetic field gradient. The magnetic particles can be paramagnetic, superparamagnetic or ferromagnetic. Ferromagnetic particles, those which posses a permanent magnetic moment, can produce forces of up to ~800 pN (118). Paramagnetic particles possess little or no magnetic moment in the absence of a magnetic field. Thermal energy is sufficient to randomise the magnetic moments of each individual atom so that the net magnetic moment is zero. As an external magnetic field is applied the magnetic moments begin to align with the field and the particle becomes magnetised, eventually the particle will become saturated when all moments are aligned. Superparamagnetic particles consist of very small ferromagnetic crystals which possess their own magnetic moment. As with paramagnetism, thermal energy will randomise the directions of these moments resulting in zero overall magnetisation. Again, in the presence of a magnetic field the moments of each crystal domain align. Forces of up to ~200 pN are achievable with para- and superparamagnetic particles. Throughout this work, 4.5 μm diameter superparamagnetic particles (Dynal, Oslo) were used. These particles posses a core of Fe_2O_3 single domain crystals and have no remnant magnetic moment in the absence of a magnetic field.

As mentioned, when a paramagnetic particle is situated within an external magnetic field it will become magnetised. The particle will then behave like an individual bar magnet and move towards the region of higher magnetic flux. The force, F on a magnetic particle in an external magnetic field gradient is given by:

$$\vec{F} = \nabla(\vec{m} \cdot \vec{B}) \qquad 2\text{-}2$$

where m is the magnetic moment of the particle and B is the magnetic field. Alternatively, Equation 2-2 can be written as:

$$\vec{F} = \frac{\partial(\vec{m} \cdot \vec{B})}{\partial x}\hat{i} + \frac{\partial(\vec{m} \cdot \vec{B})}{\partial y}\hat{j} + \frac{\partial(\vec{m} \cdot \vec{B})}{\partial z}\hat{k} \qquad 2\text{-}3$$

where:

$$\vec{m} \cdot \vec{B} = m_x B_x + m_y B_y + m_z B_z \qquad 2\text{-}4$$

In one dimension, i.e. a magnetic field gradient which exists only in the x axis, then Equation 2-3 becomes:

$$\vec{F} = m_x \frac{dB_x}{dx}\hat{i} \qquad 2\text{-}5$$

It can clearly be seen that the field gradient and not the absolute magnitude of the field generates the force. An extremely large magnetic field possessing no gradient will not induce any motion in a particle. The properties of the magnetic particles themselves also govern the magnitude of the forces generated. The magnetic moment of a particle of volume V is given by:

$$\vec{m} = \vec{M}V = \vec{M}\frac{4}{3}\pi a^3 \qquad 2\text{-}6$$

where M is the magnetisation, the amount of magnetic moment per unit volume, and a is the particle radius. The magnetic moment of a particle varies as: $m \alpha a^3$, therefore any small increase in particle radius will lead to a substantial increase in the force. Similarly, reducing the size of the particle will lead to a reduction in the available force. Particle sizes can range from nano- to micrometres in diameter. When choosing a particle it is therefore a trade off between the forces required and selecting a particle of suitable size. For

instance, extremely small particles may not generate sufficient force to deform the medium they're embedded within. On the other hand very large particles may distort their surrounding environment and alter the properties of the medium; interpretation of experimental results will be far from straightforward.

Three modes of operation are available in any active rheological measurement: constant force, step-like force and oscillatory force mode. A constant force can be used to obtain a viscosity measurement. Here, the equation of motion of a particle is given by Stokes' law:

$$F = 6\pi a \eta v \qquad 2\text{-}7$$

where F is the constant applied force, η is the fluid viscosity and v is the velocity of the particle. By using a fluid of known viscosity it is possible to calibrate the force applied to a magnetic particle as a function of the electromagnet voltage using this mode of operation (see chapter 3). A step-like force is used to measure the creep-response of a material where the time-dependent particle displacement x(t) is related to the time-dependent compliance J(t) via:

$$J(t) = \frac{6\pi a x(t)}{F} \qquad 2\text{-}8$$

here F is the amplitude of the step force applied to a particle. This mode is used extensively throughout this work. Finally, an oscillatory force is typically used to measure the frequency dependent viscoelastic moduli ($G'(\omega)$ and $G''(\omega)$) of a material. Here, particles are driven at a controlled frequency and amplitude by an oscillatory force, f(t) given by:

$$f(t) = f_0 \sin(\omega t) \qquad 2\text{-}9$$

where f_0 is the amplitude of the sinusoidal force and ω is the frequency. The time dependent displacement, x(t) of the particle is given by:

$$x(t) = x_0 \sin(\omega t + \varphi) \qquad 2\text{-}10$$

where x_0 is the maximum displacement of the particle and φ is the phase shift of the particle displacement with respect to the driving force. These two quantities can be used to calculate the frequency dependent viscoelastic moduli via:

$$G'(\omega) = \frac{f_0}{6\pi a x_0(\omega)} \cos\varphi(\omega) \qquad 2\text{-}11$$

$$G''(\omega) = \frac{f_0}{6\pi a x_0(\omega)} \sin\varphi(\omega) \qquad 2\text{-}12$$

where G′ is the storage modulus and G′′ is the loss modulus. The storage modulus is a measure of how much elastic energy is stored during deformation and gives a measure of stiffness. The loss modulus is a measure of how much energy is dissipated during deformation and gives a measure of viscosity. From the storage and loss moduli it is possible to calculate the loss tangent:

$$\tan\delta = \frac{G''}{G'} \qquad 2\text{-}13$$

which is the ratio of energy lost to energy stored during a cyclic deformation.

Oscillatory measurements are trickier to perform than the other two modes of operation. Again, using a fluid of known viscosity it is possible to calibrate the forces applied to particles. However, in addition to this, any phase shift between particle motion and driving force must also be measured. For instance, there will be a finite time delay between the signals sent to the amplifiers and the resulting magnetic field generated by the electromagnets. Also, there exists a finite time for the magnetic field to decay once the electromagnets are switched off; this causes problems when oscillating particles at high frequencies as the magnetic field does not “switch off”. Finally, in order to measure the viscoelastic moduli of a material over a range of timescales, multiple particles must be

oscillated at many different frequencies. As a result this type of measurement can be extremely time consuming to perform.

A more straightforward approach was chosen which does not rely on oscillating particles and allows the frequency-dependent viscoelastic moduli to be obtained from a step-like force mode of operation. This procedure is described in detail in Chapter 4. Details of the magnetic microrheometer used throughout this work are detailed in Chapter 3.

Chapter 3

3 Magnetic Microrheometer

The previous chapter gave a description of the experimental equipment, techniques and sample preparations used in this work. An introduction to the theory and experimental procedures of microrheology were also provided. This chapter describes the magnetic microrheometer device used to perform microrheological measurements. Experimental set-up and modelling are presented along with the force calibration procedure.

3.1 Magnetic Microrheometer Configuration

The magnetic microrheometer (see Figure 3-1) was designed and constructed by Dr R. Harrand (119). The present configuration consists of four pole pieces (core dimensions: 10 cm in length and 2 cm in diameter), made of soft iron of relatively high permeability (~250), each pole is wrapped in ~480 turns of copper wire turning it into an electromagnet. Each iron core possesses a

pointed end, based on the design of Huang *et al* (118), in order to maximize the force on the magnetic particles. The poles are all held in a soft iron frame which increases the field strength by closing the field lines and completing the magnetic circuit; increases of up to 300% have been reported (118). Each pole piece is connected to its own power supply; amplifiers are Kepco BOP 20-5M units (Kepco, Inc., NY, US). The magnets are positioned over an Olympus IX-71 inverted microscope (Olympus, UK) equipped with a 40x ultra long working distance air objective (numerical aperture 0.55).

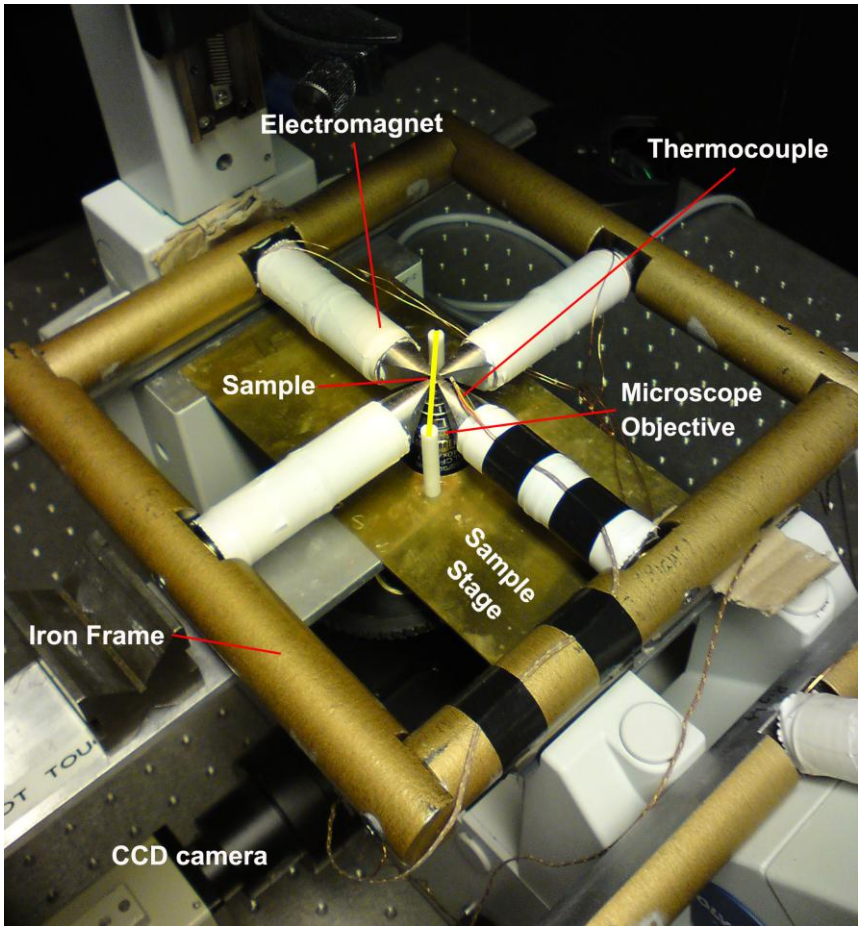

Figure 3-1: Magnetic microrheometer device. For further details on the design, construction and calibration see (119). The 4 electromagnets are held in an iron frame which sits on top of an inverted microscope. The sample holder (indicated by the yellow line) sits on 2 posts positioning it between the 4 electromagnet tips and within the optical axis of the microscope. A CCD camera attached to the microscope is used to capture images which are fed to a PC where particle tracking software analyses the images. A thermocouple is positioned within the sample area in order to measure the temperature during experiments, which can also be placed inside the sample holder.

The microscope is positioned on a vibration isolation table in order to reduce mechanical noise. Images are taken with a standard CCD camera, operating at 25 Hz, which is attached to an optical output on the microscope. The device is also covered with a thick curtain which eliminates particle drift which would normally render measurements useless. It is believed that this drift occurs due to air flow over the sample region. The sample holder for the device was built (by Dr R. Harrand) from the stage of the Olympus microscope. The sample stage is placed to one side of the microscope and a rigid arm was attached. This arm possesses two stands upon which the sample sits, this ensures the sample is positioned in the centre of the electromagnets (defined as the x-y plane) and within the optical axis (z axis) above the microscope objective. The stage can be manually moved in the x and y axes. This allows the user to scan a sample and select a suitable particle.

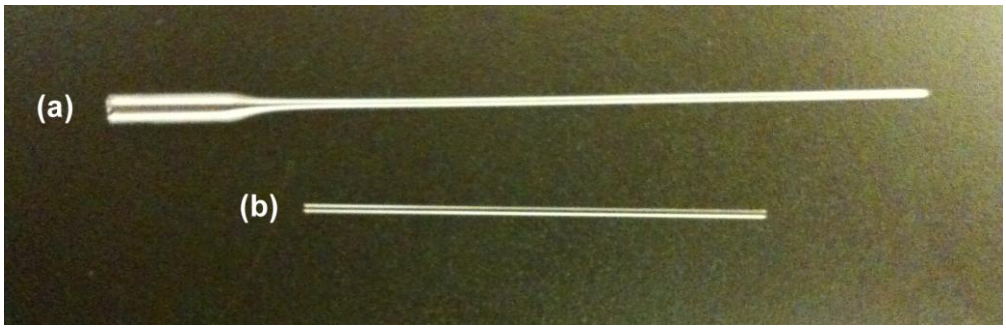

Figure 3-2: Sample holders for the magnetic microrheometer device. (a) Hildenberg capillaries used to hold glycerol and magnetic particles for force calibration experiments. (b) VitroCom microcells (50 mm length, external diameter 0.7 mm and internal diameter 0.5 mm) used to hold fibrin clots for confocal microscopy and magnetic microrheometer experiments.

Samples are held in thin glass capillaries (see Figure 3-2); either Hildenberg 8 cm long capillaries (Hildenberg GmbH, Germany) or VitroCom 5 cm long rectangular microcells (VitroCom, NJ, US). Both sample holders allow forces on the magnetic beads to be maximised by ensuring the distance between pole pieces can be minimised. The VitroCom microcells also hold very small quantities of material (< 20 µl), particularly useful for biological samples. The Hildenberg capillaries are used to hold glycerol for force calibration and have

one end which is slightly larger and can accommodate a syringe which is used to inject glycerol; owing to its high viscosity. This also allows a thermocouple to be inserted directly into the glycerol for real-time temperature measurements. The smaller VitroCom microcells are used to hold fibrin clots. After both capillaries are filled the ends are sealed with Vaseline. This minimises sample evaporation and also reduces the uptake of water by glycerol. The viscosity of glycerol will change dramatically due to its hygroscopic nature if left exposed for long periods.

In conjunction with the electromagnets and imaging system a data processing system is also required. An NI PXI-8186 (National Instruments, TX, US), external stand-alone chassis and CPU system, is used to hold the data capture and control cards. The PXI unit holds two cards, an NI IMAQ-1409 image capture card and an NI FPGA-7831R input/output card. The image card is used to capture images from the CCD camera and the FPGA (Field Programmable Gate Array) card is used to either read data from an RS-232 port or output data such as a signal to a connector block. The last piece of equipment, the NI SCB-68 signal connector block, allows the FPGA card to interface with the amplifiers; this bridges the gap between the control software and the electromagnets.

Custom written software (by Dr R. Harrand) used to control the device was written using the graphical programming language LabVIEW 7.1 (National Instruments). Several LabVIEW programs have been written in order to communicate with the NI instruments; an example of one of these is given in Figure 3-3. The particle tracking program is one in particular; this analyses images taken from the CCD camera and allows real-time tracking of the particles. The software locates a circular feature (e.g. a magnetic particle) within an area specified by the user and determines the x, y coordinates. The data is saved to an ASCII file, which avoids the need to store large amounts of data in the form of video footage.

Software has also been written to control the electromagnets (see Figure 3-3). LabVIEW generates signals which allow the voltage sent to the electromagnets to be controlled precisely. In detail, the user specifies a direction e.g. up, down,

left or right, this convention is chosen as it represents the direction the particle moves on the monitor used to output the images from the CCD camera and corresponds to movement in the x-y plane. A force is also specified by the user, the software then sends a signal to the amplifiers through the signal connector block. The software determines the magnitude of the signal and to which electromagnets it should be sent. For instance, to exert a 50 pN force on a magnetic particle in the right direction the software does the following. Firstly, it calculates what size voltage corresponds to 50 pN (see section 3.3) and then sends this voltage to electromagnet 2, and sends the opposite voltage to electromagnets 1, 3, and 4, thus setting up a magnetic field gradient across the sample region. This induces 3 north poles and 1 south pole; a field gradient is created in the direction of the south pole (see Figure 3-4).

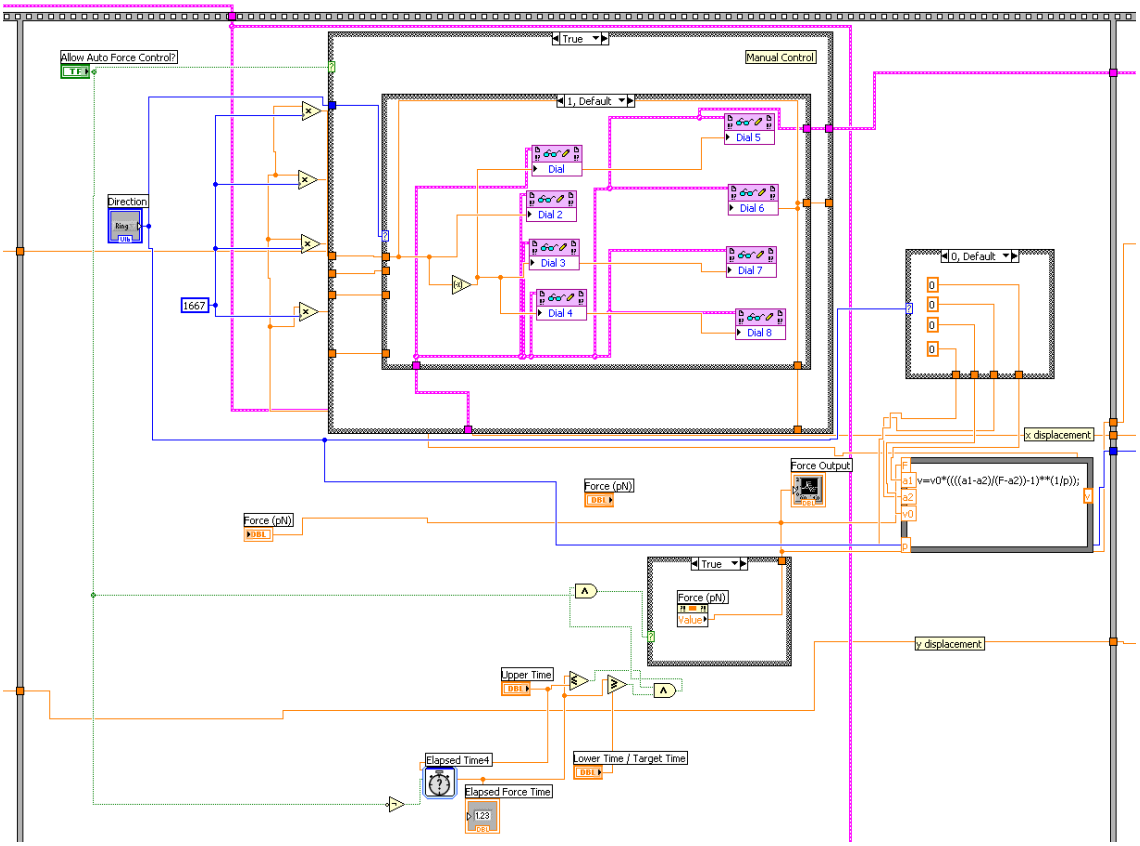

Figure 3-3: An example of a LabVIEW block diagram program. This program was written in order to apply a calibrated force pulse to a magnetic particle. The user specifies a force and the corresponding voltage is calculated. A particle can be moved in 1 of 4 directions i.e. up, down, left or right, where the directions correspond to the x and y axes.

3.2 Magnetic Modeling

The magnetic microrheometer device described here was, as mentioned, based on the design of Huang *et al.* (118) and therefore mechanisms of how to generate forces in 2D was understood. Their device consists of 8 electromagnets; four magnets in a quadrapole arrangement (as in Figure 3-1) sit on top and mirror four magnets placed below. It was shown through 3D magnetic modeling that inducing 6 north poles and 2 south poles a magnetic field gradient could be created in the direction of the 2 south poles. A reproduction of this design was chosen by (119) and using the 2D magnetic modeling program Vizimag (www.vizimag.com) alternative ideas on configurations and where to send different voltages were tried and tested.

The program Vizimag allows 2D modeling of magnetic components such as solenoids and permanent magnets, giving information on field strength and direction. The magnetic field density in any direction may also be plotted (see Figure 3-5(b)). Even though the software models in 2D, it gives all objects a circular cross-section, so a rectangle is treated as a three dimensional cylinder. This allows the electromagnets of the actual device to be modeled particularly well.

The main conclusions of the modeling carried out prior to the device being built are detailed here, for full details please see (119). Firstly, it was found using a model of a single electromagnet that there is a rapid decrease in field strength as a function of distance from the electromagnet tip. Having close proximity between sample and tip can therefore be as important as having large electromagnets and/or high currents (both important for generating high forces).

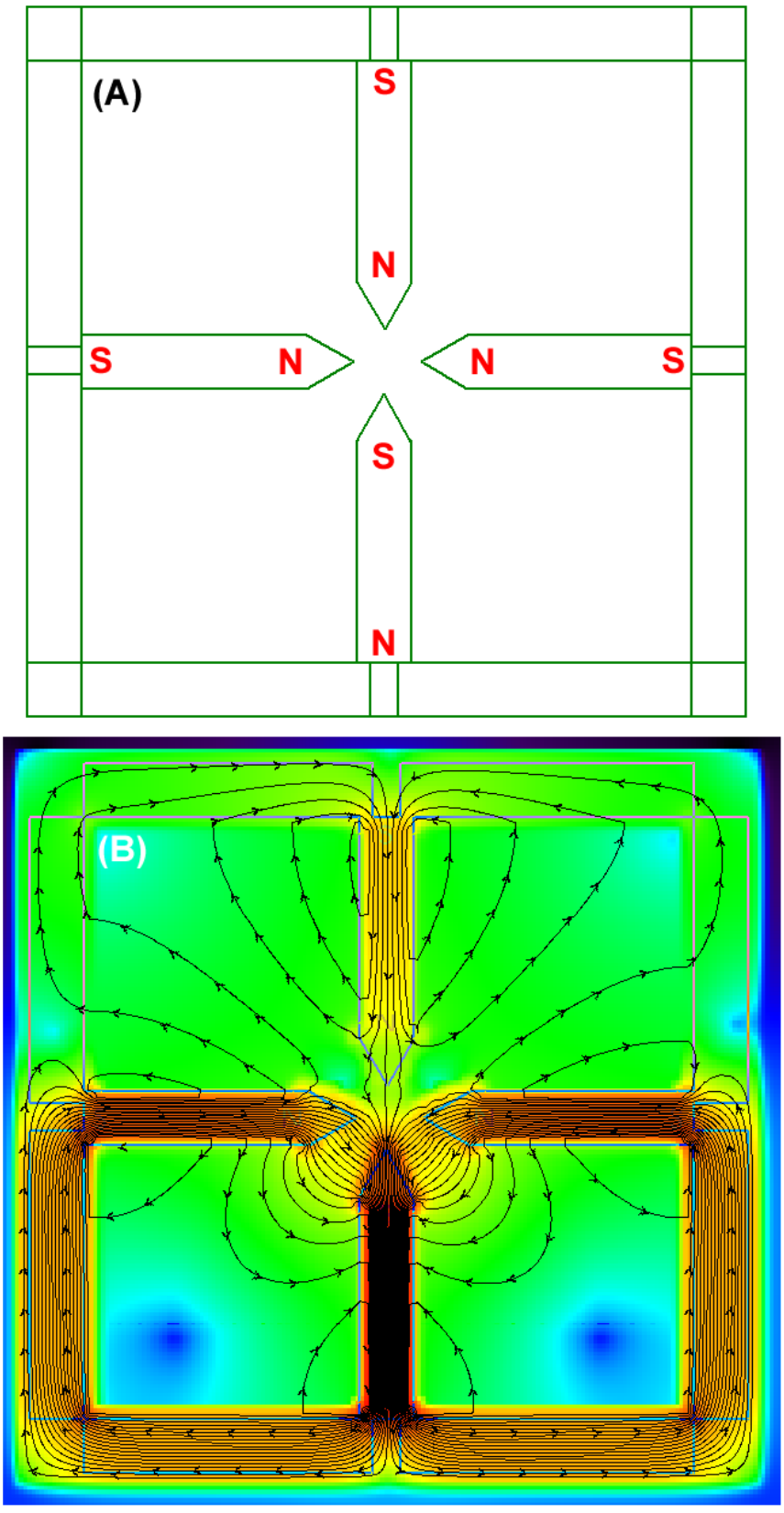

Figure 3-4: (a) Vizimag model of 4 electromagnets (3 north poles and 1 south pole) with iron frame. (b) Colour map of the flux density indicating the large amount of magnetic field density in the south pole magnet.

The entire magnetic microrheometer was modelled using 4 electromagnets held in an iron frame (see Figure 3-4). The device actually consisted of 8 electromagnets but each pair was treated as a single magnet. This represent the device particularly well as it was operated by inducing north poles in the tips of 6 electromagnets (3 magnet pairs), and 2 south poles in the remaining 2 electromagnets (1 magnet pair). It was found that this configuration produced the largest field gradient within the sample region (located equidistantly between all four electromagnets) and this was due to the upper north pole redirecting the flux from the 2 side electromagnets into the lower south pole. The back iron frame also rapidly increased the central field strength from around 500G to 3000G (500% increase) by closing the field lines and completing the magnetic circuit. For the modelling outlined here each electromagnet was represented as a solenoid possessing an iron core (permeability = 250) with a current of 1.8 A and dimensions of 10 cm in length and 2 cm in diameter. At either end of the solenoid there are regions of the same permeability which better represent the geometry of the electromagnets.

The magnetic microrheometer device consisted of 8 electromagnets and was capable of producing forces in the range of 40 to 80 pN in 2D. This somewhat restricted the device as a useful fibrin clot microrheometer as the range of fibrinogen/thrombin concentrations which could be probed was limited. For example, at higher fibrinogen concentrations the network rapidly becomes much stiffer and forces of this magnitude produce extremely small particle displacements. As such, the signal-to-noise becomes very poor and as the device has to be operated at maximum voltage, thermal noise further disrupts particle tracking. In order to increase the force range of the device a re-design was required; 4 of the electromagnets were removed and the bottom frame containing the 4 remaining magnets was raised up (see Figure 3-1 and Figure 3-5(a)). This allowed the separation of the magnets to be reduced (previously the microscope objective prevented this) and also brought the pole piece tips into much closer proximity with the sample. Previously, the tips sat above and below the sample region, now the tip and sample are located in the same plane. This new configuration was modelled and the results are shown in Figure 3-5.

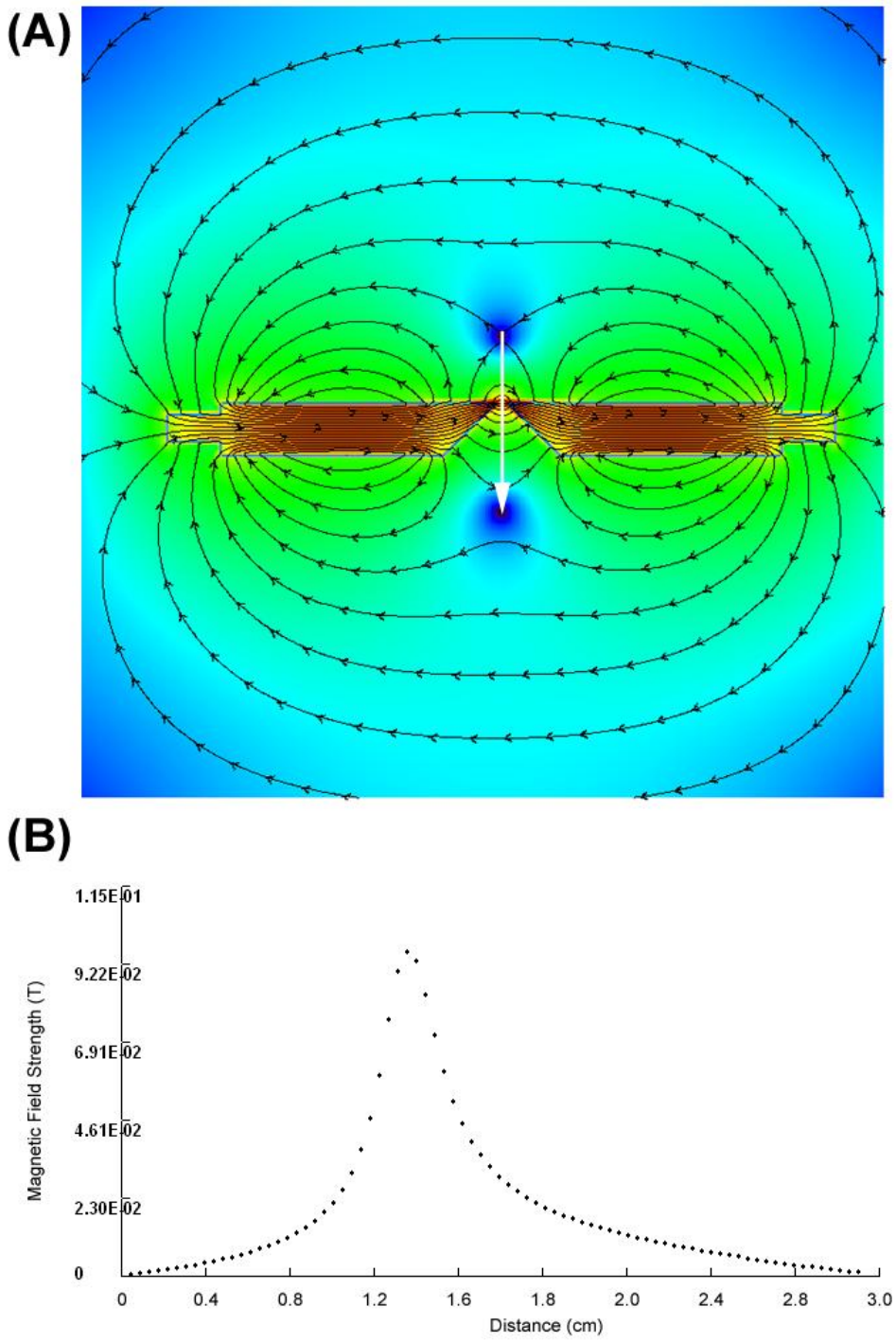

Figure 3-5: (a) Vizimag model of 2 electromagnets (1 north pole and 1 south pole). (b) Plot of the flux density moving down between the 2 pole pieces (indicated by the white arrow in (a)). It can clearly be seen that a peak in the magnetic field strength is situated between the 2 pole piece tips. A magnetic particle situated at the tip of this peak will be located in a region free of any magnetic field gradient in the z axis.

A substantial magnetic field gradient exists in the z axis (see Figure 3-5(b)) and this is known to disrupt x and y translation as a particle drifts out of the focal plane and can no longer be tracked. Eventually the particle will either be pulled or pushed into the capillary walls. However, there is a peak in the magnetic field strength which resides between the two pole piece tips, here the magnetic field reachs a plateau and there is a region free of any magnetic gradient. The sample region was positioned here resulting in x and y translation free of movement in the z axis. The device is now capable of producing forces up to 120 pN.

3.3 Force Calibration

The single most important aspect of calibration for the magnetic microrheometer, and one which must be carried out whenever the electromagnets are repositioned, is force calibration. All other calibration procedures e.g. pixel-to-distance calibration, were carried out by Dr R. Harrand. The most common method of force calibration involves Stokes' law and a fluid of known viscosity. As introduced in section 2.2.6 the force exerted on a magnetic particle in a viscous liquid can be calculated by Equation 2-7. In order to control the applied force it is necessary to know the exact relationship between the voltage of the electromagnets and this force. By analysing the motion of magnetic particles it is possible to calculate the applied force.

Calibration was performed in 99% glycerol (Sigma-Aldrich, UK) using 4.5 μm diameter particles. This glycerol solution has a viscosity of $\eta_{99\%}$ = (740 ± 20) mPa.s at 25°C (measured by Dr D. Auhl using a cone-plate rheometer). At this temperature, 99% glycerol should have a viscosity of 745.2 mPa.s (120); indeed confirming the glycerol is 99%.

Calibration samples are prepared by mixing magnetic particles with glycerol in the ratio 1:300 μl. As mentioned, this mixture is injected into a capillary which is then positioned within the microrheometer. A suitable particle is selected, one

which is located away from the capillary walls in order to minimize boundary effects, and one which is positioned away from any other particles.

Custom written LabVIEW calibration software (Dr R. Harrand) was then used to send voltages of between 0.5 and 5.5 V in 0.5 V steps to the electromagnets and move the particle in the x and y axes. This allowed the force as a function of voltage to be determined in the direction of all 4 electromagnets (see Figure 3-6). This force-voltage relationship was then programmed back into LabVIEW (see Figure 3-3) and allows the user control over the force, rather than the voltage.

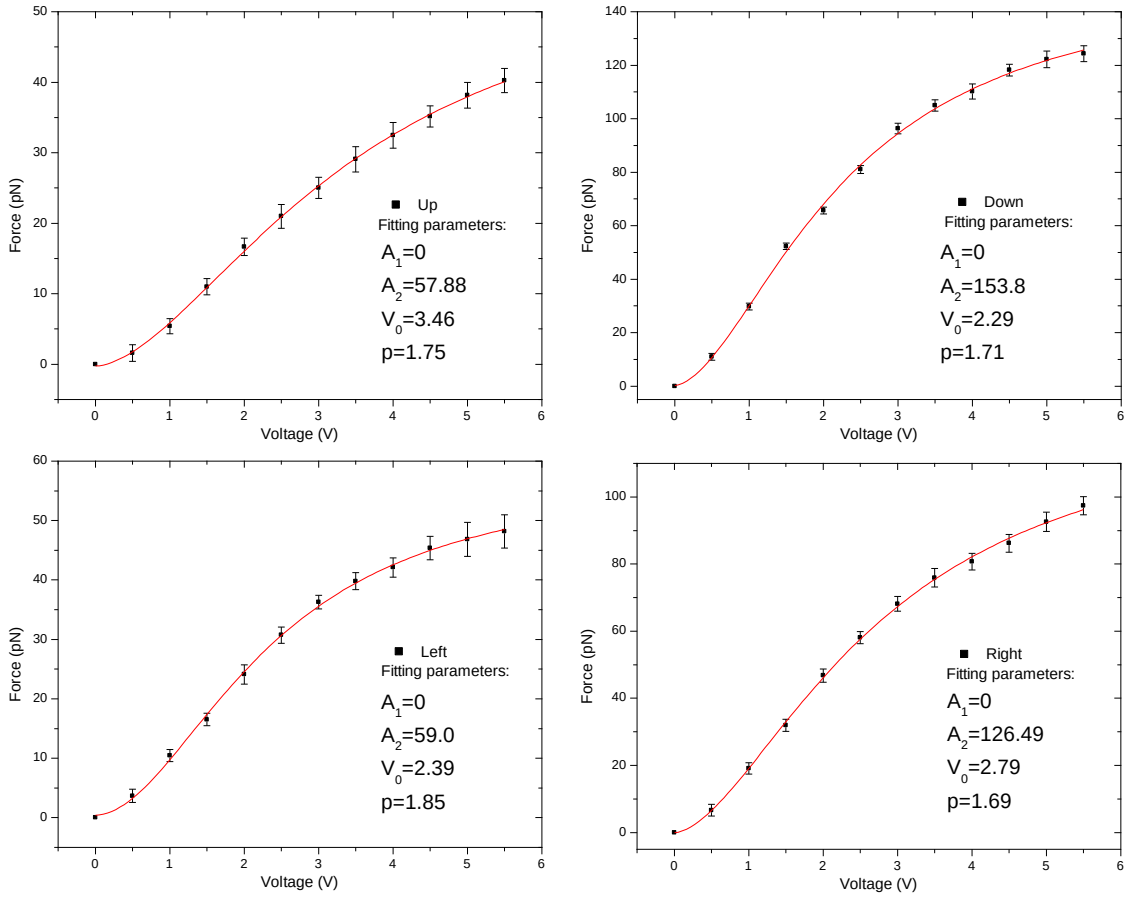

Figure 3-6: Force versus voltage calibration curves for 4.5 µm particles in 99% glycerol. The data are fitted with a sigmoidal curve of the form: $F = [(A_1 – A_2) / (1 + (V / V_0)^p] + A_2$ where F is the force, V is the voltage and A_1, A_2, V_0 and p are all fitting parameters. The parameter A_1 is set to 0 i.e. 0 force at 0 voltage. Errors represent the standard error in the mean obtained from multiple data sets.

In order to obtain the force calibration curves the data were fitted with a sigmoidal function:

$$F = \frac{A_1 - A_2}{1 + \left(\frac{V}{V_0}\right)^p} + A_2 \qquad 3\text{-}1$$

where F is the force (calculated from Equation 2-7), V is the voltage across each electromagnet and A_1, A_2, V_0 and p are all fitting parameters determined using the software OriginPro 8. This equation is rearranged, with V as the subject, and then programmed into LabVIEW (see Figure 3-3) allowing a user to specify a force. The corresponding voltage is then calculated and a signal to produce this voltage is sent to each electromagnet's amplifier.

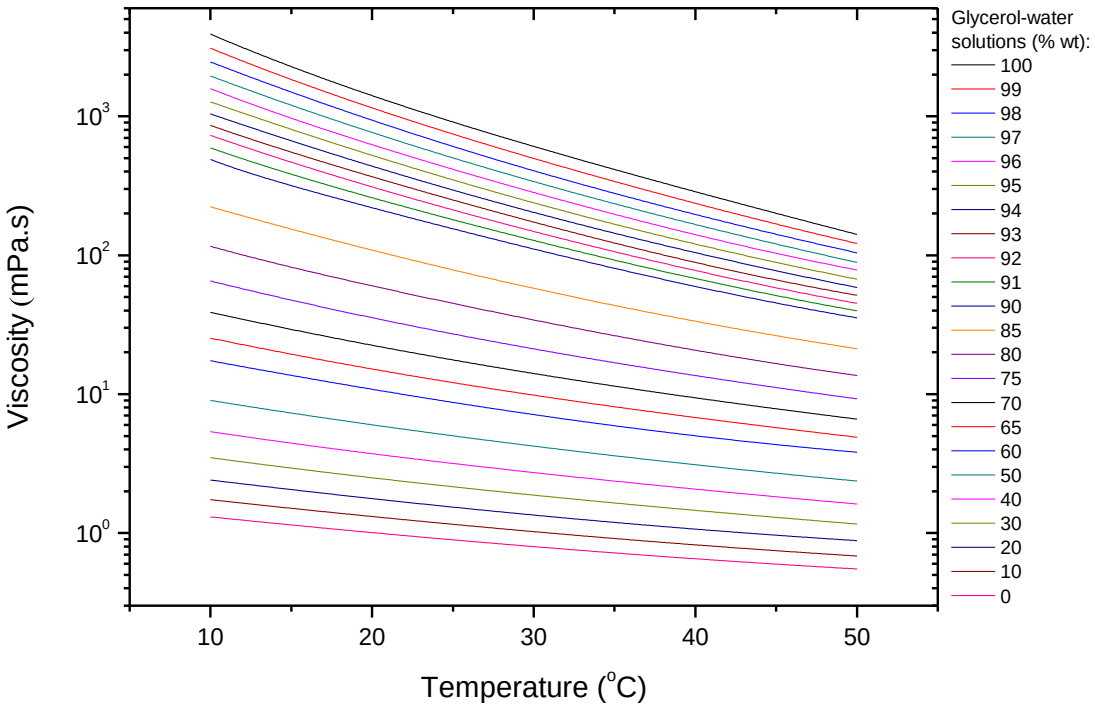

Figure 3-7: Viscosity versus temperature for different glycerol-water mixtures. Experimental data taken from (120). These data were programmed into the LabVIEW calibration program to enable real-time force calculation.

Multiple repeat measurements were taken using the automated calibration program and the results were averaged. Variations in calibration data arise due to drift within the samples. This is minimised as much as possible by sealing the capillary ends with vaseline. The viscosity of glycerol also varies considerably with temperature and water content (see Figure 3-7). Data tables relating the percentage of glycerol to temperature and viscosity were programmed into the software, and the temperature from a thermocouple was read via an RS-232 port. This allowed the viscosity of a particular percentage of glycerol/water to be calculated as the temperature fluctuated during a calibration experiment.

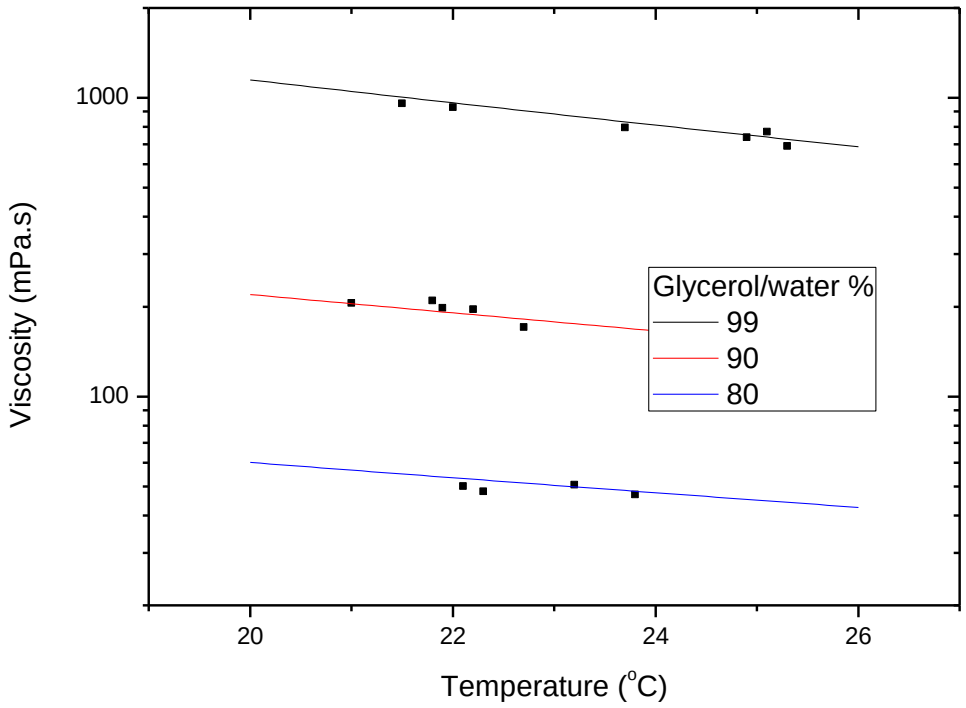

Figure 3-8: Viscosity measurements of different percentage glycerol/water mixtures. The lines are the bulk rheology measurements taken from the literature (120). Error bars (ranging between 5 and 10%) are too small to be distinguished on the logarithmic scale.

Calibration was checked by measuring the viscosity of different glycerol/water mixtures (see Figure 3-8). This is essentially an inverse of the calibration procedure; a force is applied to a particle and the subsequent motion is tracked. From this and using Equation 2-7 the viscosity of the glycerol can be calculated.

By applying a range of forces to different beads within different percentage glycerol/water samples the viscosity was measured and was in good agreement with the data from the literature. This confirms the magnetic microrheometer is a suitable device for measuring the bulk properties of materials.

Chapter 4

4 The Mechanical and Viscoelastic Properties of Fibrin Clots

4.1 Introduction

This chapter outlines the development and validation of the magnetic microrheometer as a suitable device for studying the physical properties of fibrin clots. We studied the effect of magnetic particles on clot polymerisation and structure and investigated the effects of forming clots inside microcells. We present techniques for studying the mechanical and viscoelastic properties of fibrin clots. These techniques are used to study the physical properties of fibrin clots and assess the effect of the plasma protein FXIII. We present data which provides new insight into the behaviour of fibrin clot viscoelasticity.

4.2 The Effect of Magnetic Particles on Clot Polymerisation and Structure

Turbidity measurements were performed on fibrin clots both with and without magnetic particles in order to determine the effect their presence has on clot polymerisation and structure. This is crucial to ensure the magnetic microrheometer device is a suitable microrheometer for measurements on fibrin clots as any structural alterations or effects on polymerisation may have a bearing on measurements. Samples were prepared as described in section 2.2.2 with magnetic particles added at the same concentration as that used for microrheology experiments. ERL fibrinogen at a concentration of 0.5 mg/ml was incubated with 2.5 mM $CaCl_2$ and magnetic particles. Thrombin was then added at 1.0 U/ml concentration, after which, absorbance was measured every 25 s over the first 80 mins of clotting (see Figure 4-1).

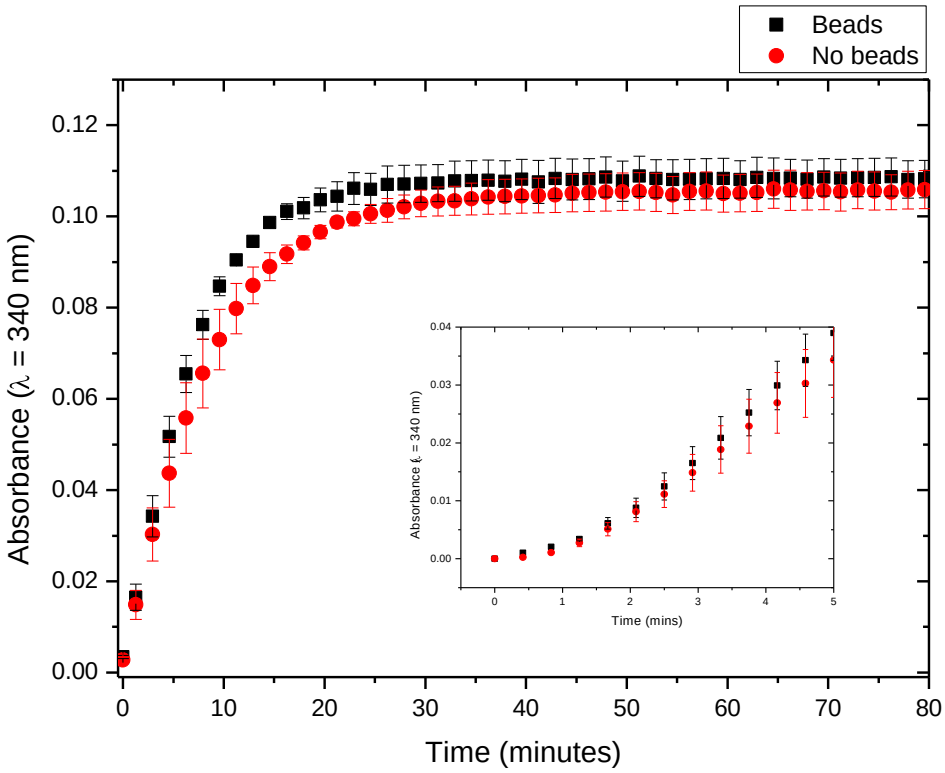

Figure 4-1: Absorbance versus time for clots formed in the presence and absence of magnetic particles. Error bars represent the standard error in the mean from 3 repeat measurements. For clarity every 4th measurement has been plotted. **Insert**: Plot shows the absorbance over the first 5 mins of clotting (the full data set is plotted).

The analysis of the turbidity data in Figure 4-1 is provided Table 4-1. From these data it can be concluded there are no significant differences in polymerisation, within experimental errors, due to the presence of the magnetic particles. The lag phase could not be determined as there was an immediate increase in turbidity for both clots. The only significant difference in turbidity occurred at ~17 mins, however, since there was no difference in the rate of polymerisation prior to this and the final plateau for both clots was identical, this transient difference appears inconsequential.

Table 4-1: Polymerisation data of clots formed with and without magnetic particles

Polymerisation Parameter	Particles	No Particles
Lag time (minutes)	n/a	n/a
Maximum rate (units min^{-1})	0.012 ± 0.001	0.010 ± 0.001
Final Absorbance	0.108 ± 0.004	0.106 ± 0.004
Plateau Time (minutes)	31 ± 2	34 ± 4

The final absorbance is related to the size and/or density of fibres in a clot e.g. a clot composed of a low density of thick fibres may have a very similar absorbance to a clot consisting of many more thin fibres. As such, turbidity does not reveal the true structural picture of what is occurring down to the single fibre level. In order to ascertain more completely the effect magnetic particles have on clot structure SEM and confocal microscopy were used to image individual particles. In this way, it is possible to determine the effect, if any, the particles have on the surrounding clot. For instance, will the fibres aggregate around the particles or will they be repelled leaving the particle in a region of lower clot density? Such minor, local structural rearrangements may have very little or no effect on the overall absorbance but will have major implications for microrheology experiments.

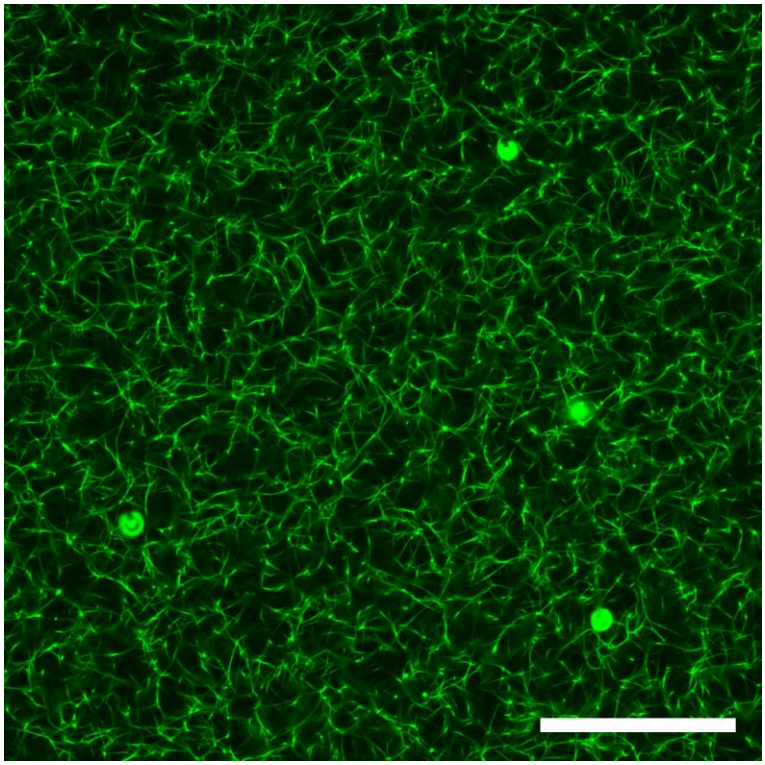

Figure 4-2: Confocal micrograph of 4.5 μm magnetic particles trapped within a clot. The bright green spots are 4 magnetic particles; they appear distorted due to either lying above or below the optical plane. This micrograph is a single optical slice. The scale bar indicates 50 μm.

Clots for SEM and confocal microscopy (see Figure 4-2 and Figure 4-3) were prepared as described in sections 2.2.4 and 2.2.5 respectively. All concentrations of particles and reactants were the same as that used for turbidity experiments described above. For both imaging techniques, samples were scanned for regions of clot containing magnetic particles and, once located, images were obtained.

From confocal imaging (see Figure 4-2), it can be seen that particles resided in regions of both high and low fibre density. In addition, particles did not appear to repel or attract the surrounding fibres, as one might expect if they were interacting in some way. Closer inspection revealed that some fibres appeared to go closely past particles and were not influenced by their presence. This indicates the particles have very little or no effect on the surrounding structure. As such, it could be assumed that the local fibre architecture around a particle is

representative of the architectural arrangements of the fibrin network throughout the clot.

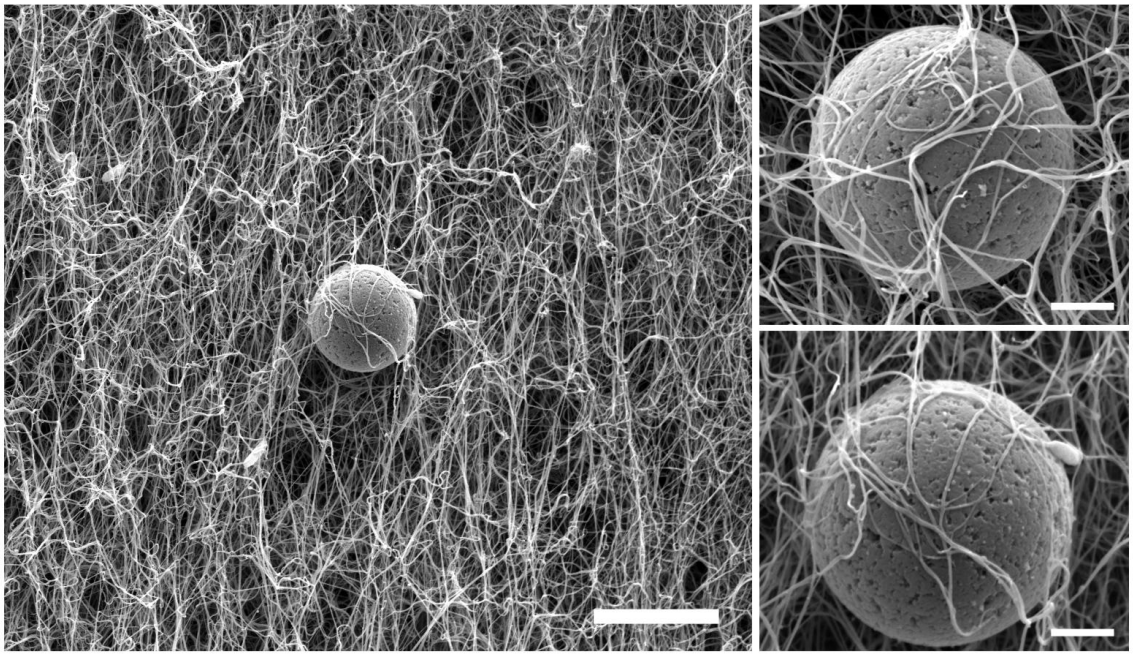

Figure 4-3: SEM micrographs of magnetic particles trapped within a clot. The large panel (10 000x) shows a magnetic particle and the surrounding clot structure, scale bar indicates 5 μm. The two smaller panels (50 000x) show how the particles interact with the individual fibres of the clot, scale bar indicates 1 μm.

Higher resolution SEM revealed particles and individual fibres in much greater detail (see Figure 4-3). Here, the fibres appeared to wrap around the particles and hold them in position. This lends support to the idea that the particles become trapped within the network by the fibres which grow around them. Microrheological measurements performed with these particles should therefore reveal the true viscoelastic properties of a clot. Deviations may occur when the characteristic length scale of the clot i.e. fibre length or mesh size, approaches that of the particle size. In this instance, the viscoelastic properties will be highly dependent upon the local fibre structure. However, repeat measurements of multiple particles distributed throughout a clot would average out these differences.

4.3 Microcell Effects on Clot Structure and Mechanical Properties

Confocal microscopy was used to image clots formed within microcells to assess the effect of the microcell on clot structure. Again, this is an important test as alterations to clot structure due to interactions with the capillary walls may affect measurements. Samples were prepared as described in section 2.2.4 with final clot concentrations the same as that used in section 4.1 for the clot containing no magnetic particles. Multiple overlapping confocal micrographs were taken from one side of the capillary to another and then stitched together to form a mosaic image of the entire capillary diameter (see Figure 4-4(A)).

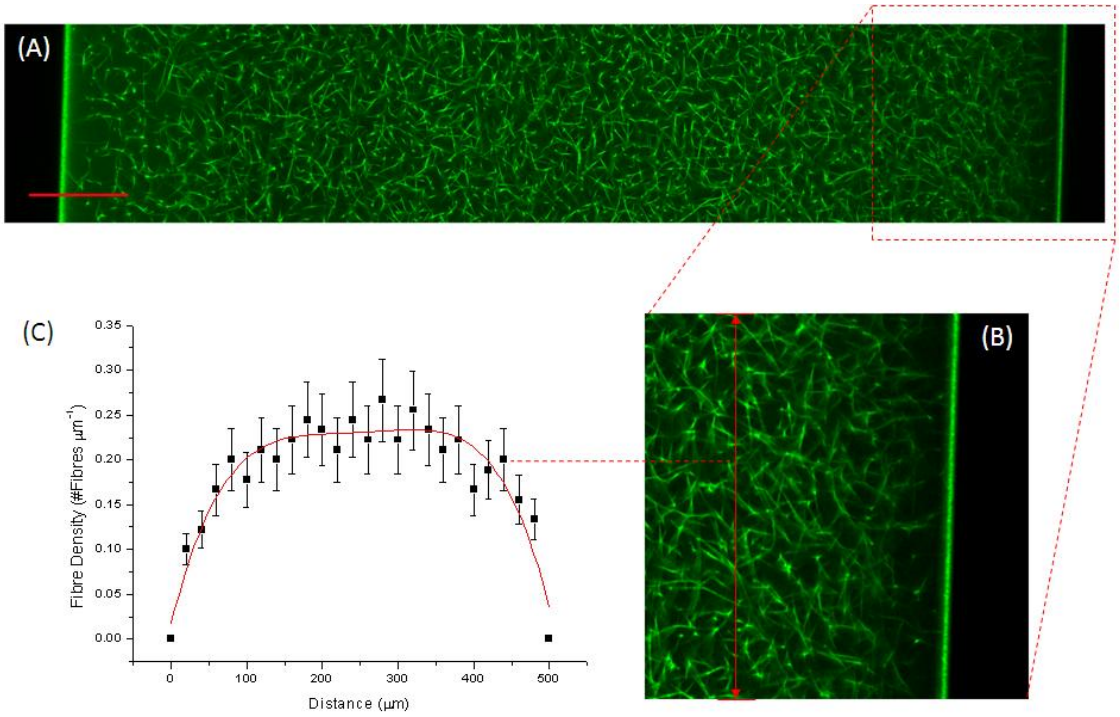

Figure 4-4: (A) Confocal microscopy mosaic image of a clot formed within a VitroCom microcell. Scale bar represents 50 µm. (B) Zoom of the capillary wall. The red line is used to determine fibre density; by counting the number of fibres which cross the line an effective fibre density can be measured. (C) Plot of fibre density across the capillary from left to right, measurements were taken at 20 µm intervals. Error bars represent the standard error in the mean from 3 repeat measurements.

Imaging revealed the capillary walls as bright green bands at either extreme of the image with a clot enclosed within. The optical plane was positioned in the centre of the capillary. A zoom of the capillary wall (see Figure 4-4(B)) revealed a dark region where there were little or no fibres. To investigate this further, fibre density was measured at regular intervals, every 20 μm, across the capillary. The fibre density at the walls was zero as no fibres crossed here. Moving from the walls of the capillary towards the centre there was an increase in fibre density. Fibre density then plateaus at around 100 μm and was constant for ~300 μm, after which it rapidly dropped off as the other wall was approached. At 20 μm from the walls the fibre density was 0.12 ± 0.02 fibres μm^{-1}, this increased to 0.23 ± 0.01 fibres μm^{-1} at the centre of the capillary. Fibre density therefore increased 1.9-times towards the centre of the microcell.

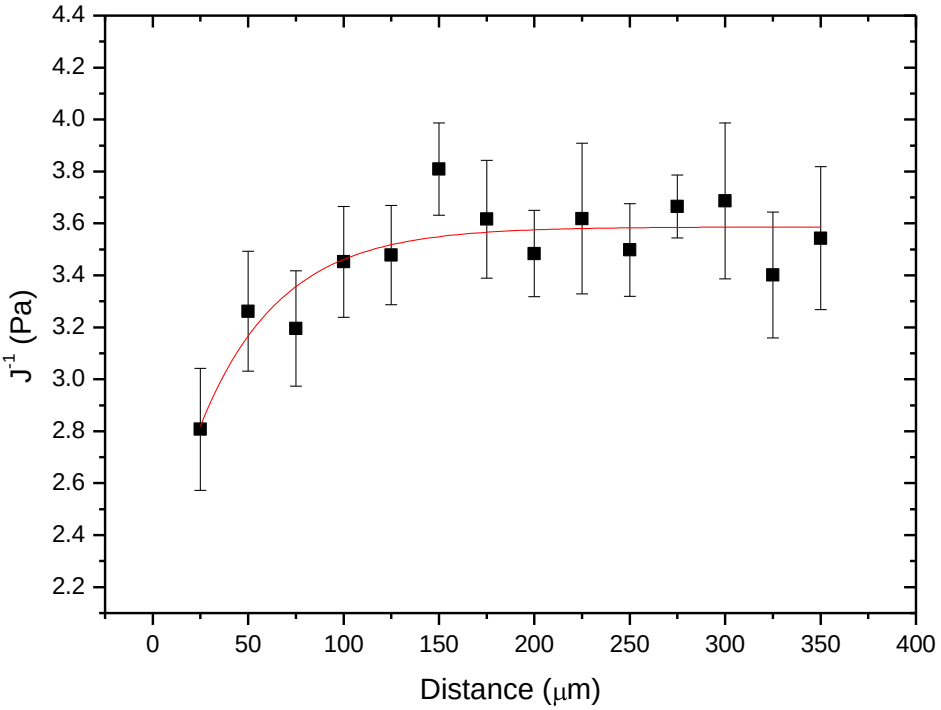

Figure 4-5: J^{-1} versus distance from wall of a clot formed inside a microcell. The inverse compliance, J^{-1} is measured as described in Figure 4-6 and is used as a measure of clot stiffness. Measurements were taken every 25 μm moving away from the microcell wall. The stiffness at 0 μm could not be determined as it was not possible to displace particles located here; it was assumed they were stuck to the wall. Error bars represent the standard error in the mean from 3 repeat measurements.

From the above observation, it was hypothesised that the location of a particle in relation to the capillary walls will have an effect on the mechanical properties measured. In order to investigate this further the stiffness as a function of distance from the capillary wall was measured. Again, samples were prepared as described in section 2.2.4 with final clot concentrations the same as that used in section 4.1 for the clot containing magnetic particles. Next, the microcell was placed inside the magnetic microrheometer and the microscope objective was focused onto the inside of the bottom capillary wall. This was defined as the starting position i.e. 0 μm. The plane of focus was then moved up through the clot at intervals of 25 μm. As the microscope is inverted the observational point is from below the clot. At each interval, 5 particles were selected; those which were in focus, and then tested. A force pulse of 2 s in duration was applied to each particle and from this the stiffness was determined (as described in Figure 4-6). In this way, the stiffness as a function of distance from the capillary wall was measured (Figure 4-5).

Particles at 0 μm could not be displaced; it is assumed that these particles are stuck to the microcell wall. When moving away from the capillary wall there was an increase in clot stiffness which reached a plateau at ~100 μm and was maintained up to 350 μm. It was not possible to see further into the microcell as the maximum working distance of the microscope objective was reached. At 25 μm from the microcell wall, the stiffness was 2.8 ± 0.2 Pa which increased to 3.6 ± 0.1 Pa. at the centre of the microcell. Stiffness increased 1.3-times when moving towards the centre of the microcell.

This correlated well with the fibre density measurements (Figure 4-4). The increase in stiffness is attributed to an increase in fibre density. Whyfibre density is lower at the microcell wall is unknown. It could be postulated that some interaction between the microcell material and fibrin inhibits fibre growth or that the wall repels the fibres. It's important to note that the clot structure observed at the centre of the capillary appeared "normal"; clots prepared within standard confocal microscopy slides showed very similar structures. For all subsequent

experiments, only particles located more than 100 μm from the microcell wall will be tested.

4.4 Stiffness during Polymerisation

Once FpA and FpB are cleaved from fibrinogen to form fibrin, this rapidly self-assembles into a 3D fibrous mesh. Depending on thrombin to fibrinogen ratio this process can occur in a time-span ranging from seconds up to minutes. Before a certain time point, defined as the gel point (see section 2.2.3), the network is a viscous liquid, after which it rapidly changes into a solid. After this time, the clot becomes viscoelastic and it is possible to measure the compliance of the clot and the subsequent rapid increase in stiffness using the magnetic microrheometer.

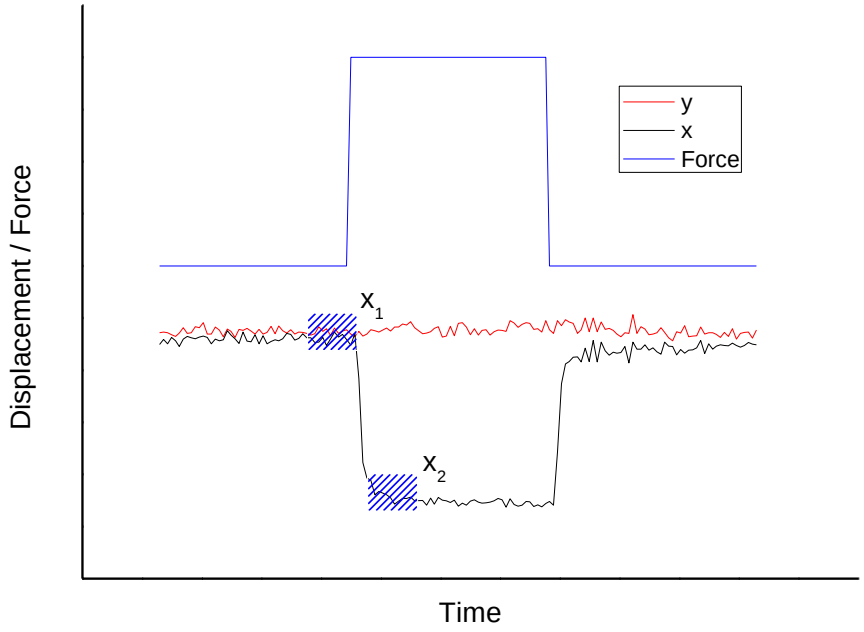

Figure 4-6: Displacement response of a particle trapped within a clot. Both the y (red) and x (black) displacement is plotted along with the step-like force pulse (blue). The blue shaded regions indicate the positions measured by the auto analysis program. Here the x displacement ($x_s = x_2 – x_1$) has been measured. In this way the analysis program can calculate the compliance ($J = 6\pi rs / F$ where $s = \sqrt{(x_s^2 + y_s^2)}$) for every force pulse applied over the course of an experiment. Typically, the inverse compliance, J^{-1} is calculated and used as a measure of clot stiffness during polymerisation.

Magnetic particles are trapped within a clot by simply mixing the particles with fibrinogen and any other reagents and then adding thrombin to initiate clotting. As the clot forms the magnetic particles become trapped by the fibres and the particle is held inside the network (Figures 4-2 and 4-3). All clots for magnetic microrheometry experiments are prepared in this way. In detail:

- Fibrinogen is mixed with magnetic particles in an Eppendorf tube. Typically 1 µl of particles in dH_2O in a final clot volume of 50 µl gives an optimum number density of particles within a clot e.g. enough particles to obtain multiple repeat measurements but not too many that it is difficult to locate a sufficiently isolated particle.
- Any other reagents are also added at this stage e.g. $CaCl_2$, FXIII, etc.
- The reactants are thoroughly mixed either using a pipette or by vortexing, after which thrombin is added.
- Immediately after this, the reactants are again mixed and then transferred to a VitroCom microcell. The microcell is placed inside the mixture and the clot is drawn up by capillary action.
- The ends of the microcell are sealed with Vaseline.
- Next the microcell is placed inside the magnetic microrheometer as quickly as possible.
- The microscope objective is focused at the centre of the capillary and the clot is scanned for a suitable particle.
- Finally, using the LabVIEW software a particle is selected and tracked while forces are applied.

One approach is to apply force pulses of the same magnitude at regular intervals e.g. 10 pN every 10 s for a duration of 2 s, as clotting proceeds. Figure 4-6 shows such a force pulse and the subsequent particle displacement measured by the tracking software. This displacement response is used to obtain a measure of clot stiffness, at that instant of time, as detailed in Figure 4-6. In this way, the time development of a clot's stiffness can be measured (see Figure 4-7). For an experiment of 1 hour, applying force pulses every 10 seconds produces

substantial amounts of data to analyse, which typically takes around 2 hours. An analysis program was written to automate this procedure, and as a result post experimental analysis time was dramatically reduced.

The early work of Roberts *et al.* (62) revealed clots undergo a rapid increase in stiffness which then reaches a plateau once the clot is formed. Following the procedures detailed above, very similar behaviour in purified fibrin clots was observed (see Figure 4-7). ERL fibrinogen at a final concentration of 0.2 mg/ml was incubated with 2.5 mM $CaCl_2$ and magnetic particles. Thrombin was then added at a concentration of 0.5 U/ml, after which, force pulses were applied every 10 s for 2 s over the first hour of clotting. Note that the magnitude of these force pulses is adjusted manually as the experiment proceeds, to ensure that the displacement response is essentially elastic (as in Figure 4-6) while maintaining a good observable displacement. This ensures minimum sample deformation while maintaining good signal-to-noise.

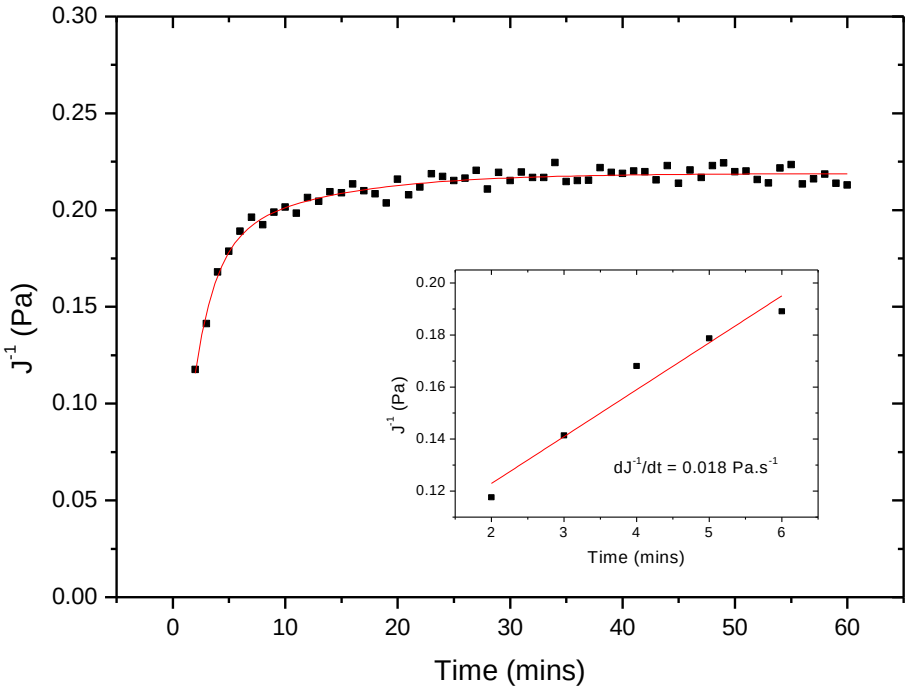

Figure 4-7: J^{-1} versus time of a clot over the first 2 hours of clotting. Much like turbidity there is an initial rapid rise in J^{-1} followed by a plateau. **Insert**: J^{-1} vs. time over the first 5 mins of clotting. The initial rate of change of J^{-1} has been measured giving information on the kinetics of fibre formation.

Initially, a rapid increase in clot stiffness was observed up to around 10 minutes, after which the stiffness began to reach a plateau. Once this plateau has been reached, a clot is assumed to be fully developed both structurally and mechanically. The viscoelastic and/or other mechanical properties of a clot can be measured once this point has been reached. In Figure 4-7, the insert shows how clotting increased over the first 5 minutes; here the rate of change of stiffness (dJ^{-1}/dt) is measured from a linear fit to the data. In a model of fibrin polymerisation as proposed by Weisel *et al*. (30) this period corresponds to when protofibrils begin to aggregate laterally. Another study by Weisel *et al*. revealed that at the gel point, ~70% of fibres have reached their maximum length and 80% of branch points have formed while fibre diameter is less than 25% (121). Our data coupled with these observations indicate that the rapid increase in stiffness may be primarily due to radial fibre growth. In addition, Ryan *et al*. reported a strong correlation between fibrin diameter and clot stiffness (84).

The earliest time at which clot stiffness can be measured is ~2 minutes. This is due to the time taken to seal the microcell, transfer it to the microrheometer and locate a suitable particle. This point was defined as the initial stiffness (J_I) and represents the mechanical properties of the nascent network before it has undergone further structural changes. As mentioned, once the curve has reached a plateau, it is assumed all structural and mechanical changes have ceased and as such this point was defined as the final stiffness (J_F). Comparison of measurements taken immediately after clot stiffness has reached a plateau with those taken many hours later (~24 hours) revealed no difference in clot stiffness. These parameters will be subsequently used to quantity the mechanical changes in clot polymerisation.

4.5 Clot Stiffness and Network Inhomogeneity

The magnetic microrheometer is capable of producing forces in two dimensions. This x-y movement is ascribed the convention up, down, left and right corresponding to the direction the particle moves on the optical display. In order

to investigate any potential directional dependence of the stiffness, a particle embedded within a clot was manipulated in 2D as the clot formed and then after clotting was complete the variation in J_F was also investigated (see Figure 4-8). Note the polymerisation is measured from a single particle as the software is not capable of tracking multiple particles. Also, the final stiffness is measured from multiple particles distributed throughout a clot.

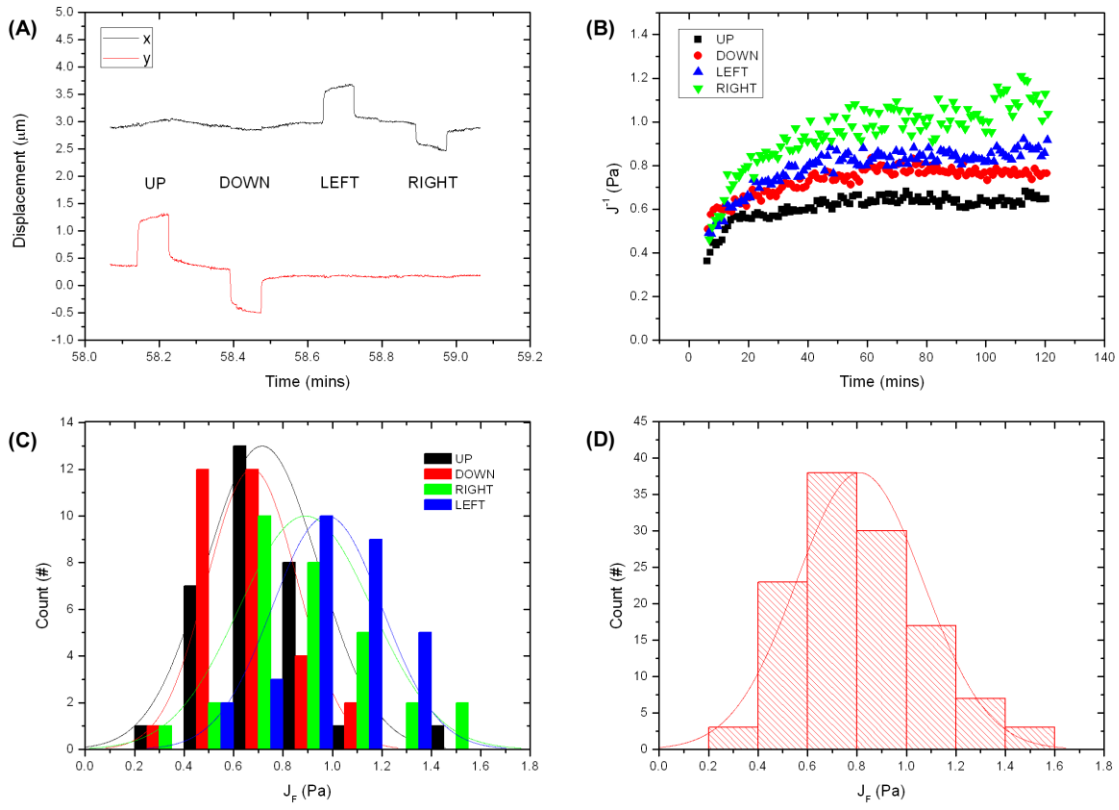

Figure 4-8: Clot stiffness and network inhomogeneity. (A) x and y displacement response of a single particle manipulated in 4 directions. The x displacement trace has been offset for clarity. **(B)** J^{-1} versus time measured in 4 directions over the first 2 hours of clotting for a single particle. **(C)** Histograms of J_F for the 4 different directions. Measurements were taken after 2 hours from multiple particles distributed throughout a clot; each particle is moved in 4 directions as in **(A)**. **(D)** Histogram of J_F for all 4 directions. Histograms are fitted with a normal distribution as a guide for the eye.

ERL fibrinogen at a concentration of 0.5 mg/ml was incubated with 2.5 mM $CaCl_2$ and magnetic particles. Thrombin was then added at a concentration of 0.5 U/ml. After this, force pulses were applied every 10 s for 5 s in four different directions

(see Figure 4-8(A)). Forces applied in the up and down directions produced a displacement in the y axis. Similarly, forces applied left and right only produced movement in the x axis. As described in section 4.4 clot stiffness is determined from this response and used to monitor clot stiffness over the first 2 hours of clotting (see Figure 4-8(B)). From the four traces, it is evident that a difference in stiffness is associated with each direction. Data from Figure 4-8(B) is presented in Table 4-2. There is a range of 0.15 Pa in the initial stiffness and this rises to 0.47 Pa in the final stiffness. The rate of change of stiffness varies by 0.012 $Pa.s^{-1}$ indicating polymerisation is also altered in different directions.

After 2 hours, the variation in the final stiffness was investigated by applying forces in four directions to multiple particles distributed throughout the clot. The results are presented in histogram form (see Figure 4-8(C)). Again, it is evident that a variation in stiffness is associated with the direction of the force. This could be an artefact due to some effect from the experimental setup. However, the trend seen in Figure 4-8(B) where right is stiffest followed by left then down and finally up being the weakest is not repeated. Similar trends between stiffness and direction were not observed in repeat experiments. This indicates the variation in stiffness arises due to differences which occur from repeated measurements of a physical system.

Table 4-2: Stiffness polymerisation data

Polymerisation Parameter	Up	Down	Left	Right	Average
J_I (Pa)	0.36	0.51	0.49	0.46	0.46 ± 0.03
J_F (Pa)	0.64	0.77	0.85	1.07	0.83 ± 0.09
dJ^{-1}/dt ($Pa.s^{-1}$)	0.020	0.022	0.014	0.026	0.021 ± 0.003

Inspection of confocal and SEM micrographs (Figure 4-2 and Figure 4-3) revealed that particles are embedded within an inhomogeneous fibrous network. Closer inspection of a single particle and the immediate surrounding fibre structure shows that the density of fibres varies around the particle. For example, in Figure 4-2, the particle located on the far left is surrounded by many fibres

except to its right where there are fewer fibres. If a force were applied in the right direction then the particle moves into the region of lower fibre density and could result in the particle displacing further, hence a lower stiffness would be measured. Alternatively, if the particle is anchored to the fibres to the left then the particle may be pulling on more fibres and it subsequently displaces less; hence greater clot stiffness is measured.

Typically, a particle was chosen and then forces were applied in one direction only. A clot was repeated at least 3 times depending upon the variation within the data. Now, each particle is moved in 4 different directions, this allows a greater proportion of the clot to be probed which subsequently results in greater data capture and better reproducibly of data. Figure 4-8(D) and Table 4-2 show the results of combining the data from multiple directions. For the final stiffness from multiple particles, a normal distribution was observed with a peak stiffness of 0.81 $\pm$ 0.02 Pa. The average final stiffness obtained from a single particle was 0.83 $\pm$ 0.09 Pa which agrees well.

The variation in mechanical properties may also be used as an indirect probe of clot structure. The mechanical properties of a clot are known to be highly dependent upon clot structure (33). For example, in a very homogeneous clot the variation in stiffness from particle to particle will be small with each particle measuring something close to that of the bulk stiffness. Contrary to this, a highly inhomogeneous clot where particles are located in regions of either high or low fibre density will result in a greater variation in stiffness being observed. In addition, it has been observed that fibres are much stiffer when stretching compared to bending (122). If a particle is attached or near a large fibre such that one direction may bend the fibre and another may stretch it then the observed stiffness could be substantially different. Hence, by comparing the variation in stiffness from particle to particle it may be possible to measure the degree of inhomogeneity within a clot.

For example, the fibrinogen variant $\gamma A/\gamma'$ is known to produce clots of an inhomogeneous structure compared with the highly uniform arrangement of fibres

within γA/γA clots. Thus, these clots provide a good test for the method outlined here. Clots were formed by the procedure detailed in section 4.4. In detail, clots were formed from 0.5 mg/ml fibrinogen, 2.5 mM $CaCl_2$, 1 mM FXIII inhibitor and 1.0 U/ml thrombin. After the required period of clotting, a particle was selected and then tested. In brief, a constant force pulse is applied to the particle for a time such that the particle stops displacing. Next, for every time point during the application of the force the compliance is calculated and then plotted as a function of time. The magnitude of the plateau compliance represents the mechanical properties of the clot on long times and therefore relates to the large-scale motion of the clot. In particular, this will be dependent upon the number/arrangement of fibres and branch points within the area surrounding the particle. In order to quantify the variation from particle-to-particle in the plateau compliance, the variance was computed. The variance indicates how spread out data is from one another.

There did not appear to be any differences in the variation between γA/γA and γA/γ′ clots. Additionally, data from microrheology experiments of purified fibrin clots where fibrinogen, thrombin and $CaCl_2$ concentrations were varied, which are known to modulate clot structure, was also analysed in this way. Again, no statistically significant difference in the variance was observed which would correlate with clot inhomogeneity. Itis suspected that the insensitivity of the microrheometer to these differences may be due to the size of the particle in relation to the characteristic network length scale. Inspection of Figure 4-2 and Figure 4-3 reveals that particles are within regions containing multiple fibres. As such when a particle strains the network it pulls on many fibres surrounding it which in turn pulls on more fibres which are attached to these fibres. Thus, the stiffness measured is close to that of the bulk stiffness of the clot. The difference in stiffness between particles distributed throughout a clot and the differences from manipulating them in multiple directions appears to be due to the fact that measurements of most physical systems result in measurements distributing normally around a mean central value.

4.6 Strain-hardening

As already seen there are different approaches to applying forces to investigate the mechanical properties of a clot. One can apply force pulses of increasing magnitude in order to test the Hookean response of a network e.g. $F = -kx$, where F is the magnitude of the force pulse, x is the particle displacement and k is the effective spring constant of the clot. Clots were prepared as described in section 2.2.4 with a final fibrinogen concentration of 0.1 mg/ml, $CaCl_2$ of 5 mM and thrombin concentration of 0.5 U/ml. Clots were allowed to form for 2 hours to ensure complete development of the mechanical properties. After this time, the clot was transferred to the magnetic microrheometer where 2 s force pulses were applied in 5 pN steps from 0 up to 80 pN. The subsequent stiffness was calculated and plotted as a function of displacement (see Figure 4-9).

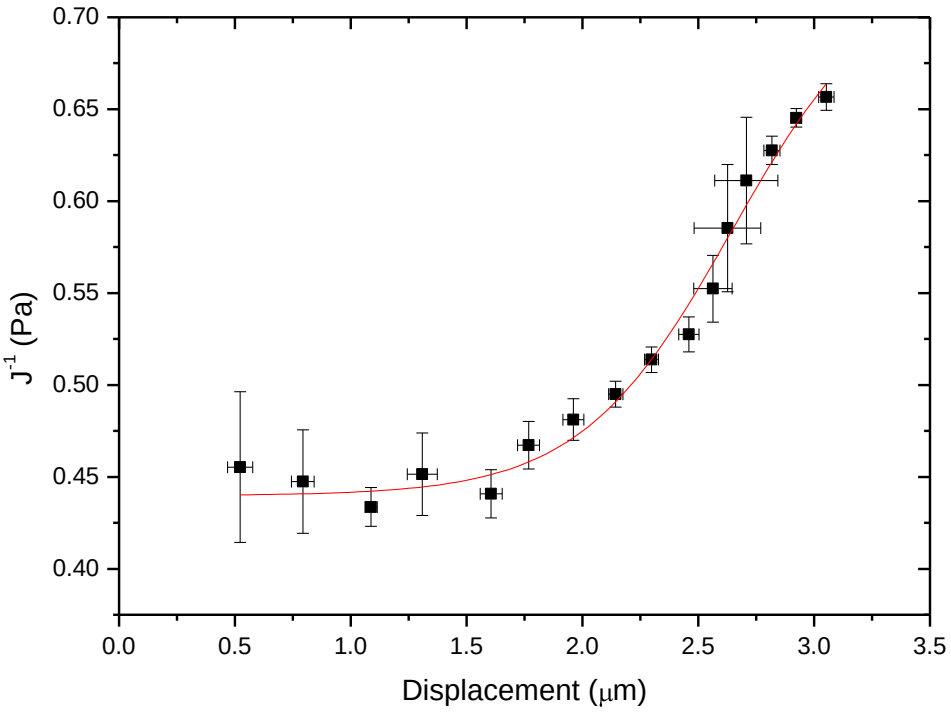

Figure 4-9: J^{-1} versus displacement of a clot displaying strain-hardening behaviour. The data is representative of 3 repeat measurements with error bars representing the standard error in the mean.

At least 5 particles distributed throughout each clot were selected and tested. It was observed that the stiffness remained constant up to bead displacements of around 2 μm, after which the stiffness began to increase as the force increased. From around 2 to 3 μm, the stiffness increased from ~0.45 Pa up to ~0.65 Pa representing an increase in stiffness of 1.4-times. It is evident from the data that fibrin clots display a non-linear elastic response and are undergoing strain-hardening.

The data presented in Figure 4-9 can be explained by several models proposed within the literature. Storm *et al*. (80) propose that reversible strain-hardening arises from the entropic response of the individual fibres. Under strain, fibres are removed from their thermodynamically stable state and the macroscopic non-linear behaviour of the clot is due to the collective response of all the fibres. The theory of Onck *et al*. (123) propose that strain-hardening arises from the stretching of fibres once they have become aligned under strain. Weigandt *et al*. (67) suggest that these models are not mutually exclusive and that both effects could be contributing to the strain-hardening response. However, Brown *et al*. report that in order to model strain-hardening, protein unfolding is required in order to fit the various models to the experimental data (81). In the framework of this model, up to displacements of ~2 μm the fibres bend and align along the direction of strain, protofibrils then untwist and then molecular domains begin to unfold. Once they have completely unfolded, the rapid rise in clot stiffness arises from the stretching of the unfolded protein chains.

The mechanism of irreversible deformation in fibrin clots is also currently unknown. Two theories have been proposed, firstly one in which the knob-hole bonds that hold fibrin molecules together break and then reform in a different location (90, 124, 125). And secondly, one where protofibrils can slip past one another and then reform bonds at different locations (13). The model proposed by Brown *et al.* (81) could explain irreversible deformation if refolding of the uncoiled domains was negligible.

Whatever the molecular mechanism of strain-hardening and irreversible deformation may be, it highlights the importance of working within the linear regime when studying fibrin clot mechanics. If for instance, a particular fibrin variant begins strain-hardening at lower strains compared to another then this would introduce complications when comparing the mechanical properties. Irreversibly deforming a clot may also alter its mechanical properties. As such, the mechanical properties of clots studied in this work have been performed within the linear strain regime. Also, as previously mentioned, when studying how clot stiffness varies over time the resulting displacement response is maintained as elastic as possible to ensure minimal sample deformation.

In addition, it was found that studying the behaviour of strain-hardening using the current experimental setup was not suitable. Due to the particularly low forces available with the magnetic microrheometer, the maximum displacements achievable are low; of the order of the bead radius. In the example above, very low fibrinogen levels were used, in order to produce a particularly weak network, which could be sufficiently strained. Despite this, the maximum displacement achieved was only around 3 μm.

4.7 Measuring the Frequency-Dependent Viscoelastic Moduli of Fibrin Clots

As mentioned in section 2.2.7, in order to measure the frequency-dependent viscoelastic moduli of materials, rheological measurements must be performed over a range of frequencies. In the case of single particle microrheology experiments, measurements must also be averaged from many different particles. This is extremely time consuming to perform and magnetic microrheometers can be limited to lower frequencies due to hysteresis effects of the magnets. Evans *et al.* provide a direct and straightforward mathematical procedure for obtaining the frequency-dependent storage and loss moduli from time-dependent experimental measurements (126).

In a creep-response measurement, as introduced in section 2.2.7, the time-dependent bead displacement is related to the time-dependent compliance through Equation 2-8. The relaxation modulus $G(t)$ is connected to the compliance $J(t)$ by a convolution (58):

$$\int_0^t G(\tau)J(t-\tau)d\tau = 1 \qquad \text{4-1}$$

where t is the time and τ is the lag time. The numerical inversion of this convolution is not a trivial task and typically involves working with the Laplace transform of Equation 4-1 (70):

$$\tilde{G}(s)\tilde{J}(s) = \frac{1}{s^2} \qquad \text{4-2}$$

where $\tilde{G}(t)$ and $\tilde{J}(t)$ are the Laplace transforms of $G(t)$ and $J(t)$ and s is the Laplace frequency. From Equation 4-2, if one function is given analytically then the other can be calculated via inverse Laplace transformation (126). The procedure of *Evans et al.* (127) bypasses this approach by working directly with the Fourier transform of the compliance. Since the complex modulus $G^*(\omega)$ is related to the relaxation modulus $G(t)$ via:

$$G^*(\omega) = F\left[\frac{dG(t)}{dt}\right] \qquad \text{4-3}$$

where *F[…]* denotes the Fourier transform, Equation 4-2 can be written as:

$$\tilde{G}^0(s) = \frac{1}{s\tilde{J}(s)} \qquad \text{4-4}$$

where $\tilde{G}^0(s)$ is the Laplace transform of the time derivative of the relaxation modulus $\dot{G}(t)$. Once $\tilde{J}(s)$ is known, the passage from $\tilde{G}^0(s)$ to $G^*(\omega)$ is

obtained by substituting the complex variable s with $i\omega$, where ω is the frequency:

$$G^*(\omega) = \frac{1}{i\omega\tilde{J}(i\omega)} \qquad 4\text{-}5$$

The determination of the quantity $\tilde{J}(i\omega)$ in this equation is the final step in obtaining the complex modulus and it represents the Fourier transform of the time-dependent compliance $J(t)$:

$$\tilde{J}(i\omega) = \int_{-\infty}^{+\infty} J(t)e^{-i\omega t}dt \qquad 4\text{-}6$$

Due to the condition that $J(t) = 0$ for $t \leq 0$ i.e. there is no response from the system before a stress is applied, then Equation 4-6 can be written as:

$$\tilde{J}(i\omega) = \int_{0}^{+\infty} J(t)e^{-i\omega t}dt \qquad 4\text{-}7$$

Due to the nature of $J(t)$, this integral diverges and therefore is not simple to solve. The procedure of Evans *et al*. (127) provides an analytical procedure which allows the calculation of Equation 4-7 once an analytical form of $J(t)$ is provided. This method requires only two conditions for $J(t)$. Firstly, that $J(t) = 0$ for $t \leq 0$, as mentioned, and secondly that in the $\lim_{t\to+\infty} J(t) \propto t$ (the long-time limit) the compliance asymptotes to a straight line with a gradient equal to the reciprocal of the steady-state viscosity, η^{-1}. In addition, there is no restriction upon the form of $J(t)$. Finally, the real and imaginary parts of Equation 4-5 represent the elastic and loss moduli respectively:

$$G^*(\omega) = G'(\omega) + iG''(\omega) \qquad 4\text{-}8$$

Figure 4-10 shows the data from a typical creep-compliance experiment performed using the magnetic microrheometer. The sample under investigation is a purified fibrin clot (discussed in detail in section 4.8). The method described here is applied to all clot types, e.g. plasma clots, studied throughout this work.

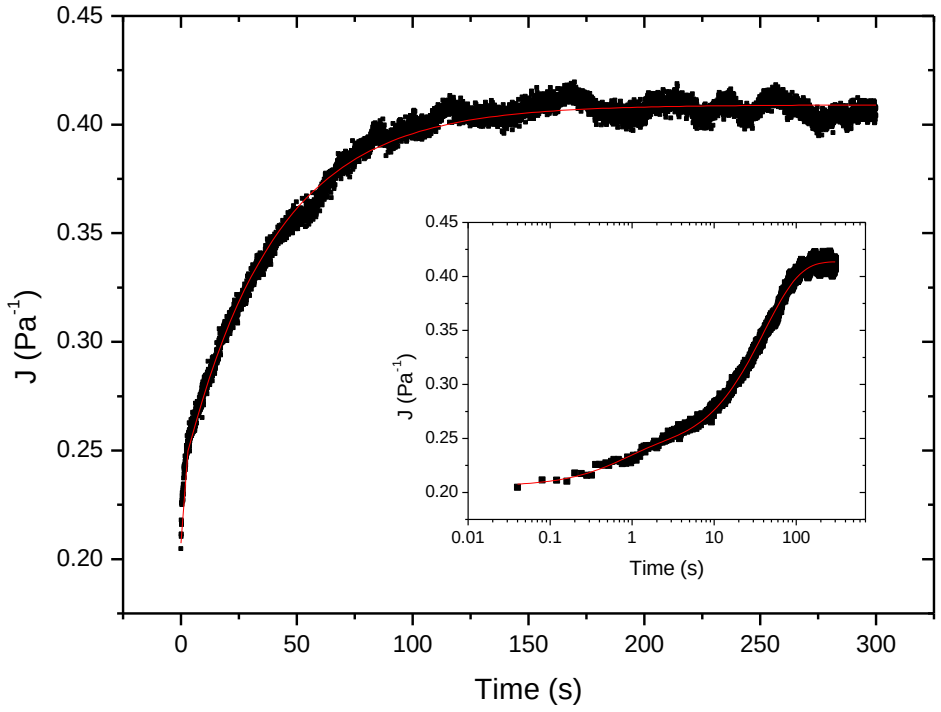

Figure 4-10: Creep-compliance versus time for a purified fibrin clot. Final clot concentrations were 0.6 mg/ml fibrinogen, 2.5 mM $CaCl_2$, 0.5 U/ml thrombin and 1 mM FXIII inhibitor. The red line is the best fit to the data using Equation 4-9. **Insert:** The same data but plotted on log-log axes.

The best fit to the experimental data in Figure 4-10 was performed by fitting the following equation:

$$J(t) = J_0 + \sum_{1}^{n} A_n e^{(-t/\tau_n)} \qquad 4\text{-}9$$

with n = 2 in this instance, n is varied to achieve the best fit to the data. J_0, A_n and τ_n represent the fitting parameters. The resulting analytical function $J(t)$ was

then used to solve Equations 4-7 and 4-5. Now the complex viscoelastic moduli can be extracted from equation 4-8. The result of this procedure is presented in Figure 4-11.

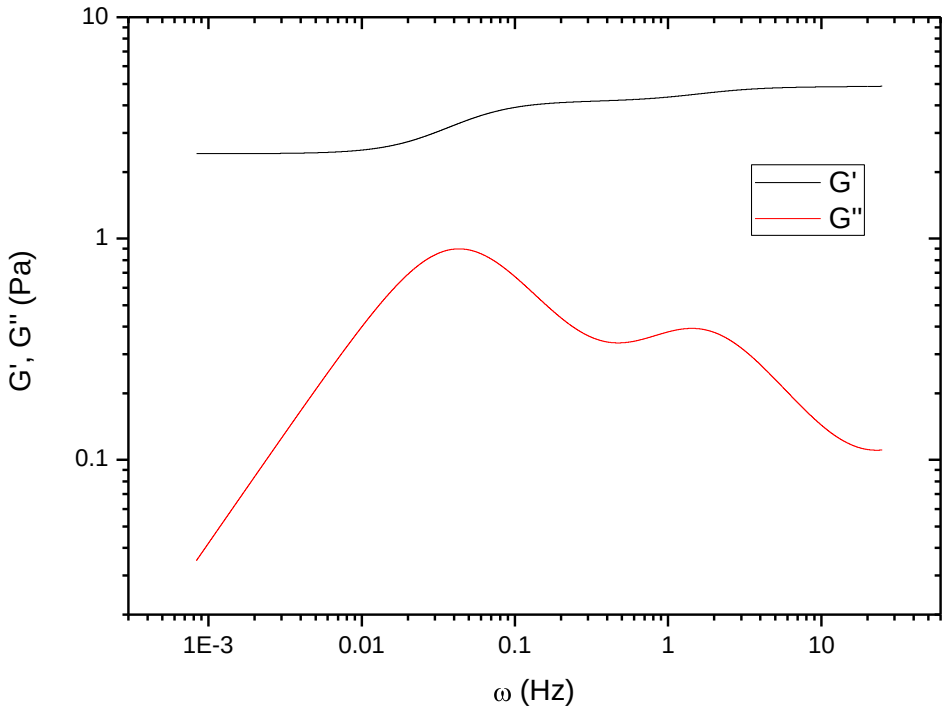

Figure 4-11: Storage (G′) and loss (G″) moduli versus frequency (ω) calculated from the data in Figure 4-10.

Using the procedure of Evans *et al*. (127), it is possible to measure the viscoelastic response of a material over a wide range of frequencies; the data in Figure 4-11 span a frequency window of 5 orders of magnitude. The lowest accessible frequency, $\omega_{min} \approx t_{max}^{-1}$ is determined by the duration of an experiment, t_{max}. This frequency can be expanded to lower frequencies once the terminal region, i.e. $J(t) \propto t$, has been reached. For oscillatory measurements, obtaining data at the same frequency would require several complete oscillations of multiple particles which would take considerably longer to perform. The highest accessible frequency, $\omega_{max} \approx t_{min}^{-1}$ is determined by the capture rate of the camera (25 Hz for all measurements presented here). For magnetic rheology, this is

particularly advantageous as hysteresis effects can hinder measurements at high frequencies. Another advantage of this approach is that any phase shift between bead displacement and the applied force does not play a role as the applied force is constant. The suitability of the procedure developed by *Evans et al*. (127) to study viscoelastic behaviour has been demonstrated by the successful application to a wide range of different systems from viscous liquids, such as glycerol, through to actin networks (128-132).

4.8 Stress Relaxation in Fibrin Clots

The procedure of Evans *et al.* (127) was applied to fibrin networks in order to extract the frequency dependent viscoelastic moduli. Clots were prepared as described in section 2.2.4 with a final fibrinogen concentration of 0.6 mg/ml, $CaCl_2$ of 2.5 mM and thrombin concentration of 0.5 U/ml. A synthetic inhibitor of FXIII (detailed in section 2.1) was included at a final concentration of 1 mM in order to inhibit cross-linking. Clots were allowed to form for 1 hour to ensure complete development of the mechanical properties. After this time the clot was transferred to the magnetic microrheometer. A constant force of 40 pN was applied for 300s and the displacement was measured. This data was used to calculate the compliance via Equation 2-8 for every time point throughout the experiment (see Figure 4-10). The steady-state viscosity is determined from the reciprocal of the gradient of the asymptote to $J(t)$ at long-times. From Figure 4-10 it is evident the steady-state viscosity approaches zero, and this is the case for all fibrin clots studied throughout this work. The initial value of the compliance, $J(0)$ is taken as the first measurable experimental point after the application of the force. This data in conjunction with the procedure of Evans *et al*. (127) was then used to compute the frequency dependent storage and loss moduli as described above. The result of this analysis is present in Figure 4-11.

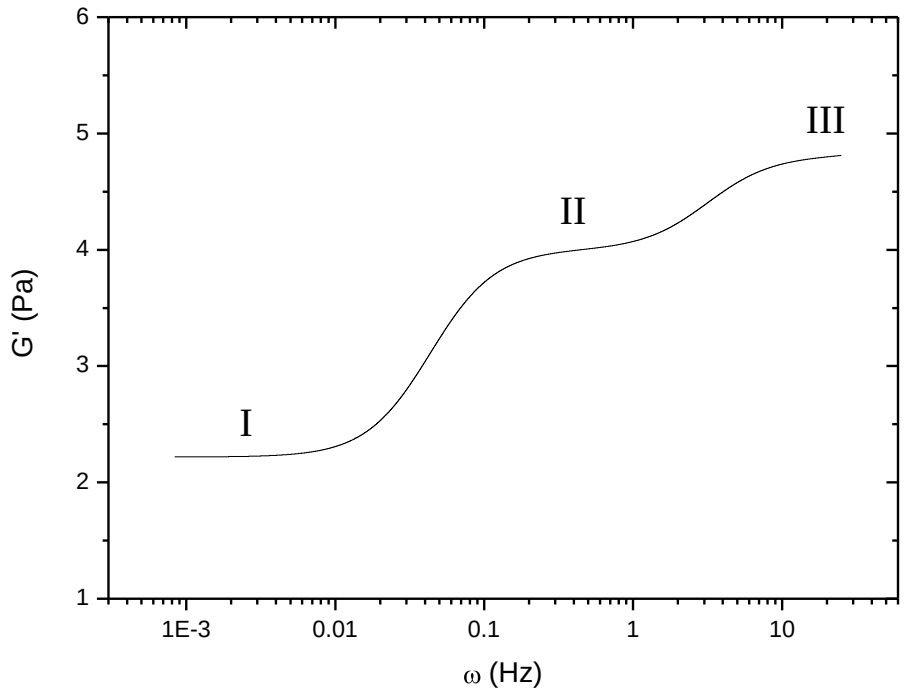

Figure 4-12: G′ vs. ω semi-log plot of a fibrin clot. Data taken from Figure 4-11. The roman numerals indicate three plateaus which represent stress relaxation mechanisms. Plateau I is orientation-dominated, plateau II is curvature-dominated and plateau III is tension-dominated, as predicted by the model of Morse (71).

The storage and loss moduli were measured over a frequency range of 0.0008 to 25 Hz. The storage modulus is approximately an order of magnitude higher than the loss modulus over the entire frequency range. This indicates the clot behaves predominately elastic on all times scales observed. A cross-over in the moduli i.e. G′′ > G′, would indicate the clot is behaving like a liquid and readily deforming. For all fibrin clots studied in this work no such cross-over behaviour was detected. The observation that on all timescales and for all fibrin types studied here the storage modulus is consistently higher than the loss modulus has interesting implications for *in vivo* clot behaviour. Within the circulatory system the rate of application of stress varies from <300 s^{-1} up to 2600 s^{-1} (60, 61). The observation that G′ > G′′ over a wide range of timescales ensures a clot maintains its integrity no matter what the rate of application of stress.

Unfortunately, it is not possible to test whether this behaviour continues up to physiologically relevant timescales as measurements at these frequencies were not possible with the current experimental setup. In addition, as time increases ($\omega < 0.01$ s^{-1}) G′ begins to plateau and G′′ diverges to smaller and smaller values. This indicates clots are highly stable on long timescales. Again, this behaviour is important physiologically as a clot must remain at the site of injury for a prolonged period until any damaged tissue is repaired.

The majority of studies conducted into the viscoelastic behaviour of fibrin clots report very little or no dependence of G′ upon frequency, see (67) for a recent example. In Figure 4-12 is a semi-log plot of the dependence of G′ upon frequency. It is evident that G′ varies with frequency and displays structure. Three plateaus at different frequencies can be identified: (I) $\omega < 0.01$, (II) $0.1 < \omega < 1$ and (III) $\omega > 10$. Each plateau corresponds to a different shear relaxation mode allowed on that timescale, as predicted by the model of Morse (71).

We can explain the stress relaxation processes occurring in fibrin within the framework of Morse's model. On long timescales (t > 100 s) plateau I corresponds to large scale motions of the fibres and branches, i.e. an orientational contribution arising from forces that resist movement of the entire fibre. We see a plateau in G′ and a divergence in G′′ as predicted by Morse for a network of branched fibres (71). Therefore, this plateau arises due to the fact that fibrin fibres form permanent branches with one another. Hudson *et al*. report on the stretching of 2D fibrin networks and find that on timescales up to 25 s, individual fibres and branch points can move distances of several micrometres (133). They also report that fibre strain-hardening acts to distribute strain equally throughout the network. The branch point therefore acts as a junction to distribute strain to other fibres. In addition, Carlisle *et al*. (34) report that fully cross-linked clots mainly fail by fibre rupture rather than branch point rupture. If one considers a branch junction of 3 fibres then if the branch point fails, all 3 fibres fail. However, if as observed, one of the fibres fails then 2 fibres are still connected which could maintain structural integrity. This demonstrates the important role branch points play in clot integrity. The data presented here also reveal the role

of branch points in the long-time elastic behaviour of fibrin networks and that they help clots maintain their integrity for prolonged periods of time.

Next, on intermediate timescales (1 s < t < 10 s), corresponding to plateau II, fibres are moving on length scales of the order of the fibre length i.e. distances between branch points. This is a curvature contribution which arises from forces that are opposing transverse deformation or rotation of the fibre. Here fibres are bending and twisting in response to an applied stress. This plateau will be dominated by the properties of the single fibres themselves and the density of branches.

Finally, on the shortest timescales (t < 0.1 s) corresponding to plateau III, fibres are compressing and stretching. This is a tension contribution which arises from tangential forces that resist stretching or compression of the fibre. Boal suggests this plateau will be dominated by molecular mechanisms. This could be either the unfolding of the coiled coil domains (81, 92, 134), the globular γ domain (135) or the αC connector region (136). It was not possible to measure the entire high frequency plateau, or any other higher frequency relaxation modes, as the acquisition rate of the optics limits higher frequency measurements. This plateau is predicted to scale with fibrinogen concentration as $G' \approx c^{2.5}$ by Mackintosh *et al*. (68), and this is tested in Chapter 5.

Liu *et al*. report on the mechanical properties of single fibrin fibres finding fibres show fast (2 - 4 s) and slow (49 - 57 s) stress relaxation times (137). They suggest these rates are due to molecular relaxation processes such as unfolding events; however they provide no further discussion. This appears at odds with the observations of Hudson *et al.* (82) and the model of Boal (69) whereby it is observed that individual fibres can move on these times and only molecular mechanisms can occur on very short times. The very short times observed by Liu *et al*. (86) could correspond to the high frequency plateau observed here with the longer times corresponding to the intermediate plateau. Differences in times could be related to the differing experimental conditions and technique used. The observation of relaxation behaviour on very long times i.e. t > 100 s, may not be

observed in the experiments of Liu *et al*. (86) as the fibre is fixed to a substrate and therefore the branches, which would normally be present, cannot move. However, it is clear from this work, and that presented within the literature, that fibrin displays multiple relaxation mechanisms on distinctly different timescales.

The various calculations by Morse of loosely- and tightly entangled and coil-like and rod-like solutions predict that each stress relaxation mode forms a hierarchy in which $G_{tens} > G_{curve} > G_{orient}$ and that each should occur on different timescales in which $\tau_{tens} < \tau_{curve} < \tau_{orient}$. Both conditions are satisfied by the data presented in Figure 4-12, and in addition all other measurements throughout this work also agree with this prediction.

The apparent discrepancy between the behaviour of G′ presented here and those presented throughout the literature appear somewhat surprising. As mentioned several authors (41, 44, 45, 67, 77) have reported measurements of $G'(\omega)$ and $G''(\omega)$ by conventional rheometry, spanning a frequency range of $\omega = 10^{-4} – 10^{4}$ Hz. However, all these studies report a single plateau in G′ and not allobserve the long-time elastic behaviour predicted by Morse's model for branched networks i.e. G′ >> G′′ as $t \rightarrow \infty$. Similar discrepancies between the results of conventional rheometry and microrheometry have been reported for studies of actin networks. Although in this instance it appears that differences arise due to microrheological techniques having the ability to access much higher frequencies. Disagreement between our results and those from the literature could be due to the differing experimental conditions used. In most studies the fibrinogen concentration is much higher than that used here; 0.6 vs. >2 mg/ml. Measurements presented in Chapter 5 reveal that at higher fibrinogen levels plateau I extends over a much broader frequency range. If this trend continued we predict that at fibrinogen levels above 2 mg/ml we would observe similar behaviour to that reported by other authors. Also, it may well be that differences arise due to the nature of the microrheological technique used.

4.9 The Effects of FXIII on Fibrin Clot Viscoelasticity

In order to assess the validity of the current experimental setup and technique the effect of FXIII on clot mechanical properties, which has been widely reported upon in the literature (29, 62, 66, 75, 79, 124, 138-143), was tested. Clots were prepared as described in section 2.2.4 with a final ERL fibrinogen concentration of 0.6 mg/ml and $CaCl_2$ of 2.5 mM. For complete cross-linking, clots were formed with a final FXIII concentration of 3.7 µg/ml. Again, the synthetic inhibitor of FXIII was included at a final concentration of 1 mM in order to inhibit cross-linking. This inhibitor has been used in other studies (33, 122) to successfully inhibit cross-linking. Thrombin was then added at a final concentration of 0.5 U/ml, after which force pulses were applied every 10 s for 2 s until a plateau in J^{-1} was observed.

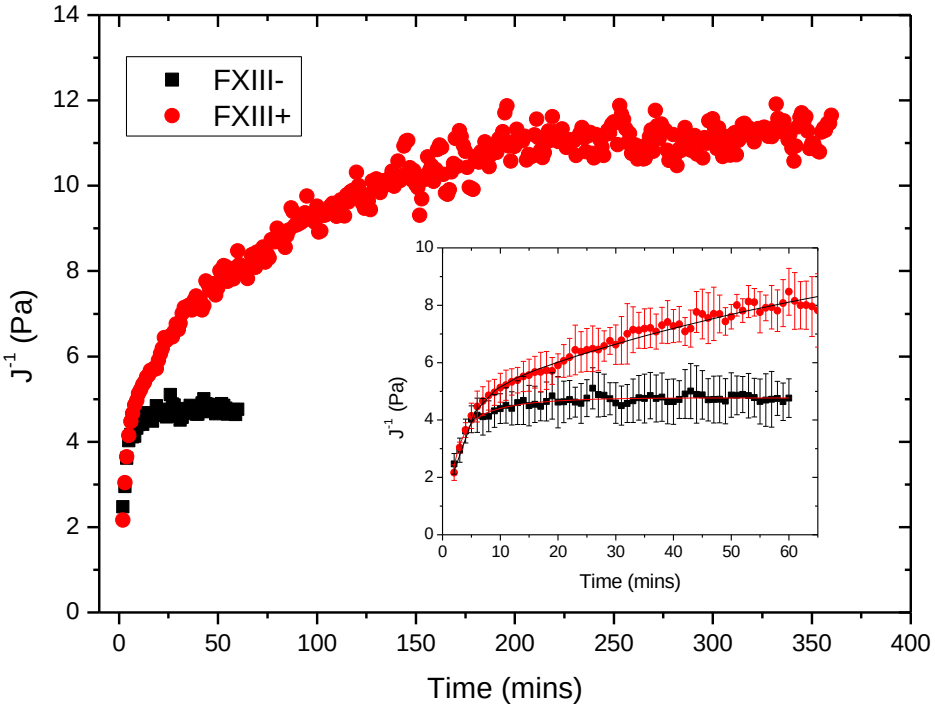

Figure 4-13: J^{-1} vs. time of clots formed with and without FXIII. Insert: J^{-1} vs. time over the 1st hour of clotting. Errors represent the standard error in the mean from 3 repeat measurements. Errors have been omitted from the main plot for clarity.

The results are displayed in Figure 4-13 and analysis is presented in Table 4-3. A plateau in J^{-1} was observed after ~20 mins in clots without cross-linking while cross-linked clots continued to increase in stiffness up to 6 hours. Cross-linking was studied using SDS-PAGE analysis in clots formed from γA/γA and γA/γ′ fibrinogen (Chapter 6) under very similar clotting conditions (0.5 mg/ml fibrinogen, 2.5 mM $CaCl_2$, 3.7 µg/ml FXIII and 1.0 U/ml thrombin). Disappearance of the α and γ chain monomers, indicating the cross-linking of these chains, in conjunction with the appearance of cross-linking products was observed at times up to 6 hours. This correlates extremely well with the observation that cross-linked clots continue to increase in stiffness on long times after the initiation of clotting. In addition, very little difference in polymerisation and clot stiffness is observed at the earliest times (see Figure 4-13 and Table 4-3). At times <5 minutes very little disappearance of the γ chain monomers has occurred and virtually no α chain monomer has disappeared due to cross-linking. Subsequent increases in clot stiffness occur due to the formation of cross-links. Once the plateau in J^{-1} was reached, the final compliance of both clots was measured and found to be 2.3-times higher in cross-linked clots, indicating a mechanically stiffer clot.

Table 4-3: Stiffness polymerisation data of clots formed with and without FXIII

Polymerisation Parameter	FXIII-	FXIII+
dJ^{-1}/dt ($Pa.s^{-1}$)	0.4 ± 0.1	0.57 ± 0.08
J_I (Pa)	2.5 ± 0.4	2.2 ± 0.3
J_F (Pa)	4.8 ± 0.8	11 ± 1
Plateau time (mins)	12 ± 2	197 ± 18

Next, the frequency dependent viscoelastic moduli were measured by the procedure detailed in section 4.7. The results are displayed in Figure 4-14. The effect of FXIII was to increase the storage and loss modulus on all timescales observed. The storage and loss moduli were extracted at frequency values of 8×10^{-4}, 0.5 and 20 Hz (Table 4-4). The 1st frequency was chosen in order to extract the plateau modulus, G'_0 which is defined as $G'_0 = G'(\omega)$ at a frequency for which

tan(δ) = G′′(ω) / G′(ω) is a minimum (70). The 2nd and 3rd frequencies were chosen in order to determine the effect of FXIII on the intermediate and high frequency plateaus.

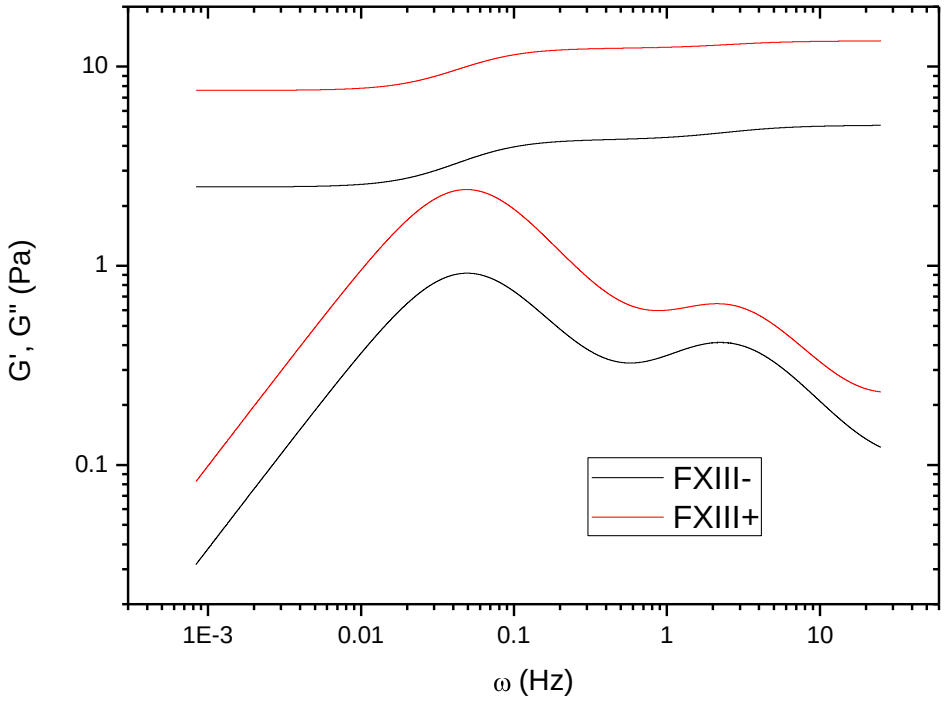

Figure 4-14: G′ and G′′ vs. ω of clots formed with and without FXIII.

An increase in the storage modulus, ranging between 2.7- and 3.1-times, at all 3 frequencies was observed in the presence of FXIII. The loss modulus increased between 1.6- and 2.6-times in the presence of FXIII. The increase in the storage over the loss modulus resulted in an increase in the loss tangent, in the absence of FXIII, by 1.2- to 1.7-times. This indicates that cross-linking increases clot stiffness and reduces viscous creep, rendering a clot more mechanically stable. Studies into the effect of FXIII on clot rheology using bulk techniques reveal cross-linking is associated with a 2- to 3.5-times increase in G′ (33, 75, 143). This demonstrates the suitability of the current experimental technique in order to study the viscoelastic behaviour of fibrin clots.

In addition, the presence of cross-linking did not significantly alter the stress relaxation behaviour of fibrin. The timescales for which the plateaus in G′ occur were not significantly altered. Similar observations were also reported by Liu *et al.* (86). These observations suggest that cross-linking does not alter the dynamics of fibrin clot behaviour. The effect of cross-linking is only to make a clot stiffer and less extensible. The effect of FXIII on clot structure has been investigated by Ryan *et al.* (84) who report an increase in fibre length and a decrease in fibre diameter, while fibre and branch point density remain unaffected. As the overall clot architecture remains essentially unchanged this most likely explains the insensitivity of the fibre dynamics to FXIII cross-linking.

Table 4-4: Viscoelastic data of clots formed with and without FXIII

Viscoelastic Parameter	**FXIII-**			**FXIII+**		
Frequency (Hz)	8×10^{-4}	0.5	20	8×10^{-4}	0.5	20
G′ (Pa)	2.5 ± 0.3	4.3 ± 0.3	5.0 ± 0.3	7.6 ± 0.1	12.4 ± 0.6	13.4 ± 0.8
G″ (Pa)	0.032 ± 0.003	0.33 ± 0.05	0.21 ± 0.05	0.08 ± 0.03	0.7 ± 0.1	0.33 ± 0.04
tanδ	0.013 ± 0.002	0.08 ± 0.01	0.04 ± 0.01	0.011 ± 0.004	0.05 ± 0.01	0.025 ± 0.004

Finally, the frequency behaviour of the loss tangent was also calculated and the results are displayed in Figure 4-15. In the presence and absence of cross-linking there is a dramatic peak in the loss tangent at ~0.04 Hz. A much smaller, 2nd peak occurs at ~2 Hz. In the absence of cross-linking there is a rapid increase in the loss tangent from 0.013 up to ~0.28. This represents a 22-times increase in the loss modulus. In the presence of cross-linking the loss tangent increases from 0.011 up to ~0.25; increasing 23-times. The loss tangent in clots without cross-linking is still higher by 1.1-times. The 2nd peak however is more dramatically affected by the presence of FXIII. In the absence of FXIII this peak is ~0.09 and in the presence of FXIII this falls to ~0.05; a decrease of around 1.8-times.

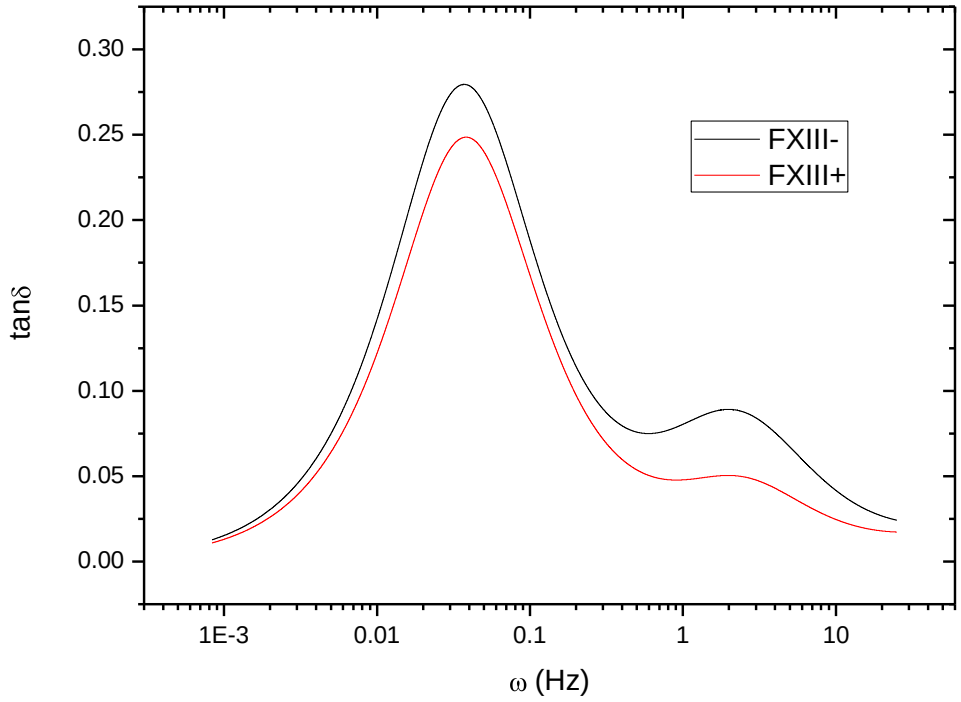

Figure 4-15: tanδ vs. ω semi-log plot of clots formed with and without FXIII.

These peaks coincide with the transitions between different stress relaxation modes. It appears that if clots are stressed on these timescales then the amount of deformation a clot undergoes is rapidly increased. These results suggest that when clots are stressed on these timescales they are unable to dissipate the stress and therefore readily deform. This highlights a weakness in fibrin clots ability to dissipate stress and could be a potential mechanism for embolism.

In addition, this highlights the important of performing viscoelastic measurements over a range of frequencies. Typically, most studies within the literature take measurements at one specific frequency. From the data, it could be inferred that fibrin clots are highly resilient to mechanical deformation as evidenced by their extremely small loss tangents. For instance, in an elastic solid tanδ << 0, therefore measurements taken on long times would indicate fibrin clots are behaving essentially elastic and do not display a large degree of viscous deformation. However, when considering measurements taken at frequencies of

~0.04 Hz this picture rapidly changes. The loss tangent begins to approach a significant fraction of unity, i.e. $\tan\delta = 1$, at which point clots are storing and dissipating similar amounts of energy and as such undergoing significant degrees of deformation. These observations highlight the importance of performing multi frequency measurements.

Chapter 5

5 Fibrin Clot Microrheology

5.1 Introduction

The aim of the work presented in this chapter was to investigate the effects of fibrinogen, thrombin and $CaCl_2$ concentrations on the viscoelastic properties of fibrin clots.

5.2 Fibrinogen Concentration

The effects of fibrinogen concentration on clot viscoelasticity were investigated using the magnetic microrheometer. The following concentrations were tested: 0, 0.2, 0.4, 0.6, 0.8 and 1 mg/ml. Clots were formed as described in section 2.2.4 with a final thrombin concentration of 0.5 U/ml, $CaCl_2$ concentration of 2.5 mM and FXIII inhibitor concentration of 1 mM. These clotting conditions, and

those subsequently used for thrombin and $CaCl_2$ experiments, were dictated by the effective working limits of the magnetic microrheometer. For instance, fibrinogen concentration is limited to ~1 mg/ml, above this concentration the clot becomes extremely stiff and as such the device is operating at maximum force in order to produce particle displacements with sufficient signal-to-noise.

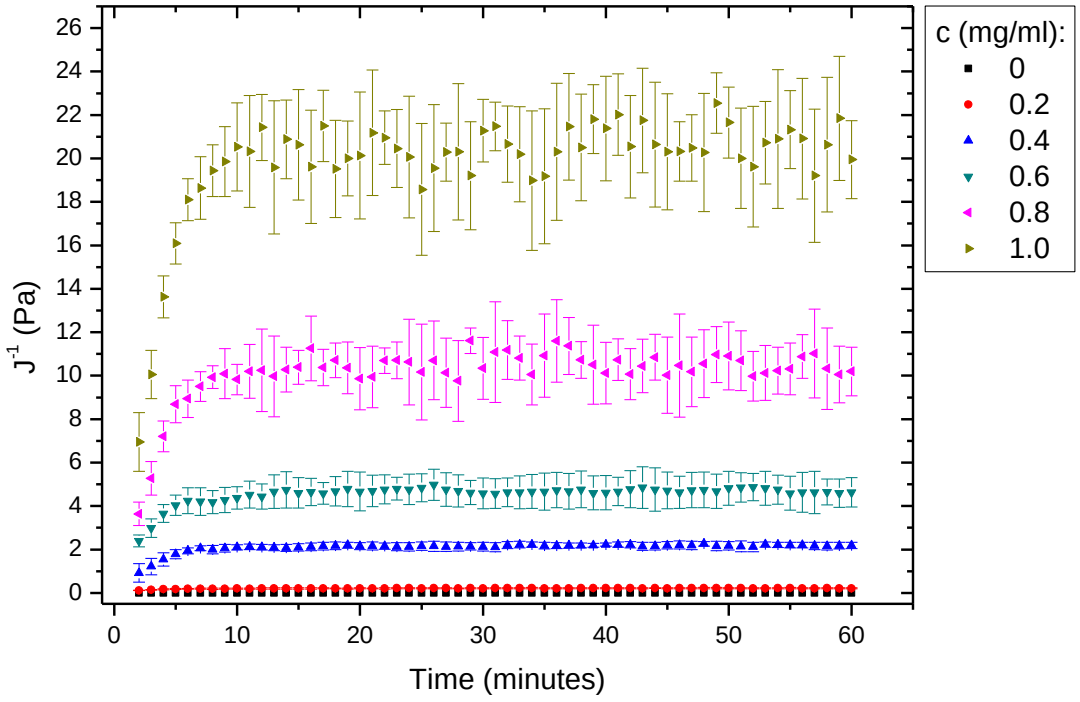

Figure 5-1: J^{-1} versus time for clots formed from different fibrinogen concentrations. Measurements were performed over the 1st hour of clotting. Fibrinogen concentration is displayed in the legend. Errors represent the standard error in the mean from 3 repeat measurements.

After the addition of thrombin, clots were transferred to the magnetic microrheometer and force pulses were applied. Pulses of 2 seconds in duration were applied every 10 seconds over the first hour of clotting. The magnitude of the force pulse is dictated by the stiffness of the network and the need to maintain a balance between sufficient signal-to-noise and minimising sample deformation. The results of these experiments are presented in Figure 5-1 and analysis is provided in Figure 5-2.

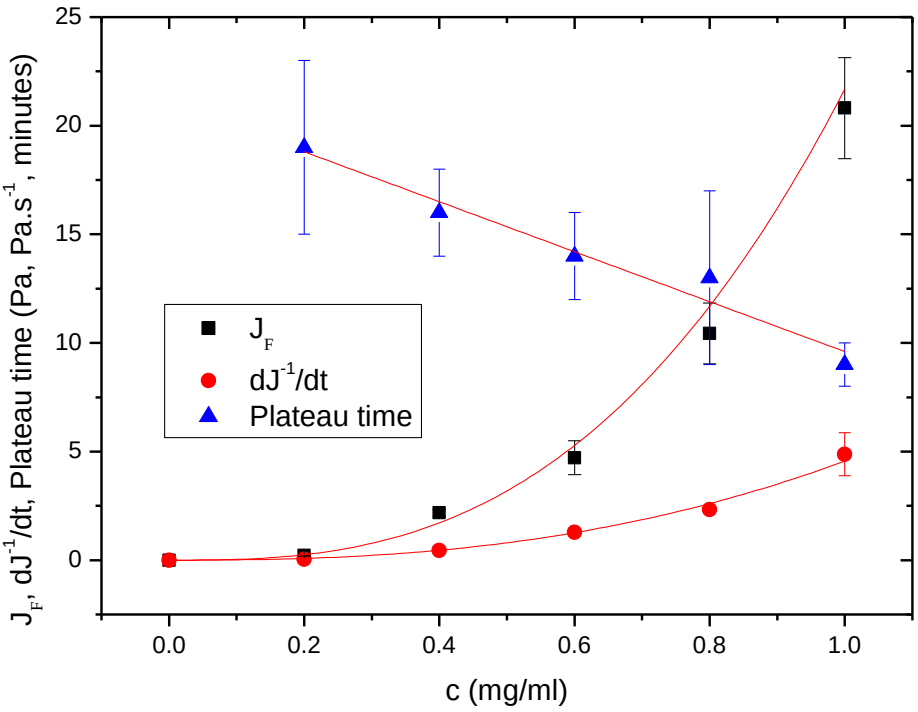

Figure 5-2: J_F, dJ^{-1}/dt and plateau time versus fibrinogen concentration. Data extracted from Figure 5-1. The J_F and dJ^{-1}/dt data have been fitted with a power law equation of the form $y \approx c^p$, where y is the measured experimental quantity, c is the fibrinogen concentration and p is the power. The plateau time data has been fit with a linear equation of the form y = mc + k, where m is the gradient and k is the intercept. dJ^{-1}/dt was calculated over the 1st minute of clotting. Errors represent the standard error in the mean from 3 repeat measurements.

A clotting period of 1 hour was more than sufficient to ensure complete mechanical development of all fibrinogen concentrations under investigation. In fact, by around 20 minutes a plateau in J^{-1} was observed for all fibrinogen concentrations (Figure 5-2). As expected no clot formation was detected at 0 mg/ml fibrinogen concentration. As the fibrinogen levels increased the final compliance increased rapidly; the data are fit by a power law relationship with $J_F \approx c^{2.9 \pm 0.1}$. For a 5-times increase in fibrinogen concentration this resulted in a 100-times increase in the final compliance. In addition, the rate of change of compliance also increased with increasing fibrinogen levels. Again, the data were well fit by a power law relationship with $dJ^{-1}/dt \approx c^{2.8 \pm 0.4}$. Similarly, for a 5-times increase in fibrinogen concentration this resulted in a 129-times increase

in the rate of change of compliance. The increased rate of mechanical development at higher fibrinogen levels is also reflected in the plateau time which decreased as fibrinogen concentration increased. The plateau time falls by ~10 minutes over the entire fibrinogen concentration range. The data presented here reveal clot polymerisation and mechanical properties are dramatically affected by small variations in fibrinogen concentration.

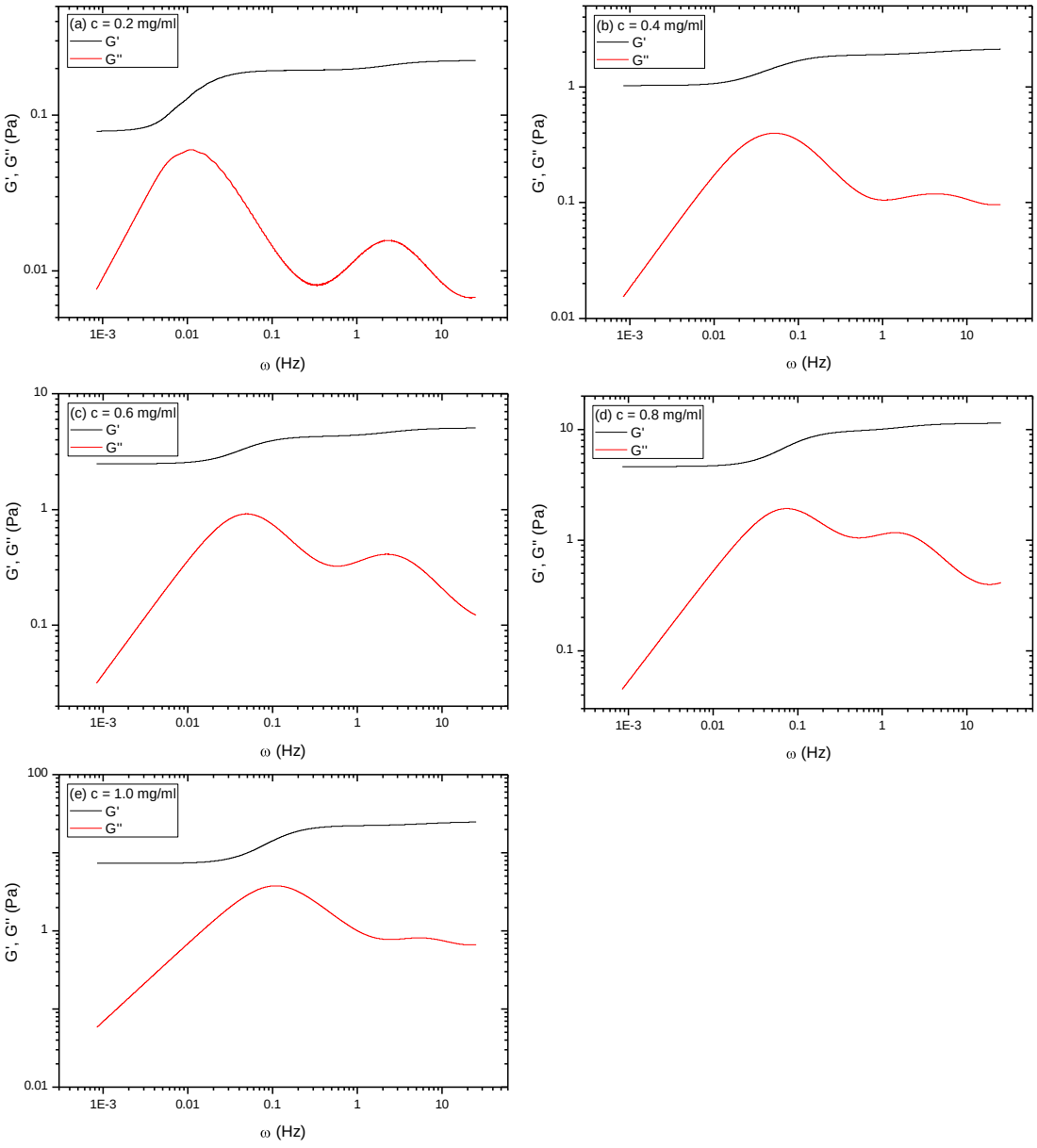

Figure 5-3 a - e: Storage and loss moduli versus frequency for clots formed at different fibrinogen concentrations. Data represent the average from 3 repeat experiments.

After a clotting period of 1 hour, the frequency dependent viscoelastic moduli were measured as described in section 4.6. The results of this analysis are displayed in Figure 5-3. The storage and loss moduli were measured over a frequency range of 0.0008 to 25 Hz. At all fibrinogen concentrations the storage modulus varied with frequency displaying three plateaus; as previously discussed in section 4.7. Again, the storage modulus was consistently higher than the loss modulus for all frequencies, indicating predominately elastic behaviour. On long-times the loss modulus diverged becoming smaller and smaller while the storage modulus reached a plateau. In order to identify the effect of fibrinogen on the different stress contributions to $G^*(\omega)$ the storage and loss moduli were extracted at 3 specific frequency values of 8×10^{-4}, 0.5 and 20 Hz corresponding to the low (hereafter I), intermediate (II) and high (III) frequency plateaus respectively. The results of this analysis are displayed in Figure 5-4.

As fibrinogen concentration increased the storage modulus increased rapidly at all frequencies. For a 5-times increase in fibrinogen concentration this resulted in a 95- to 110-times increase in the storage modulus. The dependence of the storage modulus on fibrinogen concentration was fit by a power law relationship with $G'_{I} \approx c^{2.2 \pm 0.2}$, $G'_{II} \approx c^{2.\ 8 \pm 0.2}$ and $G'_{III} \approx c^{2.7 \pm 0.2}$. Plateau III was predicted by Mackintosh *et al*. (68) to scale with concentration as $G' \approx c^{2.5}$ for branched networks of semi-flexible fibres. The value obtained in this work is slightly higher than this but still in agreement, within experimental errors, for the expected dependence. Figure 5-5 displays a plot of the data to the expected dependence and reveals good agreement between the data and the prediction. The inserts in Figure 5-4 are log-log plots and reveal good agreement between the experimental data the power law fits. There is some discrepancy between the storage modulus data and the fit at a fibrinogen concentration of 0.2 mg/ml for plateau I. This concentration was repeated but didn't result in any improvement to the fit. However, overall the data agrees extremely well with a power law relationship predicted by MacKintosh *et al*. (68).

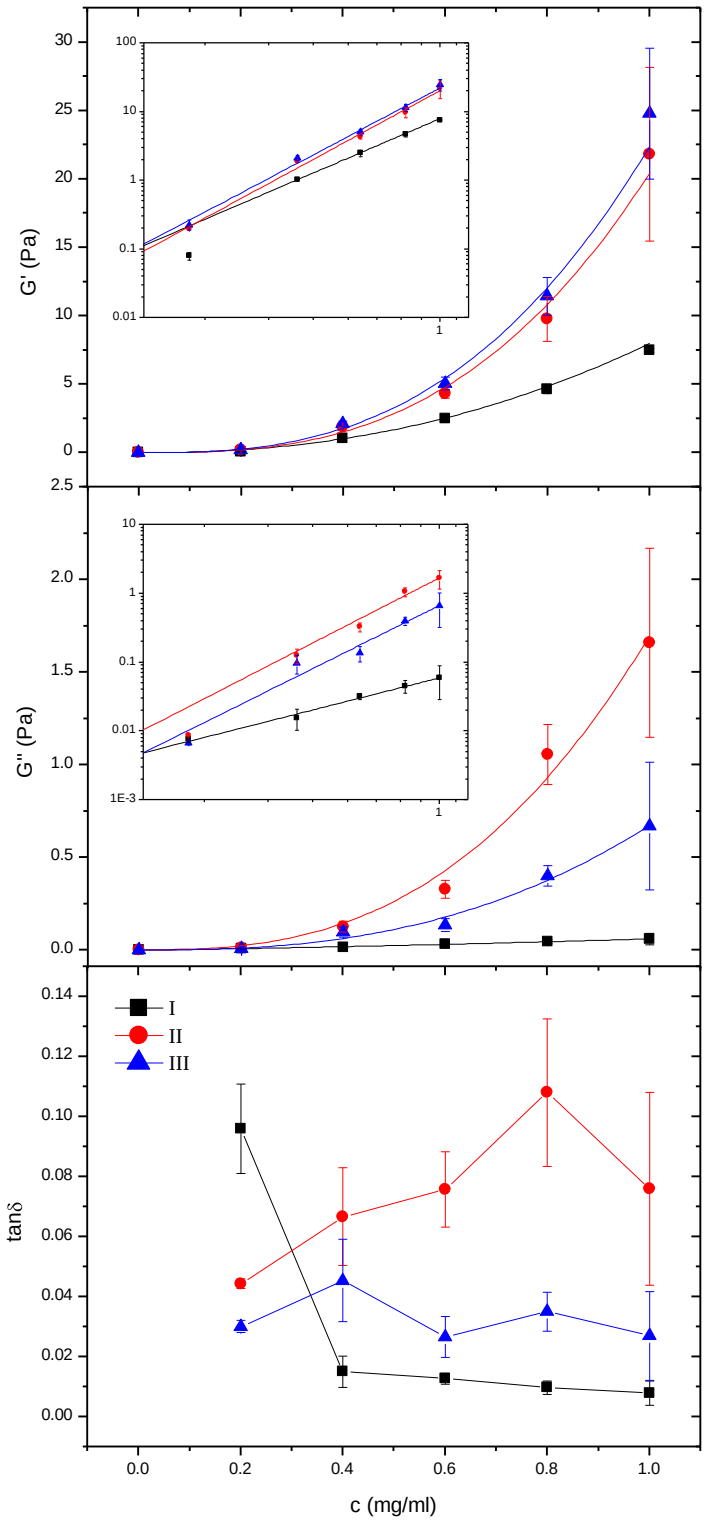

Figure 5-4: Storage modulus, loss modulus and loss tangent versus fibrinogen concentration. Data were extracted from Figure 5-3 at 3 specific frequency values; I 8 x10^{-4} (orient), II 0.5 (curvature) and III 20 (tension) Hz. Inserts depict log-log plots of the data. For G′ and G′′ the data has been fitted with the same power law relationship as in Figure 5-2. In the plot of tanδ vs. concentration the data points are joined by a linear extrapolation which is

included as a guide for the eye. Errors represent the standard error in the mean from 3 repeat experiments.

At all frequencies, the loss modulus was consistently lower than the storage modulus ranging between 10- to 130-times. The loss modulus also displayed similar behaviour to the storage modulus; increasing as fibrinogen concentration increased. For a 5-times increase in fibrinogen concentration this resulted in an 8- to 190-times increase in the loss modulus. Again, the data were fit by power law relationships with $G''_{I} \approx c^{1.32 \pm 0.07}$, $G''_{II} \approx c^{2.7 \pm 0.3}$ and $G''_{III} \approx c^{2.6 \pm 0.2}$.

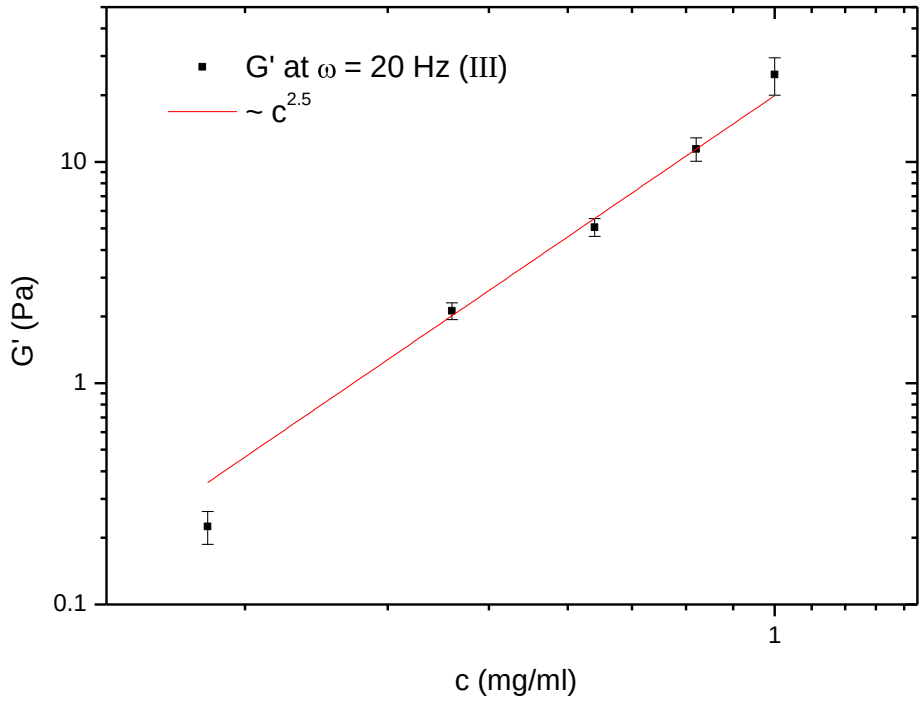

Figure 5-5: Storage modulus versus fibrinogen concentration. The storage modulus data is that in Figure 5-4 extracted at a frequency value of 20 Hz (III). The red line is the scale prediction of Mackintosh *et al*. (68) of $G' \sim c^{2.5}$. Note essentially good agreement between the data and this prediction. Errors represent the standard error in the mean from 3 repeat experiments.

For plateau I, the loss tangent decreased as fibrinogen concentration increased. At 0.2 mg/ml fibrinogen concentration the loss tangent was ~0.1 and then falls rapidly by a factor of 10, after which it remained constant, within experimental

errors, as fibrinogen concentration increased. This initial dramatic fall could be due to the lower value observed for the storage modulus, thus the loss tangent at 0.2 mg/ml is higher. In addition, the loss tangent for plateau III also remained essentially constant, within experimental errors, over the entire fibrinogen concentration range. For plateau II however the loss tangent increased up to a fibrinogen concentration of 0.8 mg/ml, after which it reduced. Overall however, the loss modulus remained essentially constant within experimental errors. It is expected that the loss tangent would begin to decrease due to the higher power dependence of the storage modulus over the loss modulus (I: 2.2 vs. 1.32). Note the loss tangent could not be calculated for clots containing no fibrinogen.

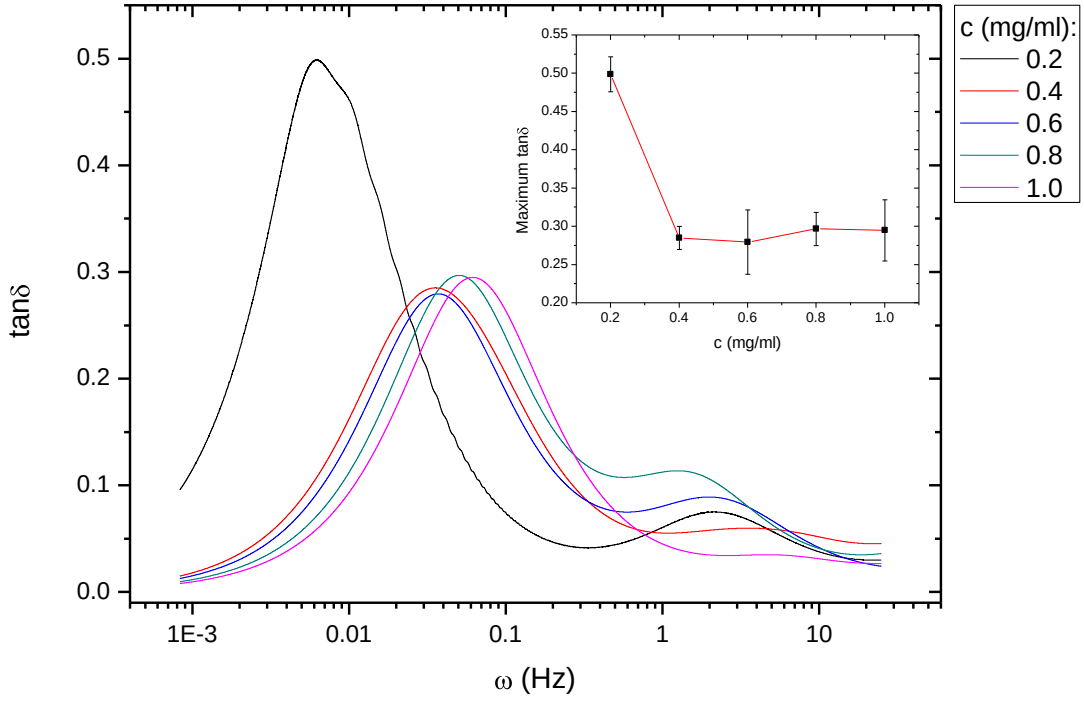

Figure 5-6: tanδ versus ω for clots formed at different fibrinogen concentrations. Insert: maximum tanδ vs. fibrinogen concentration. A linear extrapolation is included as a guide for the eye. Errors represent the standard error in the mean from 3 repeat experiments.

The dependence of the loss tangent on frequency as fibrinogen concentration is varied is displayed in Figure 5-6. Again, peaks in the behaviour of the loss tangent were observed. The maximum loss tangent was approximately a factor of 10 higher than the loss tangents displayed in Figure 5-4 and displayed very

similar behaviour as fibrinogen concentration increased. There was initially a dramatic fall in the loss tangent, as for plateau I, after which it remained constant. At 1 mg/ml fibrinogen concentration the loss tangent was 1.7-times smaller than at 0.2 mg/ml concentration. In addition, it was observed that the peak in the loss tangent was shifted to higher frequencies as fibrinogen levels increased. For example, the maximum loss tangent in clots formed at 0.2 mg/ml fibrinogen occurs at ~6 mHz while clots formed at 1.0 mg/ml the peak is shifted up to a frequency of ~70 mHz. Thus, the maximum loss tangent occurs on very different timescales; the order of minutes in clots formed at low fibrinogen levels compared to seconds for those formed at higher levels.

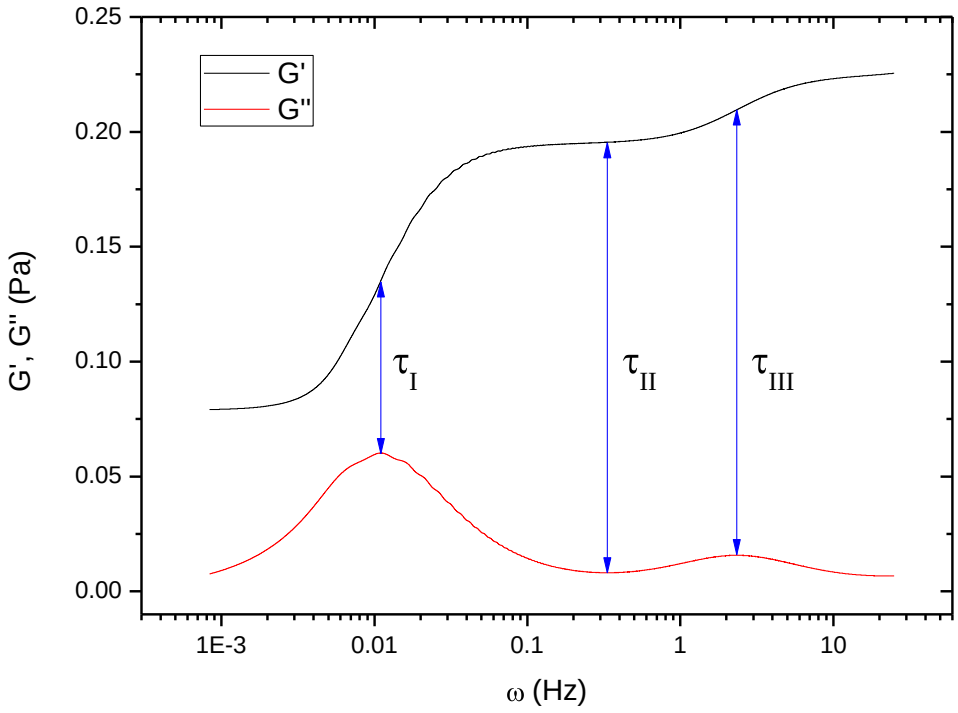

Figure 5-7: G′ and G′′ versus frequency. Clots were formed at 0.2 mg/ml fibrinogen, 0.5 U/ml thrombin, 2.5 mM $CaCl_2$ and 1 mM FXIII inhibitor. Note the plot is a linear-log plot in order to emphasize changes in the behaviour of the storage modulus. The blue arrows indicate the association between changes in the storage and loss moduli. τ_I is the time of the 1st turning point in G′′ and corresponds to the low-to-intermediate plateau transition in G′. τ_{II} is the time of the 2nd turning point in G′′ and corresponds to the intermediate plateau in G′. τ_{III} is the time of the 3rd turning point in G′′ and corresponds to the intermediate-to-high plateau transition in G′.

Analysis of the plots in Figure 5-3 reveals that fibrinogen modulates the viscoelastic dynamics of fibrin clots. Figure 5-7 reveals the association between the behaviour of the storage and loss moduli. A change in the storage modulus is accompanied by a change in the loss modulus. For example, the change between the low frequency plateau and the intermediate plateau in the storage modulus is associated with a turning point in the loss modulus and occurs within the middle of this transition. Two further turning points are associated with the intermediate plateau and the transition up to the higher frequency plateau. Due to the frequency limit of the magnetic microrheometer, as previously discussed, it is not possible to completely resolve this plateau however the transition up to this plateau can be seen. The temporal position of these turning points, designated τ_I, τ_{II} and τ_{III}, will be calculated ($\tau_n = 1 / \omega_n$) and used to quantify changes in the stress relaxation behaviour of fibrin clots as fibrinogen levels are varied (Figure 5-8).

The position of the low-to-intermediate plateau transition, given by τ_I, decreased as fibrinogen concentration increased. Initially, there was a dramatic fall of ~80 seconds as fibrinogen concentration increased from 0.2 to 0.4 mg/ml. After this τ_I continued to fall as fibrinogen levels increased, albeit less rapidly, decreasing a further 10 seconds as fibrinogen concentration reach 1.0 mg/ml. Overall, τ_I decreased ~10-times over the entire fibrinogen concentration range. As the low-to-intermediate plateau transition moves to shorter times, i.e. higher frequencies, the low frequency plateau extends over a longer time range. This results in the low frequency plateau occurring on shorter time-scales. Clots formed at 0.2 mg/ml fibrinogen plateau at ~1 mHz, as fibrinogen concentration increased up to 1.0 mg/ml this plateau begins at ~4 mHz; a time difference of ~10 minutes. Thus, as fibrinogen concentration increases clots begin to display predominately elastic behaviour on much shorter time-scales.

Next the position of the intermediate plateau, given by τ_{II}, was measured and found to decrease as fibrinogen concentration increased. Overall there was around a 3 second drop, corresponding to a 6.5-times decrease, over the entire fibrinogen concentration range. Thus, the intermediate plateau occurs at shorter times, i.e. higher frequencies, as fibrinogen concentration increases. Inspection of the curves in Figure 5-3 reveals that as the low frequency plateau grows and

the transition to the intermediate plateau moves to higher frequencies this subsequently shortens the intermediate plateau.

Finally, the position of the intermediate-to-high plateau transition, given by τ_{III}, was measured and found to show no variation, within experimental uncertainties, as fibrinogen concentration increased. It is difficult to speculate on the effect of fibrinogen on the high frequency plateau as it was not possible to measure the entire plateau. As previously mentioned, high frequency measurements are limited by the acquisition rate of the optics.

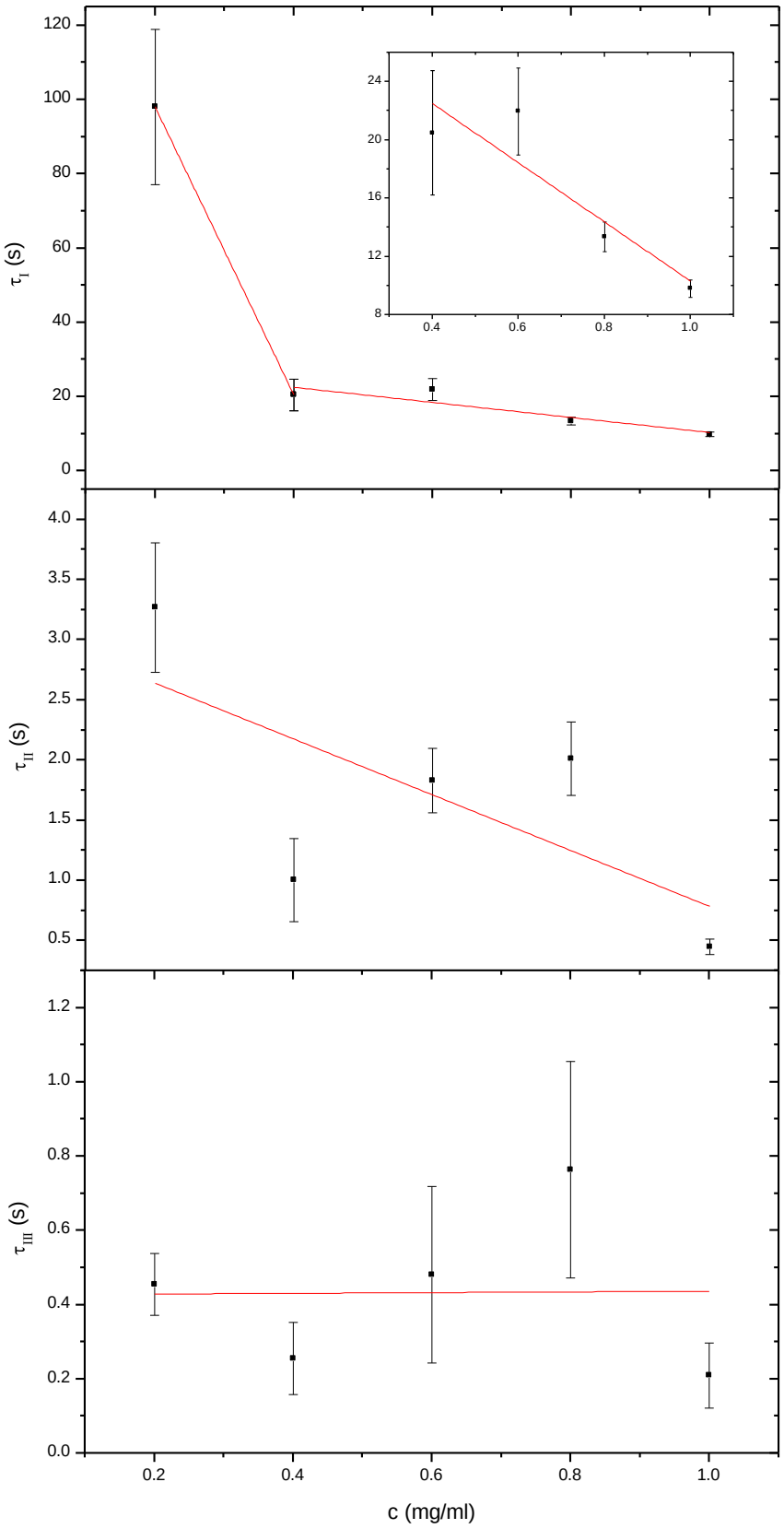

Figure 5-8: τ_I, τ_{II} and τ_{III} versus fibrinogen concentration. The data include a linear fit, of the form y = mx + c, as a guide for the eye. **Insert**: τ_I vs. fibrinogen concentration from 0.4 to 1.0 mg/ml. Errors represent the standard error in the mean from 3 repeat measurements.

5.3 Thrombin Concentration

The effects of thrombin concentration on clot viscoelasticity were investigated using the magnetic microrheometer. The following concentrations were tested: 0, 0.25, 0.5, 1 and 5 U/ml. Clots were formed as described in section 2.2.4 with a final fibrinogen concentration of 0.6 mg/ml, $CaCl_2$ concentration of 2.5 mM and FXIII inhibitor concentration of 1 mM. The lower limit of thrombin concentration was 0.25 U/ml; below this polymerisation proceeds so slowly that the magnetic particles sink out of the clot before they become trapped by the network.

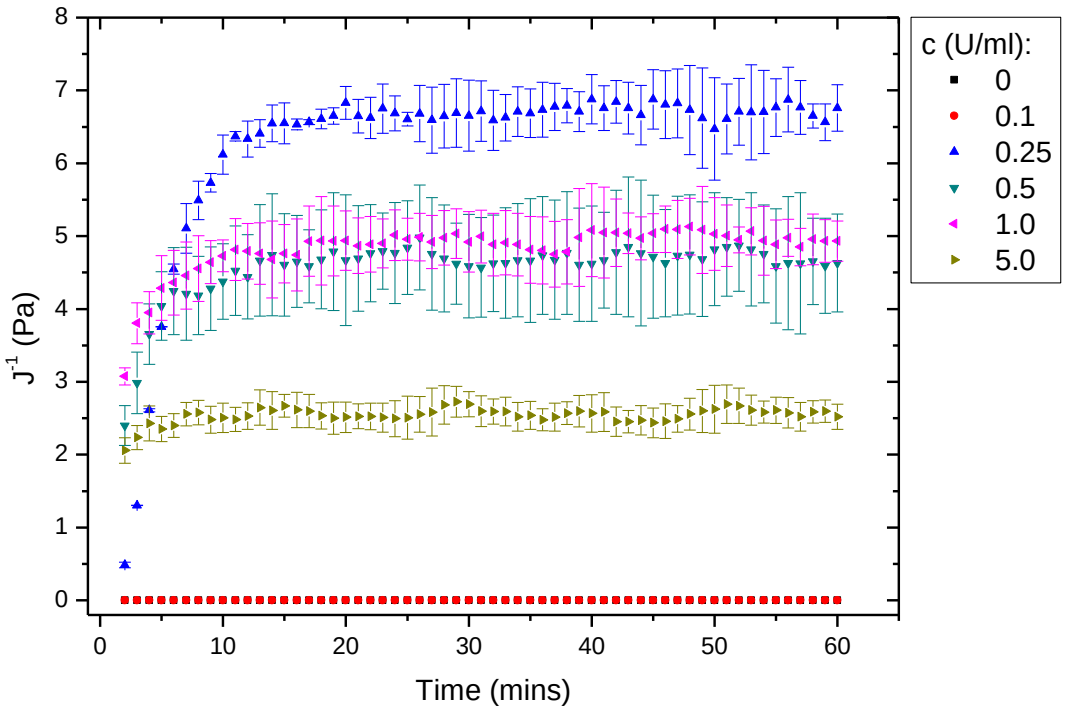

Figure 5-9: J^{-1} versus time for clots formed from different thrombin concentrations. Clotting was measured for 60 minutes and found to be sufficient for a plateau in J^{-1} to be reached for all concentrations studied. Thrombin concentration (U/ml) is displayed in the legend. Note clots formed from 0 and 0.1 U/ml thrombin concentration could not be measured. Errors represent the standard error in the mean from 3 repeat measurements.

After the addition of thrombin, clots were transferred to the magnetic microrheometer and force pulses were applied. The results of these

experiments are presented in Figure 5-9 and Figure 5-10. A clotting period of 1 hour was sufficient to ensure complete mechanical development of all thrombin concentrations investigated. As expected no clot formation was detected at 0 U/ml. In addition, it was not possible to measure clots formed at 0.1 U/ml as polymerisation preceded so slowly the magnetic particles sank out of the clot.

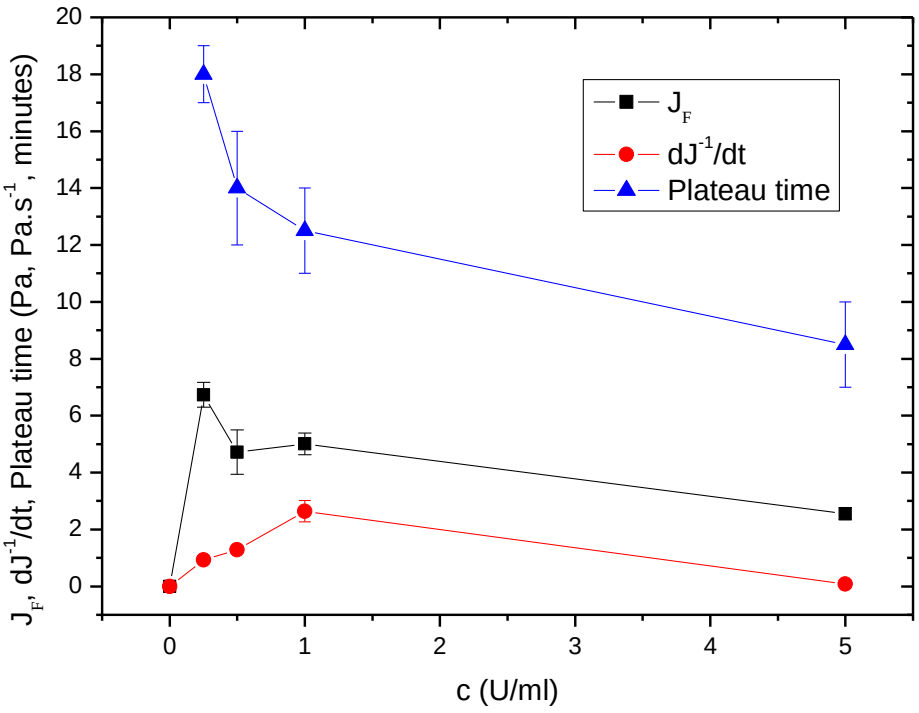

Figure 5-10: J_F, dJ^{-1}/dt and plateau time versus thrombin concentration. Data extracted from Figure 5-9. The data points are joined by linear extrapolation which is included as a guide for the eye. Note clots formed at 0 and 0.1 U/ml thrombin concentration could not be measured. The rate of change of compliance was calculated over the 1st minute of clotting. Errors represent the standard error in the mean from 3 repeat measurements.

The final compliance initially increased rapidly to a maximum and then decreased as thrombin levels increased. From 0.5 to 1 U/ml there was no change in the final compliance, falling after this as concentrations were increased to 5 U/ml. There was around a 2-times increase in the final compliance as thrombin levels were lowered to 0.25 U/ml.

The rate of change of compliance increased as thrombin concentration increased, increasing 2.8-times as thrombin increased from 0.25 to 1.0 U/ml. However, at high thrombin levels (5 U/ml) compliance rates fell to below that of the lowest thrombin levels investigated. This may be surprising as one may expect an increased rate of development at higher enzyme levels. Inspection of the data in Figure 5-9 reveal clots formed at 5 U/ml have almost reached a plateau in their compliance once measurements have commenced. The reduced compliance rate appears to be artificial and most likely arises because of the extremely rapid increase in compliance. At times below 2 minutes it was not possible to capture data with the current experimental setup hence the stiffness had nearly reached a plateau by the time the experiment commences.

The plateau time however did indicate an increased rate of mechanical development as thrombin levels increased. Between 0.25 and 1.0 U/ml there is a fall of 5.5 minutes and then a further fall of 4 minutes as thrombin concentration reaches 5 U/ml. This indicates that the plateau time is a better measure of the mechanical development in this instance. The data reveal clot polymerisation is modulated by thrombin levels, as expected, but in addition there exists an optimum level of thrombin which leads to increased mechanical strengths.

After a clotting period of 1 hour the viscoelastic moduli were measured. The results of this analysis are displayed in Figure 5-11. Similar features in the behaviour of the storage and loss modulus and their relation to one another were observed. The viscoelastic moduli were extracted at the same frequencies as that used for fibrinogen experiments in order to investigate the effect of thrombin concentration on the viscoelastic moduli (Figure 5-12).

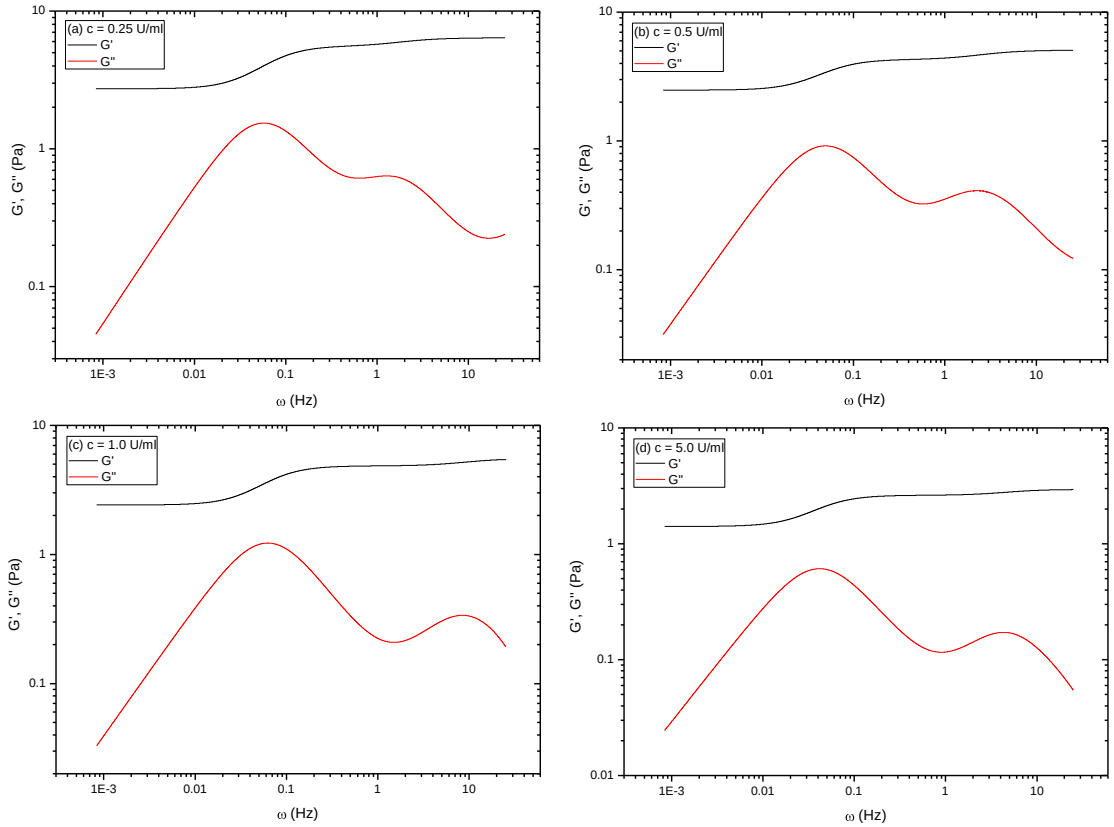

Figure 5-11 a - d: Storage and loss moduli versus frequency for clots formed at different thrombin concentrations. Data represents the average from 3 repeat experiments.

At all frequencies, the storage modulus increased sharply between 0 and 0.25 U/ml and reached a maximum. As thrombin increased to 0.5 U/ml the storage modulus decreased and stayed essentially constant up to a concentration of 1 U/ml. Further increases in thrombin concentration resulted in a decrease in the storage modulus. The storage modulus was around 2-times higher at low thrombin levels compared with maximum levels. Again, the storage modulus was consistently higher than the loss modulus; 9- to 79-times higher over the entire concentration range for all frequencies.

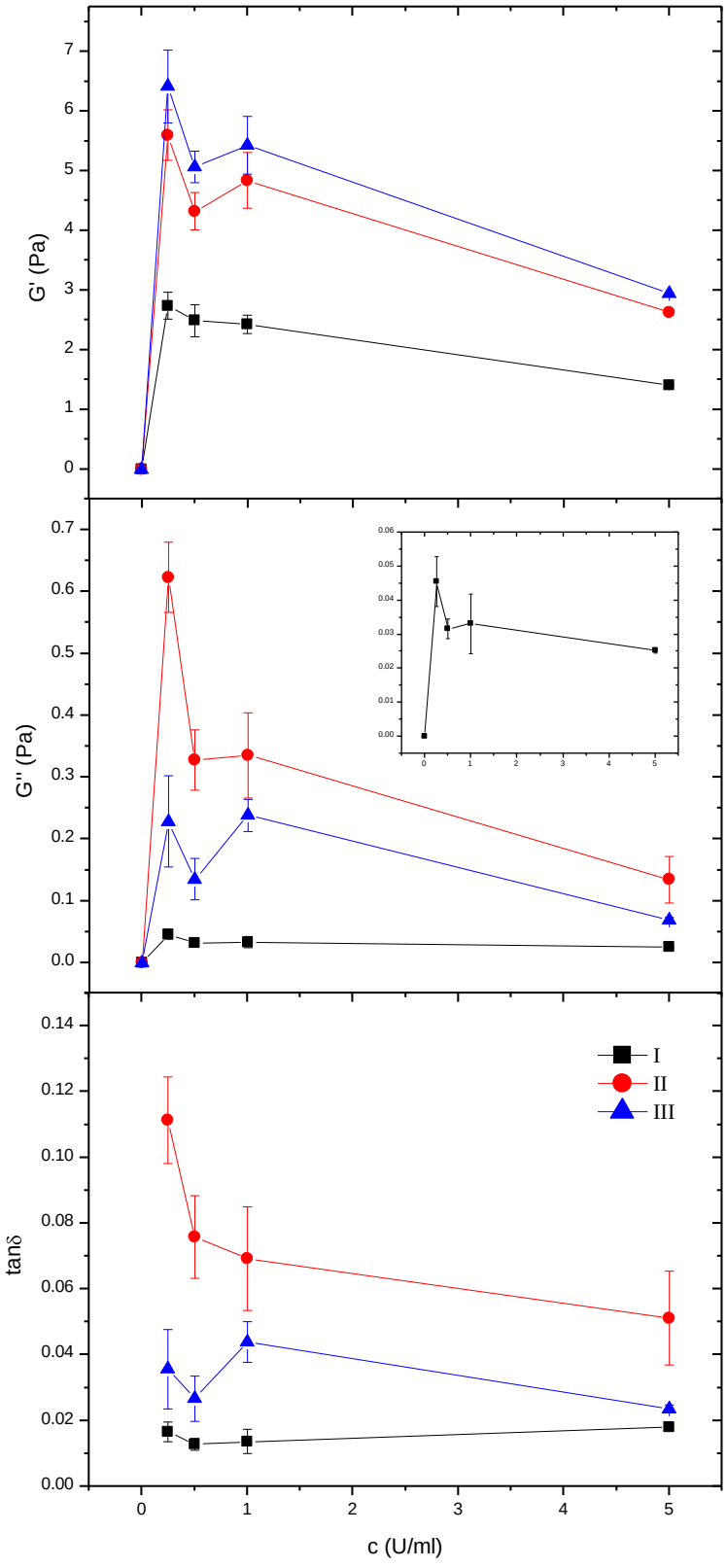

Figure 5-12: Storage modulus, loss modulus and loss tangent versus thrombin concentration. Measurements were extracted from Figure 5-11 at a at 3 specific frequency values; 8 x10^{-4} (I), 0.5 (II) and 20 (III) Hz. The data points are joined by a linear extrapolation which is included as a guide for the eye. Errors represent the standard error in the mean from 3 repeat experiments.

Again, at all frequencies the loss modulus rose sharply as thrombin concentration was raised to 0.25 U/ml. A further increase led to a fall in the loss modulus which then remained constant up to 1.0 U/ml. Except for plateau II where a dip in the loss modulus at 0.5 U/ml was observed before increasing again as levels reached 1.0 U/ml. The loss modulus again decreased as thrombin concentration reached 5 U/ml. At low thrombin levels the loss modulus was 1.8- to 4.6-times higher than at 5 U/ml.

Finally, no difference in the loss tangent for plateau I was observed as thrombin levels changed, except when comparing clots formed at 0.5 and 5 U/ml. Clots formed at the higher thrombin levels displayed increased loss tangents of around 1.4-times. For plateau II, the loss tangent dropped sharply between 0.25 and 0.5 U/ml and then decreased further beginning to plateau as thrombin levels reached 5 U/ml. Over the entire thrombin concentration range the loss modulus decreased 2.2-times. For plateau III, no difference in the loss tangent was observed, within experimental errors.

The dependence of the loss tangent on frequency as thrombin concentration varied is displayed in Figure 5-13. Once again, peaks in the behaviour of the loss tangent were observed. Thrombin had a limited effect on the height and relative frequency position of these peaks. The insert in Figure 5-13 shows the maximum loss tangent as a function of thrombin concentration. Between 0.25 and 0.5 U/ml there was a fall in the maximum loss tangent, however further increases in thrombin concentration did not significantly alter the loss tangent.

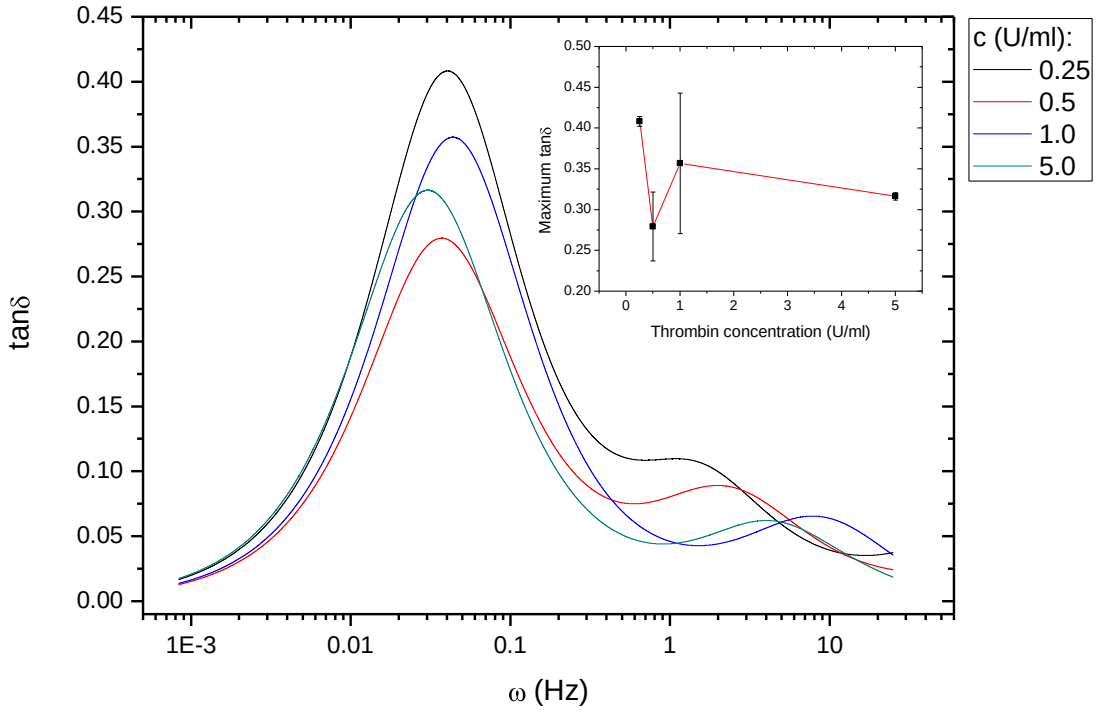

Figure 5-13: tanδ versus ω for clots formed from different thrombin concentrations. Insert: maximum tanδ vs. thrombin concentration. A linear extrapolation is included as a guide for the eye. Errors represent the standard error in the mean from 3 repeat experiments.

The insensitivity of the frequency position of the peaks in the loss tangent to thrombin levels indicates thrombin does not significantly alter the viscoelastic dynamics. In order to investigate this further, the data in Figure 5-11 was analysed, as above for fibrinogen experiments, and τ_I, τ_{II} and τ_{III} were extracted. No correlation between any of the relaxation times and thrombin concentration was detected.

5.4 $CaCl_2$ Concentration

The effects of $CaCl_2$ concentration on clot viscoelasticity were investigated using the magnetic microrheometer. The following concentrations were tested: 0, 1.5, 2.5, 5 and 10 mM. Clots were formed as described in section 2.2.4 with a final fibrinogen concentration of 0.6 mg/ml, thrombin concentration of 0.5 U/ml

and FXIII inhibitor concentration of 1 mM. It was possible to analyse clots formed at all $CaCl_2$ concentrations.

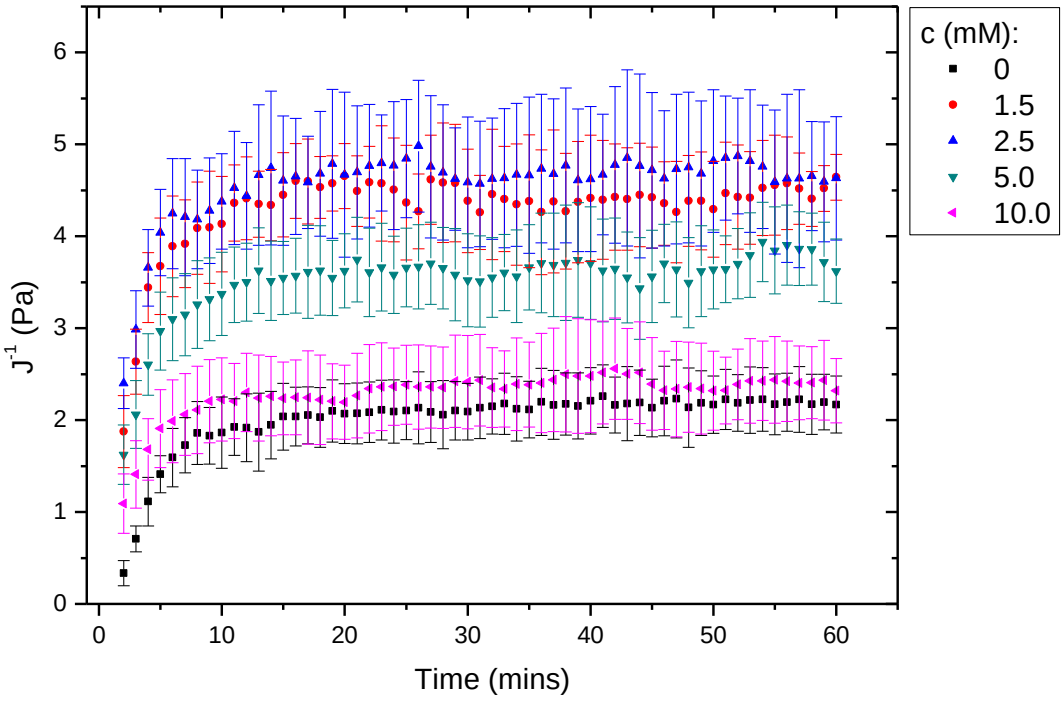

Figure 5-14: J^{-1} versus time for clots formed from different $CaCl_2$ concentrations. Clotting was measured for 60 minutes and found to be sufficient for a plateau in J^{-1} to be reached for all concentrations studied. $CaCl_2$ concentration (mM) is displayed in the legend. Errors represent the standard error in the mean from 3 repeat experiments.

After the addition of thrombin, clots were transferred to the magnetic microrheometer and force pulses were applied. The results of these experiments are presented in Figure 5-14 and Figure 5-15. Once again, a clotting period of 1 hour was sufficient to ensure complete mechanical development of all concentrations of $CaCl_2$ under investigation. Also, it was possible to analyse clots formed in the absence of $CaCl_2$.

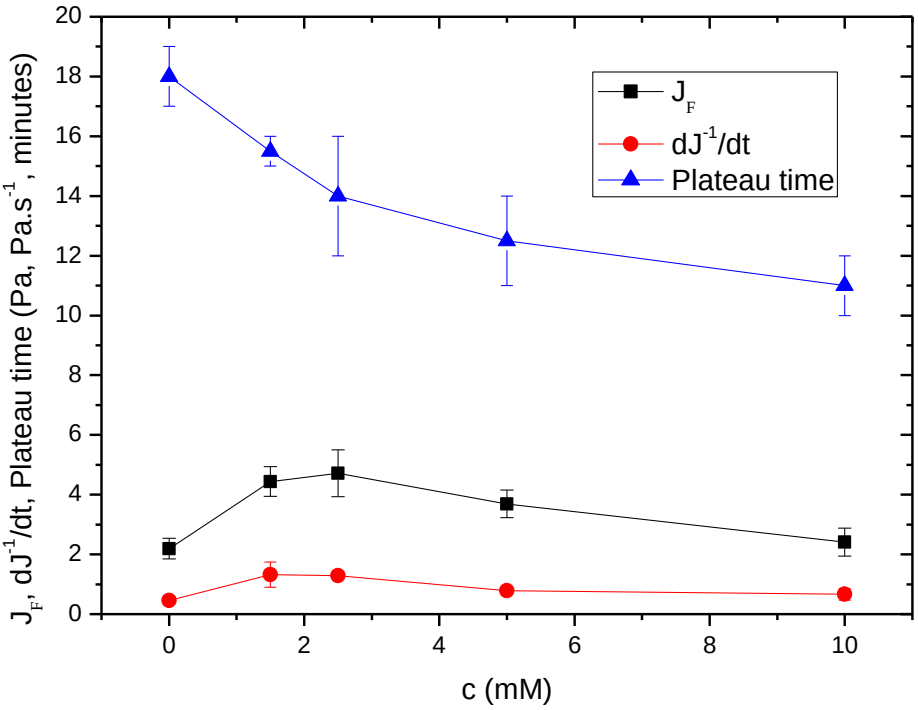

Figure 5-15: J_F, dJ^{-1}/dt and plateau time versus $CaCl_2$ concentration. Data extracted from Figure 5-14. The data points are joined by a linear extrapolation which is included as a guide for the eye. The rate of change of compliance was calculated over the 1st minute of clotting. Errors represent the standard error in the mean from 3 repeat experiments.

As $CaCl_2$ concentration increased from 0 mM, the final compliance increased reaching a maximum at 2.5 mM. As $CaCl_2$ levels increased further the final compliance began to fall; by 10 mM the final compliance was very similar to that of clots formed at 0 mM. There is around a 2-times increase in final compliance at 2.5 mM as compared with minimum and maximum $CaCl_2$ concentrations. It is interesting to note that the compliance peaks at 2.5 mM $CaCl_2$ as this is the concentration of $CaCl_2$ in plasma. The rate of change of compliance displayed remarkable similar behaviour to that of the final compliance. Initially there is an increase, which peaks between 1.5 and 2.5 mM, after which it decreases as $CaCl_2$ levels are increased. However, again the analysis of the time to plateau suggested that this drop in the rate of compliance change at high calcium chloride concentration may be an artefact from the data analysis. As $CaCl_2$ concentration increased, the time to plateau time gradually decreased. Over the

entire $CaCl_2$ concentration range the time to plateau decreased by 7 minutes indicating increased rates of mechanical development at high $CaCl_2$ levels.

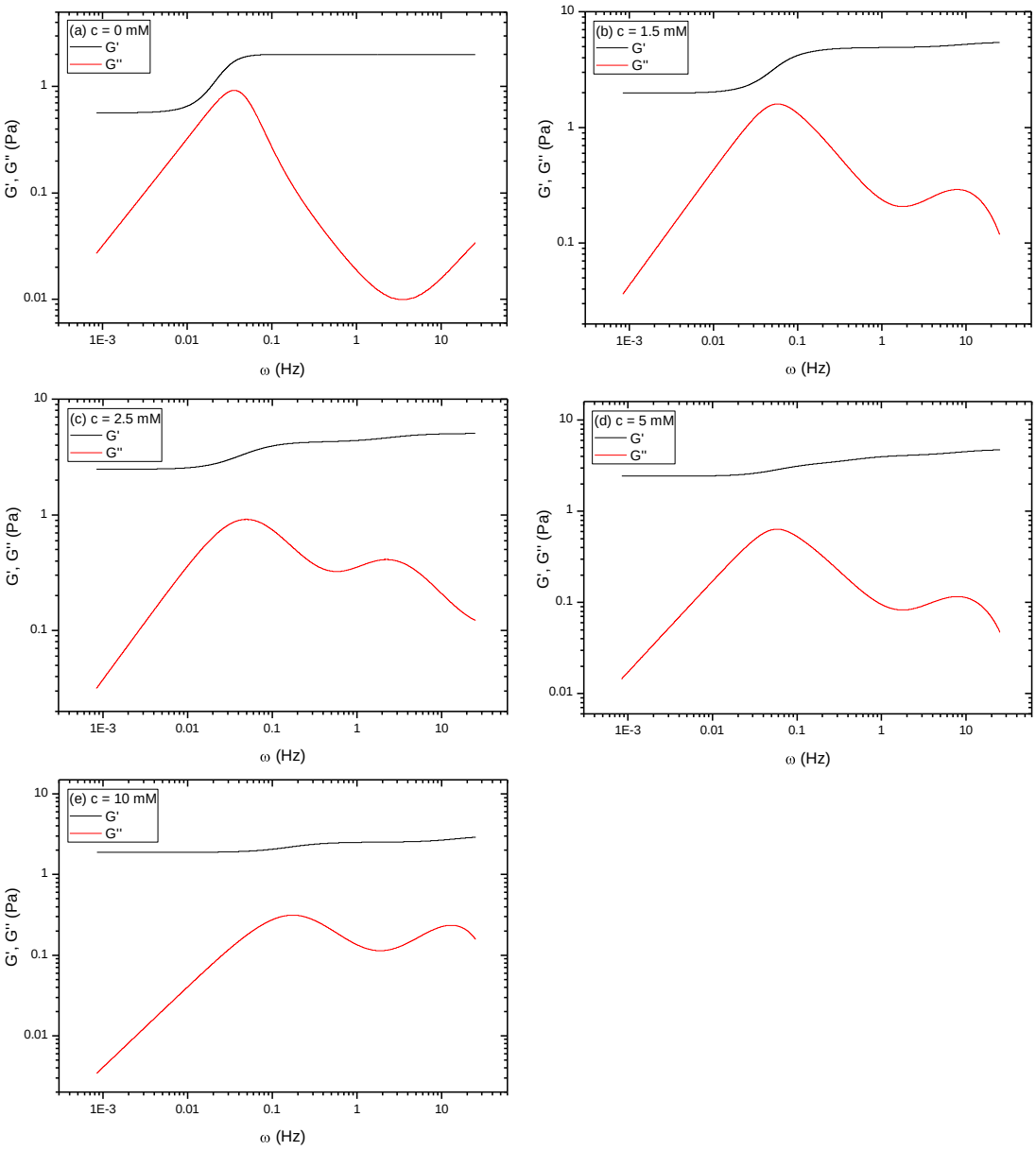

Figure 5-16 a - e: Storage and loss moduli versus frequency for clots formed at different $CaCl_2$ concentrations. Data represents the average from 3 repeat experiments.

After a clotting period of 1 hour the viscoelastic moduli were measured. The results of this analysis are displayed in Figure 5-16. Similar features in the behaviour of the storage and loss modulus and their relation to one another were observed. The viscoelastic moduli were extracted at the same frequencies

as that used for fibrinogen and thrombin experiments in order to investigate the effect of $CaCl_2$ concentration on the viscoelastic moduli (Figure 5-17).

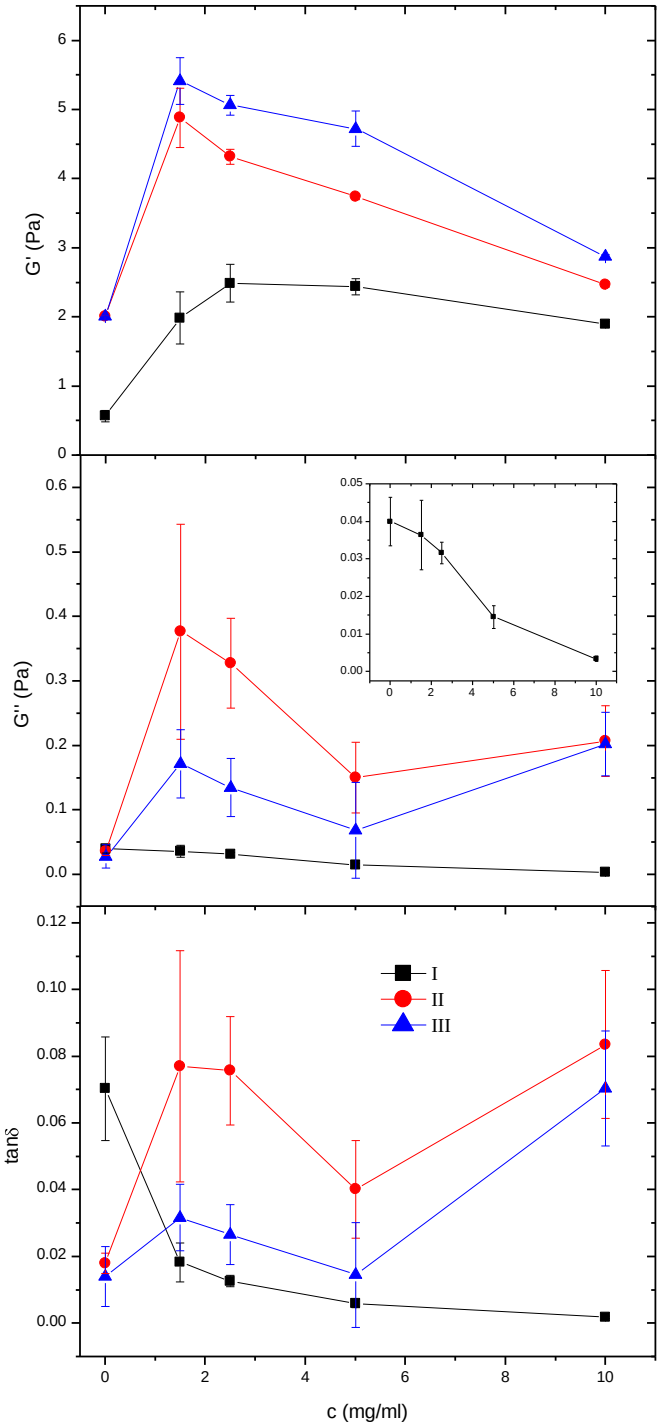

Figure 5-17: Storage modulus, loss modulus and loss tangent versus $CaCl_2$ concentration. Measurements were extracted from Figure 5-16 at 3 specific frequency values; 8 x10^{-4} (I), 0.5 (II) and 20 (III) Hz. The insert is a plot of G_I'' vs. c plotted on a different scale for clarity. The data points are joined by a linear extrapolation which is included as a guide for the eye. Errors represent the standard error in the mean from 3 repeat experiments.

The storage modulus increased sharply between 0 and 1.5 mM at all frequencies. For plateau I, the storage modulus further increased when $CaCl_2$ reached 2.5 mM and then stayed approximately constant up to 5 mM, after which it began to decrease as $CaCl_2$ levels reached 10 mM. The storage modulus was 4.3-times higher once it had reached a plateau (2.5 – 5 mM) compared with clots formed in the absence of $CaCl_2$. For plateaus II and III, the storage modulus peaked at 1.5 mM and then decreased as $CaCl_2$ concentrations increased further. The storage modulus was 2.4- and 2.7-times higher at 1.5 mM $CaCl_2$ concentration for plateaus II and III respectively compared with clots formed in the absence of $CaCl_2$. The storage modulus was consistently higher than the loss modulus; around 12- to 550-times over the entire concentration range.

For plateau I, the loss modulus decreased as $CaCl_2$ concentration increased. The loss modulus remained approximately constant, within experimental errors, up to 2.5 mM after which it decreased as $CaCl_2$ levels increased to 10 mM. The loss modulus was ~10-times lower at 10 mM $CaCl_2$ levels compared with lower levels (0 – 2.5 mM). For plateaus II and III, the loss modulus peaked at 1.5 mM then decreased as $CaCl_2$ levels reached 5 mM, before increasing again slightly as $CaCl_2$ levels reached 10 mM.

For plateau I, the loss tangent initially decreased by 3.9-times as $CaCl_2$ levels increased to 1.5 mM. As $CaCl_2$ concentration increased further, the loss tangent continued to fall, decreasing a further 10-times as $CaCl_2$ levels reached 10 mM. The loss tangent decreased 39-times over the entire $CaCl_2$ concentration range. Again, for plateaus II and III, the loss tangent peaked at 1.5 mM then decreased at 5 mM before increasing again as $CaCl_2$ concentration increased to 10 mM.

The dependence of the loss tangent on frequency as $CaCl_2$ concentration varied is displayed in Figure 5-18. Once again, peaks in the behaviour of the loss tangent were observed. It appears that $CaCl_2$ levels are modulating both the height and relative frequency position of these peaks. As $CaCl_2$ concentration increased, the maximum loss tangent decreased and moved to a

higher frequency position. The insert in Figure 5-18 shows the behaviour of the maximum loss tangent as a function of $CaCl_2$ concentration. In agreement with the loss tangent data for plateau I, presented in Figure 5-17, a reduction in the loss tangent was observed at high $CaCl_2$ concentrations. A decrease of 4.4-times over the entire $CaCl_2$ concentration range was observed. These data indicate $CaCl_2$ significantly modulates the viscoelastic dynamics of fibrin clot behaviour.

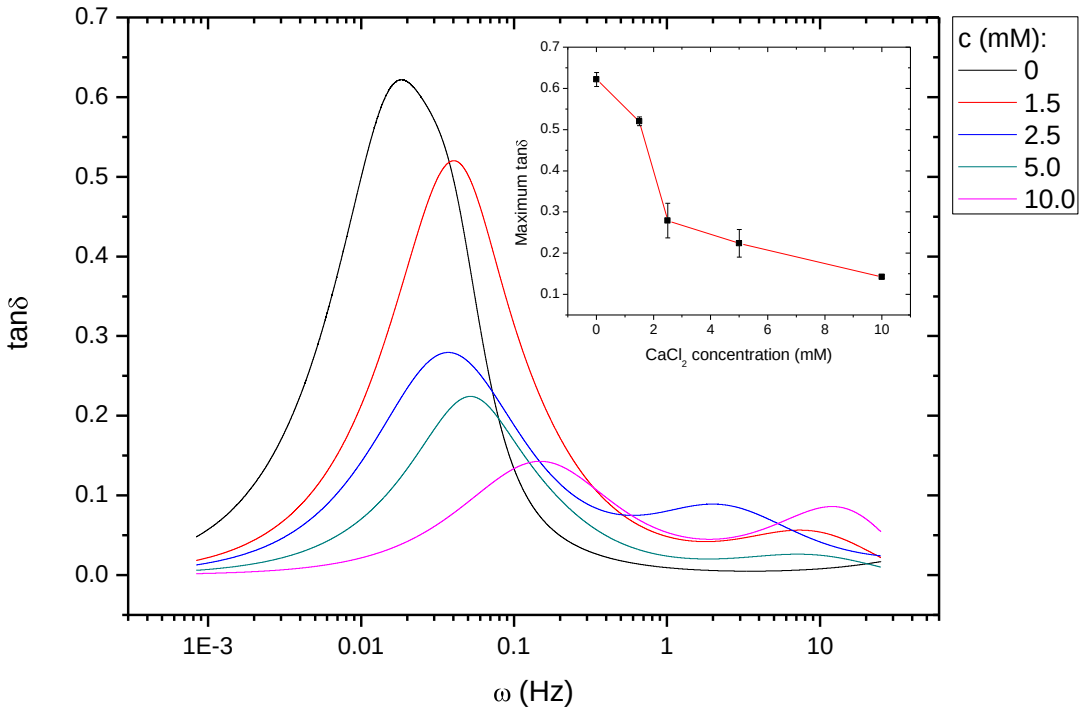

Figure 5-18: tanδ versus ω for clots formed from different $CaCl_2$ concentrations. Insert: maximum tanδ vs. $CaCl_2$ concentration. A linear extrapolation is included as a guide for the eye. Errors represent the standard error in the mean from 3 repeat experiments.

Closer inspection of the plots in Figure 5-16 reveals that $CaCl_2$ concentration does indeed modulate the viscoelastic dynamics of fibrin clots. In order to investigate this further τ_I, τ_{II} and τ_{III} were extracted from the data in Figure 5-16. The results of this analysis are displayed in Figure 5-19.

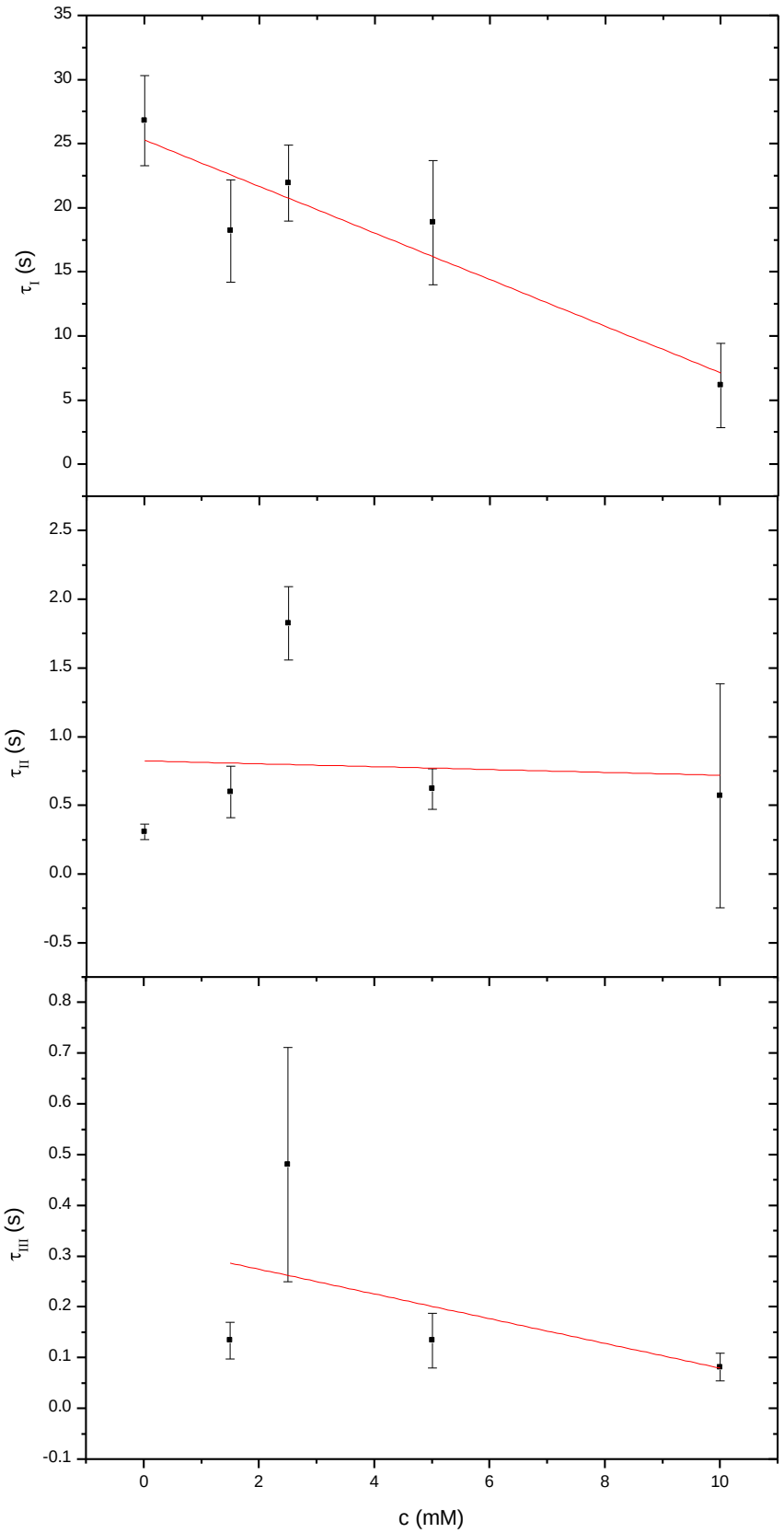

Figure 5-19: τ_I, τ_{II} and τ_{III} versus $CaCl_2$ concentration. The data include a linear fit, of the form y = mx + c, as a guide for the eye. Note τ_{III} for the 0 mM clot couldn't be measured. Errors represent the standard error in the mean from 3 repeat measurements.

The low-to-intermediate plateau transition, given by τ_I, decreased as $CaCl_2$ concentration increased. Overall, τ_I decreased by ~20 seconds corresponding to a decrease of 4.3-times over the entire $CaCl_2$ concentration range. As the low-to-intermediate plateau transition moved to shorter times, this again resulted in the low frequency plateau occurring on a much earlier time-scale, as for fibrinogen experiments. Clots formed at 0 mM $CaCl_2$ plateau at ~5 mHz, as $CaCl_2$ concentration increased up to 10 mM this plateau began at ~20 mHz; a time difference of ~2-3 minutes. Thus, as $CaCl_2$ concentration increased, clots begin to display predominately elastic behaviour on much earlier times.

Next the position of the intermediate plateau, given by τ_{II}, was measured. Overall there appeared to be little or no effect on τ_{II} as $CaCl_2$ levels increased. Initially there was a slight increase after which τ_{II} remained at ~0.5 seconds. The only exception was at 2.5 mM where τ_{II} increased up to 1.8 seconds before decreasing again as $CaCl_2$ concentration increased further. In contrast to fibrinogen experiments it appears that as the low frequency plateau increases to higher frequencies this has no effect upon the intermediate plateau.

Finally, the position of the intermediate-to-high plateau transition, given by τ_{III}, was measured. Again, as for τ_{II}, overall there was a limited effect on τ_{III} as $CaCl_2$ concentration increased. The temporal position remained at ~0.1 seconds as $CaCl_2$ increased. Except again at 2.5 mM where τ_{III} increased slightly up to 0.5 seconds before decreasing again. Note τ_{III} could not be measured for clots formed at 0 mM. Surprisingly, clots formed in the absence of $CaCl_2$ displayed only 2 plateaus in G′, a low frequency and intermediate frequency plateau.

5.5 Discussion and Conclusions

The effects of fibrinogen, thrombin and $CaCl_2$ on fibrin clot polymerisation and viscoelasticity have been studied using a magnetic microrheometer over a broad range of frequencies. It is well known that fibrin polymerisation kinetics

modulate clot structure (144-149), and furthermore it has been shown by Ryan *et al*. that clot rheology is highly sensitive to structural changes (84). In the present study, the frequency dependent viscoelastic moduli of clots formed under a range of differing concentrations have been measured. The experimental conditions selected were chosen to closely match that of the study of Ryan *et al*. (84) in order to compare our findings and also correlate changes in viscoelasticity with changes in network architecture. The data presented here are the first to study the frequency behaviour of fibrin clot viscoelasticity in combination with the effects of fibrinogen, thrombin and $CaCl_2$ on the stress relaxation behaviour of fibrin clots.

The effect of fibrinogen on clot polymerisation was studied and found to have a profound effect on the polymerisation kinetics of fibrin. As fibrinogen levels increased, the rate of change of mechanical development increased rapidly. As a result, clots formed at a higher fibrinogen concentration reached a plateau in their stiffness at earlier times. Contrary to this, measurements by Ryan *et al*. reported increased clotting times as fibrinogen concentration is raised (84). Clotting time in their study refers to the gel-point time; the time at which a clot turns from liquid to solid (100), which was detected visually. Their data however revealed no difference in clotting times, within errors, for clots formed between 0.5 and 4.5 mg/ml. Only at the highest fibrinogen levels of 6 mg/ml did they observe an increase. Inspection of their stiffness polymerisation data reveals an increased rate of mechanical development as fibrinogen levels increase, in agreement with our observations. Increased rates of mechanical development could be explained by the increased rate of monomer formation due to higher substrate levels.

Increased rates of mechanical development does not necessarily contradict a longer clotting time as suggested by Ryan *et al*. (84) as both are essentially separate process in the polymerisation reaction. Currently very little is known about fibrin gelation; recent experimental work by the Weisel group (121, 150) showed the types of structure and dynamic changes in their proportions prior to the gel point. However, they provide no model for the process of branching which is key in the gelation process. Based on the data in this thesis, it is

proposed that as fibrinogen concentration increases, protofibril formation increases while branching occurs at a slower rate, hence the prolonged clotting times. The process of lateral aggregation and radial fibre growth could then be increased due to the greater number of protofibrils available. This highlights the need for a better understanding of fibrin polymerisation prior to the gel-point.

Increased clot stiffness, indicated by G′, was associated with increased fibrinogen concentration. Similar findings have been reported by several other authors (48, 65, 67, 84, 151). An increased incidence of myocardial infarction has been associated with high levels of plasma fibrinogen and attributed to elevated clot rigidities (37). In addition, it has been found that fibrinogen concentration of *in vivo* thrombi is much higher (20 – 70 mg/ml) than normal fibrinogen plasma levels (2 – 4 mg/ml) (152). Ryan *et al*. (84) suggested that increased clot stiffness at higher fibrinogen levels is due to increased fibre density. However, increases in fibre and branch point density are only observed at the highest concentrations of fibrinogen studied (6 mg/ml). Between 0.5 and 3 mg/ml they observed no changes in clot architecture. A more recent study by Weigant *et al*. (67) used neutron scattering to probe the internal structure and radial dimensions of fibrin fibres over a fibrinogen concentration of 1 – 40 mg/ml. They reported that the internal volume fraction of protein in fibres increases while fibre diameter decreased slightly up to fibrinogen concentrations of 20 mg/ml. They proposed two different models (Figure 20): at higher fibrinogen levels individual proteins pack closer together leading to a contraction in fibre diameter or alternatively, the increased amount of protein available can correct potential defects, such as vacancies, in the internal fibre structure. Estimates for the internal volume fraction of fibrin in a fibre has been placed between 10 – 20% by Weigant *et al*. (67) and 20 – 30% by Guthold *et al*. (26). Hence, fibrin fibres are very porous structures and could potentially accommodate more protein without a change in diameter. Currently there are conflicting reports on the effects of fibrinogen on fibre diameter with some authors reporting a decrease (67, 84), some an increase (147) and others no difference (153).

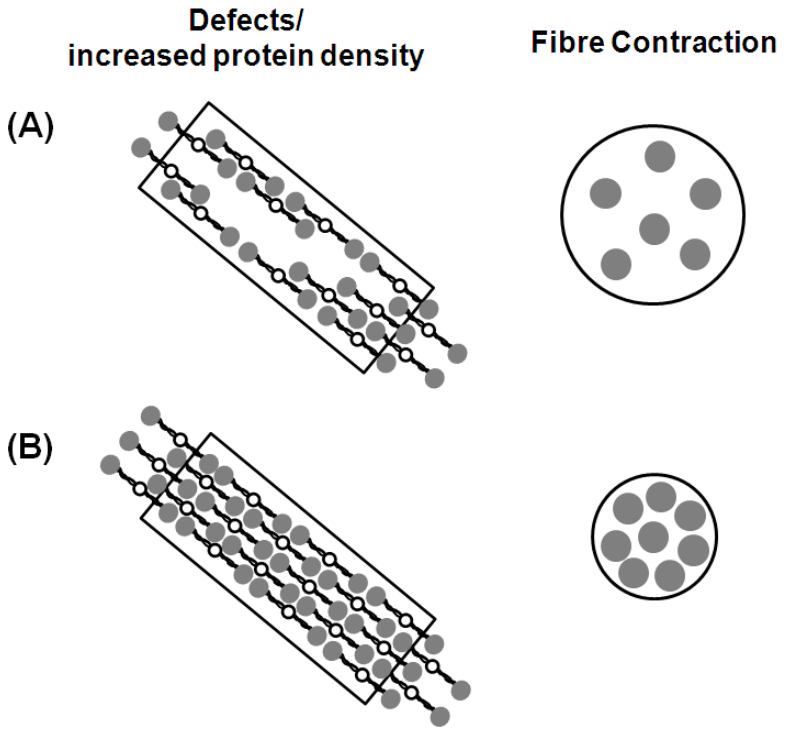

Figure 20: Schematic of two possible theories to account for the increase in internal protein fraction of fibrin fibres (adapted from (67)). (A) Low fibrinogen concentration and **(B)** high fibrinogen concentration. **Left**: increased fibrinogen levels results in fewer internal fibre defects and/or an increased internal protein density. **Right**: contraction of the proteins within the fibre results in a thinner fibre with an increased volume fraction.

In this study, fibre diameter is expected to change very little due to the very small change in fibrinogen level over the concentration ranged probed (0.2 – 1 mg/ml). Ryan et al. (84) suggested a decrease of 26 nm as fibrinogen concentration increases. However there appeared to be no statistically significant difference, within errors, in fibre diameter between the lowest (0.5 mg/ml) and highest (6 mg/ml) fibrinogen concentrations investigated. In addition, Weigant *et al*. (67) reported only a slight decrease in fibre diameter, which appeared to be <10 nm, over a much greater concentration range (2 – 20 mg/ml). Data on increased clot stiffness at higher fibrinogen concentration presented in this thesis could perhaps be attributed to an increased density of protein within each fibre. The increased amount of fibrin could potentially correct any internal fibre defects or may just result in an increased internal protein density. The net effect would be stiffer fibres resulting in a stiffer clot. As

fibrinogen concentration increased an increase in both G_{tens} and G_{curve} was observed, indicating that fibres become stiffer for both stretching and bending. In addition, G_{tens} was consistently higher than G_{curve}. That is, fibres are much stiffer for stretching than for bending, as expected from their length to diameter ratio, something which has also been confirmed by other authors (83, 154).

As previously mentioned the majority of studies reported a concentration dependence of G′ ranging between 1.5 and 2.3 Pa (48, 65, 67, 84, 151), below that predicted by Mackintosh *et al*. for a network of branched fibres ($G' \approx c^{2.5}$) (68). In this thesis, a concentration dependence of G′ is shown which is in agreement with this prediction. This indicates that fibrin fibres are semi-flexible i.e. $\ell_c \sim \ell_p$, suggesting that fibres are very straight between branches; which has indeed been observed in confocal micrographs (Figure 1-4). In addition, Storm *et al*. reported a persistence length of 0.5 μm for fibrin fibres measured from TEM micrographs (80). This is similar to fibre lengths previously reported from SEM micrographs which range between 0.3 - 5 μm (84). Mackintosh's theory proposes that elasticity in networks of semi-flexible fibres is entropic in origin. However, this does not rule out an enthalpic contribution to the elastic response. The theory of Storm *et al*. (80) proposes that at low strain entropic elasticity dominates but at higher strain an enthalpic contribution is required to fit the theory to the experimental data. This enthalpic contribution arises by assuming fibres can stretch longitudinally.

The measurements presented in this thesis of G′ vs. c show better agreement with the theory than those previously reported due to the ability of my measurements to identify the plateau modulus G_{tens} to which the theory of Mackintosh *et al*. applies (68). The majority of studies reported a value of G′ at one particular frequency. For example, Ryan *et al*. (84) performed measurements at 0.1 Hz and reported a concentration dependence of $G' \approx c^{1.67}$ which is much lower than that predicted. Similarly, Weigant *et al*. (67) reported a dependence of $G' \approx c^{2.22}$ measured at a frequency of 1 Hz. Measurements reported here reveal a lower power dependence for values of G′ measured at lower frequencies e.g. $G'_I \approx c^{2.2 \pm 0.2}$ vs. $G'_{III} \approx c^{2.7 \pm 0.2}$. In addition, the

measurements could possibly be improved using higher frequencies measurements which would enable G_{tens} to be completely measured.

Increased viscous deformation, as indicated by G′′, was also associated with increased fibrinogen concentration and closely matched the behaviour of G′. Ryan and Shan *et al*. both reported an increased storage modulus associated with an increased loss modulus (77, 84). At the lowest frequencies studied, I observed a loss modulus which displays a lower power dependence upon concentration when compared with the storage modulus ($G''_I \approx c^{1.32 \pm 0.07}$ vs. $G'_I \approx c^{2.2 \pm 0.2}$). At higher frequencies the dependence of the storage modulus was still slightly higher; however this difference was not statistically significant. As a result very little difference in the behaviour of the loss tangent with fibrinogen concentration was observed at the higher frequencies studied. The maximum loss tangent agreed well with measurements performed at the lowest frequency revealing initially a sharp decline in the loss tangent after which it remained relatively constant.

Ryan *et al*. (84) also reported very little difference in the loss tangent with increasing fibrinogen concentration. This agrees with their findings that the loss tangent is most strongly modulated by fibre diameter. They observed smaller values for tanδ in clots with thinner fibres and suggested that this was due to the greater degree of branching in these clots. The relative insensitivity of the loss tangent to fibrinogen concentration in the measurements presented in this thesis could be due to the limited effect of fibrinogen levels on fibre diameter.

Microrheological measurements performed over a broad frequency range reveal that fibrinogen modulates the viscoelastic dynamics of fibrin clots, something not previously reported in the literature. As mentioned almost all studies report little or no dependence of G′ upon frequency. In this thesis, fibrinogen concentration has a dramatic effect upon the stress relaxation behaviour of fibrin clots. As fibrinogen concentration increased, plateau I, corresponding to G_{orient}, began at a higher frequency, i.e. on a much shorter time-scale. As a result of this plateau II, corresponding to G_{curve}, was much shorter and also occurred at a higher frequency (Figure 21).

The following hypothesis can be proposed to explain this behaviour. Consider an extremely flexible fibre i.e. one formed at low fibrinogen concentration, under the influence of a stress. This fibre will stretch and bend in response to this stress and then the entire fibre will move and pull on other connected fibres. As fibrinogen concentration increases fibres become stiffer due to an increased internal protein density. Therefore fibres formed at high fibrinogen concentration under the influence of the same stress will stretch and bend less and as a result begin to move and pull on other fibres at much earlier times.

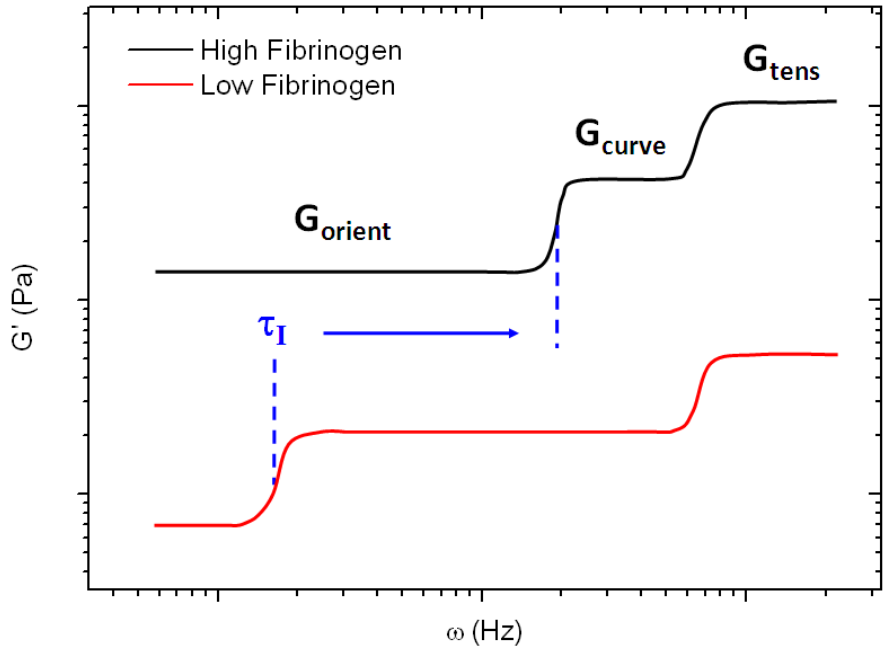

Figure 21: Schematic diagram of G′ versus frequency. The frequency behaviour is depicted for clots formed at high and low fibrinogen concentration. As fibrinogen levels are increased the stress relaxation time, τ_I moves to shorter times i.e. higher frequencies. As a result of this the G_{orient} plateau occurs at an earlier time and the G_{curve} plateau spans a smaller frequency range and also occurs at an earlier time.

Next, the effects of thrombin on clot polymerisation and viscoelasticity were investigated. Higher levels of thrombin lead to increased rates of fibrin polymerisation. The effects of thrombin on clot polymerisation measured by turbidity are well known (149). At high thrombin levels changes in concentration have little effect. While at low levels increases result in a decreased lag phase,

increased maximum rate and a decreased final absorbance. Thus, at higher thrombin levels fibrinopeptide cleavage is accelerated resulting in increased monomer formation and subsequently increased clot formation thereafter. The results reported in this thesis are consistent with turbidity measurements and agree well with those of Ryan *et al*. (84) who observed similar effects by thrombin on the mechanical development of fibrin clots.

Final compliance, indicating clot stiffness, reached a maximum at thrombin levels of 0.25 U/ml. This suggests an optimum level of thrombin exists which results in maximal clot stiffness. The effects of thrombin on clot structure have been studied by several authors who report a reduction in fibre size with increasing thrombin concentration (84, 147, 149, 153, 155-157). Reduced thrombin levels result in reduced monomer formation and subsequently protofibrils grow longer and aggregate laterally to produce networks of long, thick fibres with a low degree of branching (3, 84, 149). High thrombin levels result in rapid monomer formation compared with relatively slow longitudinal and lateral protofibril growth. As a result, clots formed at higher thrombin levels consist of thin, short and highly branched fibres (3, 84, 149). Ryan *et al*. (84) suggested that an intermediate thrombin concentration exists at which clot structure displays a balance between large fibre size and maximal branching, which occurs at 0.25 U/ml. We observed increased clot stiffness, as indicated by G′, did indeed occur at thrombin concentrations of 0.25 U/ml, in agreement with the findings of Ryan *et al*. and several other authors (158-160).

Viscous deformation, as indicated by G′′, closely matched the behaviour of G′. Subsequently the loss tangent displayed little variation as thrombin levels changed except at intermediate frequencies. Here the behaviour of tanδ closely matched that observed by other authors (84, 158) where tanδ decreased as thrombin levels were raised. This indicates clots formed at high thrombin levels will incur less permanent deformation. As clots formed at high thrombin concentration consist of short, thin fibres which are highly branched, this again points towards the importance of branching in maintaining clot integrity.

In addition, these measurements also raise the important point that clot stability is not only dependent upon stiffness. Clots formed at low thrombin levels display the greatest stiffness, however they possess the greatest loss tangents and as a result will incur more permanent deformation. These clots may therefore exhibit a greater propensity to rupture, i.e. embolise. Similarly, clots unable to deform and dissipate energy may also be more likely to rupture. Guthold *et al*. observed that the rupture force of single fibres increases with diameter (26). One would expect clots formed at low thrombin levels, which posses thick fibres, to be more mechanically stable, even though they exhibit increased deformation. Very little is currently known about the relationship between clot rupture and the viscoelastic moduli and better understanding may help to interpret *in vitro* measurements with clot embolism *in vivo*.

The effects of thrombin on the viscoelastic dynamics of fibrin clots was limited, with little or no difference in any of the stress relaxation times being observed. Changes in clot structure due to variations in thrombin are more complex than those brought about by variations in fibrinogen concentration. Changes in fibre structure are also accompanied by changes in macroscopic clot structure due to varying thrombin levels (3, 84). It could be that these changes negate one another and result in relatively little change in the stress relaxation behaviour. In addition, changes in the viscoelastic moduli were much more pronounced due to changes in fibrinogen compared with thrombin. The storage modulus increased ~100-times for fibrinogen and only 2-times for thrombin between the weakest and stiffest clots. Furthermore, in Chapter 4 measurements of clots formed in the presence and absence of FXIII revealed no change in the stress relaxation behaviour. In this instance, FXIII cross-linking resulted in an increase in stiffness of around 3-times. It could be that changes in the stress relaxation behaviour are only associated with large changes in clot stiffness. This may account for the fact that no differences in the stress relaxation behaviour were observed due to changes in thrombin concentration.

Finally, the effects of $CaCl_2$ concentration on clot polymerisation and viscoelasticity were investigated. It was observed that increasing $CaCl_2$ concentration increased the rate of fibrin polymerisation. The accelerating effect

of $CaCl_2$ on fibrin polymerisation has been demonstrated (161, 162) and attributed to the enhancement of polymerisation mechanisms after fibrinopeptide removal (24, 163-167). In particular, it has been suggested that lateral aggregation may be enhanced through either decreases in charge from calcium binding (168) and/or through the enhancement of FpB removal (169). The effect in either case, or a combination, would be an increase in fibre diameter at increased $CaCl_2$ concentrations; consistent with both turbidity (155, 170, 171) and SEM measurements (84). The presence of $CaCl_2$ has also been reported to enhance longitudinal protofibril growth (144, 172, 173), again consistent with SEM measurements (84). In addition, Ryan *et al*. (84) observed a decrease in fibre and branch point density at elevated $CaCl_2$, in agreement with observations for thrombin experiments that large fibre lengths and diameters are associated with a low degree of branching. Similarly, clots formed at low $CaCl_2$ concentrations consist of short, thin fibres with a high degree of branching. Again, indicating the existence of an optimal $CaCl_2$ concentration where clots exhibit a balance between thick fibres and maximal branching, occurring at 1.5 mM.

Peak stiffness, indicated by G′, occurred between 1.5 to 2.5 mM $CaCl_2$ concentration, consistent with the findings of several other authors (47, 48, 84, 160, 171). Ryan *et al*. (84) attribute increased clot stiffness at these $CaCl_2$ levels to the balance between large fibre diameters and maximal branching, as they do for thrombin experiments. The maximum clot stiffness observed in both $CaCl_2$ and thrombin experiments are in striking agreement with that observed by Ryan *et al*. (84) and it is therefore concluded that this is due to these clots displaying a balance between high branching density and large fibre diameters.

Viscous deformation, as indicated by G′′, did not match the behaviour of G′ at all frequencies, as was the case for fibrinogen and thrombin experiments. At intermediate and high frequencies, the behaviour was essentially the same, with a peak in G′′ occurring at 1.5 mM. The effect on the loss tangent was an overall increase as $CaCl_2$ concentration increased, consistent with previous reports (84). At elevated $CaCl_2$ levels, branching decreases, as previously discussed, and this could account for the increased values in the loss tangent, supporting

the idea that branching prevents structural rearrangements within clots. At low frequencies, G′′ consistently decreased as $CaCl_2$ concentration increased, which was also the case for the loss tangent and the maximum loss tangent. At low frequencies this corresponds to G_{orient}, the large scale motion of fibres. At maximum $CaCl_2$ concentration, fibres display some of their largest lengths and diameters which could account for the reduced loss tangent on these timescales. It has been suggested that branching reduces clot deformation, as indicated by an association with lower values of the loss tangent, however these measurements also indicate fibre thickness may play a role in maintaining clot integrity.

The effect of $CaCl_2$ on the stress relaxation behaviour of fibrin was similar to that of fibrinogen, albeit to a lesser degree. As $CaCl_2$ concentration increased plateau I occurred at a higher frequency, i.e. a shorter time, as indicated by the reduction in τ_I. Plateaus II and III remained unaffected by changes in $CaCl_2$ concentration. Again, we propose that changes in the stress relaxation behaviour arise due to changes in fibre structure. As $CaCl_2$ concentration increases fibre size increases (84) and their rupture force also increases (26). In addition, increased fibre diameters have been associated with increased clot stiffness (84). For fibrinogen experiments, it was proposed that fibres became stiffer through increased internal protein density and this resulted in the changes in the stress relaxation behaviour observed. For $CaCl_2$ experiments, it is proposed that a similar effect occurs except that fibres become stiffer due to increased radial diameter.

In addition, we observed an association between the loss tangent and the stress relaxation behaviour. For fibrinogen experiments a rapid decrease in $\tan\delta_I$ between 0.2 and 0.4 mg/ml fibrinogen concentration was observed and this coincided with a dramatic change in τ_I. Similarly, for $CaCl_2$ experiments τ_I fell consistently as concentration increased and this was associated with a similar decrease in $\tan\delta_I$. Thus, clots consisting of fibres which display less permanent deformation exhibit predominately elastic behaviour at much earlier times. Which is to be expected as a material with $\tan\delta << 1$ is essentially an elastic solid.

In this thesis, I have not only attempted to determine the effect of fibrinogen, thrombin and $CaCl_2$ on the viscoelastic moduli, but also to determine the effect on different timescales and ascertain the role, if any, that these reactants play in modulating the stress relaxation behaviour of fibrin clots. The data presented demonstrate new and important insights into the behaviour of fibrin clot viscoelasticity.

Chapter 6

6 Gamma Prime

6.1 Introduction

A variant of the common γA chain arises due to alternative processing of the mRNA chain and is called γ′ (174). This alternative form has the carboxy-terminus end 4 amino acids replaced by a new 20 amino acid sequence (175). Due to the overall negative charge of the γ′ chain, plasma fibrinogen is separable by anion-exchange chromatography into 2 major peaks (176). Peak 1 fibrinogen contains 2 γA chains and is homodimeric with respect to the γA chain (γA/γA), whereas peak 2 fibrinogen contains both a γA and a γ′ chain (Figure 6-1) and is heterodimeric with respect to the γ chain (γA/γ′) (177). Plasma fibrinogen contains approximately 8% to 15% γA/γ′ fibrinogen, whereas homodimeric γ′/γ′ fibrinogen accounts for less than 0.5% of the total fibrinogen population (178).

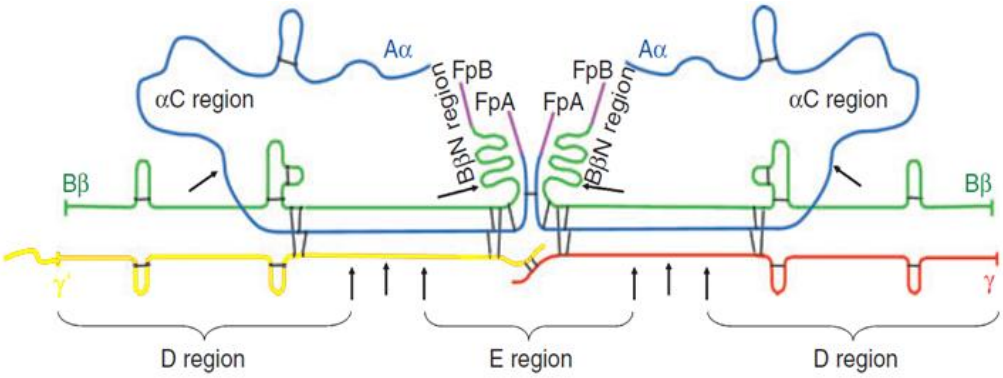

Figure 6-1: Polypeptide structure of γA/γ′ fibrinogen, adapted from (12). The individual chains, Aα, Bβ, γ and γ′ are blue, green, red and yellow respectively. The amino acid extension of the γ′ chain extends from the c-terminus of the γ chain which is located within the D region of fibrinogen. Fibrin polymerises through D-E-D interactions placing the γ′ extension at the D-D interface. The extra 16 amino acids of the γ′ chain could extend 30 to 40 Å or more depending on folding, however the structure of the γ′ chain is unknown (178).

Several studies have highlighted that plasma levels of fibrinogen γ′ may modulate thrombotic disease. Elevated levels have been associated with coronary artery disease (179), myocardial infarction (180) and stroke (181). In contrast, reduced levels have been associated with deep vein thrombosis (182) and thrombotic microangiopathy syndrome (183). Additionally, numerous functional studies have shown that clots formed from fibrinogen γA/γ′ behave differently than clots formed from fibrinogen γA/γA, with differences in polymerization rates and maximum turbidity, network structure and fibre thickness, the extent of cross-linking and resistance to fibrinolysis (96, 184-189) although there is quite some disagreement in these findings.

It has been demonstrated that the fibrinogen γ′ chain binds to thrombin with high affinity (190-192) Thrombin binds γ′ through exosite II (191) and it is thought that negatively charged residues of γ′, in particular residues 414-427 and two sulfated Tyr residues in this sequence, play a crucial role in this interaction (192). Binding of thrombin to the γ′ chain has been reported to inhibit thrombin activity and it has been suggested that this may influence clot structure (184). It

has also been reported that the γ′ chain may bind directly to FXIII (188, 193, 194) however another study could not confirm this interaction (195).

Most recently, Gersh *et al.* studied the polymerization and structure of fibrin clots formed from recombinant γA/γA, γA/γ′ and γ′/γ′ fibrinogens; the first study to include recombinant γA/γ′ fibrinogen (185). They reported that γA/γ′ clots polymerised slower than γA/γA clots but fibrinopeptide release was unaltered. In contrast to this, both Cooper *et al*. and Siebenlist *et al*. found differences in fibrinopeptide release associated with purified plasma γA/γ′ fibrinogen (96, 184).

Differences in structure have also been reported by most studies (Figure 6-2): Gersh *et al*. (196) found γA/γ′ clots had similar fibre diameters to γA/γA clots but were more inhomogeneous in structure while both Cooper *et al*. (96) and Siebenlist *et al*. (184) found γA/γ′ clots were composed of thinner more branched fibres which were arranged more uniformly. The study by Collet *et al*. which used recombinant γA/γA and γ′/γ′ fibrinogen found no differences in structure (186). The discrepancy in results between each study may be attributed to differing experimental conditions, the sources of γ′ fibrinogen and contaminating amounts of FXIII which may be present in plasma purified fibrinogen samples.

The work of Collet *et al*. (96) also showed the effect γ′ fibrinogen has on the mechanical properties of fibrin clots, the first study to attempt this. In particular, the stiffness G′ was measured using a torsion pendulum (197). They reported that in the absence of cross-linking γ′/γ′ clots have a similar stiffness to γA/γA clots, while in the presence of cross-linking γ′/γ′ clots are 3-times stiffer. They suggest this dramatic increase in stiffness is brought about by an increased amount of cross-linking. The extent of cross-linking in fibrin clots formed from γA/γ′ fibrinogen has been the subject of debate with two studies finding conflicting results. Farrell *et al*. found that γA/γ′ clots were more highly cross-linked, with more extensive γ and α chain cross-linking (187, 189). They also reported that γA/γ′ fibrinogen accelerated FXIII activation. On the contrary Siebenlist *et al*. (184) reported no measurable difference in the rate or extent of

γ chain cross-linking and the overall rate and onset of α cross-linking was slower for γA/γ′ fibrinogen. Siebenlist *et al*. (184) argue that differences in results are due to Farrell *et al*. (187, 189) having unaccounted for FXIII in their γA/γ′ fibrinogen.

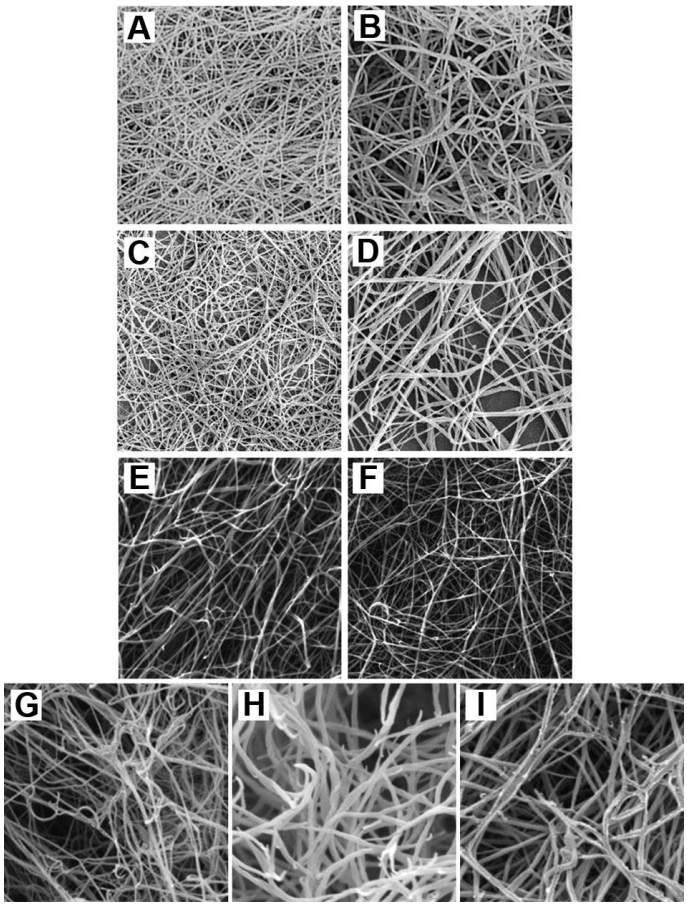

Figure 6-2: Scanning electron micrographs of fibrinogen γ-chain variants (178). A: clots made from purified γA/γ′ fibrinogen. **B:** clots made from purified γA/γA fibrinogen. Images from Cooper *et al*. (96) **C:** clots made from purified γA/γ′ fibrinogen. **D:** clots made from purified γA/γA fibrinogen. Images from Siebenlist *et al*. (184) **E:** clots made from recombinant γ′/γ′ fibrinogen. **F:** clots made from recombinant γA/γA fibrinogen. Images from Collet *et al*. (198) **G:** clots made from recombinant γ′/γ′ fibrinogen. **H:** clots made from recombinant γA/γ′ fibrinogen. **I:** clots made from recombinant γA/γA fibrinogen. Images from Gersh *et al*. (196).

The aim of the work presented here was to investigate the mechanisms underpinning the effects of fibrinogen γ′ on fibrin structure and function. We studied the effects of γ′ on protofibril formation and clot structure, and investigated the roles of thrombin and FXIII. In addition, we determined the

viscoelastic properties of γA/γ′ clots. We provide qualitative and quantitative evidence that the γ′ chain directly inhibits protofibril growth and produces a mechanically weaker clot composed of thinner fibres. Our findings provide novel insight into the early stages of protofibril formation and could help in understanding the role of the fibrinogen γ′ chain in modulating thrombotic disease.

6.2 Preparation of γA/γA and γA/γ′ Fibrinogen

γA/γA and γA/γ′ fibrinogen were purified from ERL fibrinogen as previously described (96) by Dr Shirley Uitte de Willige. In brief, the variants were separated by anion-exchange chromatography on a DE-52 column using a BioCad Sprint chromatography system (Perseptive Biosystems, Framingham, MA). Before chromatography, fibrinogen was dialyzed against equilibration buffer (0.039 M Tris, 0.005 M H_3PO_4, 0.5 mM phenylmethylsulfonyl fluoride, 1 mM benzamidine, and 5 mM aminocaproic acid, pH 8.6). Elution of the variants was established by a concave gradient from equilibration buffer to elution buffer (0.5 M Tris, 0.5 M H_3PO_4, 0.5 mM phenylmethylsulfonyl fluoride, 1 mM benzamidine, and 5 mM aminocaproic acid, pH 4.2) (193).

SDS-PAGE analysis (Figure 6-3 (A)) revealed a single band at the location of the γ chain for γA/γA fibrinogen, indicating this preparation contained only γA fibrinogen (lane 2). In contrast, the γA/γ′ fibrinogen contained two bands of approximately equal intensity but different molecular weight indicating the presence of both the γA and γ′ chains (lane 11). In all experiments (unless stated otherwise) the final concentrations were: 0.5 mg/ml fibrinogen, 1.0 U/ml thrombin (or 5 BU/ml reptilase), 2.5 mM $CaCl_2$ and either 1 mM FXIII inhibitor or 3.7 μg/ml FXIII.

6.3 Cross-linking by FXIIIa

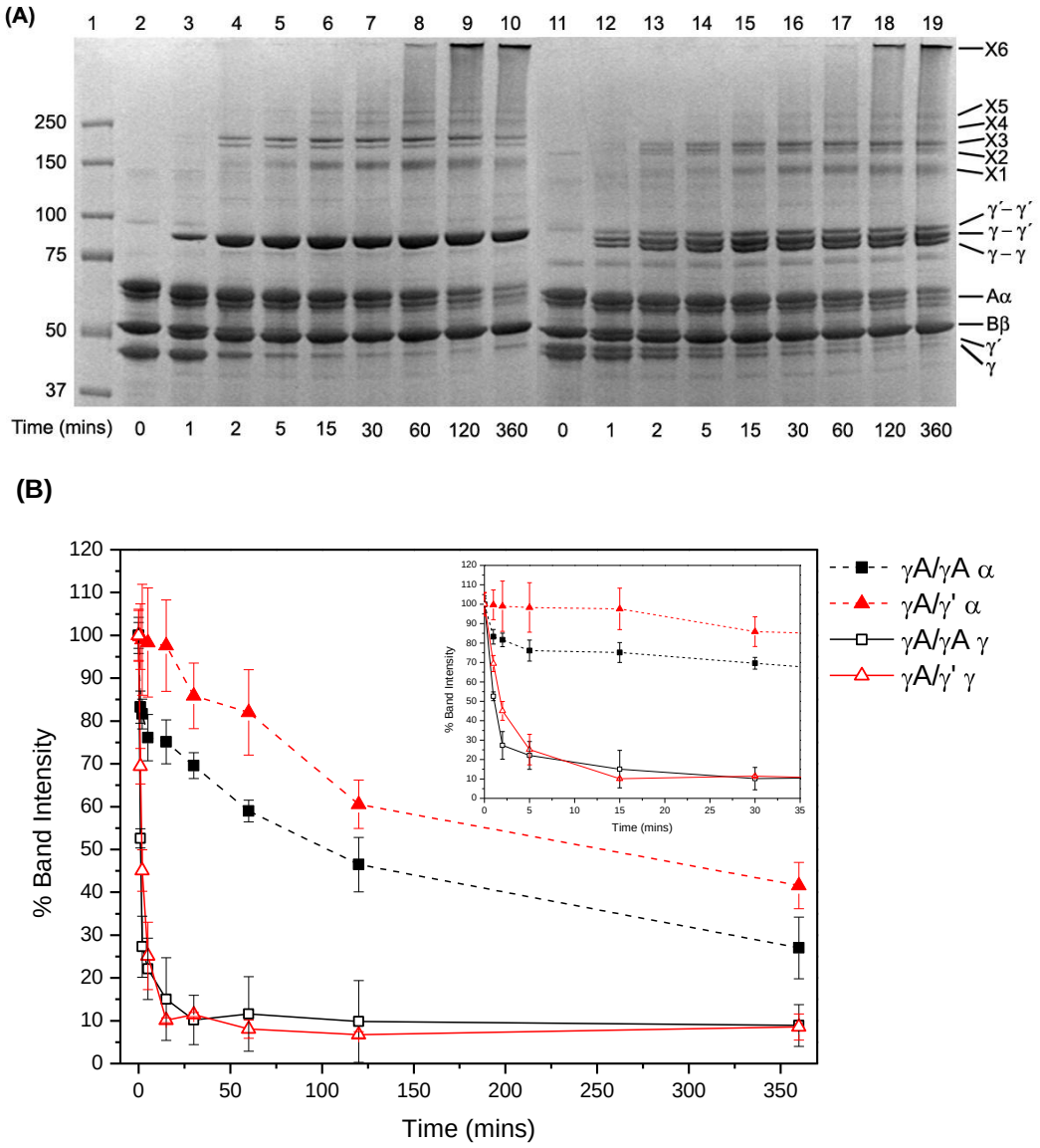

Figure 6-3: (A) Cross-linking of γA/γA and γA/γ′ fibrinogen by FXIIIa. Lane 1: molecular marker (kDa). Lanes 2-10: γA/γA fibrinogen. Lanes 11-19: γA/γ′ fibrinogen. In lanes 11-19 two γ chain bands exist corresponding to the γA and γ′ chains respectively, as compared to the single γ chain band in lanes 2-10 corresponding to the γA chain. X1-X6 denote α- and γ-multimers/polymers. **(B) Cross-linking analysis of clots formed from γA/γA and γA/γ′ fibrinogen**. The percentage intensity of the Aα and γ chains, normalized to the Bβ chain, were measured for both γA/γA and γA/γ′ fibrinogen from the SDS-PAGE gel and plotted as a function of time. The inset shows the first 30 minutes of cross-linking.

The effect of the γ′ chain on cross-linking by FXIIIa was investigated using SDS-PAGE analysis. Clots were prepared as described in section 2.2.1. Clotting was allowed to proceed for 0, 1, 2, 5, 15, 30, 60, 120 and 360 minutes at room temperature after which SDS-PAGE analysis was performed as described in section 2.2.1.

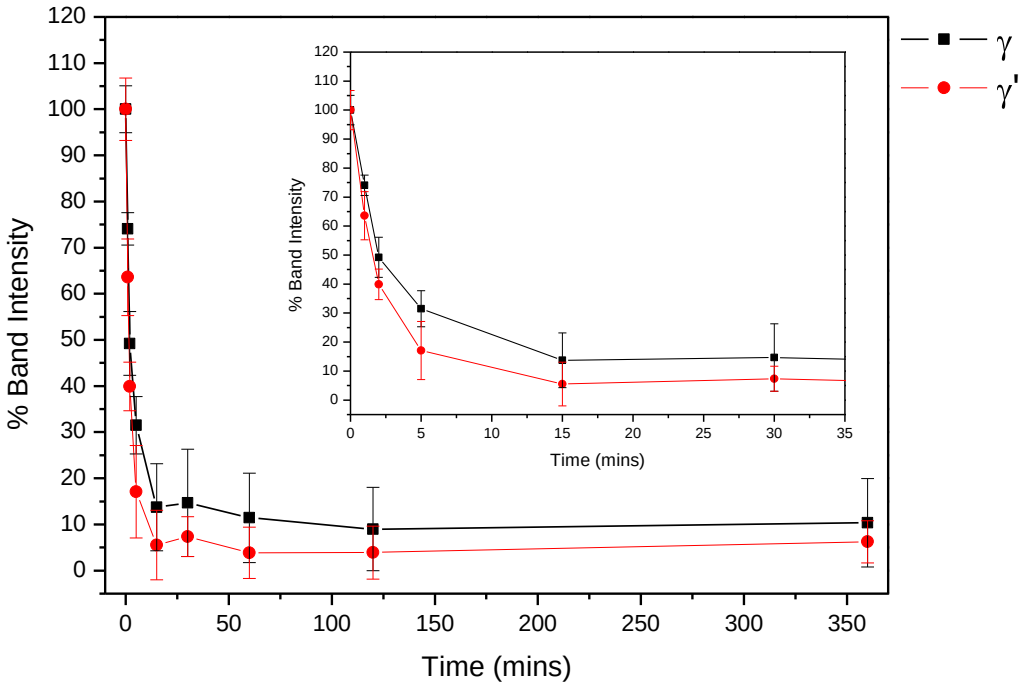

Figure 6-4: Cross-linking analysis of the γA and γ′ chains in γA/γ′ clots. The percentage intensity of the γA and γ′ chains, normalized to the Bβ chain, were measured for γA/γ′ fibrinogen from the SDS-PAGE gel in Figure 6-3(A) and plotted as a function of time. **Inset**: First 30 minutes of cross-linking. It is clear, within errors, there was no difference in the rate of cross-linking for either the γA or γ′ chains.

The decrease in intensity of the Aα and γ chain monomer bands was measured relative to that of the β chain (which is not a FXIIIa substrate and therefore does not undergo cross-linking) as a function of time to determine the relative amount of cross-linking (Figure 6-3). In both variants similar species of higher molecular weight cross-linking products were observed (X1, X2, X3, X4, X5 and X6). In γA/γ′ clots, 3 species of γ cross-link were detected corresponding to γA-γA, γA-γ′

and γ′-γ′ as opposed to the single γA-γA cross-linking band in γA/γA clots. The cross-linking rate and overall reduction in intensity of the γ chain monomer was similar when comparing γA/γ′ fibrin with γA/γA fibrin, indicating a similar amount of γ chain cross-linking (Figure 6-3 (B)). In addition, within γA/γ′ clots, the reduction rate of the individual γ-chain monomer species (γA vs. γ′) were similar (Figure 6-4). Together, these data demonstrate that FXIIIa is equally effective in cross-linking the γA- and γ′-chains.

A significant difference in cross-linking was detected between γA/γA and γA/γ′ clots in the amount of α-chain cross-linking (Figure 6-3 (B)). The reduction in α-chain monomer band was less in γA/γ′ clots, with a final intensity of 42% compared with 27% for γA/γA fibrin. These findings indicate α-chain cross-linking is reduced in γA/γ′ fibrin clots.

6.4 Fibrin Polymerisation

Polymerization of γA/γA and γA/γ′ fibrin was studied by turbidity analysis. Clots were prepared in triplicate as described in section 2.2.2. Thrombin or Reptilase was added to initiate clotting after which absorbance was measured every 12 seconds over the first 60 minutes of clotting (Figure 6-5).

The analysis of the turbidity data in Figure 6-5 is provided in Table 6-1. Turbidity initiated by thrombin showed a significant difference between polymerization of γA/γA and γA/γ′ fibrin. The maximum polymerization rate of γA/γA fibrin was 3.8-times higher than that of γA/γ′ and the time to plateau was shorter by 6 minutes (Table 6-1). Final absorbance of γA/γA fibrin was 4.1-times higher than that of γA/γ′. At equal fibrinogen concentrations, the maximum absorbance is directly related to the fibre diameter and/or the arrangement of fibres. This suggests γA/γ′ clots are either composed of thinner fibres, have an altered structure or posses thin fibres arranged non-uniformly.

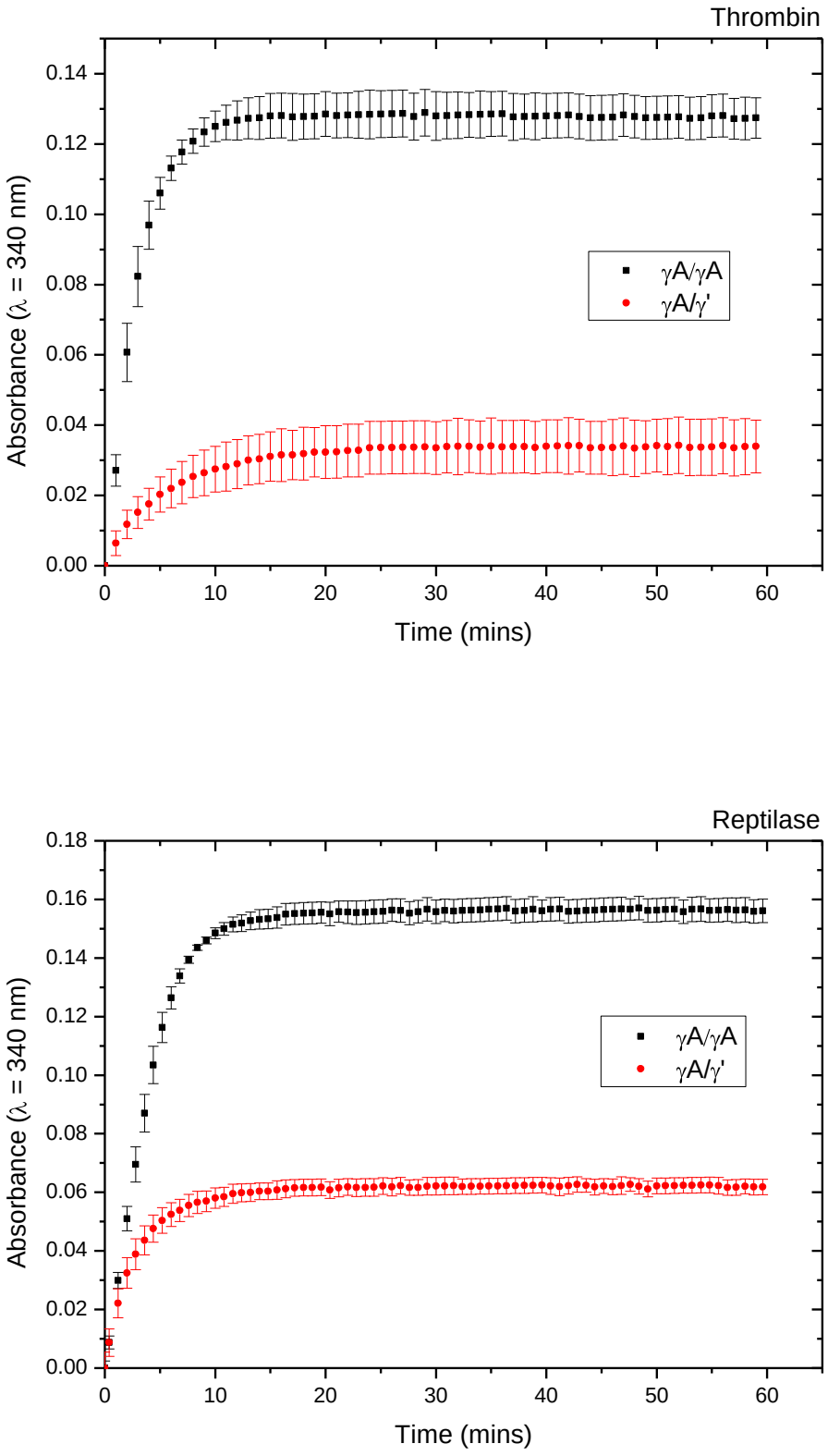

Figure 6-5: Turbidity analysis of polymerizing clots produced with γA/γA and γA/γ′ fibrinogen. Each curve is representative of 3 repeat measurements with error bars representing the standard error in the mean.

Table 6-1: Polymerisation data of clots formed from γA/γA and γA/γ′

	Thrombin		Reptilase	
Polymerisation Parameter	**γA/γA**	**γA/γ′**	**γA/γA**	**γA/γ′**
Maximum rate (units min^{-1})	0.030 ± 0.004	0.008 ± 0.001	0.026 ± 0.002	0.010 ± 0.003
Final Absorbance	0.123 ± 0.002	0.030± 0.001	0.156 ± 0.004	0.062 ± 0.003
Plateau time (minutes)	16 ± 1	22 ± 1	15 ± 2	18 ± 1

Polymerization of γA/γA and γA/γ′ fibrin was further investigated using reptilase, a snake venom enzyme which cleaves fibrinopeptide A only (unlike thrombin) and does not bind to the γ′-chain. Similar differences in polymerization were observed as with thrombin (Figure 6-5 and Table 6-1). Maximum polymerization rate of γA/γA fibrin was 2.6-times higher, and the time to plateau was shorter by 3 minutes. Final absorbance of γA/γA fibrin was 2.5-times higher than γA/γ′. These data demonstrate that the effects of γ′ on fibrin formation are independent of γ′ binding to thrombin and are likely due to a direct interference of the negatively charged peptide with fibrin formation.

The effect of FXIII inhibitor, FXIII and inhibitor-FXIII combination on polymerisation of γA/γA and γA/γ′ clots was also investigated using turbidity analysis. The results of this analysis are presented in Table 6-2. No differences were observed in any of the polymerisation parameters, within experimental errors, for γA/γA and γA/γ′ clots. It is therefore concluded that both the inhibitor and FXIII do not play a significant role in the polymerisation or final structure of either γA/γA or γA/γ′ clots.

Table 6-2: Polymerisation data of clots formed from γA/γA and γA/γ′

Polymerisation Parameter	Maximum Rate (units min^{-1})	Final Absorbance	Plateau Time (minutes)
γA/γA + In	0.127 ± 0.001	0.041 ± 0.004	14 ± 2
γA/γA + FXIII	0.133 ± 0.004	0.042 ± 0.003	14 ± 1
γA/γA + In + FXIII	0.136± 0.006	0.037 ± 0.005	15 ± 5
γA/γ′ + In	0.034± 0.002	0.009 ± 0.001	24 ± 2
γA/γ′ + FXIII	0.029 ± 0.004	0.010 ± 0.001	26 ± 4
γA/γ′ + In + FXIII	0.031 ± 0.008	0.013 ± 0.003	18 ± 4

6.5 Fibrin Structure

As suggested by turbidity analysis, γA/γ′ demonstrated a different structure than γA/γA fibrin. In order to investigate this further, LSCM (Figure 6-6) and SEM imaging (Figure 6-7) were performed as described in sections 2.2.4 and 2.2.5 respectively.

Both imaging techniques revealed a clear difference between the structure of γA/γ′ and γA/γA fibrin. The spatial distribution of fibres within γA/γ′ clots was less uniform than that of γA/γA clots. γA/γ′ fibres were arranged into tight interconnecting bundles producing large open pores. Imaging multiple optical slices which were then combined into one projection (200 x 200 x 50 μm) revealed that these pores were not localized structural inhomogeneities, but extended through the 50 μm z-stack (Figure 6-6 (C)).

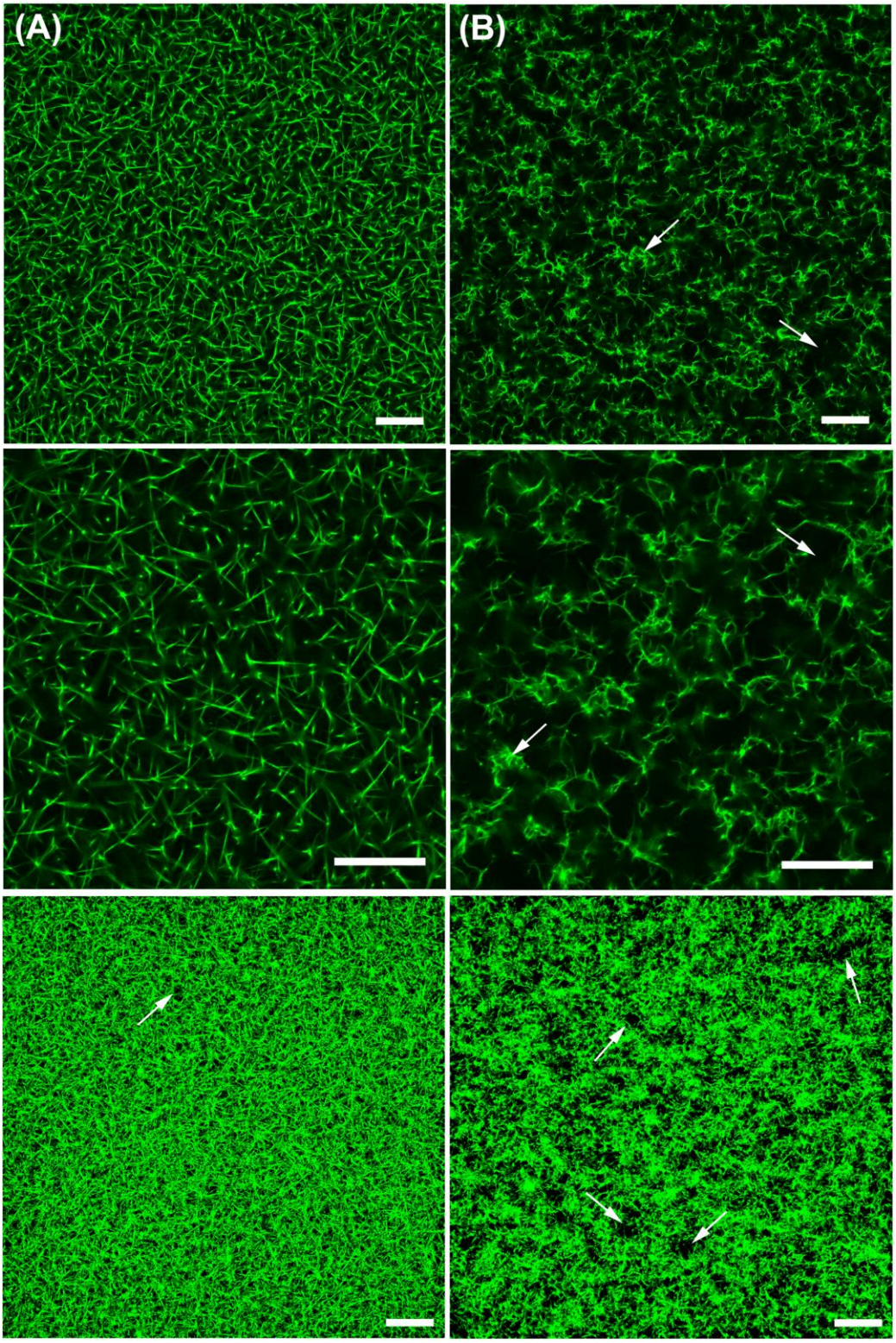

Figure 6-6: Confocal micrographs of clots formed from γA/γA (A) and γA/γ′ (B) fibrinogen. The first and second rows show micrographs, 200 x 200 μm and 100 x 100 μm respectively, of clots formed from thrombin. The third row shows three dimensionally reconstructed micrographs 200 x 200 x 50 μm. Brightness and contrast have been altered in both micrographs by the same amount. Scale bars indicate 20 μm and arrows indicate fibre bundles and pores. Final concentrations within a clot were 0.5 mg/ml fibrinogen, 5% fluorescently labelled fibrinogen 1.0 U/ml thrombin, 2.5 mM CaCl2 and 1 mM FXIII inhibitor.

SEM imaging further revealed, in agreement with lower maximum absorbance in turbidity, that γA/γ′ clots were composed of thinner fibres compared with γA/γA (Table 6-3). Fibre diameters were decreased by ~33% in γA/γ′ clots. LSCM showed lower fibre density in γA/γ′ clots, by ~22%. This decreased fibre density may be attributed to an underestimate of the fibre count in γA/γ′ clots. Many fibres were arranged into tight bundles and as such may not be resolved by confocal microscopy. However, SEM also revealed a decreased fibre density for γA/γ′ clots, although a smaller decrease of ~11% was observed.

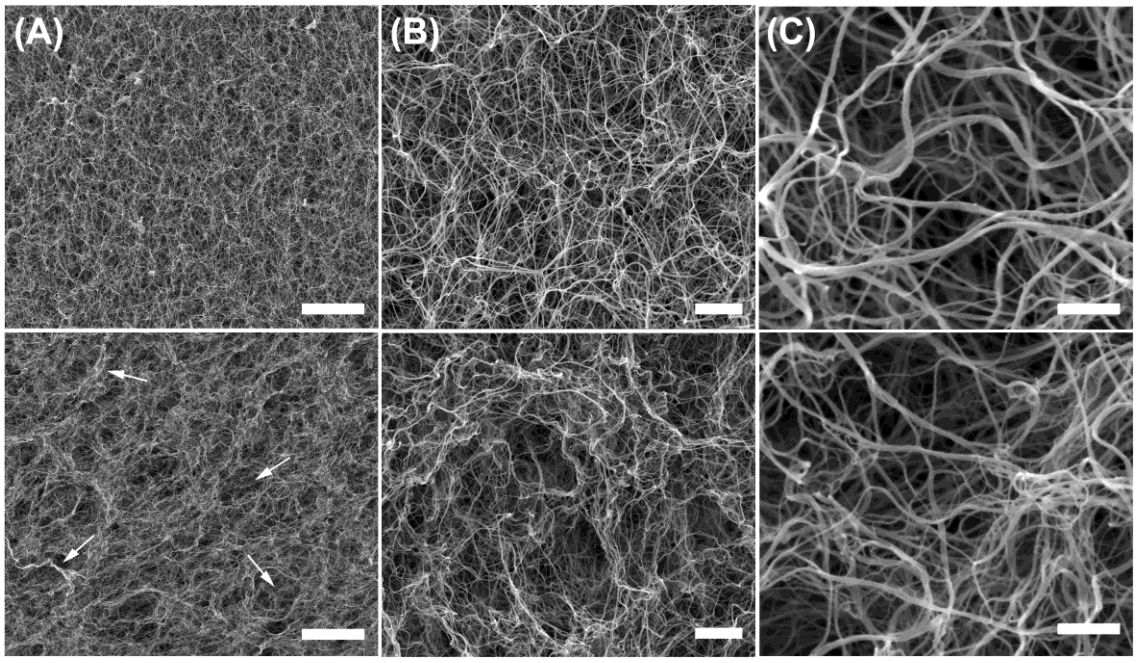

Figure 6-7: Scanning electron micrographs of clots formed from γA/γA (upper panels) and γA/γ′ (lower panels) fibrinogen. Images are (A) 5 000, (B) 20 000 and (C) 100 000 x magnification. Arrows indicate fibre bundles, pores and free fibre ends in γA/γ′ clots. Final concentrations within a clot were 0.5 mg/ml fibrinogen, 1.0 U/ml thrombin, 2.5 mM CaCl2 and 1 mM FXIII inhibitor. Scale bars represent (A) 10 µm, (B) 2 µm and (C) 500 nm.

Fibre density was much greater in SEM imaging; 49- and 43-times higher in γA/γ′ and γA/γA clots respectively compared with corresponding confocal images (Table 6-3). This discrepancy is attributed to differences in the sample preparation and imaging. SEM provides significant depth detail and will therefore show inherently more fibres in this case than the confocal microscopy images which were based on a single optical slice. In addition, clots prepared

for SEM will undergo significant shrinking as a clot consists of ~98% water (121) and must be dehydrated prior to imaging. Similar discrepancies comparing structural data from SEM and confocal imaging have been reported previously (186).

Table 6-3: Structural data of clots formed from γA/γA and γA/γ′

Structural Parameter	γA/γA	γA/γ′
Fibre diameter* (μm)	43 ± 2	29 ± 3
Fibre density* (fibres μm^{-1})	9.9 ± 0.3	8.8 ± 0.3
Fibre density† (fibres μm^{-1})	0.23 ± 0.01	0.18 ± 0.01

*SEM
†Confocal

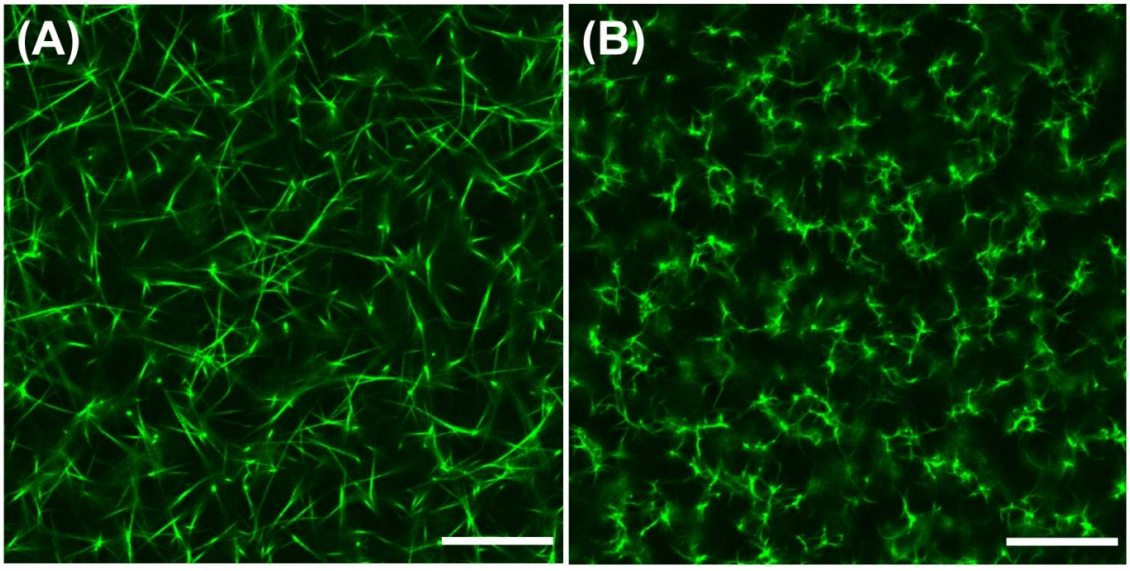

Figure 6-8: Confocal micrographs of clots formed from γA/γA (A) and γA/γ′ (B) fibrinogen by the snake venom reptilase. Micrographs are 100 x 100 μm and the scale bars indicate 20 μm. Final concentrations within a clot were 0.5 mg/ml fibrinogen, 5% fluorescently labelled fibrinogen, 5.0 BU/ml reptilase and 2.5 mM $CaCl_2$.

We next investigated whether the differences in structure between γA/γA and γA/γ′ fibrin observed by LSCM were dependent on thrombin. When reptilase was used instead of thrombin, fibrin fibres were arranged non-uniformally

producing a more porous structure in γA/γ′ clots (Figure 6-8), comparable to the structures observed with thrombin (Figure 6-6). Again, fibre density was lower in γA/γ′ clots compared with γA/γA clots ($\rho_{\gamma A/\gamma'}$ = (0.12 ± 0.01) fibres μm^{-1} vs. $\rho_{\gamma A/\gamma A}$ = (0.20 ± 0.02) fibres μm^{-1}). These data are in agreement with turbidity data (Figure 6-5) and show that the effects of γ′ on fibrin structure are independent of interaction with thrombin.

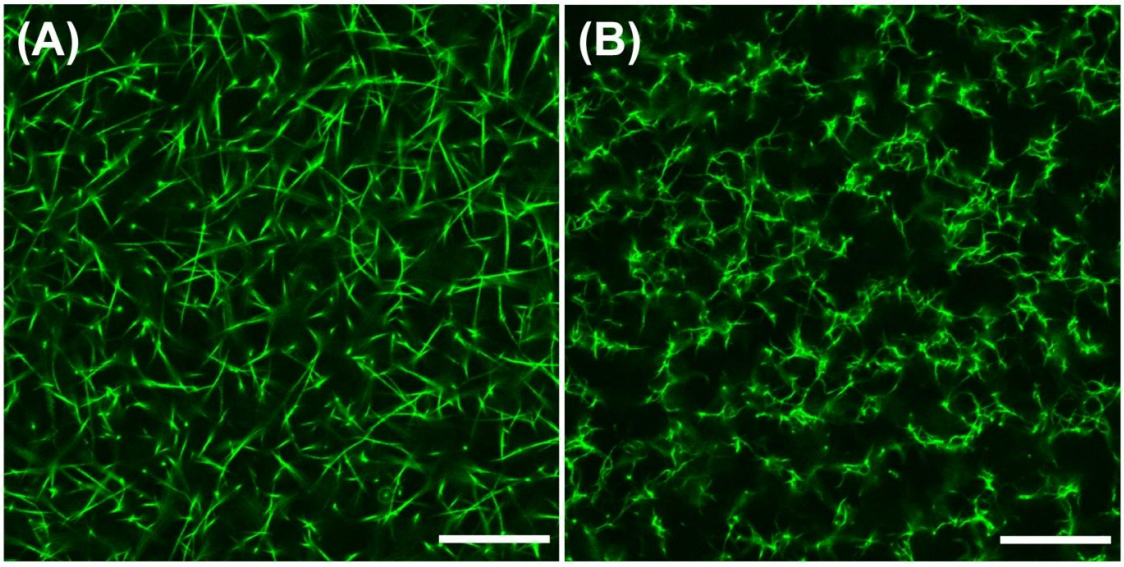

Figure 6-9: Confocal micrographs of clots formed from γA/γA (A) and γA/γ′ (B) fibrinogen in the Presence of FXIIIa. Micrographs are 100 x 100 μm and the scale bars indicate 20 μm. Final concentrations within a clot were 0.5 mg/ml fibrinogen, 5% fluorescently labelled fibrinogen, 1.0 U/ml thrombin 2.5 mM $CaCl_2$ and 3.7 μg/ml FXIIIa. Fibre density was lower in γA/γ′ clots compared with γA/γA clots.

Finally, the structure of clots formed in the presence of FXIIIa was also investigated (Figure 6-9). Once again similar differences in structure and fibre density ($\rho_{\gamma A/\gamma'}$ = (0.18 ± 0.01) fibres μm^{-1} vs. $\rho_{\gamma A/\gamma A}$ = (0.22 ± 0.01) fibres μm^{-1}) between γA/γ′ and γA/γA clots were observed. These data show that the effect of γ′ chain on fibrin structure is independent of cross-linking by FXIIIa as well.

6.6 Viscoelastic Properties

The mechanical and viscoelastic properties of γA/γA and γA/γ′ fibrin were measured using the magnetic microrheometer described in chapter 3. Samples were prepared as described in section 2.2.4. In the absence and presence of FXIIIa cross-linking there are clear differences in the mechanical properties of γA/γA and γA/γ′ clots. From the data in Figure 6-10 the following parameters were extracted: the rate of change of the compliance (dJ^{-1}/dt) during the initial 5 minutes of data capture, the initial (J_I) and final (J_F) compliances along with the plateau time which gives a measure of the kinetics of the mechanical development.

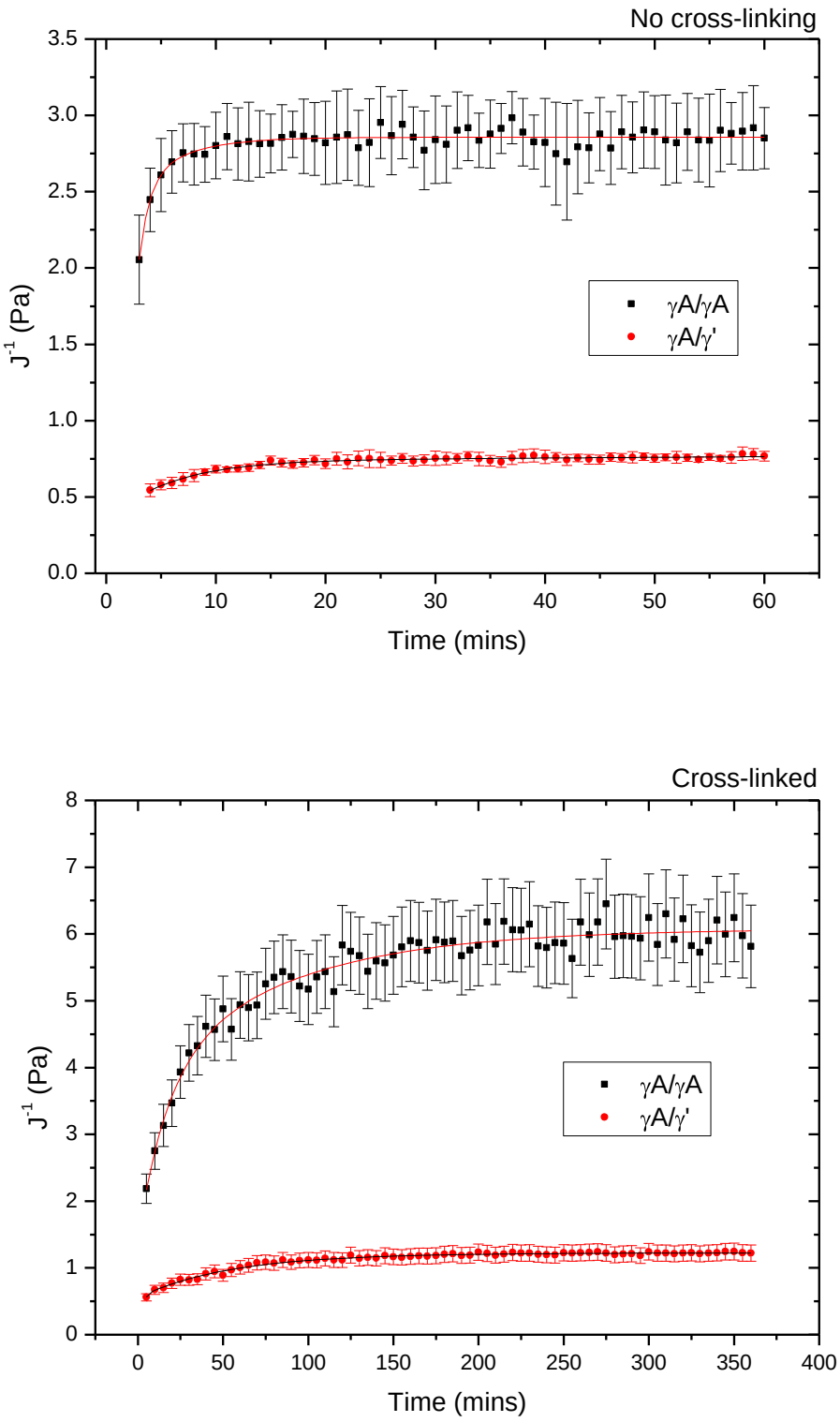

Figure 6-10: J^{-1} vs. time of clots formed from γA/γA and γA/γ′ fibrinogen in the absence and presence of FXIIIa. Each data plot is representative of 3 repeat measurements where errors are the standard error in the mean. Each data set is fitted with an exponential curve as a guide for the eye.

In the absence of cross-linking the initial compliance of γA/γA clots increased 7-times faster than γA/γ′ clots. This increased rate of compliance development is also reflected in the shorter plateau time for γA/γA clots, which is nearly half that of γA/γ′ clots, indicating an earlier plateau in the mechanical properties for γA/γA clots. This is consistent with turbidity measurements where an increased rate of development was observed for γA/γA clots. In the presence of cross-linking the rate of change of compliance increased for both γA/γA and γA/γ′ clots; increasing by 1.6- and 1.7-times respectively. However, the rate of change of compliance was still higher for γA/γA clots by 6.6-times. Again, γA/γA clots exhibited a shorter plateau time, however for both clot types these were much longer when compared to clots without cross-linking. This increased time to plateau is attributed to cross-linking which is still occurring on these timescales (Figure 6-3 (A)).

Table 6-4: Mechanical data of clots formed from γA/γA and γA/γ′

			Cross-linked	
Mechanical Parameter	**γA/γA**	**γA/γ′**	**γA/γA**	**γA/γ′**
dJ^{-1}/dt (Pa s^{-1})	0.16 ± 0.04	0.023 ± 0.002	0.25 ± 0.02	0.038 ± 0.005
J_I (Pa)	2.1 ± 0.2	0.54 ± 0.04	2.2 ± 0.2	0.56 ± 0.05
J_F (Pa)	2.87 ± 0.03	0.76 ± 0.01	6.3 ± 0.6	1.2 ± 0.1
Plateau time (minutes)	10 ± 1	20 ± 3	175 ± 18	200 ± 12

The initial compliance of γA/γA clots was ~3.9-times higher than γA/γ′ clots both in the presence and absence of cross-linking. This indicates that the nascent network of the clot is mechanically stiffer prior to further fibre growth, branch point formation and cross-linking. The final compliance of γA/γA clots was 3.8-times higher than γA/γ′ clots in the absence of cross-linking, this difference increased to 5.3-times in the presence of cross-linking. Since there is little change in the initial compliance for both clots with and without cross-linking this

suggests the increased final compliance in γA/γA clots over γA/γ′ clots is due to increased amounts of α-chain cross-linking as observed in SDS-PAGE analysis.

There was also a significant difference in the viscoelastic properties of γA/γA and γA/γ′ clots (Table 6-5). In the absence of cross-linking, γA/γA clots were 2.7-times stiffer than γA/γ′ clots, as shown by the difference in the storage modulus G′. In the presence of cross-linking this difference increased, with γA/γA clots becoming 4.6-times stiffer than γA/γ′ clots. Therefore, γA/γA clots became 3.9-times stiffer and γA/γ′ clots 2.3-times stiffer due to cross-linking. These data show that cross-linking by FXIIIa induces a greater increase in stiffness in γA/γA than in γA/γ′ clots. As mentioned above this is attributed to the increased amounts of α-chain cross-linking observed.

Table 6-5: Viscoelastic data of clots formed from γA/γA and γA/γ′

			Cross-linked	
Viscoelastic Parameter	**γA/γA**	**γA/γ′**	**γA/γA**	**γA/γ′**
G′ (Pa)	1.5 ± 0.2	0.56 ± 0.06	5.8 ± 0.2	1.27 ± 0.09
G′′ (mPa)	8 ± 2	40 ± 10	1.2 ± 0.4	7 ± 2
tanδ (10^{-3})	5 ± 3	71 ± 43	0.2 ± 0.1	5 ± 3

The energy dissipated by deformation processes as indicated by the loss modulus G′′ was around 5-times higher in γA/γ′ clots than in γA/γA clots, both with and without cross-linking. This suggests that γA/γ′ clots are more likely to deform compared with γA/γA clots. In addition, the loss tangent of γA/γ′ clots was 14- and 25-times greater than that of γA/γA clots in the absence and presence of cross-linking respectively. Altogether these data indicate that the decreased stiffness and increased viscosity render γA/γ′ clots less resistant to deformation than γA/γA clots.

6.7 Protofibril Arrangements

The AFM was used to visualise protofibril formation during the very early stages (< 1min) of fibrin polymerization and investigate the molecular mechanisms underpinning the role of γ′ in fibrin structure. Samples were prepared and imaged as described in section 2.2.6. Prior to imaging fibrin polymerisation, the binding of γA/γA and γA/γ′ fibrinogen to the mica substrate was measured in order to investigate any potential differences.

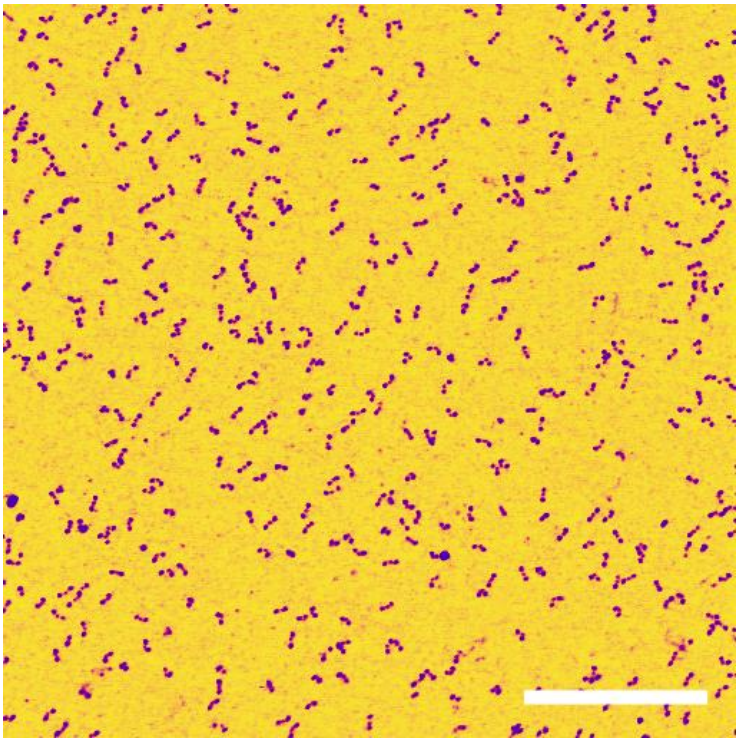

Figure 6-11: AFM image of γAγA fibrinogen on a mica substrate. Multiple 2 x 2 μm images were obtained and the surface density of molecules was measured. The scale bar represents 500 nm.

γA/γA and γA/γ′ fibrinogen were diluted in TBS buffer to ~1 μg/ml, placed onto the $NiCl_2$ treated mica surface and allowed to incubated for 2 minutes. Multiple images of fibrinogen molecules distributed across the surface were obtained and the surface density of molecules was measured (Figure 6-11). No difference between the surface binding of γA/γA and γA/γ′ fibrinogen was observed ($\rho_{\gamma A/\gamma'}$ = (121 ± 6) molecules μm^{-2} vs. $\rho_{\gamma A/\gamma A}$ = (108 ± 8) molecules μm^{-2}; n = 5, p = 0.19).

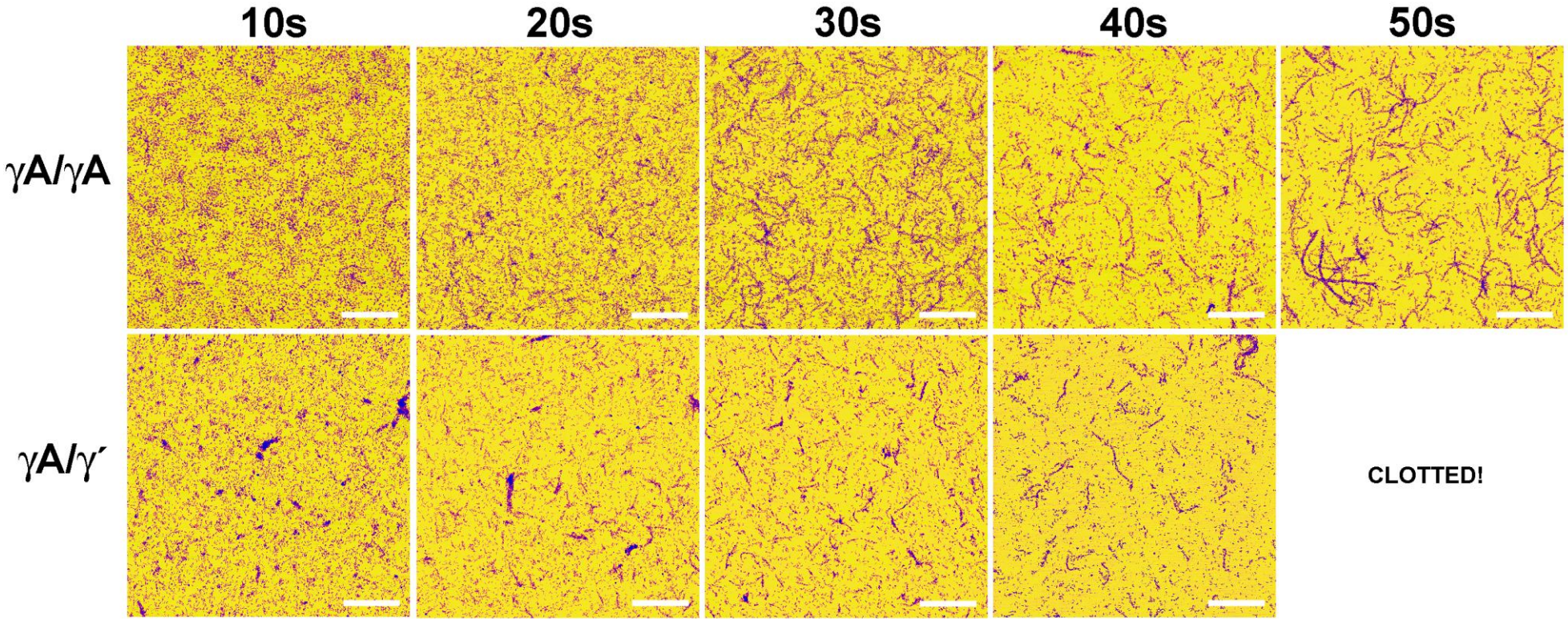

Figure 6-12: AFM imaging of γA/γA and γA/γ′ polymerization. Each image is 5 x 5 μm and the scale bar indicates 1 μm. It wasn't possible to image up to 50 seconds for the γA/γ′ clot as the clot had gelled by this time.

Next, the AFM was used to visualize protofibril formation during the initial stages of polymerization after the addition of thrombin (Figure 6-12). After 10 seconds of polymerization there was already a notable difference; fibrin monomers arranged themselves into loose associations on the surface in γA/γA clots, these could be seen as regions of higher density fibrin. However, in γA/γ′ clots, large agglomerations of fibrin monomers were observed. By 20 seconds oligomer formation appeared more extensive in γA/γ′ clots. At 30 seconds oligomer formation and growth was observed in both γA/γA and γA/γ′ clots. At 40 seconds γA/γA fibrinogen oligomers were 96 nm longer than γA/γ′ fibrinogen oligomers ($L_{\gamma A/\gamma A}$ = (327 ± 11) nm (n = 229) vs. $L_{\gamma A/\gamma'}$ = (231 ± 12) nm (n = 218); $p < 0.0001$). At 50 seconds, γA/γA oligomers continued to grow longer, reaching 526 ± 6 nm in length, and appeared to be forming protofibrils and fibres. It was not possible to image γA/γ′ clots at 50 seconds as the network had gelled by this time. These data show that the γ′-chain directly interferes with oligomer formation and protofibril growth.

6.8 Gel time

The gel point was analyzed both manually and with a coagulometer as described in section 2.2.3. Manual inspection showed that γA/γ′ clots gelled between 40 and 45 and γA/γA clots between 50 and 55 seconds. Using the coagulometer, we found that γA/γ′ clots gelled ~10 seconds quicker than γA/γA clots ($t_{\gamma A/\gamma'}$ = 32.9 ± 0.9 vs. $t_{\gamma A/\gamma A}$ = 43.4 ± 0.3 seconds; $p < 0.001$). We attribute the overall quicker gelling time observed with the coagulometer to the experiment being performed at 37°C as opposed to room temperature for the manual test. The instrument has no temperature control hence it wasn't possible to perform both experiments under the same conditions. Nevertheless, both measurements agreed that γA/γ′ fibrin gels earlier by ~10 seconds.

6.9 Fibrinolysis

Fibrinolysis of γA/γA and γA/γ′ fibrin was studied by turbidity analysis. Clots were prepared in triplicate as described in section 2.2.2. Plasminogen (final concentration of 0.3 μM) was incubated with fibrinogen and then a mixture of thrombin and tPA (final concentration of 1 nM) was added to initiate coagulation and fibrinolysis simultaneously. Changes in absorbance were measured every 12 seconds over the first 80 minutes of clotting (Figure 6-13).

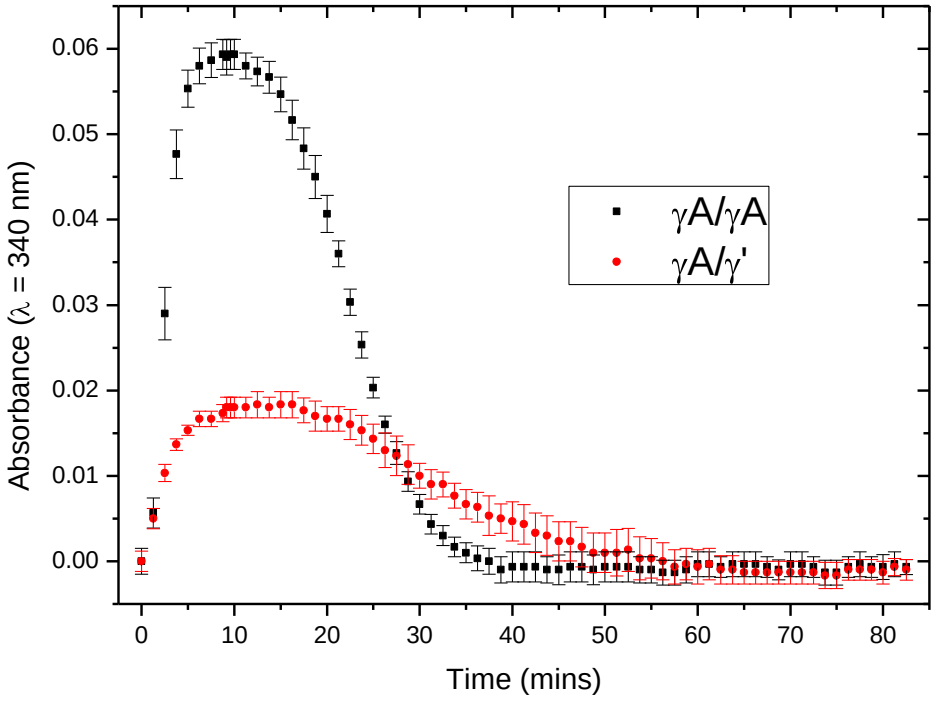

Figure 6-13: Turbidity analysis of fibrinolysis in clots formed from γA/γA and γA/γ′ fibrinogen. Each curve is representative of 3 repeat measurements with error bars representing the standard error in the mean.

The analysis of the turbidity data in Figure 6-13 is provided in Table 6-6. In agreement with turbidity measurements we observed both an increased maximum rate and higher absorbance for γA/γA clots. The maximum polymerization rate of γA/γA fibrin was 4.2-times higher than that of γA/γ′. The maximum absorbance of γA/γA fibrin was 3.2-times higher than that of γA/γ′.

Again, there was no observable lag phase for either fibrinogen variant. The lysis time, defined as the time taken to reach half the peak absorbance, was longer in γA/γ′ clots by 5 minutes.

Table 6-6: Fibrinolysis data of clots formed from γA/γA and γA/γ′

Fibrinolysis Parameter	γA/γA	γA/γ′
Maximum Rate (units min^{-1})	0.022 ± 0.002	0.0052 ± 0.0004
Maximum Absorbance	0.059 ± 0.001	0.0187 ± 0.0003
Lysis time*	14 ± 1	19 ± 2

*Lysis time is defined as the time taken to reach half the peak absorbance

6.10 Discussion and Conclusions

Our study shows major differences in the viscoelastic properties of clots produced with a naturally occurring fibrinogen γ chain splice variant (γ′), with reduced stiffness and increased deformation for γ′ fibrin. These differences in stiffness and deformation occurred both with and without cross-linking by FXIIIa. In addition, we present qualitative and quantitative evidence that the γ′ chain inhibits protofibril growth directly. We show dramatic differences in fibrin polymerization and structure, and show that these are independent of thrombin binding to the γ′ chain and of its interactions with FXIII. This direct interference of the γ′ chain with protofibril growth provides a potential mechanism that explains the altered structure and mechanical properties of γA/γ′ fibrin.

We found a reduced maximal rate of polymerisation and final absorbance associated with the γ′ chain in turbidity measurements, in agreement with previous observations (96, 185). Our data suggest that clot formation is slowed through a decrease in lateral aggregation, resulting in a clot consisting of thinner fibres. This interpretation is consistent with the observation from scanning electron microscopy, where we observed γA/γ′ clots consist of thinner

fibres. In addition, magnetic microrheometer measurements also reveal the rate of mechanical stiffness development is reduced in γA/γ′ clots. Again, consistent with the idea of reduced radial fibre growth.

Two possible models have previously been suggested to explain the role of the γ′ chain in clot polymerization. Firstly, one in which the binding of the γ′ chain to thrombin inhibits its activity (190). And secondly, one whereby the γ′ chain disrupts protofibril and fibre formation through charge-charge interactions (185). A study by Siebenlist *et al.* suggested that thrombin binding to the γ′ chain results in delayed release of fibrinopeptide A and that this may be responsible for the observed structural alterations between γA/γ′ and γA/γA clots (184). In order to elucidate the mechanism responsible for altered polymerization we formed clots with either thrombin or reptilase; a snake venom which cleaves fibrinopeptide A but does not bind to the γ′ chain. Turbidity data clearly showed that a decreased maximum rate and final absorbance remained associated with the γ′ chain when clots were formed with reptilase, demonstrating that the effect of the γ′ chain on fibrin structure is independent of its interactions with thrombin. There were some minor differences in polymerization when comparing thrombin to reptilase, which may be explained by differences in enzyme concentrations or fibrinopeptide release rates, however the difference between γA/γ′ and γA/γA fibrin remained clear. Confocal microscopy imaging also showed minor overall differences in clot structure between clotting with thrombin or reptilase, but again a striking difference between γA/γ′ and γA/γA fibrin was apparent. It has been observed that thrombin remains active while bound to the γ′ chain (191). In addition, previous studies from our laboratory and others reported normal fibrinopeptide A release from recombinant γA/γ′ fibrinogen by thrombin (96, 185). Our current data provide new evidence that the differences in polymerization arise from direct disruption of clot formation by the γ′ chain through physical interaction and not through inhibition of thrombin.

In the present study we find that γA/γ′ fibrinogen formed clots composed of thinner fibres and found that they are arranged non-uniformly. Several reports in the literature show changes in clot structure for γ′ fibrin, however, the reports

have not been entirely consistent. Part of these differences may be due to the different source materials used (recombinant versus plasma purified) and the experimental conditions. Previous studies from our laboratory and from Siebenlist *et al.* found an association between γ′ and thinner fibres (96, 184). Gersh *et al.* find no difference in fibre diameter between recombinant γA/γA and γA/γ′ clots, however they did observe thinner fibres in γ′/γ′ clots (185). Both Siebenlist *et al.* and our previous study found that γ′ was associated with a more branched network (96, 184). Gersh *et al.* reported that clots formed from γA/γ′ fibrinogen were non-uniform with fibres that bundled together and produced large open pores (185). The latter authors also reported the presence of free fibre ends, which they suggested arise when multiple γ′ ends come together and terminate the polymerization process due to the concentration of negative charge. In agreement with this, the SEM and confocal imaging carried out in our current study show the presence of structures that were non-uniform. The heterogeneity of the γ′ fibrin structure was particularly evident at lower SEM magnification (5000x), which may explain why this aspect was not observed in our previous study in which fibrin was imaged at higher magnification (185). Overall, most studies appear to confirm an effect of the γ′ chain on fibrin structure and most studies agree with a decrease in fibre diameter for γ′ fibrin.

Magnetic microrheometer measurements reveal that γA/γ′ clots are inherently weaker, independently of cross-linking by FXIIIa, and that these mechanical properties are attributable to differences in their fibrin structure. Larger fibres are associated with maximum rigidities in clots (33). Thus, the thinner and shorter fibres in γA/γ′ clots, combined with a non-uniform distribution of the fibres, may lead to the reduced stiffness observed. Collet *et al.* previously reported on the role of the fibrinogen γ′ chain in modulating fibrin viscoelasticity (186). However, their study refers to homodimers of γ′/γ′ fibrin (produced by recombinant expression), which occur at a maximum concentration of 0.5% in human plasma, while the heterodimer γA/γ′ presented in our current study circulates at a concentration of 8-15% of total fibrinogen. They observed no difference in stiffness between clots made with recombinant γ′/γ′ clots and γA/γA clots in the absence of cross-linking. Instead an increase in stiffness of around

3-times was observed in recombinant γ′/γ′ clots over γA/γA clots in the presence of cross-linking. Other studies have suggested that γ′ fibrin undergoes more cross-linking by FXIIIa (187, 189). We suggest that the discrepancy between our findings and those of Collet *et al.* (198) may be due in part to differences in source material (recombinant γ′/γ′ compared with plasma purified γA/γ′).

The extent of cross-linking in clots produced with γA/γ′ fibrinogen has been subject of debate. Farrell *et al*. found that γA/γ′ clots were more highly cross-linked, with more extensive γ- and α-chain cross-linking (187, 189). They also reported that γA/γ′ fibrinogen accelerated FXIII activation. On the contrary, Siebenlist *et al*. found no measurable differences in the rate or extent of γ-chain cross-linking, whereas the overall rate and onset of α-cross-linking was slower for γA/γ′ fibrinogen (184). In agreement with the latter study, our data show that γA/γ′ fibrin is associated with reduced α-chain cross-linking. In the presence of FXIIIa cross-linking, we observed a smaller increase in stiffness in γA/γ′ clots when compared with γA/γA clots. The combination of thinner, less uniform fibres with less extensive α-chain cross-linking is likely responsible for the reduced stiffness observed in γA/γ′ clots.

To elucidate the mechanism by which the γ′ chain alters clot polymerization we performed AFM imaging during the early stages of polymerization. Fibrin polymerization studies are typically performed by analyzing the lag phase via turbidity. However, turbidity only increases during the phase of lateral aggregation of fibrin protofibrils (30) and therefore does not provide information on protofibril formation. Recently, Chernysh *et al* (199). visualized and characterized structures formed during the early stages of fibrin polymerization using transmission electron microscopy. Here, we used the AFM to directly visualize and measure protofibril formation. We report that the presence of the γ′ chain inhibits protofibril growth. One hypothesis may be that normal protofibril growth occurs through either γA-γA or γA-γ′ chain combinations at the D-D interface, but when two γ′ chains come together at this interface, they disrupt the growth of the protofibril. Turbidity data indicating that the γ′ chain disrupts polymerization and the existence of free fibre ends in SEM micrographs as

observed by Gersh *et al*. (196) gives further support to this hypothesis. However, in absence of structural information on the γ′ C-terminal extension, the orientation of γ′ with respect to the D-D interface remains unknown.

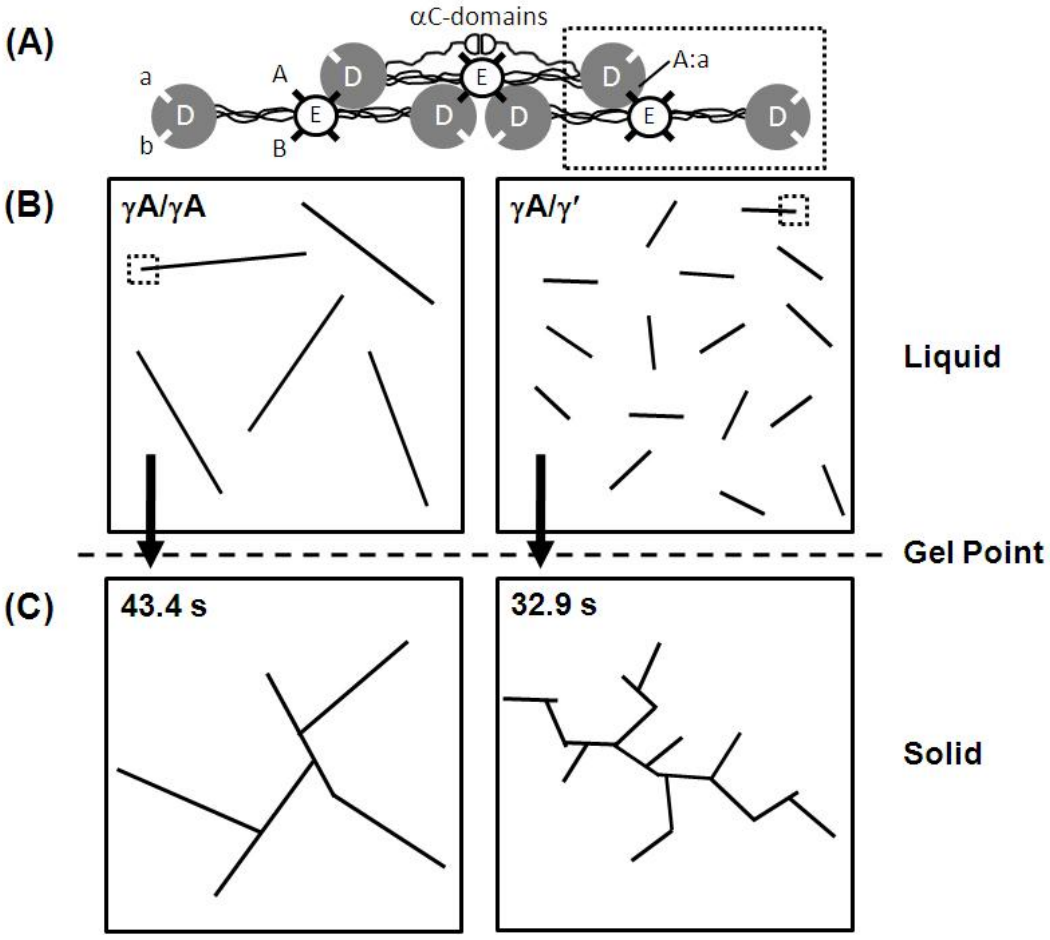

Figure 6-14: Schematic diagram of network formation in γA/γA and γA/γ′ clots. (A) diagram representing the "knob-hole" interaction of 3 fibrinogen molecules (adapted from Medved et al.(11)). The αC-domains are shown only in the upper molecule for clarity. Protofibril growth occurs through highly specific A:a interactions,(16) as indicated in the dashed box which highlights the exposed binding sites at the ends of the protofibril. (B) Schematic representation of γA/γA and γA/γ′ clots prior to the gel-point. The same amount of material is present within both clots but distributed differently. γA/γ′ clots are composed of a greater number of smaller protofibrils, the result is many more biochemically "sticky" ends (dashed box) are present within the same volume of clot as compared with γA/γA clots. (C) γA/γA and γA/γ′ clots after the gel-point. At this stage the protofibrils have branched and produced an interconnected path of fibrils which spans the clot structure. As seen by the experimentally determined gel-point time this process occurs ~10 seconds quicker in γA/γ′ clots.

In addition to differences in protofibril growth, γA/γ′ protofibrils gelled earlier than γA/γA. It has been reported that 70% of fibres have reached their maximum length at the gel-point (121). Weisel and Nagaswami developed a model to predict fibrin formation based on fibrinopeptide A release, protofibril formation and lateral aggregation of the protofibrils to form fibres (149). This model predicts that longer protofibrils lead to increased lateral aggregation, in agreement with our findings of increased fibre diameter for γA/γA fibrin which showed longer protofibrils by AFM. However, this model cannot predict our findings with regards to the earlier gel-point in γA/γ′ fibrin, which produced shorter protofibrils and thinner fibres. We therefore propose a working model hypothesis of gel formation to explain the relationship between inhibition of protofibril growth in γA/γ′ fibrin, reduced gel formation time and differences in fibrin structure (Figure 6-14). In this model hypothesis, inhibiting protofibril growth would lead to a greater number of smaller protofibrils in a given area. Assuming that only the ends of a fibrin protofibril are biochemically active (with at least half of the binding sites on the E-region and all those of one D-region still exposed), these can therefore attach to another fibril or to another fibrin monomer. In γA/γ′ clots, which contain a larger number of protofibril ends per given area, there may therefore be a greater likelihood of protofibril interaction and branching, resulting in a higher chance for the occurrence of an interconnected path of fibrils which spans a length scale long enough to turn a clot from liquid to gel (defined as the gel point (100)). This model could explain why γA/γ′ clots gel while protofibrils are still in this premature stage. The model could also agree with the formation of a non-uniform structure due to early gelling of highly branched, short protofibrils. However, a note of caution needs to be added that this model represents a simplified working hypothesis, and that it is therefore likely incomplete and speculative, until further experimental data is obtained to support it.

Finally, we observed longer lysis times in γA/γ′ clots. Delayed clot lysis rates have been associated with altered fibre and clot architecture (200-202). Thinner fibres support a slower rate of tPA-mediated plasmin generation (203) reducing the fibrinolytic activity of the clot. It has also been observed that clots consisting of thinner fibres are more resistant to fibrinolysis. This is attributed to the fact

that clots consisting of thinner fibres form a tighter and less porous network (33, 200-204). Our observations of slowed lysis in γA/γ′ clots are consistent with these findings. The thinner fibres of γA/γ′ clots will result in reduced plasmin generation. This coupled with the non-linear structure where fibres form dense knots will further reduce the fibrinolytic activity of γA/γ′ clots. In addition, our findings are consistent with other studies in the literature reporting an association between the γ′ chain and reduced fibrinolysis (184, 186, 187).

In conclusion, we provide evidence that the γ′ chain alters fibrin polymerization and that this is independent of the γ′ chain binding to thrombin or FXIIIa. Direct imaging of protofibril formation reveals that the γ′ chain is associated with inhibition of protofibril growth. Our data are consistent with a model hypothesis whereby shorter, more numerous protofibrils could lead to earlier gelling of γA/γ′ clots. Subsequently, this results in a clot which is altered both structurally and mechanically. γA/γ′ clots are composed of thinner, shorter fibres arranged non-uniformly producing large open pores which extend throughout the clot structure. The production of a mechanically weaker, non-uniform fibrin clot which results in delayed lysis may help to explain the differential association of fibrinogen γ′ with thrombosis in the venous and arterial vascular beds.

Chapter 7

7 Plasma Clots

7.1 Introduction

The aim of the work presented within this chapter was to investigate the effect of different plasma proteins on clot polymerisation and structure and determine the subsequent effect on clot mechanical properties and viscoelasticity. Four different plasma proteins, factor VIIa, IXa, XIIa and XIII, were chosen and each displayed a range of different effects on clot behaviour.

7.2 Sample Preparation

Clots were formed using FVII-, FIX-, FXII- and FXIII-deficient plasmas with and without reconstitution with purified human proteins. The plasma was diluted 1/6 in the final reaction mixture, so the final fibrinogen concentration was assumed

to be around 0.5 mg/ml, which represents a 6-times dilution from normal *in vivo* plasma concentration. Final thrombin concentration was 0.5 U/ml with a final $CaCl_2$ concentration of 7.5 mM. The final concentration of plasma protein was as follows,

- FVIIa: 83 ng/ml
- FIXa: 0.83 µg/ml
- FXIIa: 5 µg/ml
- FXIII: 3.7 µg/ml

All of which represent 1/6 *in vivo* zymogen plasma concentration. For FXIIa clots an intermediate concentration of 1.25 µg/ml, representing 25% of the corresponding plasma level, was also tested. For details of all plasmas and their respective proteins please see section 2.1.

7.3 FVIIa

The effect of FVIIa on clot polymerization was studied by turbidity analysis. Clots were prepared as described in section 2.2.2 with 5 repeats being made for each clot type. Thrombin was added to initiate clotting after which absorbance was measured every 12 seconds over the first 60 minutes of clotting (Figure 7-1). This procedure was used to investigate the overall effects of the selected plasma proteins on clot polymerisation.

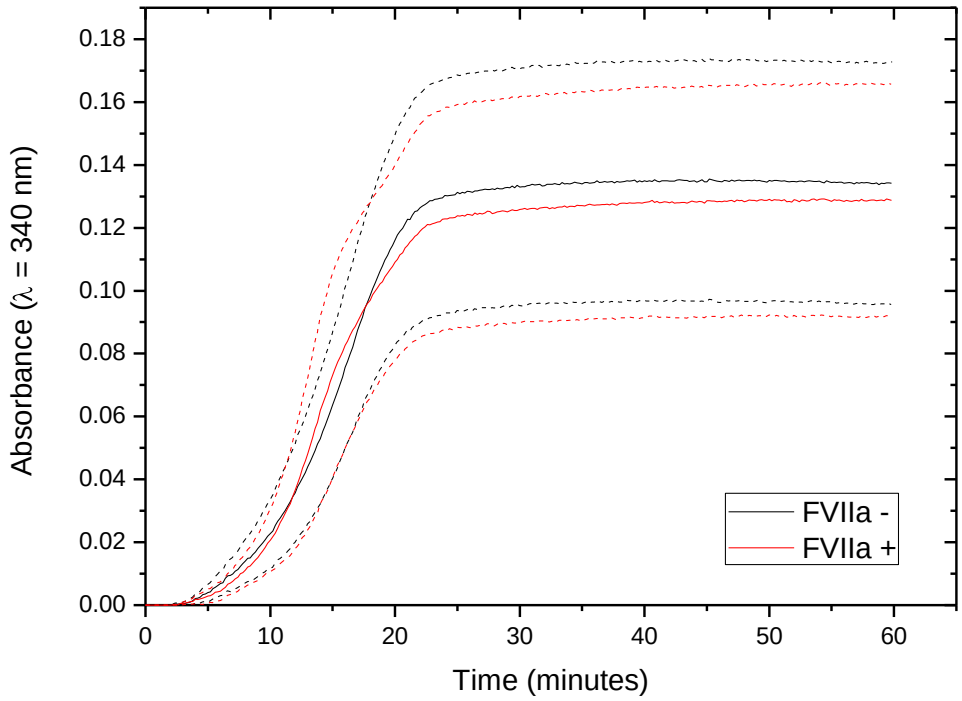

Figure 7-1: Absorbance vs. time for clots formed from FVII-deficient plasma in the absence and presence of FVIIa. Each curve is representative of 3 repeat measurements. The dashed lines represent the standard error in the mean from 3 repeat measurements.

The analysis of the turbidity data in Figure 7-1 is provided in Table 7-1. It is clear from this analysis that FVIIa had no major effect on the polymerisation of fibrin. No significant changes in lag phase, maximum rate, final absorbance or plateau time were detected within the experimental uncertainties. It is therefore concluded that FVIIa had little or no direct effect upon clot structure.

Table 7-1: Polymerisation data of clots formed from FVII-deficient plasma in the absence and presence of FVIIa

	FVIIa -	**FVIIa +**
Lag time (minutes)	3.7 ± 0.5	3.6 ± 0.6
Maximum rate (units min^{-1})	0.015 ± 0.003	0.018 ± 0.005
Final absorbance	0.13 ± 0.03	0.13 ± 0.03
Plateau time (minutes)	23 ± 2	25 ± 2

In order to investigate clot structure further, clots were investigated by SEM analysis. Samples were prepared (with above concentrations of thrombin, $CaCl_2$ and fibrinogen), and further processed, imaged and analysed as described in section 2.2.5. All clots studied in this chapter were allowed to form for 6 hours in a humidity chamber at room temperature. The results of this analysis are presented in Figure 7-2 and Table 7-2. As expected no difference in structure was detected between clots formed in the presence or absence of FVIIa. Both clots displayed a homogeneous arrangement of fibres. Analysis of SEM micrographs revealed fibre diameter and density were unchanged in the presence of FVIIa.

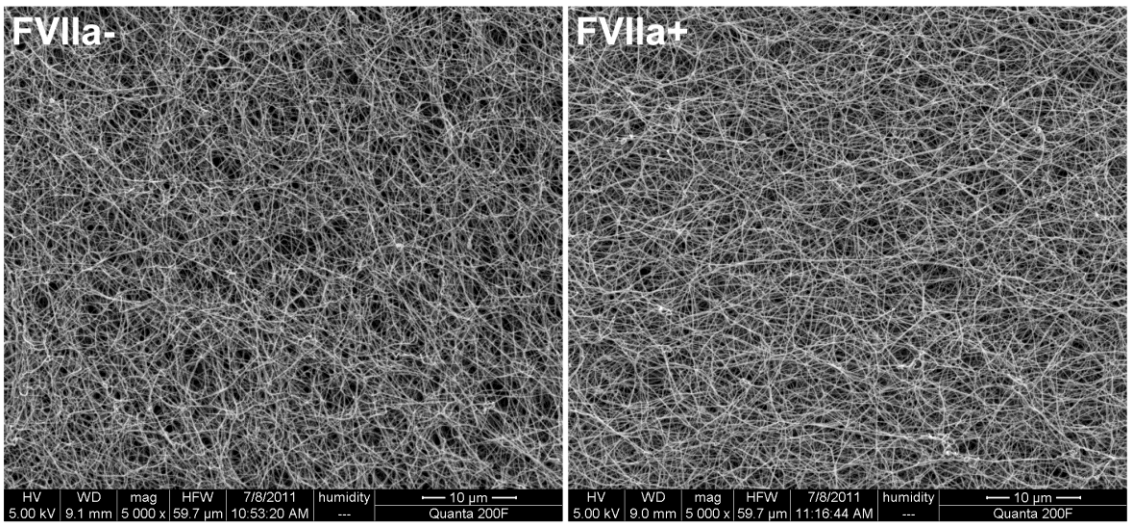

Figure 7-2: Scanning electron micrographs of clots formed from FVII-deficient plasma in the absence (left) and presence (right) of FVIIa. Images are 5 000 x magnification.

Table 7-2: Structural data of clots formed from FVII-deficient plasma in the absence and presence of FVIIa

	FVIIa -	**FVIIa +**
Fibre diameter (nm)	84 ± 3	85 ± 3
Fibre density (#fibres μm^{-1})	3.3 ± 0.2	3.0 ± 0.1

Next, the mechanical properties were measured using the magnetic microrheometer described in chapter 3. Samples were prepared as described in section 2.2.4. The mechanical data during clot polymerisation is presented in

Figure 7-3 and the analysis is provided in Table 4-2. Minimal differences in the mechanical development of clots formed with or without FVIIa were observed.

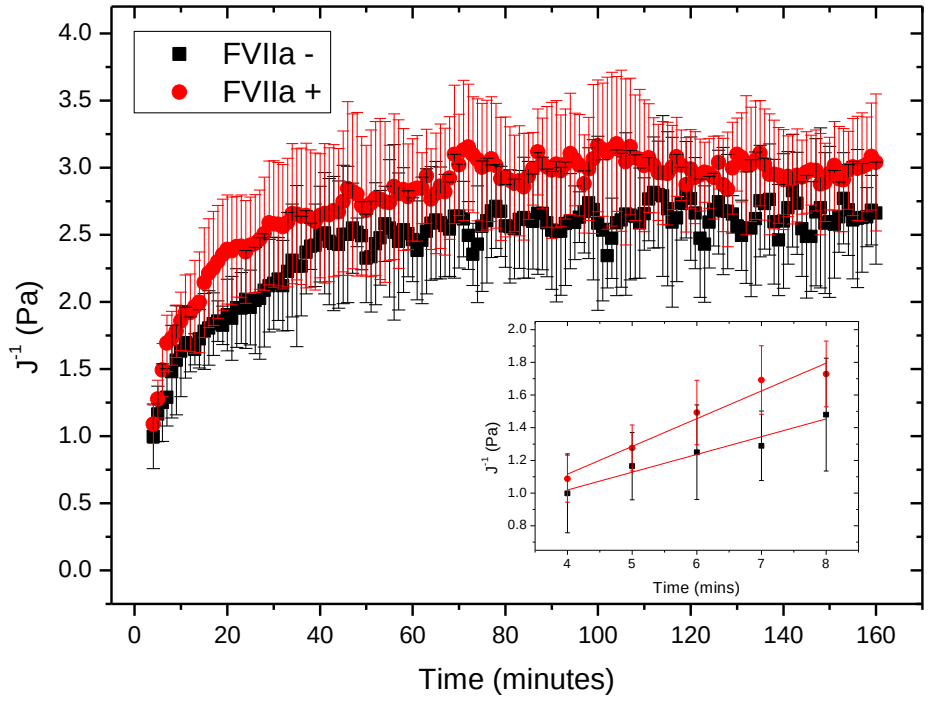

Figure 7-3: J^{-1} vs. time for clots formed from FVII-deficient plasma in the absence and presence of FVIIa.

Table 7-3: Stiffness polymerisation data of clots formed from FVII-deficient plasma in the absence and presence of FVIIa

	FVIIa -	**FVIIa +**
dJ^{-1}/dt ($Pa.s^{-1}$)	0.11 ± 0.02	0.17 ± 0.03
J_I (Pa)	1.0 ± 0.2	1.1 ± 0.1
J_F (Pa)	2.6 ± 0.4	3.0 ± 0.3
Plateau time (minutes)	68 ± 3	74 ± 4

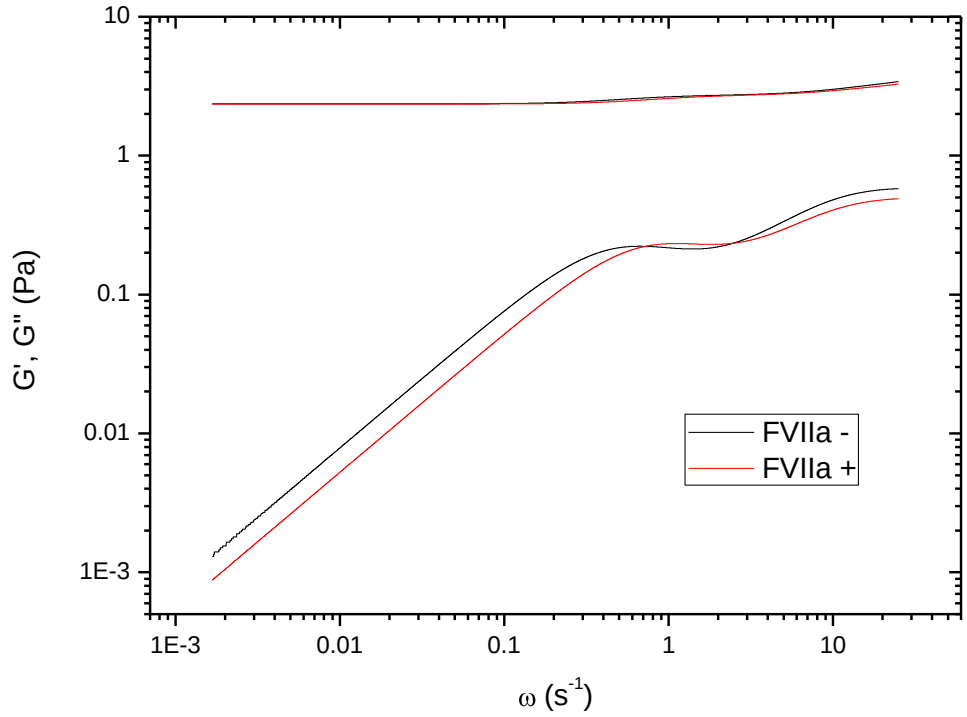

Figure 7-4: G′ and G″ vs. frequency for clots formed from FVII-deficient plasma in the absence and presence of FVIIa.

Table 7-4: Viscoelastic data of clots formed from FVII-deficient plasma in the absence and presence of FVIIa

	FVIIa -	FVIIa +
G′ (Pa)	2.4 ± 0.3	2.4 ± 0.1
G″ (x10^{-3} Pa)	1.3 ± 0.3	0.9 ± 0.1
tanδ (x10^{-3})	0.5 ± 0.1	0.38 ± 0.04

Finally, the viscoelastic properties were also measured using the magnetic microrheometer. The viscoelastic data are presented in Figure 7-4 and the analysis is provided in Table 7-4. No significant differences in the viscoelastic behaviour were observed over the entire frequency probed. There appeared to be some differences at very low frequencies, however the data provided in Table 7-4 indicate that these differences were not statistically significant. Similar

comparisons were made at multiply frequencies with no differences detected. As such there was no difference in the loss tangent either.

7.4 FIXa

The effect of FIXa on clot polymerization was studied by turbidity analysis. The data are presented in Figure 7-5 and the analysis is provided in Table 7-5.

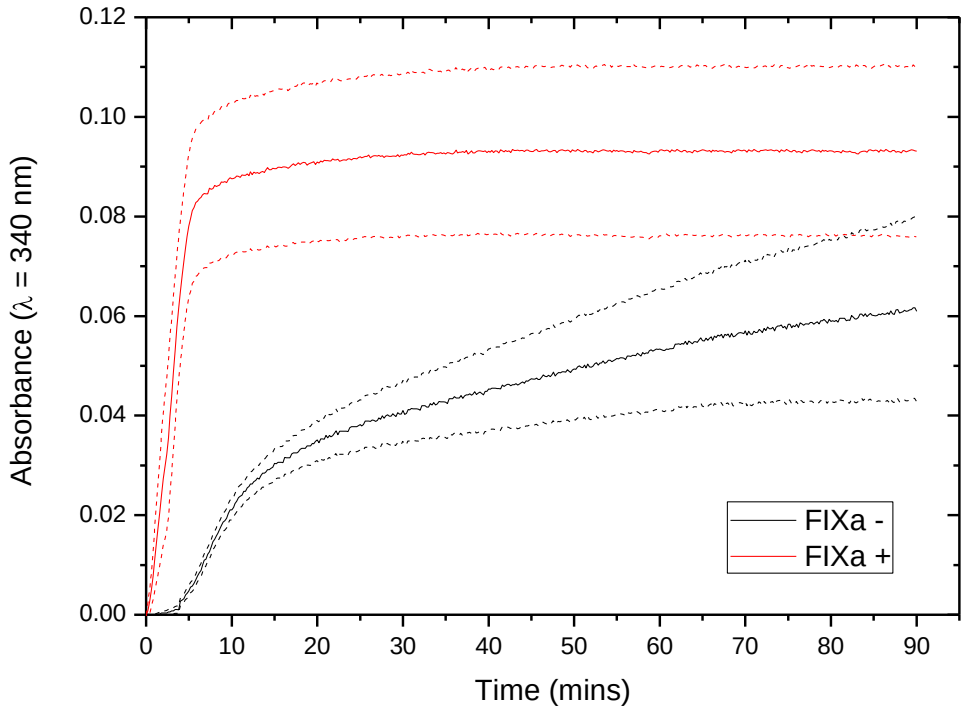

Figure 7-5: Absorbance vs. time for clots formed from FIX-deficient plasma in the absence and presence of FIXa. Each curve is repeated at least 5 times. The dashed lines represent the standard error in the mean of each curve**.**

It is evident that the presence of FIXa has a strong effect on clot polymerisation. In the presence of FIXa the lag phase was shorter by 2.9 minutes, the maximum rate was 6-times higher and the final absorbance at 60 minutes was 1.5-times higher. However, at 60 minutes the absorbance of clots without FIXa was still continuing to increase and ~30 minutes later (at 90 minutes) there was no difference in absorbance within experimental errors.

The shortening of the lag phase and the increased maximum rate indicate that protofibril formation and lateral aggregation are both enhanced in the presence of FIXa. These effects are in keeping with the central role that FIXa plays in enhancing intrinsic thrombin generation during the consolidation phase of coagulation. However, it appears that these differences may have little or no effect upon clot structure as eventually the final absorbance remains unchanged, indicating similar fibre diameter and/or fibre distribution.

Table 7-5: Polymerisation data of clots formed from FIX-deficient plasma in the absence and presence of FIXa

	FIXa -	FIXa +
Lag time (minutes)	4 ± 1	1.1 ± 0.4
Maximum rate (units min^{-1})	0.006 ± 0.001	0.036 ± 0.002
Final absorbance (at 90 minutes)	0.06 ± 0.02	0.09 ± 0.02
Plateau time (minutes)	91 ± 5	15 ± 2

Clot structure was investigated by SEM analysis. The results of this analysis are presented in Figure 7-6 and Table 7-6. Fibre arrangement appeared less homogeneous than FVIIa clots with regions of higher fibre density forming. However, the difference in structure between clots formed with and without FIXa appeared minimal. Analysis of SEM micrographs revealed fibre diameter remained unchanged while fibre density was 1.2-times higher in clots formed with FIXa.

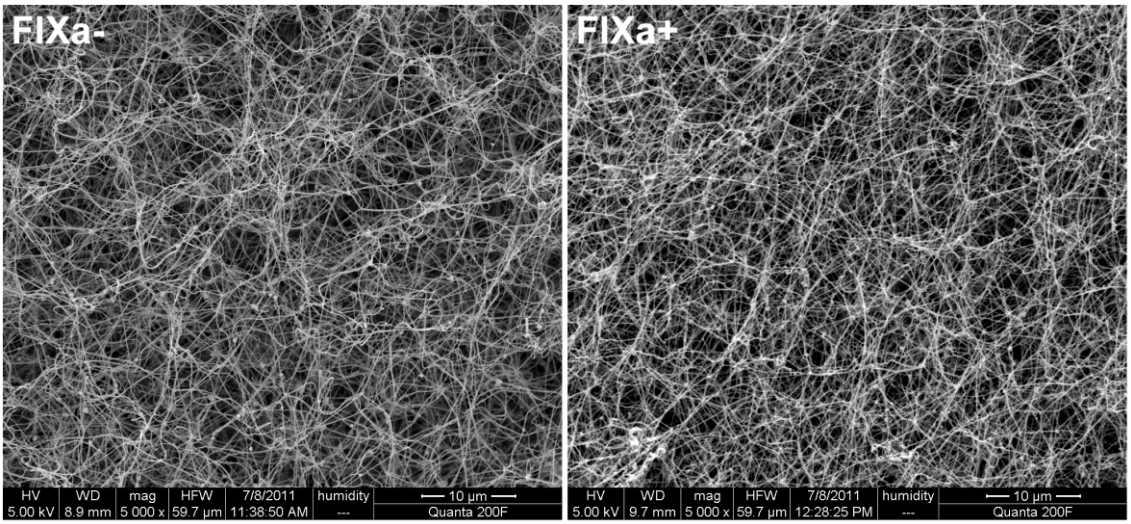

Figure 7-6: Scanning electron micrographs of clots formed from FIX-deficient plasma in the absence (left) and presence (right) of FIXa. Images are 5 000 x magnification.

Table 7-6: Structural data of clots formed from FIX-deficient plasma in the absence and presence of FIXa

	FIXa -	**FIXa +**
Fibre diameter (nm)	88 ± 2	92 ± 2
Fibre density (#fibres μm^{-1})	2.9 ± 0.1	3.4 ± 0.1

Next, the mechanical properties during polymerisation were measured. The data are presented in Figure 7-7 and the analysis is provided in Table 7-7. The initial compliance and the rate of change of compliance remained unchanged within the experimental uncertainties. However, in the presence of FIXa the final compliance was found to be 1.4-times higher and the time to plateau was shorter by 31 minutes. Thus, the mechanical properties of the clot develop at an increased rate, indicating fibre and/or branch point formation is altered in the presence of FIXa. The resulting final clot was therefore mechanically stiffer due to the presence of FIXa.

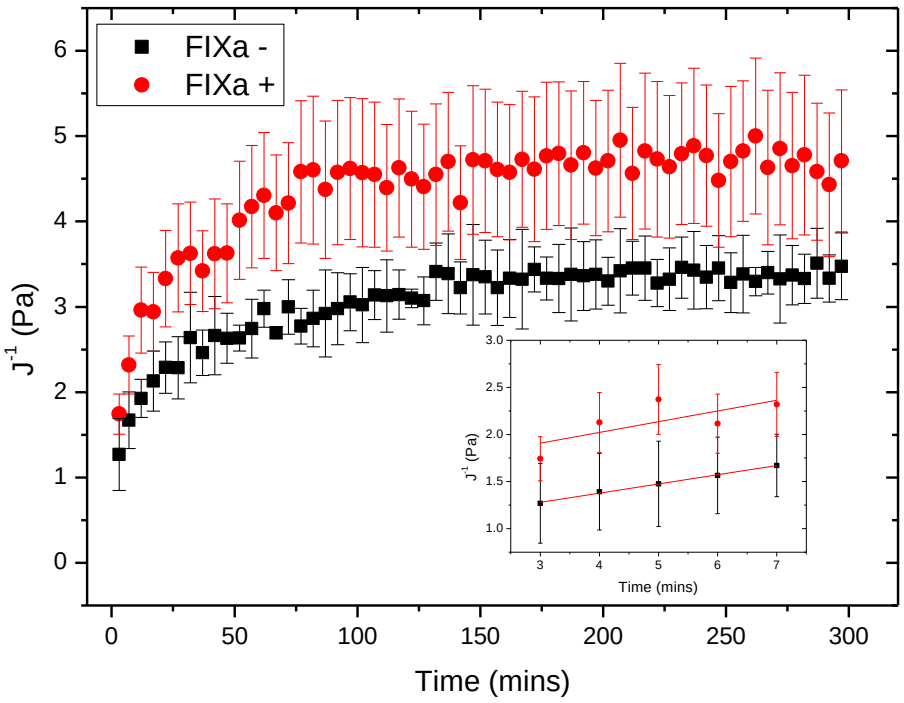

Figure 7-7: J^{-1} vs. time for clots formed from FIX-deficient plasma in the absence and presence of FIXa.

Table 7-7: Stiffness polymerisation data of clots formed from FIX-deficient plasma in the absence and presence of FIXa

	FIXa -	FIXa +
dJ^{-1}/dt (Pa.s^{-1})	0.098 ± 0.004	0.11 ± 0.06
J_I (Pa)	1.3 ± 0.4	1.7 ± 0.2
J_F (Pa)	3.3 ± 0.4	4.6 ± 0.8
Plateau time (mins)	145 ± 3	114 ± 5

Finally, the viscoelastic properties were also measured using the magnetic microrheometer. The viscoelastic data are presented in Figure 7-8 and the analysis is provided in Table 7-8. Differences in the viscoelasticity due to the presence of FIXa were apparent. The storage modulus was 1.4-times higher in the presence of FIXa. Also, the storage modulus was consistently higher over

the entire frequency range. In addition, no major differences in the viscoelastic dynamics were observed.

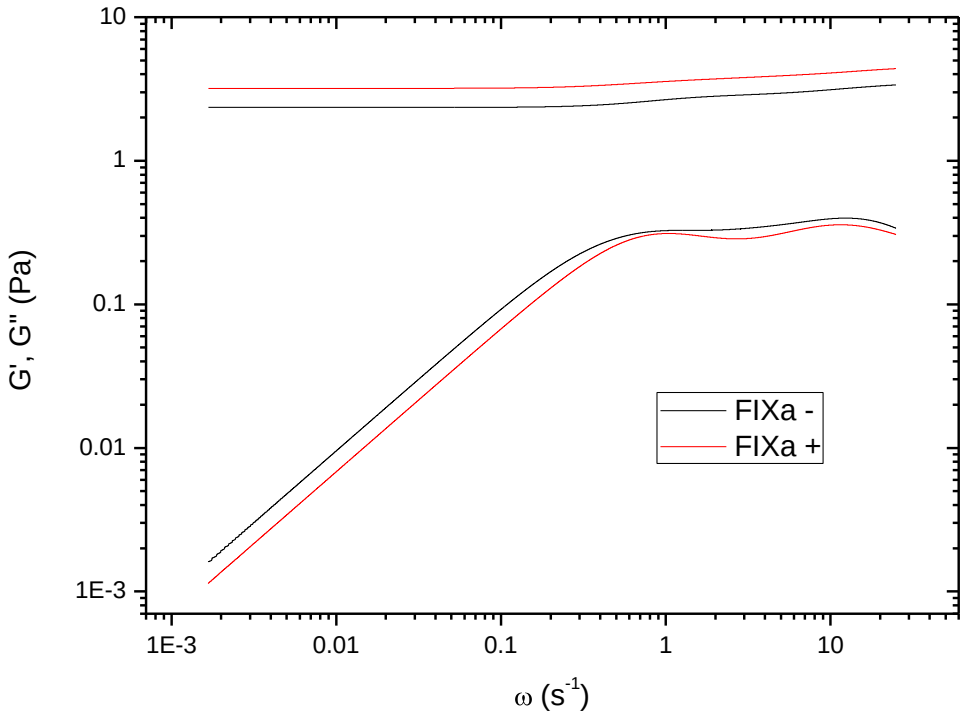

Figure 7-8: G′ and G′′ vs. frequency for clots formed from FIX-deficient plasma in the absence and presence of FIXa.

Table 7-8: Viscoelastic data of clots formed from FIX-deficient plasma in the absence and presence of FIXa.

	FIXa -	**FIXa +**
G′ (Pa)	2.35 ± 0.07	3.2 ± 0.1
G′′ (x10^{-3} Pa)	1.6 ± 0.1	1.1 ± 0.1
tanδ (x10^{-3})	0.68 ± 0.04	0.34 ± 0.01

The loss modulus was found to be 1.5-times higher in the absence of FIXa. The loss tangent was therefore 2-times higher in clots without FIXa. The increased storage modulus and reduced loss modulus of clots formed in the presence of FIXa render them stiffer and more resistant to deformation.

7.5 FXIIa

The effect of FXIIa on clot polymerization was studied by turbidity analysis. The data are presented in Figure 7-9 and the analysis is provided in Table 7-9. There is a clear difference in polymerisation due to the presence of FXIIa. The lag phase was shorter by 2.1 minutes and the maximum rate was 2.7-times higher in the presence of FXIIa. The effect of this increased polymerisation was that FXIIa clots reached a plateau in their absorbance around 30 minutes earlier. However, the final absorbance of clots formed without FXIIa was 1.8-times higher.

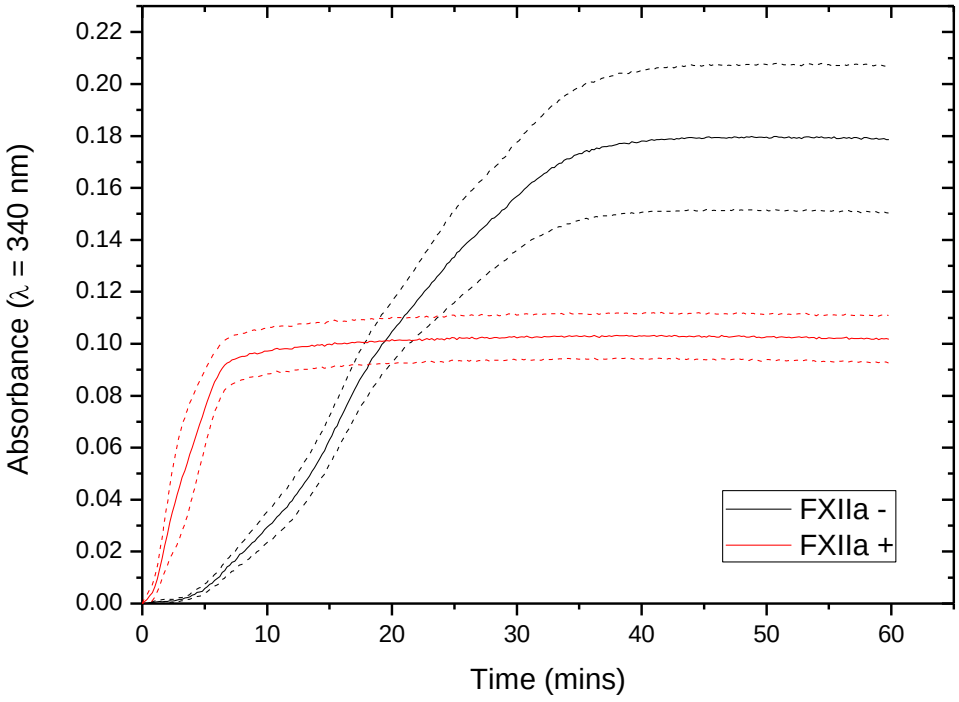

Figure 7-9: Absorbance vs. time for clots formed from FXII-deficient plasma in the absence and presence of FXIIa. Each curve is repeated at least 5 times. The dashed lines represent the standard error in the mean of each curve.

Again, as with FIXa clots, the shorter lag phase coupled with the increased maximum rate indicate that protofibril formation and lateral aggregation are enhanced by the presence of FXIIa. This resulted in a much shorter plateau

time as the network formed quicker. However, the final absorbance was much lower indicating that clots formed in the presence of FXIIa were comprised of thinner fibres and/or an altered fibre arrangement.

Table 7-9: Polymerisation data of clots formed from FXII-deficient plasma in the absence and presence of FXIIa

	FXIIa -	FXIIa +
Lag time (mins)	3.1 ± 0.9	1.0 ± 0.7
Maximum rate (units min^{-1})	0.015 ± 0.001	0.041 ± 0.006
Final Absorbance	0.18 ± 0.03	0.10 ± 0.01
Plateau time (mins)	39 ± 4	8 ± 1

Clot structure was investigated by SEM analysis. The results of this analysis are presented in Figure 7-10 and Table 7-10. Both clots displayed a homogeneous arrangement of fibres. Analysis of SEM micrographs revealed that fibre density was increased 1.1-times in FXIIa clots while fibre diameters were significantly thinner (by 29 nm on average) in FXIIa clots.

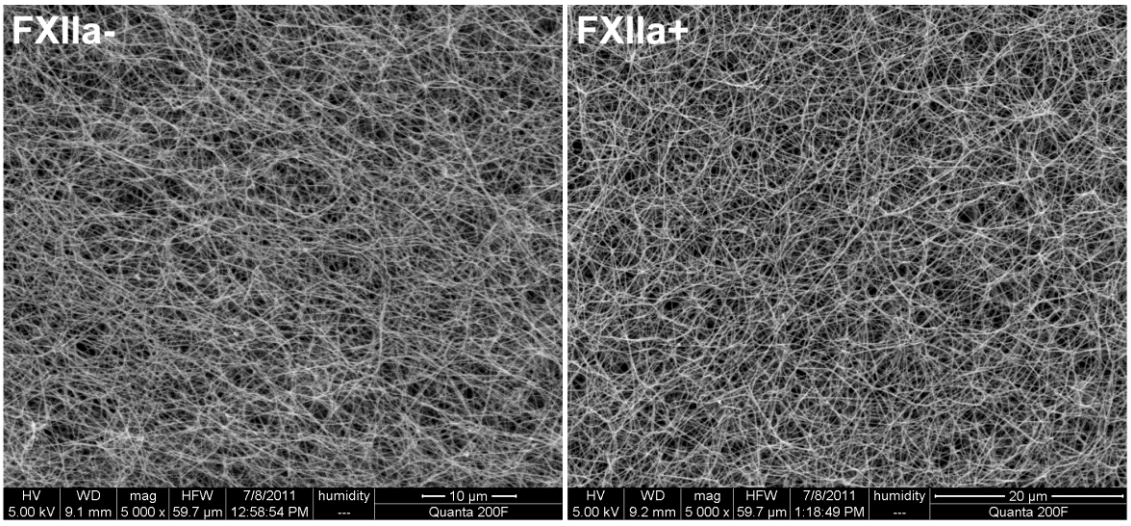

Figure 7-10: Scanning electron micrographs of clots formed from FXII-deficient plasma in the absence (left) and presence (right) of FXIIa. Images are 5 000 x magnification.

Table 7-10: Structural data of clots formed from FXII-deficient plasma in the absence and presence of FXIIa

	FXIIa -	FXIIa +
Fibre diameter (nm)	104 ± 4	75 ± 2
Fibre density (#fibres μm^{-1})	3.4 ± 0.1	3.71 ± 0.07

Next, the mechanical properties during polymerisation were measured. The data are presented in Figure 7-11 and the analysis is provided in Table 7-11. The initial compliance was 1.8-times higher in the presence of FXIIa. In addition, the final compliance was higher, albeit slightly less so, for FXIIa clots by 1.2-times. Inspection of both curves revealed little difference between their time-development and this was reflected in the plateau time which remained unchanged. It appears that the effect of FXIIa was to increase the mechanical stiffness of the network prior to further fibre growth and branch point formation.

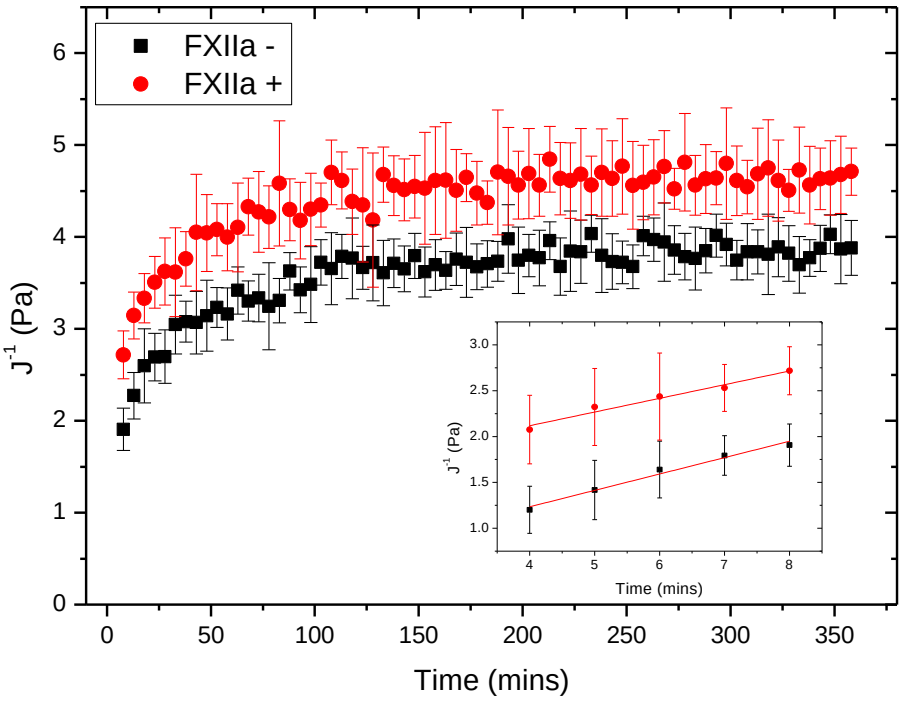

Figure 7-11: J^{-1} vs. time for clots formed from FXII-deficient plasma in the absence and presence of FXIIa.

Table 7-11: Stiffness polymerisation data of clots formed from FXII-deficient plasma in the absence and presence of FXIIa

	FXIIa -	FXIIa +
dJ^{-1}/dt (Pa.s^{-1})	0.18 ± 0.02	0.15 ± 0.03
J_I (Pa)	1.2 ± 0.3	2.1 ± 0.4
J_F (Pa)	3.9 ± 0.3	4.6 ± 0.4
Plateau time (mins)	170 ± 22	162 ± 15

Finally the viscoelastic properties were measured. The viscoelastic data are presented in Figure 7-12 and the analysis is provided in Table 7-12. An additional intermediate concentration, representing 25% of *in vivo* levels, was also tested. Differences in the viscoelasticity due to the presence of FXIIa were apparent. The presence of FXIIa resulted in an increase in the storage modulus over all frequencies. Similarly, the loss modulus was higher in the presence of FXIIa, except at high frequencies for 100% FXIIa. No differences in the viscoelastic dynamics were observed due to the presence of FXIIa.

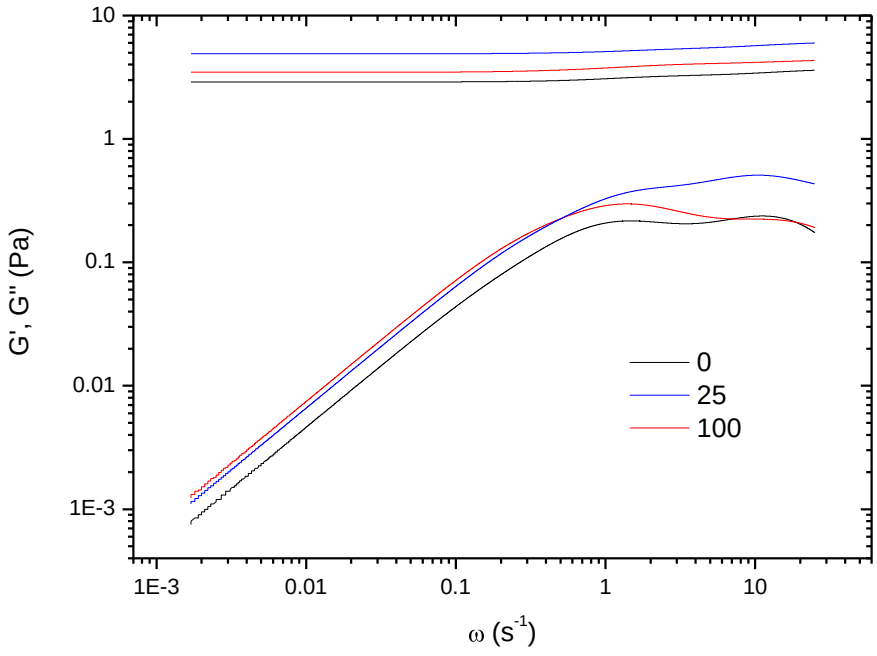

Figure 7-12: G′ and G″ vs. frequency for clots formed from FXII-deficient plasma in the absence and presence of FXIIa.

Table 7-12: Viscoelastic data of clots formed from FXII-deficient plasma in the absence and presence of FXIIa

% FXIIa	0	25	100
G′ (Pa)	2.89 ± 0.05	4.9 ± 0.2	3.47 ± 0.05
G′′ (x10^{-3} Pa)	0.8 ± 0.1	1.1 ± 0.2	1.2 ± 0.1
tanδ (x10^{-3})	0.28 ± 0.02	0.22 ± 0.04	0.36 ± 0.02

A non-linear increase in the storage modulus is associated with the presence of FXIIa. The storage modulus increased 1.7-times with 25% FXIIa and 1.2-times with 100% FXIIa. The loss modulus remained unchanged with 25% FXIIa but increased 1.5-times with 100% FXIIa. No difference in loss tangent was observed at 25% FXIIa while at 100% FXIIa there was an increase of 1.3-times.

The increased storage modulus and unchanged loss modulus of clots formed with 25% FXIIa indicates these clots are stiffer and more resistant to deformation compared with clots formed from 0 and 100% FXIIa. In addition, increased FXIIa levels of 100% lower the storage modulus and increase the loss modulus. This results in an elevated loss tangent compared with 0 and 25% FXIIa clots. Thus, clots formed with 100% FXIIa will deform more and as such are mechanically weaker. The increase in clot stiffness at intermediate FXIIa concentrations generally agrees with the U-shaped curve of other functions of FXIIa and is typical of contact-mediated reactions. Recent studies suggest that FXIIa binds strongly to fibrin, so the fibrin clot itself could provide a surface that mediates the effects of FXIIa on clot structure and stiffness (205).

7.6 FXIII

The effect of FXIII on clot polymerization was studied by turbidity analysis. The data are presented in Figure 7-13 and the analysis is provided in Table 7-13. In this experimental set-up, the presence of FXIII had no effect upon clot polymerisation. No change in lag phase, maximum rate, final absorbance or

plateau time was detected within the experimental uncertainties. It is therefore assumed that FXIII had little or no effect upon clot structure.

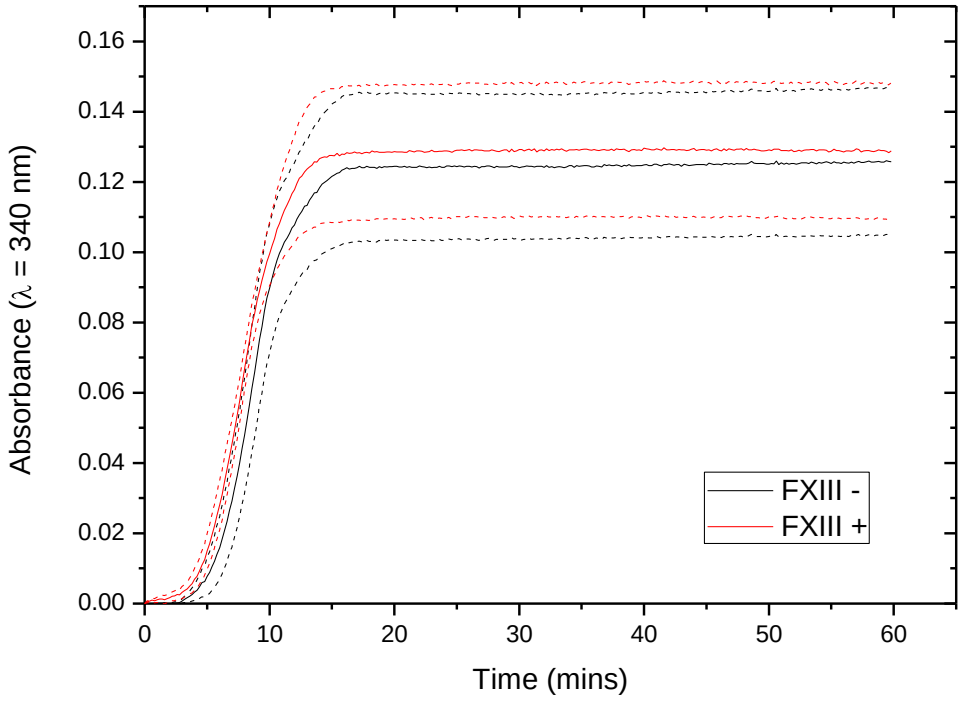

Figure 7-13: Absorbance vs. time for clots formed from FXIII-deficient plasma in the absence and presence of FXIII. Each curve is repeated at least 5 times. The dashed lines represent the standard error in the mean of each curve.

Table 7-13: Polymerisation data of clots formed from FXIII-deficient plasma in the absence and presence of FXIII

	FXIII -	**FXIII +**
Lag time (mins)	4.1 ± 0.8	2.8 ± 0.7
Maximum rate (units min^{-1})	0.026 ± 0.002	0.026 ± 0.001
Final Absorbance	0.13 ± 0.02	0.13 ± 0.02
Plateau time (mins)	16 ± 3	15 ± 4

Clot structure was investigated by SEM analysis. The results of this analysis are presented in Figure 7-14 and Table 7-14. There was very little difference in clot structure associated with FXIII. Analysis of SEM micrographs revealed a fall in

fibre density of 1.1-times was associated with FXIII. No difference in fibre diameter was detected.

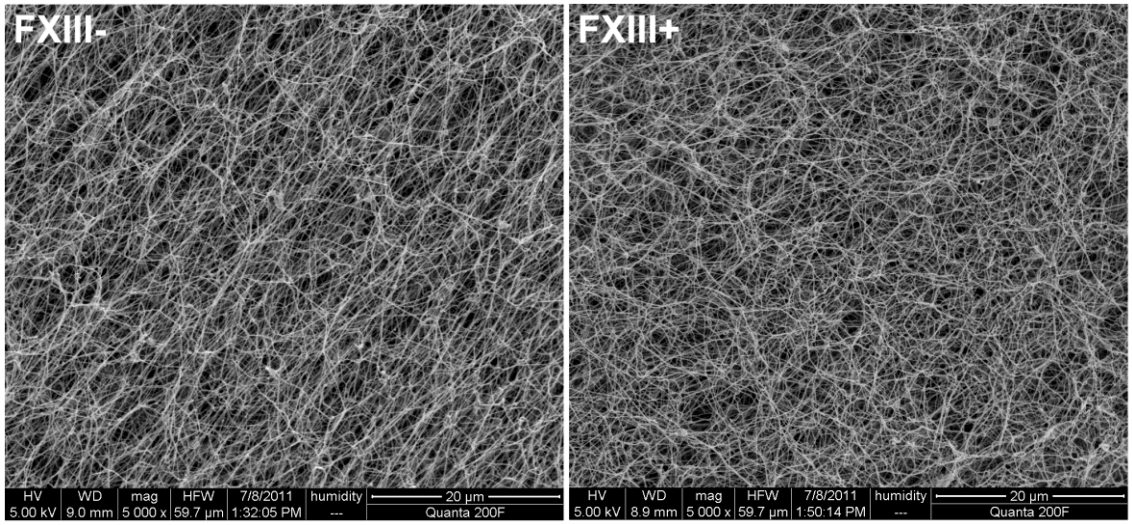

Figure 7-14: Scanning electron micrographs of clots formed from FXIII-deficient plasma in the absence (left) and presence (right) of FXIII. Images are 5 000 x magnification.

Table 7-14: Structural data of clots formed from FXIII-deficient plasma in the absence and presence of FXIII

	FXIII -	FXIII +
Fibre diameter (nm)	92 ± 4	87 ± 12
Fibre density (#fibres μm^{-1})	3.4 ± 0.1	3.1 ± 0.1

Next, the mechanical properties during polymerisation were measured. The data are presented in Figure 7-15 and the analysis is provided in Table 7-15. The initial compliance and rate of change of compliance remained unchanged. However, the final compliance was 2.1-times higher in the presence of FXIII. There was also a striking difference between the rates at which each clot developed over time as indicated by the difference in plateau time. Clots formed in the presence of FXIII took an additional 147 minutes to reach a plateau in their compliance. As discussed in chapter 4 clots formed in the presence of FXIII continue to stiffen for much longer periods due to the formation of cross-links.

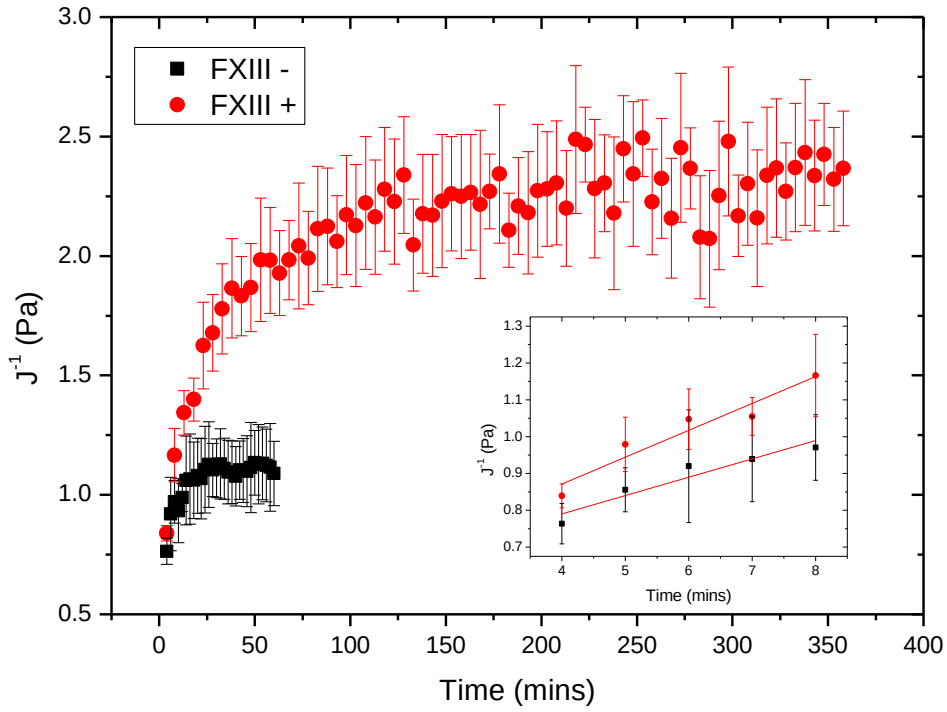

Figure 7-15: J^{-1} vs. time for clots formed from FXIII-deficient plasma in the absence and presence of FXIII.

Table 7-15: Stiffness polymerisation data of clots formed from FXIII-deficient plasma in the absence and presence of FXIII

	FXIII -	FXIII +
dJ^{-1}/dt ($Pa.s^{-1}$)	0.05 ± 0.01	0.07 ± 0.01
J_I (Pa)	0.76 ± 0.05	0.84 ± 0.4
J_F (Pa)	1.1 ± 0.2	2.3 ± 0.2
Plateau time (mins)	15 ± 2	162 ± 12

Finally the viscoelastic properties were measured. The viscoelastic data are presented in Figure 7-16 and the analysis is provided in Table 7-16. Differences in the viscoelasticity due to the presence of FXIII were apparent. The presence of FXIII resulted in an increased storage and loss modulus over all frequencies. No differences in the viscoelastic dynamics were observed due to the presence of FXIII.

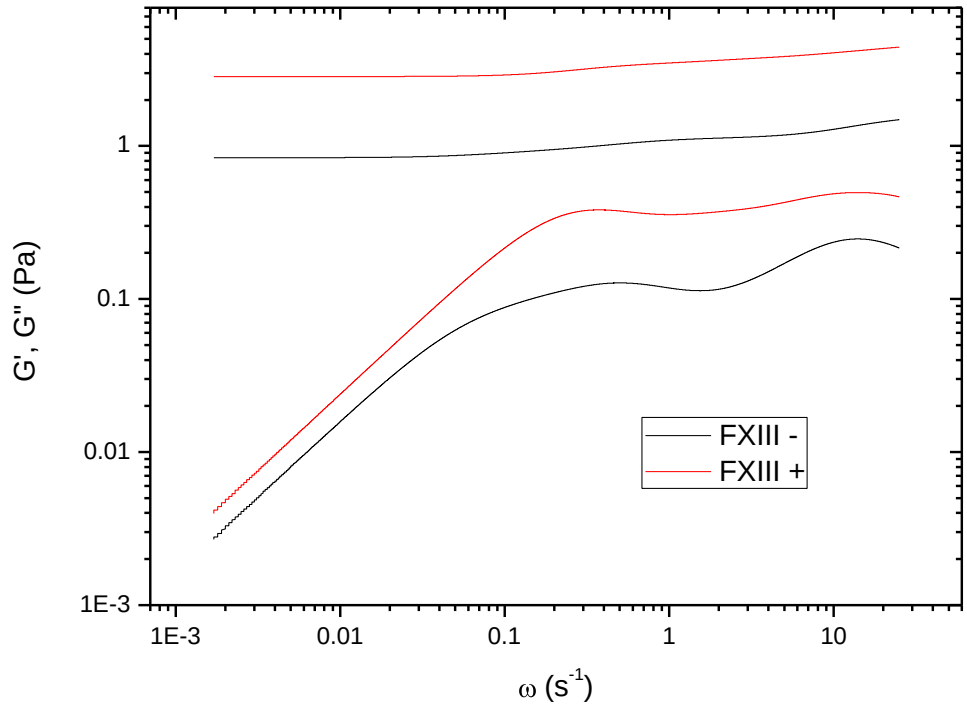

Figure 7-16: G′ and G″ vs. frequency for clots formed from FXIII-deficient plasma in the absence and presence of FXIII.

Table 7-16: Viscoelastic data of clots formed from FXIII-deficient plasma in the absence and presence of FXIII

	FXIII -	FXIII +
G′ (Pa)	0.84 ± 0.08	2.8 ± 0.7
G″ (x10^{-3} Pa)	2.7 ± 0.8	4.0 ± 0.5
tanδ (x10^{-3})	3.2 ± 0.5	1.4 ± 0.3

The storage modulus was 3.3-times higher and loss modulus was 1.5-times higher in the presence of FXIII. It has been reported that cross-linking is associated with a 2- to 3.5-times increase in G′ (33, 75, 143). However, the loss tangent was 2.3-times higher in clots without FXIII. This indicates that clots formed in the presence of FXIII are stiffer and will deform less when stressed.

7.7 Discussions and Conclusions

The effects of four different plasma proteins, factors VIIa, IXa, XIIa and XIII, on clot polymerisation, structure, and mechanical and viscoelastic properties were studied. The data presented here reveal that combinations of different effects on clot behaviour are associated with each individual plasma protein.

Firstly, FVIIa was studied and found to have no effect on clot behaviour. Polymerisation was unaltered in the presence of FVIIa. In agreement, SEM imaging revealed no differences in clot structure i.e. the presence of fibre bundling or pores, due to FVIIa. No difference in fibre diameter or density were detected either. A study by He *et al*. report a minimal effect on clot permeability, a direct measure of pore size, by the addition of recombinant FVIIa in normal plasma suggesting clot structure remains unaltered (206). In addition, we measured no differences in the mechanical or viscoelastic properties. This agrees with the work of Carr *et al*. who found recombinant FVIIa has a minimal effect on clot stiffness in normal blood clotted with thrombin (207). The insensitivity of the mechanical properties to the presence of FVIIa most likely arises due to the negligible effect FVIIa has on clot structure, which is known to modulate clot viscoelasticity (33). These data reveals that FVIIa does not play a significant role in clot formation in a plasma system where clotting is initiated by the addition of thrombin. *In vivo* FVIIa is involved in the initiation and generation of thrombin (202) through activation of FIX and FX by the TF-VIIa complex (208). However, in the system used here a large amount of thrombin is added, which will immediately convert fibrinogen to fibrin triggering immediate fibrin polymerisation. Any additional, thrombin generated through the addition of FVIIa could well be negligible in comparison to this and/or play a limited role as the nascent network may already have formed.

Secondly, the effects of FIXa were studied and found to modulate clot polymerisation. In the presence of FIXa, clots polymerised at a quicker rate as indicated by a shorter lag time and increased maximum rate. In addition, the absorbance reached a plateau at a shorter time. However, in the absence of FIXa clots still reached a very similar final absorbance, albeit at a much later

time. Similar values for the final absorbance suggest FIXa does not play a significant role in modulating clot structure. No significant differences in the macroscopic structure of clots formed with or without FIXa were detected in SEM micrographs. In addition, analysis of these micrographs revealed fibre diameter remained unchanged. This most likely explains the insensitivity of the final absorbance to the presence of FIXa. However, FIXa was associated with a slight increase in fibre density.

Measurements of the mechanical properties during polymerisation revealed that in the presence of FIXa initially clot stiffness was the same and developed at a similar rate. However, FIXa clots eventually became stiffer at an earlier time. This agrees with turbidity measurements which show quicker clot formation in the presence of FIXa. In addition, viscoelastic measurements revealed that clots were stiffer in the presence of FIXa and were less susceptible to permanent deformation. The study of Carr *et al*. report that FIX deficient patients form clots with a reduced stiffness as compared to controls (207). We attribute the increased mechanical stability of FIXa clots to the increased fibre density, and therefore branch point density, as observed in SEM micrographs, which is known to elevate clot stiffness (84).

The effect of FIXa on clot polymerisation and structure is interesting. Typically, increased polymerisation rates, due to higher levels of thrombin, are associated with denser clots composed of thinner fibres. We observe increased polymerisation where a denser structure forms but fibre diameter remains unaltered. It appears that protofibril formation is enhanced but lateral aggregation remains unaffected. One potential mechanism could be that FIXa enhances FpA but not FpB cleavage. Thus, more protofibrils form resulting in a denser structure but lateral aggregation proceeds at the same rate leading to similar fibre diameters. However, it is not clear what the potential mechanism could be by which FIXa modulates fibrinopeptide release.

Next, the effects of FXIIa were studied; differences in polymerisation, structure and mechanical and viscoelastic properties were all observed. In the presence of FXIIa the lag time was shorter and the maximum rate was higher resulting in

a lower final absorbance occurring. The study of Konings *et al*. reported very similar observations and suggested increased polymerisation in plasma is due to increased thrombin generation via FXI activation (205). In agreement with turbidity measurements, SEM imaging revealed FXIIa resulted in a denser clot composed of thinner fibres. A denser clot would typically increase the final absorbance; the decrease was attributed to the more dramatic change in fibre diameter. Similar observations have also been reported from confocal microscopy, SEM and permeation experiments (205). As FXIIa concentration increased from 0% to 25% and then up to 100% fibre density increased but fibre diameter decreased (Figure 7-17) (205).

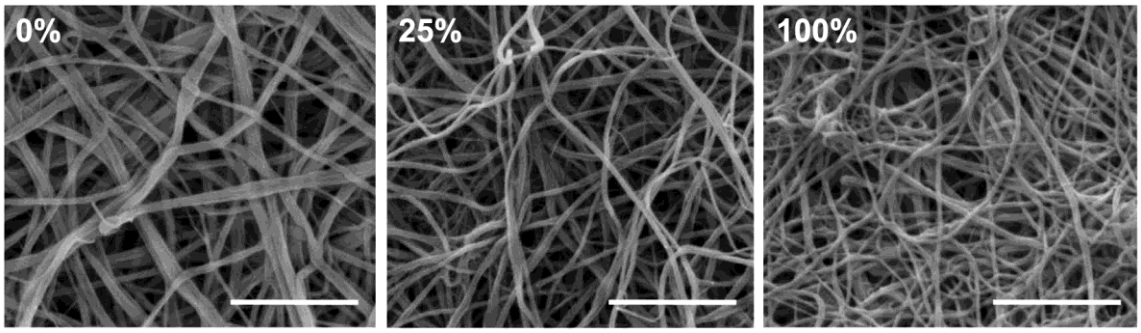

Figure 7-17: Scanning electron micrographs of plasma clots formed in the presence of 0, 25 and 100% FXIIa (taken from konings *et al*. (205)). Fibre density increased from left to right while fibre diameter increased from right to left. At 25% FVIIa clots displayed a balance between maximal fibre diameter and density. Scale bar represents 1 μm.

Measurements of the mechanical properties during polymerisation revealed that FXIIa had a limited effect on the mechanical development. Clots formed in the presence of 100% FXIIa are initially stiffer and then develop at a very similar rate with no further increases in stiffness observed. Additionally, viscoelastic measurements revealed an increase in stiffness associated with FXIIa. However this was accompanied by an increase in the viscous component. The result is that clots formed from 100% FXIIa are mechanically weaker and will undergo permanent deformation more easily than clots formed from 0% FXIIa.

At 25% FXIIa levels, however, clot stiffness reached a maximum and the viscous component remained unchanged. This resulted in a stiffer clot which will undergo less permanent deformation than clots formed at either high or low

FXIIa levels. Thus, at intermediate FXIIa levels clots displayed an optimal viscoelastic balance; possessing maximal stiffness and displaying minimum deformation. This correlates particularly well with structural data from SEM imaging which revealed that an optimal balance between fibre branching and diameter are achieved at 25% FXIIa levels. Maximal clot stability has been correlated with a balance between large fibre diameters and increased branching (33). Konings *et al*. (205) proposed that, in addition to increased thrombin generation in plasma which influences clot structure, FXIIa also modulates fibrin clot structure independently of thrombin generation through direct binding of the N-terminus of FXIIa to fibrinogen and fibrin.

Finally, the effects of FXIII were studied. Clot polymerisation was found to be unaffected by the presence of FXIII in this experimental set-up. In addition, clot structure was only minimally affected, with a slight decrease in fibre density due to FXIII. Previous studies (33, 75, 154, 209) observed minimal effects of FXIII on clot structure, although some authors reported slight decreases in fibre diameter and increases in fibre density. In contrast, the mechanical properties during polymerisation showed a much more dramatic influence due to the presence of FXIII. The initial stiffness and rate of development remained unchanged. However, after around 10 minutes clotting displayed a marked difference. In the absence of FXIII, stiffness reached a plateau very early while in the presence of FXIII clots continued to stiffen for a sustained period. Similar effects have been observed in a purified system where cross-linking was controlled with a synthetic inhibitor (84). As previously discussed in chapter 4, clots formed in the presence of FXIII continued to stiffen due to the formation of cross-links. In addition, the viscoelastic properties revealed that an increase in stiffness was also accompanied by an increase in the viscous component. However, a greater increase in the stiffness rendered the loss tangent lower in the presence of FXIII. Thus, FXIII clots were stiffer and more resistant to deformation. Previous studies reporting on the mechanical properties of single fibres found that in the presence of FXIII, fibres were stiffer and less extensible (83, 86). We therefore infer that the increased stiffness of cross-linked clots is due to the stiffening of the individual fibres as opposed to structural alterations.

The data presented here demonstrate that the effect of FXIII is very similar in both purified and plasma systems.

Chapter 8

8 Summary and Conclusions

This project has used multiple complimentary techniques in order to study fibrin clot polymerisation, structure and viscoelasticity. The initial stages of this work were concerned with adapting and developing a magnetic microrheometry device in order to measure the frequency dependent viscoelastic moduli ($G'(\omega)$ and $G''(\omega)$) of fibrin clots over a broad frequency range. The latter stages of the project were then concerned with applying this magnetic microrheometry technique to a range of different fibrin samples. Both purified and plasma systems were studied along with the fibrinogen variant γ' as well as the effects of the plasma proteins FVII, FIX, FXII and FXIII. In addition, viscoelastic measurements were correlated with fibrin clot structure and polymerisation as measured by turbidity, confocal microscopy, SEM and AFM techniques.

The magnetic microrheometer used throughout this work was designed and constructed by Dr R. Harrand (210) and was based on the design of Huang *et al*. (211) to perform active particle tracking microrheology measurements. The

device originally consisted of 8 electromagnets and was capable of producing forces of ~60 pN in magnitude. Initially, work focused on increasing the force range of the device and this was achieved by removing 4 of the electromagnets and reconfiguring the device based upon magnetic modelling data. This resulted in an increase in the available force up to 120 pN; a 2-fold increase in the maximum force. This was achieved by positioning the electromagnet tips in the plane of the sample region, and not slightly above and below as was the previous configuration. The device was then tested with standard fluids of water-glycerol mixtures and found to agree well with bulk measurements presented within the literature. This had previously been demonstrated along with the ability to correctly measure the viscoelastic properties of polyacrylamide solutions (210).

Prior to proceeding onto a comprehensive study of the mechanical and viscoelastic behaviour of fibrin clots, the suitability of the device to study clots was assessed. The effect of magnetic particles on fibrin polymerisation and structure was investigated by turbidity, confocal microscopy and SEM. This was important as any alterations would affect the interpretation of results. The presence of magnetic particles was found to have no effect upon clot polymerisation or structure as indicated by turbidity analysis. In order to directly visualise the effect the magnetic particles were having on clot structure, SEM and confocal microscopy were employed. Imaging revealed particles had little or no effect upon the fibres surrounding them and that they became trapped within the clot as the network grew around them.

The effect of the microcell, used to hold clots for microrheology experiments, has on clot structure was also studied by confocal microscopy. The fibre density as a function of distance from the microcell wall was measured. This revealed fibre density was ~2-times lower within the vicinity of the microcell wall. Moving away from the wall, the fibre density increased and reached a plateau where the fibre density was constant throughout the centre of the capillary. Next, clot stiffness as a function of distance from the microcell wall was measured. This revealed clot stiffness increased with distance from the microcell wall and then reached a plateau. This correlated well with fibre density measurements and the

increased stiffness was attributed to increased fibre density. The reason for the decrease in fibre density at the microcell wall was not ascertained but the effect on the overall clot structure appeared minimal. These observations reveal that forming clots within microcells and embedding magnetic particles within them does not significantly alter the structural or mechanical properties.

After validation of the magnetic microrheometer as a suitable device, different techniques and approaches were developed to study the mechanical and viscoelastic properties of fibrin clots. One such approach was to measure the change in stiffness of a clot during polymerisation which allows kinetic information on clot formation to be gathered. It was observed that clots undergo a rapid increase in stiffness which then reaches a plateau once the clot has formed. It was assumed that once this plateau had been reached, a clot was fully formed both structurally and mechanically. Further measurements revealed that the final stiffness did not change significantly over prolonged periods of time giving justification to this claim.

The variation in clot stiffness from particle-to-particle and also the variation due to the direction of manipulation of a magnetic particle were also investigated. Measurements revealed that there was a difference in stiffness depending upon which direction a magnetic particle was moved. However, no one direction was consistently associated with either a higher or lower measure of clot stiffness. In addition, the variation in stiffness from particle-to-particle also revealed a distribution in stiffness. This variation was investigated as an indirect probe of clot structure, which is known to modulate clot viscoelasticity. However, measurements of clots formed from $\gamma A/\gamma A$ and $\gamma A/\gamma'$ fibrinogen, two clots known to have very different structures, revealed no correlation between stiffness variation and clot inhomogeneity. It is thought that differences in clot stiffness arise from repeated measurements of a physical system where measurements distribute normally.

The non-linear behaviour of clot elasticity, termed strain-hardening, was also investigated with the magnetic microrheometer. It was possible to resolve some relatively weak clots undergoing strain-hardening behaviour. At low strains the

stiffness remained essentially constant but as strain increased, clots displayed increased stiffness. This approach was investigated as a potential diagnostic of fibrin clot elasticity. However, due to the low forces achievable with the magnetic microrheometer it was not possible to strain clots sufficiently to observe and compare their non-linear response. As fibrinogen levels increase and clots become stiffer their elastic response approaches that of Hooke's Law.

Next, a method to measure the frequency dependent viscoelastic moduli was developed. The author of (210) had previously developed a technique with the current magnetic microrheometer and studied the viscoelasticity of polyacrylamide solutions. However, a study of the frequency dependent viscoelastic moduli of fibrin clots was not carried out. In order to do so with the current magnetic microrheometer and the method of (210) would be extremely time consuming to perform and as such it was decided to implement a more straightforward approach. Using the procedure of Evans *et al*. (127) the frequency dependent viscoelastic moduli were calculated directly from time dependent creep compliance measurements. This approach allowed the viscoelastic moduli of clots to be measured over a frequency range spanning 5 orders of magnitude.

This approach was used to investigate the viscoelastic behaviour of purified fibrin clots. It was observed that fibrin clot behaviour was predominantly elastic on all timescales. Furthermore, it was observed that fibrin clots were highly stable on very long times. This was the case for all fibrin types studied throughout this work. This behaviour could account for the stability and integrity of clots *in vivo* which must withstand varying degrees of shear stress and maintain their integrity for prolonged periods during wound repair.

To date, very little or almost nothing has been reported upon the frequency dependence of the storage modulus. Most studies report a storage modulus which remains constant with frequency. Measurements in this work revealed that the storage modulus varied with frequency and displayed three distinct plateaus. Each plateau corresponds to a different shear relaxation mechanism as predicted by the model of Morse (71). On long-times the behaviour is

dominated by large scale motions of the fibres and branches, i.e. an orientational contribution, G_{orient} arising from forces that resist movement of the entire fibre. In addition, the plateau in G′ and the divergence of G′′ to smaller values as predicted by Morse for a network of branched fibres was also observed. This reveals the role of branch points in the long-time elastic behaviour of fibrin networks in that they help maintain clot integrity on long timescales. At intermediate times, fibres are moving on length scales of the order of the fibre length, i.e. distances between branch points. This is a curvature contribution, G_{curve} which arises from forces that are opposing transverse deformation or rotation of the fibre. Finally, on very short times fibres are compressing and stretching. This is a tension contribution, G_{tens} which arises from tangential forces that resist stretching or compression of the fibre. This plateau is predicted to scale with fibrinogen concentration as $G' \approx c^{2.5}$ by Mackintosh *et al*. (68) and measurements in this work were found to agree well with this scaling prediction. We believe that discrepancies between our observations of relaxation behaviour and that presented within the literature may arise due to differing experimental conditions and/or the microrheological technique employed. Other micron based measurements of single fibrin fibres also report relaxation behaviour on differing timescales (86).

In addition, the effect of FXIII on clot mechanical and viscoelasticity properties, which has been widely reported upon in the literature, was tested with the magnetic microrheometer. This also serves as a validation for the procedure of Evans *et al*. (127) which previously has not been applied to the study of fibrin clots. The polymerisation of clot stiffness displayed a marked difference in the presence of FXIII. Initially, at times <5 minutes there was no difference in polymerisation. However, after this time clots formed in the presence of FXIII displayed an increased stiffness and continued to stiffen for up to 6 hours. This was attributed to cross-linking of the α- and γ-chains. Viscoelastic measurements revealed clot stiffness increased ~3-times, agreeing well with previous measurements presented in the literature (33, 75, 143). Also, cross-linking reduced viscous creep, thus overall a clot is rendered more mechanically stable. In addition, it was observed that cross-linking did not significantly alter the stress relaxation behaviour of fibrin. As clot architecture remains essentially

unchanged this most likely explains the insensitivity of the fibre dynamics to FXIII cross-linking.

Measurements of the frequency behaviour of the loss tangent revealed that cross-linking decreased the loss tangent on all times. In addition, increases in the loss tangent were observed at two specific frequencies. These peaks in the loss tangent coincide with the transitions between different stress relaxation modes. This indicates that when clots are stressed at these specific times they incur a greater degree of deformation which could be a potential mechanism for embolism. These observations also highlight the importance of performing multi frequency measurements as clot viscoelastic behaviour is highly dependent upon the timescale on which one observes.

A comprehensive study to investigate the frequency dependent viscoelastic behaviour of purified fibrin clots was performed. Specifically, the effects of fibrinogen, thrombin and calcium concentration on clot viscoelasticity were investigated. The work presented in this thesis is the first to study fibrin in this way under such conditions. Increased clot stiffness was associated with increased fibrinogen concentration and attributed to an increase in the internal protein density of fibres. Good agreement between experimental data and the scaling prediction of G' with fibrinogen concentration, as proposed by Mackintosh *et al*. (68), was observed. Indicating fibrin fibres are semi-flexible and that fibrin clot elasticity is essentially entropic in origin. However, other theories suggest that at high strain an enthalpic contribution may also play a role in fibrin elasticity. It was observed that fibrinogen concentration also had an effect upon the stress relaxation behaviour of fibrin clots; at higher fibrinogen levels G_{orient} and G_{tens} occurred at earlier times. This indicates that as fibres become stiffer they alter the intermediate- and long-timescale behaviour of fibrin clot viscoelasticity. Under varying thrombin levels, increased clot stiffness occurred at intermediate thrombin levels. Similarly, maximal clot stiffness was also observed at intermediate calcium levels. It is concluded that clots formed at these intermediate concentrations display a balance between a degree of branching and large fibre diameters, both of which are known to increase clot stiffness.

Next, the molecular mechanisms underpinning the effects of the fibrinogen γ′ chain on clot polymerisation, structure and viscoelasticity, still currently under debate, were investigated. We observed that the presence of the fibrinogen γ′ chain slows fibrin polymerization and that this is independent of the γ′ chain binding to thrombin or FXIII. It was also observed that protofibril formation is inhibited by the presence of the γ′ chain, and this is through either electrostatic or steric effects. Surprisingly, the γ′ chain was also associated with an earlier clotting time. In order to explain these apparently conflicting observations, a model hypothesis was developed whereby shorter, more numerous protofibrils lead to earlier gelling of γA/γ′ clots. Subsequently, this results in a clot composed of thinner, shorter fibres arranged non-uniformly producing large open pores which extend throughout the clot structure. This non-uniform structure is mechanically weaker and results in prolonged lysis times. Such observations may help to explain the differential association of fibrinogen γ′ with thrombosis in the venous and arterial vascular beds.

Finally, the effects of the plasma proteins FVIIa, FIXa, FXIIa and FXIII on plasma clot behaviour were also studied. It was observed that FVIIa had no effect on clot behaviour. This is believed to be due to the use of thrombin to initiate coagulation which dwarfs any thrombin generated through reactions involving FVIIa. The presence of FIXa was found to increase polymerisation and alter clot structure with an increase in fibre density observed. Viscoelastic measurements revealed clots were stiffer and less susceptible to permanent deformation in the presence of FIXa. This increased mechanical strength was attributed to increased fibre density.

Differences in polymerisation, structure and viscoelasticity were observed due to the presence of FXIIa. Clot polymerisation was quicker and is believed to be due to increased thrombin generation via FXI activation. As FXIIa concentration increased, fibre density increased while fibre diameter decreased. Viscoelastic measurements revealed that clots formed at 100% FXIIa levels are mechanically weaker and will undergo permanent deformation more easily than clots formed in the absence of FXIIa. At 25% FXIIa levels clots displayed an

optimal viscoelastic balance; possessing maximal stiffness and displaying minimum deformation. This correlates with structural data indicating that an optimal balance between fibre branching and diameter are achieved at these levels. Konings *et al*. (205) proposed that, in addition to increased thrombin generation which influences clot structure, FXIIa also modulates clot structure through direct binding of the N-terminus of FXIIa to fibrinogen and fibrin.

FXIII had little or no effect on either clot polymerisation or structure but did, as expected, alter clot viscoelasticity. In the presence of FXIII, plasma clots continued to increase in stiffness for prolonged periods due to the formation of cross-links by FXIII. Viscoelastic measurements revealed clots were stiffer and more resistant to deformation when formed in the presence of FXIII. In addition, the effects of FXIII in purified and plasma systems are very similar.

Chapter 9

9 Future Work

9.1 High Frequency Measurements

A relatively simple and straightforward improvement to the magnetic microrheometer would be to replace the current CCD camera with a higher capture rate camera. Currently, measurements are limited to frequencies < 25 Hz and as seen in this work it was not possible to completely measure G_{tens}, the high frequency contribution to $G^*(\omega)$. The ability to access higher frequencies may also result in the detection of further stress relaxation mechanisms in fibrin and more specifically molecular stress contributions.

9.2 AFM Study of Early Stage Fibrin Polymerisation

Currently the accepted model for fibrin polymerisation is that the release of FpA results in the formation of fibrin oligomers which grow longitudinally to form protofibrils. These protofibrils, upon the release of FpB, aggregate laterally to form fibres. Protofibril divergence and interaction result in the formation of branch points. Experimental evidence has shed light on this process; increased polymerisation rates result in networks with a high degree of branching consisting of thin fibres while, decreased polymerisation rates result in networks consisting of thick fibres with a low degree of branching. However, a definitive model of branch point formation has yet to be agreed upon and the role of FpB is still poorly understood. Using the AFM, as in this work, it is possible to directly image the time development of this process and gather quantitative information. Through the use of snake venoms which cleave only one set of Fps, e.g. reptilase which cleaves only FpA, or by mutating functional sites of fibrinogen, it would be possible to study the roles of FpA and FpB in the very early stages of fibrin polymerisation helping to develop a more complete model of fibrin polymerisation and branch point formation.

9.3 Computational Modelling of Fibrin Clots

To date, a model to predict the viscoelastic behaviour of fibrin networks does not exist. Morse (71-73) and Mackintosh *et al*. (68) have both developed models in order to compute the viscoelastic properties of networks of concentrated isotropic solutions of semi-flexible filaments for a range of concentrations and chain lengths. This model is most applicable to solutions of actin filaments. The effect of permanent branches on these networks was computed and found to agree with measurements for fibrin presented in this work. We propose that a model for fibrin could be developed based on the

branched model of Morse (71). Magnetic microrheometer measurements could be used to validate and test predictions from such a model.

References

1. Mann, K. G. 1999. Biochemistry and physiology of blood coagulation. *Thromb Haemost* **82**:165.
2. Heemskerk, J. W. M., E. M. Bevers, and T. Lindhout. 2002. Platelet activation and blood coagulation. *Thrombosis and Haemostasis-Stuttgart* **88**:186-194.
3. Wolberg, A. S. 2007. Thrombin generation and fibrin clot structure. *Blood Rev* **21**:131-142.
4. Colman, R. W., and A. H. Schmaier. 1997. Contact system: a vascular biology modulator with anticoagulant, profibrinolytic, antiadhesive, and proinflammatory attributes. *Blood* **90**:3819.
5. http://en.wikipedia.org/wiki/File:Coagulation_full.svg
6. Doolittle, R. F. 1984. *Anal Rev Biochem* **53**:195-229.
7. Mosesson, M. W. 2005. Fibrinogen and fibrin structure and functions. *J Thromb Haemost* **3**:1894-1904.
8. Blomback, B., B. Hessel, and D. Hogg. 1976. Disulfide bridges in NH2-terminal part of human fibrinogen. *Thromb Res* **8**:639-658.
9. Zhang, J. Z., and C. M. Redman. 1992. Identification of B beta chain domains involved in human fibrinogen assembly. *J Biol Chem* **267**:21727.
10. Henschen, A., F. Lottspeich, M. Kehl, and C. Southan. 1983. Covalent structure of fibrinogen. Annals of the New York Academy of Sciences 408:28-43.
11. Medved, L., and W. Nieuwenhuizen. 2003. Molecular mechanisms of initiation of fibrinolysis by fibrin. Thrombosis and haemostasis 89:409-419.
12. Medved, L., and J. W. Weisel. 2009. Recommendations for nomenclature on fibrinogen and fibrin. *J Thromb Haemost* **7**:355-359.
13. Weisel, J. W. 2004. The mechanical properties of fibrin for basic scientists and clinicians. Biophysical chemistry 112:267-276.

14. Weisel, J. W. 1986. Fibrin assembly. Lateral aggregation and the role of the two pairs of fibrinopeptides. *Biophys J* **50**:1079-1093.
15. Olexa, S. A., and A. Z. Budzynski. 1980. Evidence for four different polymerization sites involved in human fibrin formation. *Proc Natl Acad Sci* **77**:1374.
16. Litvinov, R. I., O. V. Gorkun, S. F. Owen, H. Shuman, and J. W. Weisel. 2005. Polymerization of fibrin: specificity, strength, and stability of knob-hole interactions studied at the single-molecule level. Blood 106:2944.
17. Weisel, J. W., Y. Veklich, and O. Gorkun. 1993. The sequence of cleavage of fibrinopeptides from fibrinogen is important for protofibril formation and enhancement of lateral aggregation in fibrin clots. *J Mol Biol* **232**:285-297.
18. Bale, M. D., M. F. Müller, and J. D. Ferry. 1985. Rheological studies of creep and creep recovery of unligated fibrin clots: comparison of clots prepared with thrombin and ancrod. *Biopolymers* **24**:461-482.
19. Lewis, S. D., P. P. Shields, and J. A. Shafer. 1985. Characterization of the kinetic pathway for liberation of fibrinopeptides during assembly of fibrin. *J Biol Chem* **260**:10192.
20. Ruf, W., A. Bender, D. A. Lane, K. T. Preissner, E. Selmayr, and G. Müller-Berghaus. 1988. Thrombin-induced fibrinopeptide B release from normal and variant fibrinogens: influence of inhibitors of fibrin polymerizatno. *Biochimica et Biophysica Acta (BBA)-General Subjects* **965**:169-175.
21. Shainoff, J. R., and B. N. Dardik. 1979. Fibrinopeptide B and aggregation of fibrinogen. *Science* **204**:200.
22. Mosesson, M. W., J. P. DiOrio, M. F. Muller, J. R. Shainoff, K. R. Siebenlist, D. L. Amrani, G. A. Homandberg, J. Soria, C. Soria, and M. Samama. 1987. Studies on the ultrastructure of fibrin lacking fibrinopeptide B (beta-fibrin). *Blood* **69**:1073.
23. Hogan, K. A., B. Bolliger, N. Okumura, and S. T. Lord. 2001. The Formation of β Fibrin Requires a Functional a Site. *Annals New York Acad Sci* **936**:219-222.

24. Blombäck, B., B. Hessel, D. Hogg, and L. Therkildsen. 1978. A two-step fibrinogen--fibrin transition in blood coagulation. *Nature* **275**:501.
25. Weisel, J. W., and L. Medved. 2001. The structure and function of the C domains of fibrinogen. *Annals New York Acad Sci* **936**:312-327.
26. Guthold, M., W. Liu, B. Stephens, S. T. Lord, R. R. Hantgan, D. A. Erie, R. M. Taylor Jr, and R. Superfine. 2004. Visualization and mechanical manipulations of individual fibrin fibers suggest that fiber cross section has fractal dimension 1.3. *Biophys J* **87**:4226-4236.
27. Medved, L., T. Ugarova, Y. Veklich, N. Lukinova, and J. Weisel. 1990. Electron microscope investigation of the early stages of fibrin assembly:: Twisted protofibrils and fibers. *J Mol Biol* **216**:503-509.
28. Weisel, J. W., C. Nagaswami, and L. Makowski. 1987. Twisting of fibrin fibers limits their radial growth. *Proc Natl Acad Sci* **84**:8991.
29. Nelb, G. W., C. Gerth, J. D. Ferry, and L. Lorand. 1976. Rheology of fibrin clots:: III. Shear creep and creep recovery of fine ligated and coarse unligated clots. Biophysical Chemistry 5:377-387.
30. Weisel, J. W., and C. Nagaswami. 1992. Computer modeling of fibrin polymerization kinetics correlated with electron microscope and turbidity observations: clot structure and assembly are kinetically controlled. Biophysical journal 63:111-128.
31. Mosesson, M. W., J. P. DiOrio, K. R. Siebenlist, J. S. Wall, and J. F. Hainfeld. 1993. Evidence for a second type of fibril branch point in fibrin polymer networks, the trimolecular junction. *Blood* **82**:1517.
32. Mosesson, M. W., K. R. Siebenlist, and D. A. Meh. 2001. The structure and biological features of fibrinogen and fibrin. *Annals New York Acad Sci* **936**:11-30.
33. Ryan, E. A., L. F. Mockros, J. W. Weisel, and L. Lorand. 1999. Structural origins of fibrin clot rheology. Biophysical journal 77:2813-2826.
34. Carlisle, C. R., E. A. Sparks, C. Der Loughian, and M. Guthold. Strength and failure of fibrin fiber branchpoints. *J Thromb Haemost* **8**:1135-1138.

35. Weisel, J. W. 1986. The electron microscope band pattern of human fibrin: various stains, lateral order, and carbohydrate localization. *J Ultra Mol Struc Res* **96**:176-188.
36. Fatah, K., A. Silveira, P. Tornvall, F. Karpe, M. Blombäck, and A. Hamsten. 1996. Proneness to formation of tight and rigid fibrin gel structures in men with myocardial infarction at a young age. *Thromb Haemost* **76**:535-540.
37. Scrutton, M. C., S. B. Ross-Murphy, G. M. Bennett, Y. Stirling, and T. W. Meade. 1994. Changes in clot deformability--a possible explanation for the epidemiological association between plasma fibrinogen concentration and myocardial infarction. *Blood Coag Fibrinolys* **5**:719.
38. Collet, J. P., Y. Allali, C. Lesty, M. L. Tanguy, J. Silvain, A. Ankri, B. Blanchet, R. Dumaine, J. Gianetti, and L. Payot. 2006. Altered fibrin architecture is associated with hypofibrinolysis and premature coronary atherothrombosis. *ATVB* **26**:2567-2573.
39. Carr, M. E., E. J. Martin, J. G. Kuhn, and S. V. Seremetis. 2003. Effects of recombinant factor VIIa on platelet function and clot structure in blood with deficient prothrombin conversion. *Thrombosis and Haemostasis-Stuttgart* **89**:803-811.
40. Lorand, L. 1994. Acquired inhibitors of fibrin stabilization: a class of hemorrhagic disorders of diverse origins. *Anticoagulants, Physiologic, Pathologic and Pharmacologic*:169–191.
41. Nelb, G. W., C. Gerth, J. D. Ferry, and L. Lorand. 1976. Rheology of fibrin clots:: III. Shear creep and creep recovery of fine ligated and coarse unligated clots. *Biophys Chem* **5**:377-387.
42. Ferry, J. D., M. Miller, and S. Shulman. 1951. The conversion of fibrinogen to fibrin. VII. Rigidity and stress relaxation of fibrin clots; effect of calcium* 1. *Biochem Biophys* **34**:424-436.
43. L. Roberts, W. W. L. a. L. F. M. 1973. Viscoelastic properties of fibrin clots. *Biorheology* **10**:29-42.

44. Roberts, W. W., O. Kramer, R. W. Rosser, F. H. M. Nestler, and J. D. Ferry. 1974. Rheology of fibrin clots. I.:: Dynamic viscoelastic properties and fluid permeation. *Biophys Chem* **1**:152-160.
45. Gerth, C., W. W. Roberts, and J. D. Ferry. 1974. Rheology of fibrin clots II:: Linear viscoelastic behavior in shear creep. *Biophys Chem* **2**:208-217.
46. Mockros, L. F., W. W. Roberts, and L. Lorand. 1974. Viscoelastic properties of ligation-inhibited fibrin clots. *Biophys Chem* **2**:164.
47. Shen, L. L., R. P. McDonagh, J. McDonagh, and J. Hermans. 1974. Fibrin gel structure: influence of calcium and covalent cross-linking on the elasticity. *Biochem Biophys Res Comm* **56**:793-798.
48. Shen, L. L., J. Hermans, J. McDonagh, R. P. McDonagh, and M. Carr. 1975. Effects of calcium ion and covalent crosslinking on formation and elasticity of fibrin gels. *Thromb Res* **6**:255-265.
49. Rosser, R. W., W. W. Roberts, and J. D. Ferry. 1977. Rheology of fibrin clots:: IV. Darcy constants and fiber thickness. *Biophys Chem* **7**:153-157.
50. Nelb, G. W., G. W. Kamykowski, and J. D. Ferry. 1981. Rheology of fibrin clots. V. Shear modulus, creep, and creep recovery of fine unligated clots. *Biophys Chem* **13**:15-23.
51. Janmey, P. A., E. J. Amis, and J. D. Ferry. 1983. Rheology of fibrin clots. VI. Stress relaxation, creep, and differential dynamic modulus of fine clots in large shearing deformations. *J Reol* **27**:135.
52. Shen, L., and L. Lorand. 1983. Contribution of fibrin stabilization to clot strength. Supplementation of factor XIII-deficient plasma with the purified zymogen. *J Clin Invest* **71**:1336.
53. Shimizu, A., and J. D. Ferry. 1988. Clots of beta-fibrin. Viscoelastic properties, temperature dependence of elasticity, and interaction with fibrinogen-binding tetrapeptides. *Biophys J* **53**:311-318.
54. Ryan, E. A., L. F. Mockros, A. M. Stern, and L. Lorand. 1999. Influence of a natural and a synthetic inhibitor of factor XIIIa on fibrin clot rheology. *Biophys J* **77**:2827-2836.

55. Mallett, S. V., and D. J. A. Cox. 1992. Thrombelastography. *Brit J Anaesthsia* **69**:307.
56. Wenker, O. C., Z. Wojciechowski, R. Sheinbaum, and E. Zisman. 2000. Thrombelastography. *The Internet Journal of Perfusionists* **1**.
57. Hartert, H. 1948. Blutgerinnungsstudien mit der Thrombelastographie, einem neuen Untersuchungsverfahren. *J Mol Med* **26**:577-583.
58. Ferry, J. D. 1980. Viscoelastic properties of polymers, 3rd ed. Wiley, New York.
59. Macosko, C. W., and R. G. Larson. 1994. Rheology: principles, measurements, and applications. VCH New York.
60. Neeves, K. B., D. A. R. Illing, and S. L. Diamond. Thrombin Flux and Wall Shear Rate Regulate Fibrin Fiber Deposition State during Polymerization under Flow. Biophysical journal 98:1344.
61. Fressinaud, E., K. S. Sakariassen, C. Rothschild, H. R. Baumgartner, and D. Meyer. 1992. Shear rate-dependent impairment of thrombus growth on collagen in nonanticoagulated blood from patients with von Willebrand disease and hemophilia A. *Blood* **80**:988.
62. Roberts, W. W., L. Lorand, and L. F. Mockros. 1973. Viscoelastic properties of fibrin clots. *Biorheology* **10**:29.
63. Weisel, J. W. 2004. The mechanical properties of fibrin for basic scientists and clinicians. *Biophys Chem* **112**:267-276.
64. Carr Jr, M. E., and J. Hermans. 1978. Size and density of fibrin fibers from turbidity. Macromolecules 11:46-50.
65. Fukada, E., and M. Kaibara. 1973. The dynamic rigidity of fibrin gels. *Biorheology* **10**:129.
66. Glover, C. J., L. V. McIntire, C. H. Brown 3rd, and E. A. Natelson. 1975. Rheological properties of fibrin clots. Effects of fibrinogen concentration, Factor XIII deficiency, and Factor XIII inhibition. The Journal of laboratory and clinical medicine 86:644.
67. Weigandt, K. M., D. C. Pozzo, and L. Porcar. 2009. Structure of high density fibrin networks probed with neutron scattering and rheology. *Soft Matter* **5**:4321-4330.

68. MacKintosh, F. C., J. Kas, and P. A. Janmey. 1995. Elasticity of semiflexible biopolymer networks. *Phys Rev Lett* **75**:4425-4428.
69. Boal, D. H. 2002. Mechanics of the Cell. Cambridge Univ Pr.
70. Tassieri, M. 2007. Microrheology of semflexible polymers. PhD thesis, University of Leeds, Leeds.
71. Morse, D. C. 1998. Viscoelasticity of concentrated isotropic solutions of semiflexible polymers. 2. Linear response. *Macromolecules* **31**:7044.
72. Morse, D. C. 1998. Viscoelasticity of concentrated isotropic solutions of semiflexible polymers. 1. Model and stress tensor. *Macromolecules* **31**:7030.
73. Morse, D. C. 1998. Viscoelasticity of concentrated isotropic solutions of semiflexible polymers. 3. Nonlinear rheology. *Macromolecules* **32**:5934.
74. Collet, J. P., J. L. Moen, Y. I. Veklich, O. V. Gorkun, S. T. Lord, G. Montalescot, and J. W. Weisel. 2005. The C domains of fibrinogen affect the structure of the fibrin clot, its physical properties, and its susceptibility to fibrinolysis. *Blood* **106**:3824.
75. Standeven, K. F., A. M. Carter, P. J. Grant, J. W. Weisel, I. Chernysh, L. Masova, S. T. Lord, and R. A. S. Ariëns. 2007. Functional analysis of fibrin -chain cross-linking by activated factor XIII: determination of a cross-linking pattern that maximizes clot stiffness. Blood 110:902.
76. Baradet, T. C., J. C. Haselgrove, and J. W. Weisel. 1995. Three-dimensional reconstruction of fibrin clot networks from stereoscopic intermediate voltage electron microscope images and analysis of branching. *Biophys J* **68**:1551-1560.
77. Shah, J. V., and P. A. Janmey. 1997. Strain hardening of fibrin gels and plasma clots. *Rheologica Acta* **36**:262-268.
78. Doi, M., and N. Y. Kuzuu. 1980. Nonlinear elasticity of rodlike macromolecules in condensed state. Journal of Polymer Science: Polymer Physics Edition 18:409-419.

79. Janmey, P. A., E. J. Amis, and J. D. Ferry. 1983. Rheology of fibrin clots. VI. Stress relaxation, creep, and differential dynamic modulus of fine clots in large shearing deformations. Journal of Rheology 27:135.
80. Storm, C., J. J. Pastore, F. C. MacKintosh, T. C. Lubensky, and P. A. Janmey. 2005. Nonlinear elasticity in biological gels. *Nature* **435**:191-194.
81. Brown, A. E. X., R. I. Litvinov, D. E. Discher, P. K. Purohit, and J. W. Weisel. 2009. Multiscale mechanics of fibrin polymer: gel stretching with protein unfolding and loss of water. *Science* **325**:741.
82. Hudson, N. E., J. R. Houser, E. T. O'Brien Iii, and R. M. Taylor. Stiffening of individual fibrin fibers equitably distributes strain and strengthens networks. *Biophys J* **98**:1632.
83. Collet, J. P., H. Shuman, R. E. Ledger, S. Lee, and J. W. Weisel. 2005. The elasticity of an individual fibrin fiber in a clot. *Proc Natl Acad Sci* **102**:9133.
84. Ryan, E. A., L. F. Mockros, J. W. Weisel, and L. Lorand. 1999. Structural origins of fibrin clot rheology. *Biophys J* **77**:2813-2826.
85. Liu, W., L. M. Jawerth, E. A. Sparks, M. R. Falvo, R. R. Hantgan, R. Superfine, S. T. Lord, and M. Guthold. 2006. Fibrin fibers have extraordinary extensibility and elasticity. *Science* **313**:634.
86. Liu, W., C. R. Carlisle, E. A. Sparks, and M. Guthold. The mechanical properties of single fibrin fibers. *J Thromb Haemost* **8**:1030-1036.
87. Mosesson, M. W. 2004. The fibrin cross linking debate: cross linked chains in fibrin fibrils bridge ‘transversely’between strands: yes. *J Thromb Haemost* **2**:388-393.
88. Weisel, J. W. 2004. Cross linked chains in fibrin fibrils bridge transversely between strands: no. *J Thromb Haemost* **2**:394-399.
89. Roska, F. J., and J. D. Ferry. 1982. Studies of fibrin film. I. Stress relaxation and birefringence. *Biopolymers* **21**:1811-1832.
90. Ferry, J. D. 1988. Structure and rheology of fibrin networks. Biological and Synthetic Polymer Networks. Amsterdam: Elsevier:41–55.

91. Brown André, E. X., R. I. Litvinov, D. E. Discher, and J. W. Weisel. 2007. Forced unfolding of coiled-coils in fibrinogen by single-molecule AFM. *Biophys J* **92**:L39-L41.
92. Lim, B. B. C., E. H. Lee, M. Sotomayor, and K. Schulten. 2008. Molecular basis of fibrin clot elasticity. Structure 16:449-459.
93. Veklich, Y. I., O. V. Gorkun, L. V. Medved, W. Nieuwenhuizen, and J. W. Weisel. 1993. Carboxyl-terminal portions of the chains of fibrinogen and fibrin: localization by electron microscopy and the effects of isolated C fragments on polymerization. *J Biol Chem* **268**:13577-13585.
94. Ariëns, R. A. S., H. Philippou, C. Nagaswami, J. W. Weisel, D. A. Lane, and P. J. Grant. 2000. The factor XIII V34L polymorphism accelerates thrombin activation of factor XIII and affects cross-linked fibrin structure. *Blood* **96**:988.
95. Mihalyi, E. 1968. Physicochemical studies of bovine fibrinogen. IV. Ultraviolet absorption and its relation to the structure of the molecule. Biochemistry 7:208-223.
96. Cooper, A. V., K. F. Standeven, and R. A. S. Ariëns. 2003. Fibrinogen gamma-chain splice variant {gamma}'alters fibrin formation and structure. Blood 102:535.
97. Freund, K. F., K. P. Doshi, S. L. Gaul, D. A. Claremon, D. C. Remy, J. J. Baldwin, S. M. Pitzenberger, and A. M. Stern. 1994. Transglutaminase inhibition by 2-[(2-oxopropyl) thio] imidazolium derivatives: mechanism of factor XIIIa inactivation. Biochemistry 33:10109-10119.
98. http://upload.wikimedia.org/wikipedia/commons/0/04/Beer_lambert
99. Mullin, J. L., O. V. Gorkun, and S. T. Lord. 2000. Decreased Lateral Aggregation of a Variant Recombinant Fibrinogen Provides Insight into the Polymerization Mechanism†. Biochemistry 39:9843-9849.
100. Jones, R. A. L. 2002. Soft condensed matter. Oxford University Press, USA.
101. http://www.olympusfluoview.com/theory/index.html
102. Knoll, M. 1935. Zeit Techn Phys 11:467.

103. http://en.wikipedia.org/wiki/File:Schema_MEB_(en).svg
104. Hawkes, P. W., and J. C. H. Spence. Science of microscopy.
105. Binnig, G., C. F. Quate, and C. Gerber. 1986. Atomic force microscope. Physical review letters 56:930-933.
106. Moreno-Herrero, F., M. Perez, A. M. Baro, and J. Avila. 2004. Characterization by atomic force microscopy of Alzheimer paired helical filaments under physiological conditions. Biophysical journal 86:517-525.
107. Abou-Saleh, R. H., S. D. Connell, R. Harrand, R. A. Ajjan, M. W. Mosesson, D. A. M. Smith, P. J. Grant, and R. A. S. Ariëns. 2009. Nanoscale Probing Reveals that Reduced Stiffness of Clots from Fibrinogen Lacking 42 N-Terminal B [beta]-Chain Residues Is Due to the Formation of Abnormal Oligomers. Biophysical journal 96:2415-2427.
108. Meyer, G., and N. M. Amer. 1988. Applied Physics Letters 53:1045.
109. http://knol.google.com/k/atomic-force-microscopy-afm#
110. http://en.wikipedia.org/wiki/Atomic_force_microscopy
111. MacKintosh, F. C., and C. F. Schmidt. 1999. Microrheology. Current Opinion in Colloid & Interface Science 4:300-307.
112. Waigh, T. A. 2005. Microrheology of complex fluids. Reports on Progress in Physics 68:685.
113. Keller, M., J. Schilling, and E. Sackmann. 2001. Oscillatory magnetic bead rheometer for complex fluid microrheometry. Review of Scientific Instruments 72:3626.
114. Mason, T. G., and D. A. Weitz. 1995. Optical measurements of frequency-dependent linear viscoelastic moduli of complex fluids. Physical review letters 74:1250-1253.
115. Crick, F. H. C., and A. F. W. Hughes. 1950. The physical properties of cytoplasm:: A study by means of the magnetic particle method Part I. Experimental. Experimental Cell Research 1:37-80.
116. Amblard, F., B. Yurke, A. Pargellis, and S. Leibler. 2009. A magnetic manipulator for studying local rheology and micromechanical

properties of biological systems. Review of Scientific Instruments 67:818-827.

117. Gosse, C., and V. Croquette. 2002. Magnetic tweezers: micromanipulation and force measurement at the molecular level. Biophysical Journal 82:3314-3329.

118. Huang, H., C. Y. Dong, H. S. Kwon, J. D. Sutin, R. D. Kamm, and P. T. C. So. 2002. Three-dimensional cellular deformation analysis with a two-photon magnetic manipulator workstation. Biophysical journal 82:2211-2223.

119. Harrand, R. 2007. The viscoelastic properties of fibrin clots studied using magnetic tweezers. PhD thesis, University of Leeds.

120. Gustavo, J. 2003. PhD thesis, California Institute of Technology, Pasadena, California.

121. Chernysh, I. N., and J. W. Weisel. 2008. Dynamic imaging of fibrin network formation correlated with other measures of polymerization. Blood 111:4854.

122. Collet, J. P., H. Shuman, R. E. Ledger, S. Lee, and J. W. Weisel. 2005. The elasticity of an individual fibrin fiber in a clot. Proceedings of the National Academy of Sciences of the United States of America 102:9133.

123. Onck, P. R., T. Koeman, T. van Dillen, and E. van der Giessen. 2005. *Phys Rev Lett* **95**.

124. Nelb, G. W., G. W. Kamykowski, and J. D. Ferry. 1981. Rheology of fibrin clots. V. Shear modulus, creep, and creep recovery of fine unligated clots. Biophysical Chemistry 13:15-23.

125. Schindlauer, G., M. D. Bale, and J. D. Ferry. 1986. Interaction of fibrinogen binding tetrapeptides with fibrin oligomers and fine fibrin clots. Biopolymers 25:1315-1336.

126. Evans, R. M. L., M. Tassieri, D. Auhl, and T. A. Waigh. 2009. Direct conversion of rheological compliance measurements into storage and loss moduli. Physical Review E 80:12501.

127. Evans, R. M. L., M. Tassieri, D. Auhl, and T. A. Waigh. 2009. Direct conversion of rheological compliance measurements into storage and loss moduli. *Phys Rev E* **80**:12501.
128. Squires, T. M., and T. G. Mason. Fluid mechanics of microrheology. Annual Review of Fluid Mechanics 42:413-438.
129. Tassieri, M., G. M. Gibson, R. M. L. Evans, A. M. Yao, R. Warren, M. J. Padgett, and J. M. Cooper. 2009. Measuring storage and loss moduli using optical tweezers: Broadband microrheology. Arxiv preprint arXiv:0910.1339.
130. Spruijt, E., J. Sprakel, M. Lemmers, M. A. C. Stuart, and J. van der Gucht. Relaxation Dynamics at Different Time Scales in Electrostatic Complexes: Time-Salt Superposition. Physical review letters 105:208301.
131. Tassieri, M., T. A. Waigh, J. Trinick, A. Aggeli, and R. M. L. Evans. Analysis of the linear viscoelasticity of polyelectrolytes by magnetic microrheometry—Pulsed creep experiments and the one particle response. Journal of Rheology 54:117.
132. Preece, D., R. Warren, R. M. L. Evans, G. M. Gibson, M. J. Padgett, J. M. Cooper, and M. Tassieri. Optical tweezers: wideband microrheology. Journal of Optics 13:044022.
133. Hudson, N. E., J. R. Houser, E. T. O'Brien Iii, and R. M. Taylor. Stiffening of individual fibrin fibers equitably distributes strain and strengthens networks. Biophysical journal 98:1632.
134. Brown André, E. X., R. I. Litvinov, D. E. Discher, and J. W. Weisel. 2007. Forced unfolding of coiled-coils in fibrinogen by single-molecule AFM. Biophysical journal 92:L39-L41.
135. Averett, L. E., C. B. Geer, R. R. Fuierer, B. B. Akhremitchev, O. V. Gorkun, and M. H. Schoenfisch. 2008. Complexity of “Aa” knob-hole fibrin interaction revealed by atomic force spectroscopy. Langmuir 24:4979-4988.
136. Falvo, M. R., D. Millard, E. T. O’Brien, R. Superfine, and S. T. Lord. 2008. Length of tandem repeats in fibrin’s αC region correlates with

fiber extensibility. Journal of Thrombosis and Haemostasis 6:1991-1993.

137. Liu, W., C. R. Carlisle, E. A. Sparks, and M. Guthold. The mechanical properties of single fibrin fibers. Journal of Thrombosis and Haemostasis 8:1030-1036.

138. Ferry, J. D., M. Miller, and S. Shulman. 1951. The conversion of fibrinogen to fibrin. VII. Rigidity and stress relaxation of fibrin clots; effect of calcium* 1. Archives of Biochemistry and Biophysics 34:424-436.

139. Gerth, C., W. W. Roberts, and J. D. Ferry. 1974. Rheology of fibrin clots II:: Linear viscoelastic behavior in shear creep. Biophysical Chemistry 2:208-217.

140. Mockros, L. F., W. W. Roberts, and L. Lorand. 1974. Viscoelastic properties of ligation-inhibited fibrin clots. Biophysical chemistry 2:164.

141. Shen, L. L., J. Hermans, J. McDonagh, R. P. McDonagh, and M. Carr. 1975. Effects of calcium ion and covalent crosslinking on formation and elasticity of fibrin gels. Thrombosis research 6:255-265.

142. Shen, L., and L. Lorand. 1983. Contribution of fibrin stabilization to clot strength. Supplementation of factor XIII-deficient plasma with the purified zymogen. Journal of Clinical Investigation 71:1336.

143. Ryan, E. A., L. F. Mockros, A. M. Stern, and L. Lorand. 1999. Influence of a natural and a synthetic inhibitor of factor XIIIa on fibrin clot rheology. Biophysical journal 77:2827-2836.

144. Hantgan, R. R., and J. Hermans. 1979. Assembly of fibrin. A light scattering study. *J Biol Chem* **254**:11272.

145. Wolfe, J. K., and D. F. Waugh. 1981. Relations between enzymatic and association reactions in the development of bovine fibrin clot structure* 1. *Arch Biochem Biophys* **211**:125-142.

146. Blombäck, B., and M. Okada. 1982. Fibrin gel structure and clotting time. *Thromb Res* **25**:51-70.

147. Shah, G. A., C. H. Nair, and D. P. Dhall. 1985. Physiological studies on fibrin network structure. *Thromb Res* **40**:181-188.

148. Carr Jr, M. E., D. A. Gabriel, and J. McDonagh. 1986. Influence of Ca2+ on the structure of reptilase-derived and thrombin-derived fibrin gels. *Biochem J* **239**:513.
149. Weisel, J. W., and C. Nagaswami. 1992. Computer modeling of fibrin polymerization kinetics correlated with electron microscope and turbidity observations: clot structure and assembly are kinetically controlled. *Biophys J* **63**:111-128.
150. Chernysh, I. N., C. Nagaswami, and J. W. Weisel. 2011. Visualization and identification of the structures formed during early stages of fibrin polymerization. *Blood* **117**:4609.
151. Glover, C. J., L. V. McIntire, C. H. Brown 3rd, and E. A. Natelson. 1975. Rheological properties of fibrin clots. Effects of fibrinogen concentration, Factor XIII deficiency, and Factor XIII inhibition. *J Lab Clin Med* **86**:644.
152. Anand, S., and S. L. Diamond. 1996. Computer simulation of systemic circulation and clot lysis dynamics during thrombolytic therapy that accounts for inner clot transport and reaction. *Circulation* **94**:763.
153. Blombäck, B., D. Banerjee, K. Carlsson, A. Hamsten, B. Hessel, R. Procyk, A. Silveira, and L. Zacharski. 1990. Native fibrin gel networks and factors influencing their formation in health and disease. *Advan Exp Med Biol* **281**:1.
154. Muller, M. F., H. Ris, and J. D. Ferry. 1984. Electron microscopy of fine fibrin clots and fine and coarse fibrin films* 1:: Observations of fibers in cross-section and in deformed states. *J Mol Biol* **174**:369-384.
155. Carr, M. E. 1988. Fibrin formed in plasma is composed of fibers more massive than those formed from purified fibrinogen. Thromb Haemost **59**:535.
156. Blomback, B., K. Carlsson, K. Fatah, B. Hessel, and R. Procyk. 1994. Fibrin in human plasma: gel architectures governed by rate and nature of fibrinogen activation. *Thromb Res* **75**:521-538.
157. Blomback, B., K. Carlsson, B. Hessel, A. Liljeborg, R. Procyk, and N. Aslund. 1989. Native fibrin gel networks observed by 3D microscopy,

permeation and turbidity. *Biochimica et Biophysica Acta (BBA)-Protein Structure and Molecular Enzymology* **997**:96-110.

158. Kaibara, M., and E. Fukada. 1971. The influence of the concentration of thrombin on the dynamic viscoelasticity of clotting blood and fibrinogen-thrombin systems. *Biorheology* **8**:139.
159. Kaibara, M. 1973. Dynamic viscoelastic study of the formation of fibrin networks in fibrinogen-thrombin systems and plasma. *Biorheology* **10**:61-73.
160. Marx, G. 1988. Elasticity of fibrin and protofibrin gels is differentially modulated by calcium and zinc. *Thromb Haemost* **59**:500.
161. Rosenfeld, G., and B. Janszky. 1952. The accelerating effect of calcium on the fibrinogen-fibrin transformation. *Science* **116**:36.
162. Ratnoff, O. D., and A. M. Potts. 1954. The accelerating effect of calcium and other cations on the conversion of fibrinogen to fibrin. *J Clin Invest* **33**:206.
163. Lorand, L., and K. Konishi. 1964. Activation of the fibrin stabilizing factor of plasma by thrombin. *Arch Biochem Biophys* **105**:58-67.
164. Boyer, M. H., J. R. Shainoff, and O. D. Ratnoff. 1972. Acceleration of fibrin polymerization by calcium ions. *Blood* **39**:382.
165. Endres, G. F., and H. A. Scheraga. 1972. Equilibria in the fibrinogen-fibrin conversion* 1:: IX. Effects of calcium ions on the reversible polymerization of fibrin monomer. *Biochem Biophys* **153**:266-278.
166. Brass, E. P., W. B. Forman, R. V. Edwards, and O. Lindan. 1978. Fibrin formation: effect of calcium ions. *Blood* **52**:654.
167. Hardy, J. J., N. A. Carrell, and J. McDonagh. 1983. Calcium ion functions in fibrinogen conversion to fibrin. *Annals New York Acad Sci* **408**:279-287.
168. Dang, C. V., C. K. Shin, W. R. Bell, C. Nagaswami, and J. W. Weisel. 1989. Fibrinogen sialic acid residues are low affinity calcium-binding sites that influence fibrin assembly. *J Biol Chem* **264**:15104.
169. Mihalyi, E. 1988. Clotting of bovine fibrinogen. Calcium binding to fibrin during clotting and its dependence on release of fibrinopeptide B. *Biochemistry* **27**:967-976.

170. Okada, M., and B. BlombÃ¤ck. 1983. Calcium and fibrin gel structure. *Thromb Res* **29**:269-280.
171. Carr Jr, M. E., and S. L. Carr. 1995. Fibrin structure and concentration alter clot elastic modulus but do not alter platelet mediated force development. *Blood Coag Fibrinolys* **6**:79.
172. Hantgan, R., W. Fowler, H. Erickson, and J. Hermans. 1980. Fibrin assembly: a comparison of electron microscopic and light scattering results. *Thromb Haemost* **44**:119.
173. Hantgan, R., J. McDonagh, and J. Hermans. 1983. Fibrin assembly. *Annals New York Acad Sci* **408**:344-366.
174. Chung, D. W., and E. W. Davie. 1984. Gamma and γ' chains of human fibrinogen are produced by alternative mRNA processing. *Biochemistry* **23**:4232-4236.
175. Wolfenstein-Todel, C., and M. W. Mosesson. 1981. Carboxy-terminal amino acid sequence of a human fibrinogen γ-chain variant (γ'). Biochemistry 20:6146-6149.
176. Mosesson, M. W., and J. S. Finlayson. 1963. Subfractions of human fibrinogen; preparation and analysis. The Journal of laboratory and clinical medicine 62:663.
177. Mosesson, M. W., J. S. Finlayson, and R. A. Umfleet. 1972. Human fibrinogen heterogeneities: 3. Identification of chain variants. Journal of Biological Chemistry 247:5223-5227.
178. Uitte de Willige, S., K. F. Standeven, H. Philippou, and R. A. S. Ariëns. 2009. The pleiotropic role of the fibrinogen {gamma}'chain in hemostasis. *Blood* **114**:3994.
179. Lovely, R. S., L. A. Falls, H. A. Al-Mondhiry, C. E. Chambers, G. J. Sexton, H. Ni, and D. H. Farrell. 2002. Association of γA/γ' Fibrinogen Levels and Coronary Artery Disease. Thrombosis and Haemostasis 88:26-31.
180. Mannila, M. N., R. S. Lovely, S. C. Kazmierczak, P. Eriksson, A. Samnegård, D. H. Farrell, A. Hamsten, and A. Silveira. 2007. Elevated plasma fibrinogen gamma' concentration is associated with myocardial infarction: effects of variation in fibrinogen genes and

environmental factors. Journal of Thrombosis and Haemostasis 5:766-773.

181. Cheung, E. Y. L., S. Uitte de Willige, H. L. Vos, F. W. G. Leebeek, D. W. J. Dippel, R. M. Bertina, and M. P. M. de Maat. 2008. Fibrinogen {gamma}'in Ischemic Stroke: A Case-Control Study. Stroke 39:1033.

182. Uitte de Willige, S., M. C. H. de Visser, J. J. Houwing-Duistermaat, F. R. Rosendaal, H. L. Vos, and R. M. Bertina. 2005. Genetic variation in the fibrinogen gamma gene increases the risk for deep venous thrombosis by reducing plasma fibrinogen {gamma}'levels. Blood 106:4176.

183. Mosesson, M., I. Hernandez, T. Raife, L. Medved, S. Yakovlev, and P. Simpson-Haidaris. 2007. Plasma Fibrinogen Gamma Prime Chain Content in the Thrombotic Microangiopathy Syndrome. Journal of Thrombosis and Haemostasis 5:62-69.

184. Siebenlist, K. R., M. W. Mosesson, I. Hernandez, L. A. Bush, E. Di Cera, J. R. Shainoff, J. P. Di Orio, and L. Stojanovic. 2005. Studies on the basis for the properties of fibrin produced from fibrinogen-containing {gamma}'chains. Blood 106:2730.

185. Gersh, K. C., C. Nagaswami, J. W. Weisel, and S. T. Lord. 2009. The presence of γ' chain impairs fibrin polymerization. Thrombosis research 124:356-363.

186. Collet, J. P., C. Nagaswami, D. H. Farrell, G. Montalescot, and J. W. Weisel. 2004. Influence of {gamma}'fibrinogen splice variant on fibrin physical properties and fibrinolysis rate. Arteriosclerosis, thrombosis, and vascular biology 24:382.

187. Falls, L. A., and D. H. Farrell. 1997. Resistance of γA/γ' fibrin clots to fibrinolysis. Journal of Biological Chemistry 272:14251.

188. Moaddel, M., D. H. Farrell, M. A. Daugherty, and M. G. Fried. 2000. Interactions of Human Fibrinogens with Factor XIII: Roles of Calcium and the γ' Peptide†. Biochemistry 39:6698-6705.

189. Moaddel, M., L. A. Falls, and D. H. Farrell. 2000. The role of γA/γ' fibrinogen in plasma factor XIII activation. Journal of Biological Chemistry 275:32135-32140.

190. Meh, D. A., K. R. Siebenlist, and M. W. Mosesson. 1996. Identification and characterization of the thrombin binding sites on fibrin. Journal of Biological Chemistry 271:23121.

191. Lovely, R. S., M. Moaddel, and D. H. Farrell. 2003. Fibrinogen γ' chain binds thrombin exosite II. Journal of Thrombosis and Haemostasis 1:124-131.

192. Meh, D. A., K. R. Siebenlist, S. O. Brennan, T. Holyst, and M. W. Mosesson. 2001. The amino acid sequence in fibrin responsible for high affinity thrombin binding. Thrombosis and haemostasis 85:470-474.

193. Siebenlist, K. R., D. A. Meh, and M. W. Mosesson. 1996. Plasma factor XIII binds specifically to fibrinogen molecules containing γ' chains. Biochemistry 35:10448-10453.

194. Kazama, M., J. McDonagh, R. H. Wagner, R. D. Langdell, and R. P. McDonagh. 1976. Purification and immunochemical characterization of human plasma factor XIII. Pathophysiology of Haemostasis and Thrombosis 5:329-340.

195. Gersh, K. C., and S. T. Lord. 2006. An Investigation of Factor XIII Binding to Recombinant {gamma}'/{gamma}' and {gamma}/{gamma}' Fibrinogen. *ASH Annual Meeting Abstracts* **108**:1705.

196. Gersh, K. C., C. Nagaswami, J. W. Weisel, and S. T. Lord. 2009. The presence of γ' chain impairs fibrin polymerization. *Thromb Res* **124**:356-363.

197. Janmey, P. A. 1991. A torsion pendulum for measurement of the viscoelasticity of biopolymers and its application to actin networks. Journal of biochemical and biophysical methods 22:41-53.

198. Collet, J. P., C. Nagaswami, D. H. Farrell, G. Montalescot, and J. W. Weisel. 2004. Influence of {gamma}'fibrinogen splice variant on fibrin physical properties and fibrinolysis rate. *ATVB* **24**:382.

199. Chernysh, I. N., C. Nagaswami, and J. W. Weisel. Visualization and identification of the structures formed during early stages of fibrin polymerization. Blood 117:4609.

200. Collet, J. P., D. Park, C. Lesty, J. Soria, C. Soria, G. Montalescot, and J. W. Weisel. 2000. Influence of fibrin network conformation and fibrin fiber diameter on fibrinolysis speed: dynamic and structural approaches by confocal microscopy. Arteriosclerosis, thrombosis, and vascular biology 20:1354-1361.

201. Collet, J. P., J. Soria, M. Mirshahi, M. Hirsch, F. B. Dagonnet, J. Caen, and C. Soria. 1993. Dusart syndrome: a new concept of the relationship between fibrin clot architecture and fibrin clot degradability: hypofibrinolysis related to an abnormal clot structure. Blood 82:2462.

202. Wolberg, A. S. 2007. Thrombin generation and fibrin clot structure. Blood reviews 21:131-142.

203. Gabriel, D. A., K. Muga, and E. M. Boothroyd. 1992. The effect of fibrin structure on fibrinolysis. Journal of Biological Chemistry 267:24259.

204. Carr Jr, M. E., and B. M. Alving. 1995. Effect of fibrin structure on plasmin-mediated dissolution of plasma clots. Blood coagulation & fibrinolysis: an international journal in haemostasis and thrombosis 6:567.

205. Konings, J., J. W. P. Govers-Riemslag, H. Philippou, N. J. Mutch, J. I. Borissoff, P. Allan, S. Mohan, G. Tans, H. ten Cate, and R. A. S. Ariëns. 2011. Factor XIIa regulates the structure of the fibrin clot independently of thrombin generation through direct interaction with fibrin. *Blood* **118**:3942-3951.

206. He, S., M. Blombäck, G. Jacobsson Ekman, and U. Hedner. 2003. The role of recombinant factor VIIa (FVIIa) in fibrin structure in the absence of FVIII/FIX. Journal of Thrombosis and Haemostasis 1:1215-1219.

207. Carr, M. E., E. J. Martin, J. G. Kuhn, and S. V. Seremetis. 2003. Effects of recombinant factor VIIa on platelet function and clot structure in blood with deficient prothrombin conversion. Thrombosis and Haemostasis-Stuttgart 89:803-811.

208. Davidson, C. J., E. G. Tuddenham, and J. H. McVey. 2003. 450 million years of hemostasis. *J Thromb Haemost* **1**:1487-1494.
209. Carr Jr, M. E., D. A. Gabriel, and J. McDonagh. 1987. Influence of factor XIII and fibronectin on fiber size and density in thrombin-induced fibrin gels. *J Lab Clin Med* **110**:747.
210. Harrand, R. 2007. The viscoelastic properties of fibrin clots studied using magnetic tweezers. PhD thesis, University of Leeds, Leeds.
211. Huang, H., C. Y. Dong, H. S. Kwon, J. D. Sutin, R. D. Kamm, and P. T. C. So. 2002. Three-dimensional cellular deformation analysis with a two-photon magnetic manipulator workstation. *Biophys J* **82**:2211-2223.